

ISIS

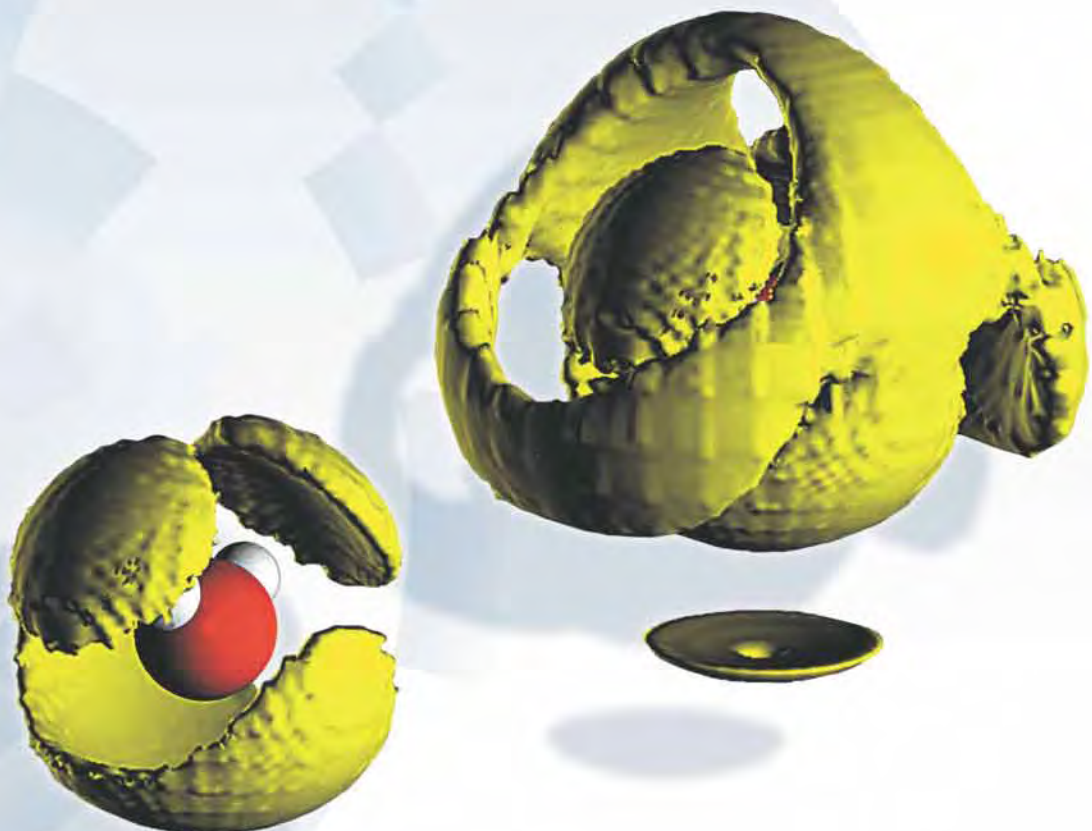


2002

ISIS Facility Annual Report 2001-2002

*For the financial year
1 April 2001 to 31 March 2002*

This document and the experimental reports for 2001- 2002 are contained on the CD inside the back cover in PDF format. ISIS 2002, including experimental reports, is also available on the ISIS web site <http://www.isis.rl.ac.uk>



Highlights of ISIS Science (pages 17 - 74)

- 18 *Structural phase transitions in minerals at low temperatures*
- 20 *An unusual molecular glue – unconventional di-hydrogen bonds in boraneamines*
- 22 *Location of hydrogen in ternary transition metal hydrides*
- 24 *Isotopic substitution with combined Rietveld analysis methods for definitive structural information from powder neutron diffraction*
- 26 *Formation of isomorphic Ir³⁺ and Ir⁴⁺ octamers and spin dimerization in the spinel CuIr₂S₄*
- 28 *The structures of high and low density amorphous ice*
- 30 *Acetylcholine in water*
- 32 *Observing magnetically patterned structures on CRISP*
- 34 *Thermal denaturation of interfacial protein layers*
- 36 *Combining small-angle X-ray and neutron scattering to elucidate complex layer structures in model polymers*
- 38 *Formation mechanisms in surfactant templated films*
- 40 *Polymer diffusion in supercritical fluids*
- 42 *Bose-Einstein condensation in disorder*
- 44 *Understanding the origin of non-Fermi liquid behaviour in doped Kondo insulators*
- 46 *Vibrational studies on disaccharide/H₂O systems*
- 48 *Quantum melting in magnetic metals*
- 50 *Spin polaron in a quantum spin liquid*
- 52 *The application of INS spectroscopy in heterogeneous catalysis: methyl chloride synthesis*
- 54 *Hydrogen spillover on carbon-supported metal catalysts*
- 56 *Pressure effect on water dynamics in TBA-water mixtures*
- 58 *Measurement of the proton wave function in hydrogen bonds by eV neutron scattering*
- 60 *Magnetic correlations vs anisotropic Kondo fluctuations*
- 62 *Vortex motion in type-II superconductors probed by muon spin rotation*
- 64 *Very low-frequency excitations in frustrated antiferromagnets*
- 66 *Internal strain and texture evolution in piezoelectric ceramics*
- 68 *Revealing the missing-link with Bayes and MaxEnt*
- 70 *Successful operation of the ISIS radio frequency quadrupole*
- 72 *A fast beam chopper for the ESS*



Foreword	v
Science at ISIS	1
Highlights of ISIS Science	17
Instrument Developments	75
Accelerator and Target	83
User Interaction and Support	91
Publications	105

contents

*Professor Werner Press
(Kiel University, Germany) with
Uschi Steigenberger (ISIS) during
his visit in April (02RC1968).*

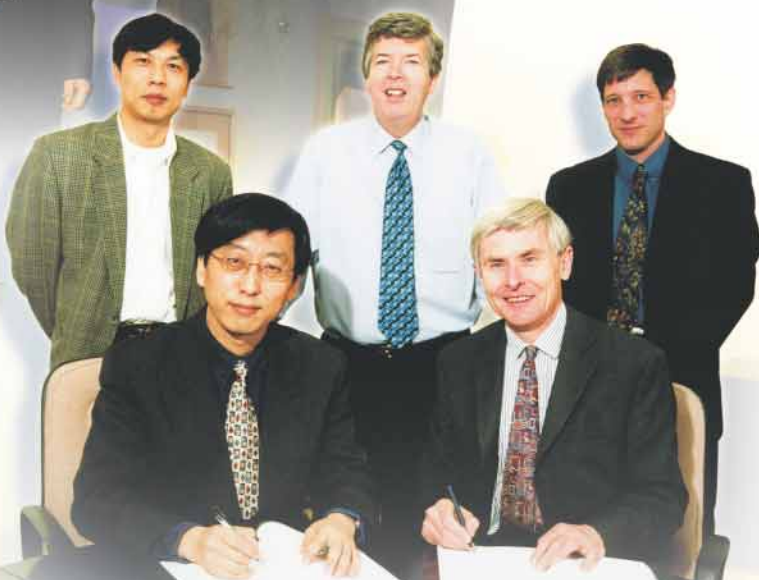


*Professor Murray Gibson
(Director, Advanced Photon
Source, Argonne, USA) with
Andrew Taylor and Roger
Eccleston (ISIS) (02RC2009).*

*Professor Flavio Toigo (INFN,
Italy) toasting the new VESUVIO
spectrometer with Andrew Taylor
(ISIS, left) and David Schildt
(CLRC) at the inauguration
ceremony in April (02RC2051).*



*Dr François Gounand and
Dr Yves Terrien (CEA-Saclay)
discussing ISIS developments
with Andrew Taylor, ISIS Director
(02RC3320).*



*Professor Jie Zhang (Chinese Academy of Sciences) and Professor John
Wood (Chief Executive, CLRC) signing a Memorandum of Understanding on
the development of future neutron sources, with Dr. Jichen Li (UMIST),
Andrew Taylor and Steve Bennington (ISIS) (02RC1971).*

Foreword

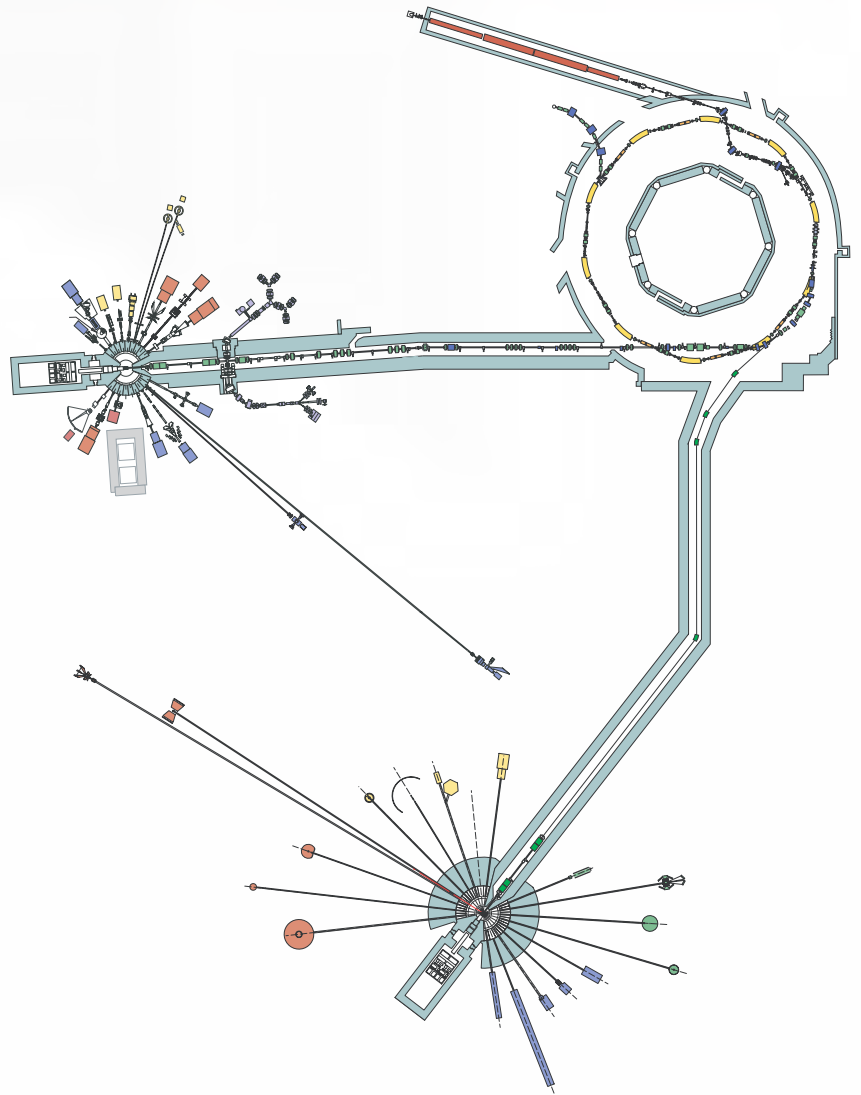
Interesting times!

Earlier this year, the report on the second stage of the Quinquennial Review of CCLRC was published. A key aspect of the outcome is that from April 2003 onwards, all CCLRC's facilities will be *free at the point of access* for UK users. CCLRC will be responsible for both the peer review and the scheduling of proposals for ISIS, and for funding the developments of the facility needed by the user community. We strongly welcome these new arrangements and look forward to developing mechanisms with the community which will maximise the scientific returns from this major investment in UK science.

The momentum for the ISIS Second Target Station continues to build: the project is progressing well through the Government's 'Gateway' process and is anticipating major funding in the Autumn Spending Review.

The Gateway review team were particularly impressed by the clarity of the project and the strong connection established between the facility and the users. They had no doubts that it would deliver opportunities for exciting science as demanded by the UK community. The newly formed Science Advisory Committee is now canvassing views through the User Groups on the development of the instrument suite, and funding is already in place to move 350,000 m³ of earth as part of the site preparation phase of the project!

Last year the accelerator delivered a record 725 mA.hr of protons into the enhanced tungsten target, enabling some 700+ experiments to be performed. Major refurbishment of the accelerator is well underway – an upgraded extraction system is already operational; the RFQ (due to replace the long-serving Cockcroft-Walton next year) has had many hundreds of hours of successful operation on its test stand; and we are halfway through installing the dual harmonic rf system. Please bear with us while we deliver these upgrades which – in the long term – will greatly enhance the overall performance of ISIS.



ENGIN-X has now entered its commissioning phase – with the knock-on effect that the very successful high pressure programme will also double by the end of the year. The last spare beam position on the first ISIS target station has now been earmarked for MERLIN, the latest in a long line of pioneering chopper spectrometers.

It is very satisfying to be able to report such progress on all fronts!

Plan of ISIS with the proposed Second Target Station.

ANTHONY

Dr Bob McGuiness (Managing Director, National Physical Laboratory, centre left) and Professor Andrew Wallard (Deputy Director and Chief Metrologist of the NPL, centre right) touring ISIS with Andrew Taylor and Bill David (01RC4545).

Science and Technology Officers from the Foreign and Commonwealth Office visited ISIS in April (02RC1963).



Professor John Durrell (University of Manchester, left) and Professor David Williams (University of Liverpool, centre right), members of the CLRC Council, visiting ISIS with Jeff Penfold and Bill David (ISIS) (02RC2356).



Professor Helmut Rauch (TU Wien, Austria) explaining the significance of the VESTA (Viennese nEutron Storage Apparatus) experiment for the storage of cold neutrons at the VESTA-II inauguration in December (01RC4655).



Members of the Tokai-mura Assembly visiting ISIS as part of the plans for the JAERI and KEK High Intensity Proton Accelerator Project (02RC1825).





Science at ISIS

ISIS is the world's most powerful pulsed spallation neutron source. The facility provides beams of neutrons and muons that enable scientists to probe the structure and dynamics of matter in areas encompassing Physics, Chemistry, Earth Science, Materials Science, Engineering and Biology. An overview of ISIS science is given here; specific highlights can be found in the next chapter, and reports describing the experiments performed in the last year can be found on the accompanying CD.

1

Introduction to ISIS

ISIS is the world's most intense pulsed neutron and muon source and the major facility at CLRC's Rutherford Appleton Laboratory. First neutrons were produced in 1984, and over the past eighteen years the facility has developed into a major force in condensed matter research and attracted substantial international investment.

Why neutrons and muons?

The neutron is a powerful probe for the study of the microscopic structure and dynamics of condensed matter, having significant advantages over other forms of radiation. Detailed information obtained from neutron scattering has had a major impact on our understanding of the microscopic nature of materials, from magnetism and superconductivity to chemical surfaces and interfaces. Muons are an alternative probe of condensed matter, giving complementary information on structure and dynamics.

Fig. 1.1.
The ISIS experimental hall
(98RC1178).



Neutron production

Neutrons are produced at ISIS by the spallation process. A heavy metal target is bombarded with pulses of highly energetic protons from a synchrotron accelerator, driving neutrons from the nuclei of the target atoms. This results in an extremely intense neutron pulse, delivered with only modest heat production in the neutron target. The neutrons produced have very high energies, and are slowed to speeds (wavelengths) useful for condensed matter research by an array of hydrogenous moderators around the target. They are then directed to some 20 neutron instruments, each optimised to explore different properties of the microscopic structure of materials.

Muons

ISIS also produces intense pulsed beams of muons, via the insertion of a thin graphite intermediate target into the extracted proton beam. These are fed to seven experimental areas for condensed matter investigations and other muon physics studies.

A user facility

ISIS is a User Facility, providing a fully supported instrument suite to enable visiting teams to exploit the neutron and muon techniques. Experiments carried out at ISIS typically complement work programmes performed at home laboratories. The 1600 or so researchers who visit annually come from over 30 different countries, and include both academic and industrial scientists. Experiments are selected by a peer review process, with almost 1000 proposals being received per year. ISIS also proves an excellent training ground for young researchers, with a large number of visiting scientists being aged 30 or under.

ISIS Instruments

MAPS

Single Crystal Excitations
Toby Perring, ext. 5428,
T.G.Perring@rl.ac.uk

VESUVIO

Electron Volt Spectroscopy
Jerry Mayers, ext. 5882,
J.Mayers@rl.ac.uk

SXD

Single Crystal Diffraction
Matthias Gutmann, ext. 6397,
M.J.Gutmann@rl.ac.uk

MARI

S(Q,ω) Vibrational & Magnetic Spectroscopy
Bjorn Fåk, ext. 5453,
B.Fak@rl.ac.uk

GEM

General Purpose Diffraction, Liquids and Amorphous Structures
Paolo Radaelli, ext. 5685,
P.G.Radaelli@rl.ac.uk
Alex Hannon, ext. 5358,
A.C.Hannon@rl.ac.uk

HRPD

High Resolution Powder Diffraction
Richard Ibberson, ext. 5871,
R.M.Ibberson@rl.ac.uk

PEARL

Engineering & High Pressure Instrument
Mark Daymond, ext. 5434,
M.R.Daymond@rl.ac.uk,
Bill Marshall, ext. 5414,
W.G.Marshall@rl.ac.uk

ENGIN-X

Engineering Instrument
Mark Daymond ext. 5434,
M.R.Daymond@rl.ac.uk

DEVA

Muon Development Beam
James Lord, ext. 5674, J.S.Lord@rl.ac.uk

MuSR, EMU

Implanted Muon Spectroscopy
Stephen Cottrell, ext. 5352,
S.P.Cottrell@rl.ac.uk
Adrian Hillier, ext. 6001,
A.D.Hillier@rl.ac.uk
Francis Pratt, ext. 5135,
F.L.Pratt@rl.ac.uk

SANDALS

Small Angle Liquids & Amorphous Diffraction
Daniel Bowron, ext. 6397,
D.T.Bowron@rl.ac.uk

PRISMA

Coherent Excitations & Critical Scattering
Martyn Bull, ext. 5805,
M.J.Bull@rl.ac.uk

ROTAX

Multiple Purpose Diffractometer
Winfried Kockelmann, ext. 6731,
W.Kockelmann@rl.ac.uk

CRISP, SURF

Neutron Reflectometry
Sean Langridge, ext. 5269,
S.Langridge@rl.ac.uk
John Webster, ext. 6381,
J.R.P.Webster@rl.ac.uk

LOQ

Small Angle Scattering
Richard Heenan, ext. 6744
R.K.Heenan@rl.ac.uk

OSIRIS

Long Wavelength Diffractometer; Development of Polarisation Analysis
Mark Telling, ext. 5529,
M.Telling@rl.ac.uk

IRIS

Low Energy Spectroscopy; Long d-spacing Diffraction
Mark Adams, ext. 6157,
M.A.Adams@rl.ac.uk

POLARIS

High Intensity Powder Diffraction
Steve Hull, ext. 6628, S.Hull@rl.ac.uk

TOSCA

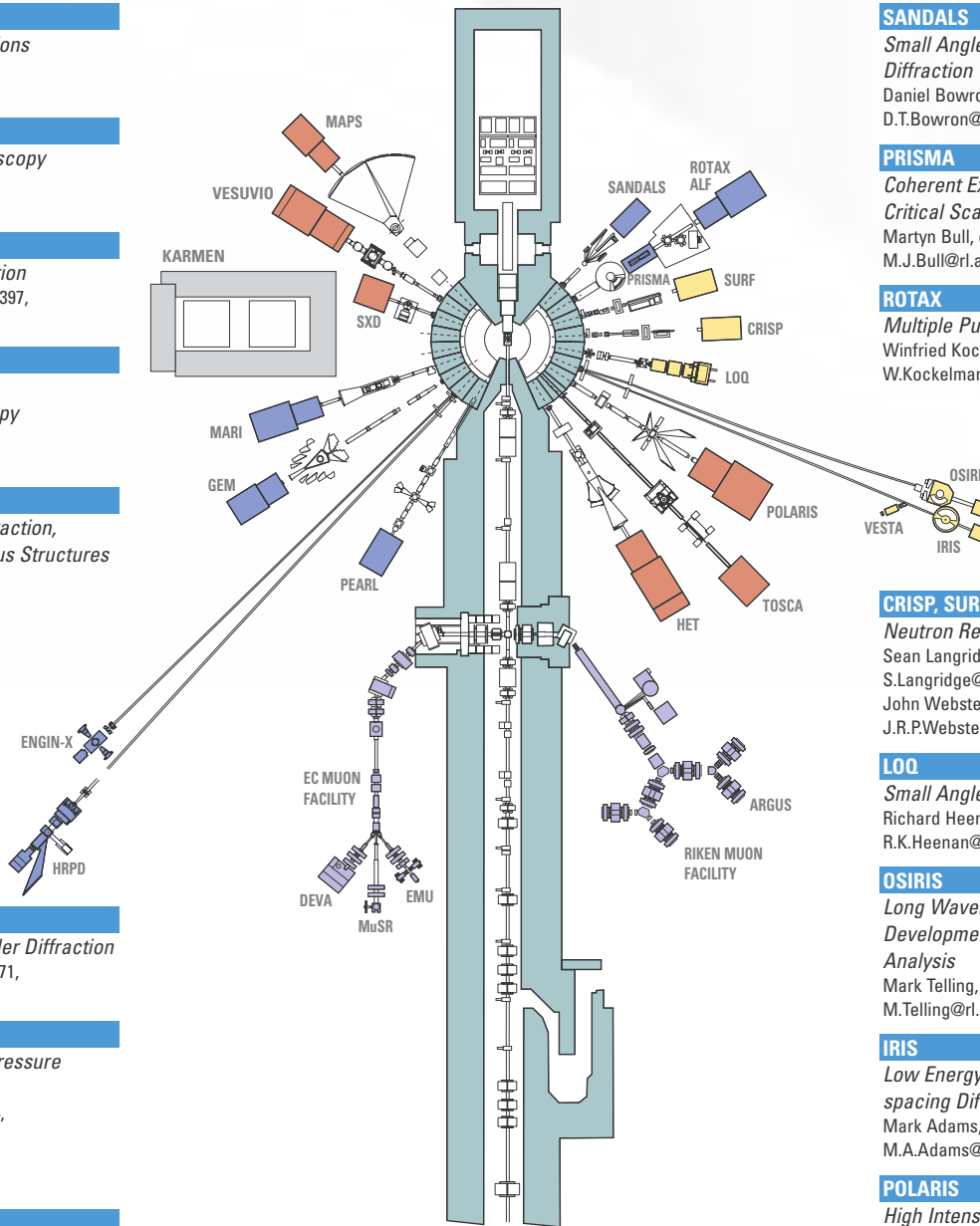
Molecular Spectroscopy & Crystal Fields
Stewart Parker, ext. 5797,
S.F.Parker@rl.ac.uk

HET

Excitations at Low Momentum Transfer
Rob Bewley, ext. 5797,
R.I.Bewley@rl.ac.uk

RIKEN

Surface & Decay Line Muon Facility
Katsu Ishida, ext. 6802, K.Ishida@rl.ac.uk



Moderators:

- Liquid Hydrogen, 20 K
- Liquid Methane, 100 K
- Water, 316 K

Crystallography

GEM • HRPD • POLARIS • SXD • HiPr/PEARL

The Crystallography instruments POLARIS, HRPD, GEM, HiPr/PEARL and SXD all operate busy user programmes. These straddle the areas of Chemistry, Materials, Physics and Earth Science, and offer a very diverse portfolio of structural science.



Fig. 1.2. Bas Van Aken, Anne Dros and Thomas Palstra (University of Groningen, The Netherlands), preparing a cryostat for their POLARIS experiment (01RC4019).

The high intensity powder diffractometer POLARIS continues to support vigorous programmes in various aspects of solid state chemistry, such as oxides, nitrides, chalcogenides and intercalates, and materials science, including ferroelectrics, battery materials and the area of novel metal hydride and nitride systems synthesised at high pressure, studied both on POLARIS and HRPD (see the Highlight on page 22). Among recent trends in the science have been studies of a wide range of defect and non-stoichiometric systems, particularly in the areas of ionic and superionic conductivity. The theme of complex sample environment, including chemical reactivity, continues to be strongly emphasised.

The high resolution powder diffractometer HRPD continues to provide a powerful tool for studies of phase transitions (see the Highlight on page 18), subtle structural effects in a range of materials including oxides, sulphides (see the Highlight on page 26), ionic conductors, dielectric ceramics and molecular systems. The new 90° bank has had a high impact on the programme in the areas of small molecular systems, magnetic diffraction and high pressure studies.

GEM offers rapid counting times coupled with high resolution, making studies of small

samples and rapid scanning diffraction routine, along with a large programme in magnetic diffraction. Total scattering (measuring and modelling Bragg and diffuse scattering together) continues to be prominent on GEM, and novel approaches to parametric diffraction enabled by the high count-rate are also being implemented. The wide range of materials science investigations include studies of manganites and novel spinel phases (see the Highlight on page 26), solid state chemistry applications including magnetic structures, and the use of small samples in isotope substitution experiments (see the Highlight on page 24). Time and temperature-resolved studies of, for example, battery electrode materials and NTE-related phases are also a significant theme, along with studies of disordered materials.

The high pressure user programme is principally carried out on the HiPr high pressure instrument on the PEARL beamline exploiting the Paris-Edinburgh cell, though some ambient temperature work in this cell is still carried out on POLARIS. Highlight areas include continuing studies of novel phases of small molecule systems, hydrogen bonded systems, increasingly complex mineral phases, studies of magnetic structures under pressure and increased exploitation of variable temperature and pressure investigations.

The programme on SXD, the single crystal diffractometer, covers both the study of molecular systems and areas such as diffuse scattering, quasicrystals and incommensurate structures. Capabilities in all of these have been substantially enhanced by the completion of the first phase of the instrument upgrade (see page 76). There has been an emphasis on the use of the new 5 kbar He pressure cell to allow for variable temperature/variable pressure studies of molecular systems, in particular in the study of hydrogen bonding. Supramolecular chemistry and crystal engineering, and the associated understanding of weak or unusual intermolecular interactions, also continue to feature strongly (see the Highlight on page 20).

Contact:

Chick Wilson
c.c.wilson@rl.ac.uk
01235 445137

Disordered Materials

GEM • SANDALS

The ISIS Disordered Materials Group provides the neutron scattering instruments GEM and SANDALS for characterising the atomic scale structure of liquids and disordered solids. In addition it supports a suite of data analysis programs and is developing novel techniques for the interpretation of neutron scattering data from disordered systems in terms of three-dimensional atomic models.

The nature of the order in a material is determined from whether or not crystalline Bragg peaks are present in its diffraction pattern. Radial distribution functions give a view of a material that is complementary to that of the crystal peaks. They portray the instantaneous correlations within a material, while Bragg peaks determine the average atomic positions. For a liquid or truly amorphous material the atoms can occur anywhere in the sample and so Bragg peaks are absent. An increasing number of ISIS proposals are investigating the nature of the order-disorder transition as materials go from being either liquid or amorphous to being crystalline.

Neutrons are complementary to X-rays for studying disordered materials because they are scattered strongly by important light atoms. In addition, in a number of cases it is possible to extract the individual site-site correlations from a diffraction pattern by the technique of isotope substitution, since different isotopes of some atoms have markedly different neutron scattering lengths.

SANDALS is used for most of the work on liquids owing to its large detector solid angle and fairly low scattering angles (below 40°) which help to minimise the effect of recoil distortion in the diffraction pattern. There have also been some excellent studies of amorphous solids as well on SANDALS, in cases where high real-space resolution was not required. A recent highlight has been the detailed study of amorphous ice in several different forms. In addition, the instrument is being increasingly used to study complex liquids, such as the imidazolium ionic liquids, mixed with other solvents like benzene. In this past year there was a pioneering study of an alanine peptide chain in water.

GEM, with its huge solid angle and broad range of scattering angles, is good for studying amorphous solids where maximum real space resolution is required. For example an interesting structural feature of vanadium tellurite glasses is the varying proportions of TeO_3 and TeO_4 units, depending on the composition. The high real-space resolution of GEM was most beneficial in revealing the detailed behaviour of the Te-O correlation. In addition, studies of the amorphous to crystalline (or liquid to crystalline) transition are becoming an important part of GEM's programme, owing to its excellent Q-resolution.

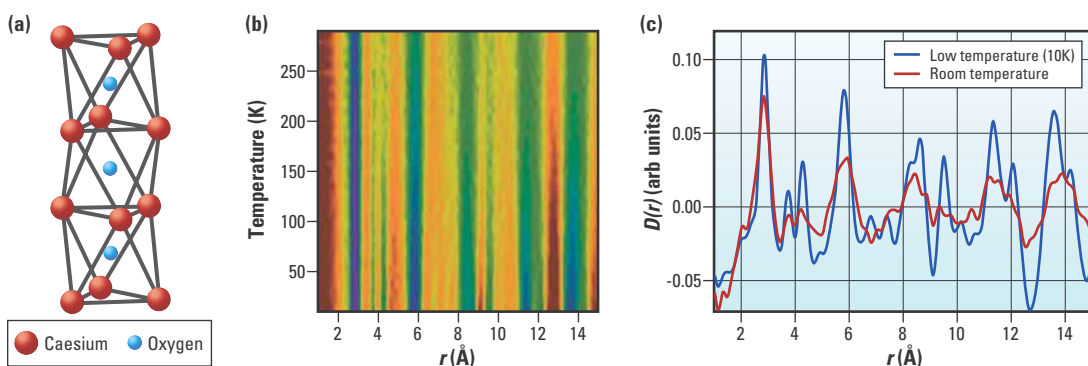


Fig. 1.3. The basic crystal structure of caesium suboxide (a), Cs_3O , has been known for many years. However, at room temperature the material is highly disordered. GEM was used to study the structure of $\text{Cs}_3\text{O}_{0.93}$ as a function of temperature from 10 K to 290 K to reveal the nature of the disorder in this material (b). Surprisingly a large amount of motion of the massive caesium atoms is found at room temperature, as shown by the decay of the features in the data as a function of temperature (b, c).

Contact:
Alan Soper
a.soper@rl.ac.uk
01235 445543

Large Scale Structures

LOQ • SURF • CRISP

Small Angle Neutron Scattering, SANS (LOQ) and Neutron Reflectivity (SURF, CRISP) are important techniques for the study of many of today's key scientific and technological materials, which are dominated by the nanometer to micron length scales. SANS probes meso-scale structures in the size range 20 to 1000 Å. Specular reflectivity provides structural information orthogonal to the surface or interface in the length scale range 10 to 4000 Å, and off-specular scattering probes in-plane structural correlations on the length scale of microns.

In both SANS and reflectivity there is a broad experimental programme in Soft Condensed Matter, Bio-materials and Materials Science, with an emphasis on the study of complex multi-component systems, sophisticated sample environments and kinetics.

In SANS a new 1.6 kBar pressure cell is now in routine use, to study aggregation in super-critical CO₂ at elevated temperatures (work of Holmes and Eastoe), and the new plate-plate rheometer being developed (Clarke, Higgins, King) will further extend the applications of SANS to aspects of polymer processing. Linked to the problems in processing concentrated mesophases, Penfold *et al* have demonstrated how Couette shear flow can be used to separate and identify the scattering from lamellar and micellar components in mixed di-chain cationic–nonionic surfactant mixtures. Measurements in the tangential scattering geometry show the scattering from a highly aligned lamellar phase in such concentrated dispersions; those in the radial scattering

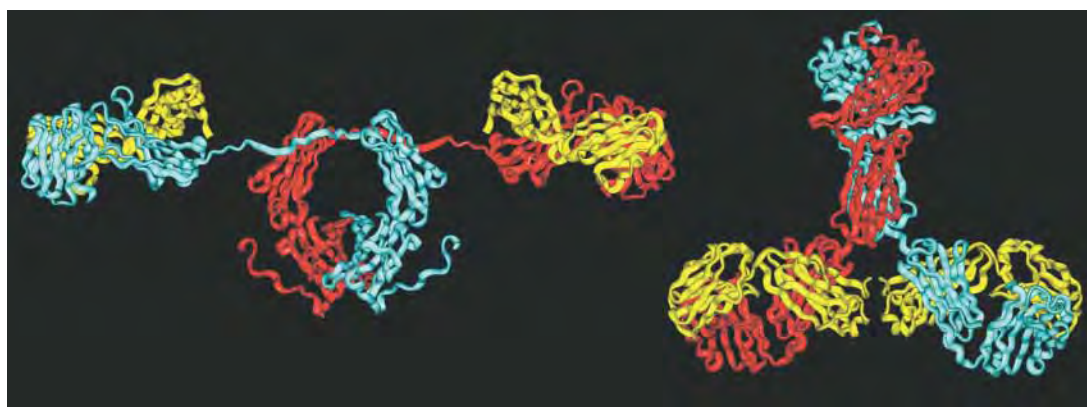
geometry reveal the micellar component which is in equilibrium with the lamellar phase.

Eastoe *et al* have demonstrated how the kinetics of light-induced transitions can be followed in photo-sensitive stilbene containing Gemini surfactants. Photo-induced dimerisation produces a vesicle to spherical micelle transition. Advanced modelling, using known fragment structures, and a combination of SANS and SAXS, provides the opportunity to study large macromolecular assemblies in solution, such as immunoglobulin (Fig. 1.4). The shorter hinge in the IgA2 compared to IgA1 may account for its unique immune role in plasma and mucosa.

In reflectometry the Highlight by Russel *et al* (see page 40) illustrates the use of complex environments and kinetics in the study of polymer-polymer inter-diffusion. Bucknall *et al* have extended *in situ* investigations in polymer films to measurement intervals as short as 20 seconds, enabling them to study plasticiser and solvent ingress. Fig. 1.5 shows the evolution of reflectivity as a function of time for the plasticiser dioctyl phthtalate diffusing into a deuterated poly-methylmethacrylate thin film. At early times the variation in film thickness (swelling) shows a linear dependence, consistent with case II diffusion.

The use of sophisticated sample environments is epitomised by the work of Bain and Eastoe on the measurement of

Fig 1.4.
The structures of human immunoglobulin, IgA1 and IgA2 (work in progress) determined by Perkins *et al*.



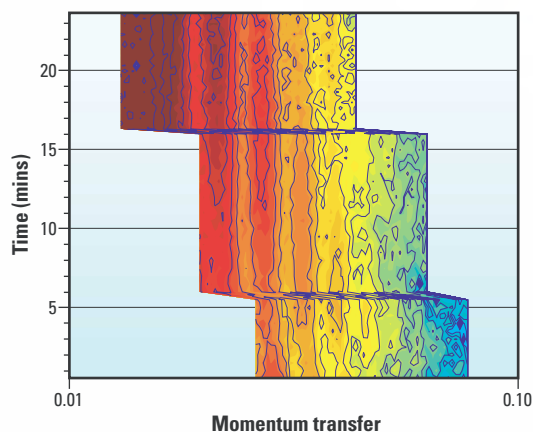


Fig. 1.5. Reflectivity as a function of time for the plasticiser dioctyl phthalate diffusing into a deuterated polymethylmethacrylate thin film.

dynamic surface excess on a flowing liquid surface. Measurements of the dynamic surface excess for C_{14} TAB and C_{18} TAB were compared with static values previously measured by neutron reflectivity, and are broadly consistent with theoretical expectations. This provides the essential input required to model the adsorption kinetics of surfactants. The work of Thomas *et al* on polymer-surfactant mixtures is an example of the powerful combination of reflectivity and contrast to study the adsorption and organisation of complex mixtures at interfaces. At low surfactant concentrations the surface layer consists of a monolayer containing both surfactant and polymer, whereas at higher concentrations ordered polymer-surfactant layers are formed below the surface layer. The neutron reflection measurements on this and a range of polyelectrolyte / surfactant mixtures have now provided the essential information to understand the surface behaviour and interpret the complex surface tension patterns that arise.

Glidle *et al* used neutron reflectivity to follow the temporal and spatial profile of the modification of electroactive polymeric interfaces *in situ* in an electrochemical cell. Electropolymerised films of the functionalised pyrrole, pentafluorophenyl-3-(pyrrol-1-yl)

propionate, were reacted with a solution phase nucleophile, ferrocene ethylamine. The *in situ* neutron reflection, in combination with XPS and FT-IR measurements, showed that the progress of the reaction within the polymer film is limited by the transport of reacting species in the dense region on the membrane that are further from the solution interface.

The polarised neutron mode of CRISP supports a growing and important programme in thin film magnetism (see the Highlight by Grundy *et al* on page 32). An important aspect of these studies is the increasing use of off-specular scattering. Fig. 1.6 shows spin parallel intensity for a Fe/Cr multilayer (Takeda *et al*), showing the anti-ferromagnetic and structural 'Bragg' peaks. The off-specular scattering, coincident with the AF peak, is allied with conformal interfacial roughness, and is closely associated with the magnitude of the GMR effect.

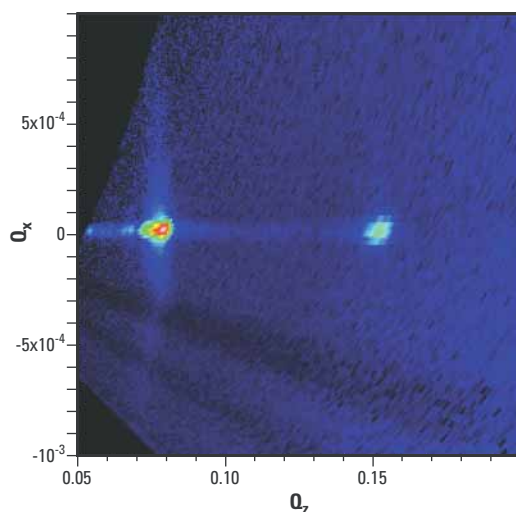


Fig. 1.6. Polarised neutron reflectivity data from a Fe/Cr multilayer.

Contact:

Jeff Penfold
j.penfold@rl.ac.uk
01235 445681

Excitations

MAPS • HET • MARI • PRISMA • ROTAX • ALF

The Excitations Group operates the three chopper spectrometers, HET, MARI and MAPS, the single crystal spectrometer PRISMA, the diffractometer ROTAX and the single crystal alignment facility ALF. The scientific programme of the group spans a wide range of disciplines from the investigation of model magnetic systems to the dynamics of disordered materials and quantum fluids.

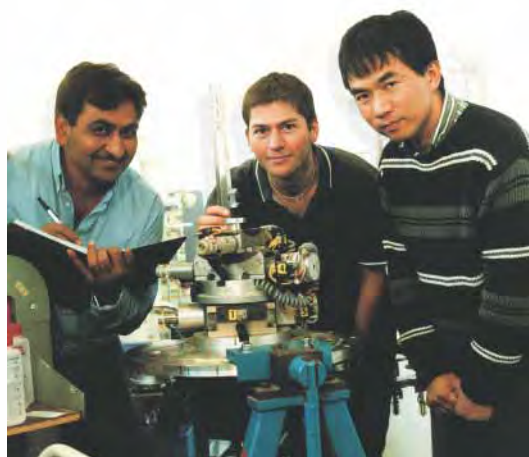


Fig. 1.7.
Penchang Dai (University of Tennessee, USA, right) with Rob Bewley (centre) and Adroja (ISIS) preparing their HET experiment (01RC4425).

In its diffraction mode, PRISMA is an ideal instrument for studies of weak magnetic moments and diffuse magnetic scattering owing to its exceptionally good signal-to-noise ratio, good Q -resolution and large Q -coverage. Recent examples include studies of short-range spin correlations in frustrated magnetic systems (spin ice), incommensurate magnetic order in a magnetic field in DyRu_2Si_2 , magnetic structures in PrSi , and the search for novel forms of order in URu_2Si_2 . This latter experiment showed just how good the signal-to-noise is on the instrument: the magnetic Bragg peaks associated with the very small moment of $0.03\mu_B/\text{U-ion}$ were easily seen. An increasing fraction of experiments on PRISMA are making use of its extreme sample environment capabilities, requiring combinations of milli-Kelvin temperature, high pressure, and high magnetic field, coupled with the need to rotate the crystal relative to the scattering vector.

The last year witnessed the development on MAPS of both the variety of the science studied and also its international appeal. In addition to well established programs in magnetism, in high temperature superconductors and transition metals, recent

experiments have also encompassed the itinerant ferrimagnet UGe_2 , incommensurate correlations in $\text{La}_{1.8}\text{Sr}_{0.2}\text{NiO}_4$, phonons in a high temperature superconductor and high-energy excitations (0.5 eV) in a 1D antiferromagnet.

MARI has as diverse a scientific programme as ever, including studies of sugars in solution, hydrogen on catalysts, nano-crystals, quasi-crystals, molecular magnets, and thermoelectric materials. The disordered materials programme is still strong and includes work on fragile glassy polymers as well as the start of a programme to extract partial density of states using isotopically enriched GeSe_2 . The large programme studying the effects of disorder and confinement on superfluidity continued with work on helium in vycor and SBA-15. On the magnetism front, studies have included systems close to a quantum critical point such as CeIn_3 and CePd_2Si_2 , the frustrated exchange system Pr_2NiO_4 , and spin exchange in high- T_c superconductors such as $\text{Pr}_{0.8}\text{LaCe}_{0.12}\text{CuO}_{4+y}$.

The majority of HET's single crystal experiments have now moved to MAPS, although this has not diminished the quality and range of experiments performed on the instrument. Recent studies have included 1D and 2D magnetic quantum systems as well as quantum critical behaviour, crystal fields, heavy fermion compounds, mixed valence, anisotropic Kondo systems, and compounds exhibiting coexisting magnetism and superconductivity. The instrument has also seen successful pressure experiments, together with novel biological studies of bone and antifreeze proteins.

ROTAX continues to run a diffraction programme that is primarily aimed at the German neutron user community, providing quick and informal access to a spallation source instrument. The programme is as diverse as ever, including the non-destructive testing of archaeological objects using neutron diffraction.

The design and detailed project planning for the MERLIN spectrometer is well underway now and more information can be found on page 80.

Contact:

Steve Bennington
s.m.bennington@rl.ac.uk
01235 445193

Molecular Spectroscopy

IRIS • OSIRIS • TOSCA • VESUVIO

The Molecular Spectroscopy Group operate four spectrometers: IRIS and OSIRIS enable investigation of biological and large scale chemical systems with very high energy resolution at very low energies; TOSCA provides good energy resolution over a wide energy range for chemical catalysis and materials studies; and VESUVIO offers modest energy resolution at the very highest energies for fundamental studies into quantum entangled states and Bose condensation.



Fig. 1.8.
Greg Chaboussant and
Andreas Sieber (Burn
University, Switzerland)
studying magnetic
excitations in mixed Mn (II,
III) clusters using IRIS
(01RC4030).

The use of IRIS for single-crystal magnetism studies continues to grow, with studies of magnetic materials in general now accounting for approximately half of the allocated beamtime. Amongst the other investigations, polymer dynamics and liquid helium confined in porous media continue to be of interest.

OSIRIS also operates as a diffractometer for measuring at long d-spacings with high resolution. Incident neutron wavelengths of up to 70 Å can be selected for measuring at d-spacings of up to 35 Å. Parametric studies are enhanced by the ability to adjust the chopper frequency to 'zoom in' on small regions in Q with a very high counting rate.

The science on TOSCA is as diverse as ever. Well-established programmes on hydrogen-bonded systems and catalysts continue to flourish. In the latter case, investigations have been extended to studies of the formation of cobalt-aluminium-phosphates. These materials exhibit many structural forms depending on the preparation conditions and particularly the choice of template molecule. Inelastic Neutron Scattering allows the study of the precursor solutions both with and without template. In addition, the template in the final product is also readily studied to give information about the interactions between the template and framework. The catalyst work has had a useful spin-off; the methodology developed to allow *in situ* adsorption of reactants on a catalyst can also be used to study the interaction of hydrogen with different forms of carbon ranging from single-walled nanotubes to high-surface area materials. These materials are potentially useful as hydrogen storage compounds.

Considerable attention has been devoted in recent years to the study of methane clathrate owing to its abundance and the problems of clogging of pipelines for the petroleum industry. Experiments on TOSCA show the effects of clathrate formation on the local structure of ice. Further studies are looking at how the presence of inhibitors effects the structure for methane clathrate and related materials.

A successful programme on the study of the simple quantum fluids, liquid and solid hydrogen has been extended to include mixtures of hydrogen with deuterium or neon and to studies at high pressure.

The old eVS beamline has undergone a major upgrade over the past year, with the installation of the EEC funded modifications, and was re-inaugurated as VESUVIO. These modifications will considerably improve the resolution for measurements at back scattering, particularly for studies of quantum fluids; further details can be found in Chapter 3.

Contact:

John Tomkinson
j.tomkinson@rl.ac.uk
01235 446686

Muons

EMU • MuSR • DEVA • RIKEN

The μ SR instruments MuSR, EMU, ARGUS and DEVA run a very diverse science programme, using implanted positive muons both as magnetic probes, in magnetism, superconductivity and charge transport, and as proton analogues in chemical physics, including investigations of hydrogen behaviour in semiconductors, molecular dynamics and light particle diffusion. Muon catalysed fusion studies and fundamental muon physics investigations are also carried out at the RIKEN-RAL muon facility.

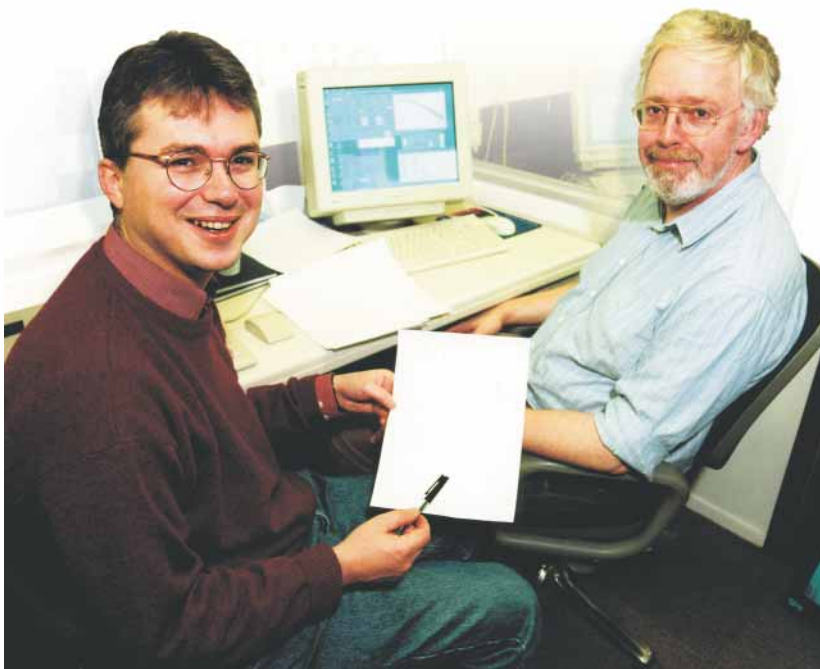


Fig. 1.9. Laurence Siebbeles and Dirk Visser (TU-Delft, The Netherlands) studying delayed muonium formation on MuSR (01RC4403).

Magnetism continues to be a strong area of application of the muon technique, making use of the special sensitivity of the muon to weak magnetic ordering and to short range correlations. Examples of magnetic systems studied this year include magnetically frustrated systems, spin ice, molecular magnetic clusters and spin-crossover systems. Orbital ordering and the dynamical Jahn-Teller effect are under investigation in several different systems, and various forms of magnetic carbon are now being studied.

In semiconductor research, the positive muon is used to mimic hydrogenic species. Shallow and deep level states have been identified in many semiconductors from the III-V and II-VI families, and attention is now being paid to state formation mechanisms and

to the energy barriers between the different states. Chemical physics studies this year have included high pressure phases of ice, muonium in hydrocarbons, hydrogen spillover in catalysts and muonium in powdered silica.

Investigating the diffusion of charged species in materials is another area of application for muons, and both ionic and electronic charge motion can be probed. Electron conduction studies have covered topics ranging from electron diffusion in condensed Kr to polaron diffusion in conducting polymers, discotic liquid crystals and DNA. Ionic conductor studies include Li battery materials, polymer electrolytes and proton conducting KHSO_4 .

Muons provide a powerful tool in the study of superconductors, particularly when investigating the interplay between magnetism and superconductivity and when studying the properties of superconducting vortices. The superconductor studies this year have included MgB_2 and MgCNi_3 , BETS-based molecular magnetic superconductors and studies of magnetic stripe phases in high- T_c systems.

Significant developments over the year at the RIKEN-RAL muon facility have included the first production of slow muons using the laser-ionisation method, and the completion of the construction of a fourth RIKEN experimental port which will be used initially for the study of muonic atoms. The research programme on muon catalysed fusion has succeeded in measuring the fusion cycling rate for a non-equilibrium D_2+T_2 liquid target and in determining the conversion rate from non-equilibrium D_2+T_2 to equilibrium $\text{D}_2+2\text{DT}+\text{T}_2$. Condensed matter studies using the ARGUS spectrometer have included observations of the non-magnetic impurity effect on the dynamical stripes in the LSCO high- T_c superconducting oxides, novel magnetism in electron-doped zeolite compounds and electron transport in double-stranded DNA.

Contact:

Philip King
p.j.c.king@rl.ac.uk
01235 446117

Engineering

ENGIN • ENGIN-X

Engineering measurements are based on Bragg diffraction, yielding information on the distortion of the atomic lattice, typically as a function of position, or applied thermal and / or mechanical loads. This information is used to shed light on deformation mechanisms, processing and manufacturing routes, and failure mechanisms in real components and test samples.

This year has seen the ISIS Engineering team continuing to provide scientific support on the existing engineering beamline, ENGIN, for a wide-ranging user program. Experiments undertaken have again involved users from a wide research base within Materials Science, Engineering and Geology.

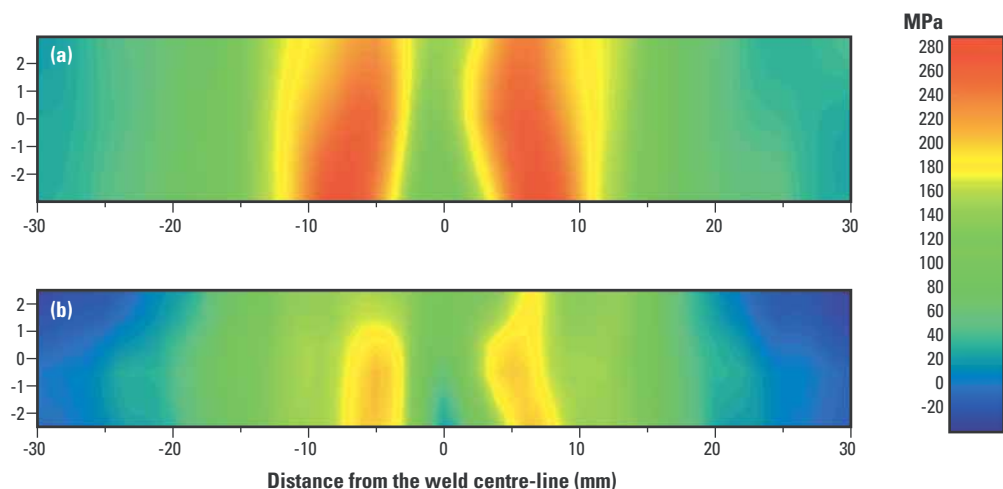
Successful engineering investigations in the past year have considered two basic areas. First, studies of fundamental material behaviour including investigations of basic deformation mechanisms in metals, as well as phase transformation studies in shape memory alloys and domain flip during loading of ferroelectrics (see the Highlight on page 66). Secondly, several experiments have focused on producing strain or stress maps as a function of position in components, often to provide data for the verification of finite element modelling predictions of engineering processes or for comparison with other methods of residual stress measurement. The

processes investigated have included forging of nickel based superalloys and novel 'low temperature' welding techniques such as Friction Stir Welding and Inertia Welding.

For example, a team of experimenters from the Open University has been investigating the residual stresses in 7150 alloy components which have undergone Metal Inert Gas (MIG) welding. This technique is currently being considered as a cost-effective alternative to mechanical fastening for aircraft metallic structures and components. During a series of experiments they have examined the effect of machining to typical finished size on the stress distribution in candidate welds. Fig. 1.10 shows the longitudinal residual stresses before and after machining. It can be seen that machining produces considerable stress relief in the most highly stressed areas, which correspond to the weld heat affected zone.

This year also see the long awaited construction of ENGIN-X (see Instrument Developments, page 79) which will greatly expand the capabilities of the engineering programme at ISIS when the user programme is transferred from PEARL (ENGIN) in early 2003.

Fig. 1.10.
The longitudinal residual stresses in the 7150 weld (a) before and (b) after machining to size.



Contact:

Mark Daymond
m.r.daymond@rl.ac.uk
01235 445414

Data Analysis

The Data Analysis and Visualisation Group develops algorithms and software in a number of areas that impact upon science performed at ISIS, especially in the area of powder diffraction.

The Data Analysis Group, in close collaboration with Professor Bill David, has continued to innovate in the area of analysis of powder diffraction data, both from a structure determination and a structure refinement perspective. The ISIX project, which aims to produce an object oriented Rietveld analysis package for the refinement of neutron and X-ray diffraction data, has continued to develop at the level of base classes. Developing collaborations with authors working towards similar aims should encourage the re-use of lower level routines and thus allow for development of the higher level ones needed to adapt the code to the requirement of ISIS powder diffraction instruments.

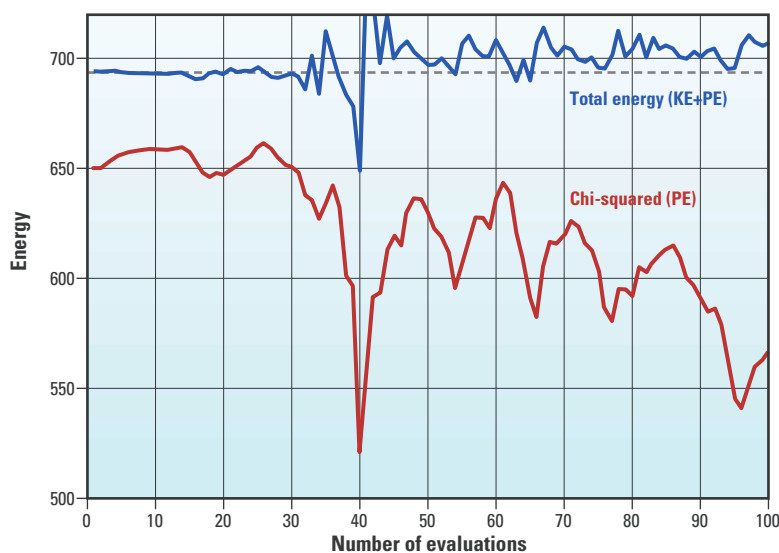


Fig. 1.11. The potential energy and total energy (kinetic energy plus potential energy) evaluated over a single MD trajectory during the crystal structure solution of capsaicin from powder diffraction data by the HMC method. The initial total energy is shown as a dotted line in order to highlight the total energy fluctuations arising from the finite MD step size.

In the area of structure determination, highlights have included a new release of the DASH software package, the development of a maximum likelihood approach, and the implementation of a hybrid Monte-Carlo

global search method. This latter technique, originally developed for large-scale simulations, combines the best features of molecular dynamics and Monte-Carlo methods in a single algorithm, and has proven to be a fast and efficient way of searching space in a structure determination context (Fig. 1.11). More recently, a framework for the problem of utilising solid-state NMR-derived conformational information in structure determination has also been developed. Also in the area of crystallography, a combination of Bayesian methods and maximum entropy phase extension has proven to be particularly powerful in elucidating subtle structural details that would otherwise be missed (see the Highlight on page 68). Outside this area, work has been undertaken in the analysis of reflectivity data, the analysis of muon data, and the extraction of weak intensity features from neutron detectors.

The Group also acts as the point-of-contact for the development of e-Science projects within ISIS. Working closely with the CLRC e-Science centre, two projects have been identified: first, work is beginning on designing efficient ways of capturing, tagging and registering ISIS data with the CLRC Data Portal. The Data Portal will allow users to search, explore and retrieve data sets with ease, whichever CLRC facility was their source. Secondly, work has begun on a technological solution to the problem of interacting with multidimensional data collected from the MAPS instrument. Critical to realising the potential of this instrument is the ability to explore the experimental data rapidly and the proposed solution will achieve this using modern computing methodologies. However, the emphasis is firmly on allowing users to utilise the improved data processing whether they are conducting an experiment or analysing it off-line.

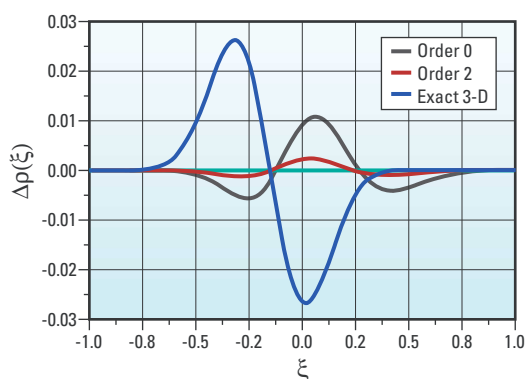
Contact:
Kenneth Shankland
k.shankland@rl.ac.uk
01235 446381

Theory

The Theory Division support experimental work using neutrons, muons and X-rays, developing models to explain experimental results and propose new experimental work.

A new class of magnetic peaks in the neutron diffraction pattern of V_2O_3 has been predicted on the basis of a successful interpretation of resonant X-ray diffraction data. The space-group forbidden reflections are created by the V octupole moment. Using a V wavefunction, inferred from X-ray data, the intensity of the octupole reflections is estimated to be three orders of magnitude smaller than the strongest reflection created by the V magnetic moment. An observation of the octupole reflections by neutron diffraction will confirm a radical development in our understanding of the wealth of fascinating properties displayed by an archetypal Mott-Hubbard insulator.

Fig. 1.12. Results for the ground state of the water molecule. Density differences from the full SCF or Hartree solution (green line), for the optimal coordinate that is very close to the bending normal mode, in the cases: full BO result (exact 3-D, blue line), second, (red), and zero-order, (black). The comparison of the results for the other two normal modes (breathing and asymmetric stretching) is even better.



One of the most interesting experiments reported in the resurgence of work on rare-earth hexaborides is the observation of Bragg reflections from CeB_6 held at a low temperature (<3.2 K) that are forbidden with the Cs Cl-type structure established at room temperature. The observations, using nonresonant (Thomson) and resonant X-ray Bragg diffraction, are a direct confirmation that Ce ions in the low temperature phase II of CeB_6 occupy sites with a low spatial symmetry. It has been shown that all the X-ray data can be interpreted by assuming that CeB_6 adopts a structure consistent with Fmmm with Ce ions at sites 8(f) and a point-group symmetry 222 (D_2). In particular, the

distorted structure supports a motif of Ce quadrupoles which transform according to the Γ_3 representation. This finding ties in with data obtained for the Ce crystal field states by using neutron-beam spectroscopy.

Electronic structure calculations within Density Functional Theory (DFT) are normally carried out in the clamped nuclei (classical nuclei) approximation. While this approach is realistic for many systems of interest, the quantum mechanical treatment of nuclear degrees of freedom is still desirable in a wide variety of situations. These range from molecules and molecular clusters involving light-mass atoms, like H or first-row elements, to liquids like water, and to solids like hydrogen and hydrogen-bonded molecular crystals.

Even within the usual Born-Oppenheimer (BO) separation of nuclear and electronic degrees of freedom, the problem remains formidable. In order to appreciate the complexity, consider a molecule with N atoms. The number of spatial degrees of freedom of the nuclei is $3N$, which reduces to $3N-6$ after separating the centre of mass translation and the rigid rotations of the molecule. For a tetratomic molecule this means 6 variables. In order to plot the Potential Energy Surface, allocating, e.g. 100 points to each internal degree of freedom, one would need 100^6 points, i.e., in an *ab initio* scheme, one would have to perform a trillion electronic ground state energy calculations for the various nuclear configurations!

We have developed a fast and efficient method, based on approximating the nuclear wavefunction with a self-consistent-field (SCF) or Hartree-product wavefunction. The ‘orbitals’ and the set of collective nuclear coordinates are both optimally chosen to minimize the expectation value of the nuclear Hamiltonian with respect to the product ansatz wavefunction. The new method allows substantial reduction of the computational cost from 100^{3N-6} to $100 \times (3N-6)$ (zero-order), or $3 \times 100 \times (3N-6)$ (second order) with a very small compromise in accuracy, as tests on triatomic molecules show (Fig. 1.12).

Contact:

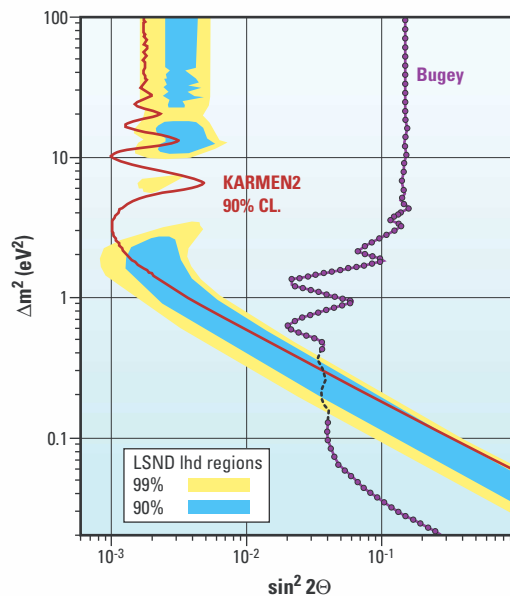
Stephen Lovesey
s.lovesey@rl.ac.uk
01235 446359

KARMEN

ISIS provides the world's most intense pulsed source of low energy neutrinos from the decays of pions and muons produced by the 800 MeV proton beam in the spallation target. The KARMEN (Karlsruhe Rutherford Medium Energy) Experiment has exploited the unique features of this neutrino source to investigate the interactions of neutrinos with nuclei and to search for neutrino oscillations.

Having successfully completed more than 10 years of measurements in March 2001, the KARMEN experiment has been dismantled almost completely over the last year. At the same time, the careful analysis of the entire neutrino data taken has continued and several final experimental results have been published.

Fig. 1.13.
Comparison of the exclusion curves (90% confidence limit) of the KARMEN experiment (1997-2001) and the Bugey reactor experiment with the oscillation parameter region favoured by the LSND experiment.



The measurements of KARMEN have an impact on two key areas of astroparticle physics. First, the investigation of neutrino-nucleus interactions in the energy range up to 50 MeV adds to a better understanding of the important role of neutrinos in core-collapse supernovae, in particular to open problems in neutrino-induced element synthesis. Secondly, the search for neutrino oscillations at short baseline can answer the question of whether neutrinos do have a cosmologically significant mass and act as Hot Dark Matter in the evolution of large-scale structures in the universe.

The KARMEN data analysis focuses on the search for flavour oscillations between muon anti-neutrinos and electron anti-neutrinos. The appearance of electron anti-neutrinos, which are not produced at ISIS, at a distance of 17.6 m from the spallation target would be a strong hint for neutrino oscillations with short baseline, as claimed in 1995 by the LSND experiment at Los Alamos. A genuine *short-baseline* oscillation signal, in addition to the well-established oscillation signals from solar and atmospheric neutrinos at much larger baseline, would require the introduction of *sterile* neutrinos, which do not interact with ordinary matter. For these reasons, a thorough test of the LSND results is very important. The most sensitive test of LSND so far is based on the high-quality KARMEN measurements from 1997-2001.

A signal of neutrino oscillations would be the detection of inverse beta-decay reactions on the free protons of the 56 tonne liquid scintillation calorimeter. Following various software cuts on the 3.7×10^9 events of the raw data, 15 oscillation candidates survive the most stringent selection criteria, compared with the background expectation of 15.8 ± 0.5 events, resulting mostly from conventional neutrino interactions. A more detailed spectral analysis shows no hint of oscillation events in the data, and the resulting upper limit on the ν -oscillation probability $P < 0.85 \times 10^{-3}$ contradicts the LSND signal of $P = 2.64 \pm 0.67 \times 10^{-3}$. The corresponding exclusion plot (Fig. 1.13) for the oscillation parameters $\sin^2 2\theta$ (mixing angle) and Δm^2 (squared mass difference) rules out the high Δm^2 region of LSND and only leaves a narrow range of oscillation parameters at small values ($\Delta m^2 < 1 \text{ eV}^2$), which is statistically compatible with both experiments.

With this clear and unequivocal oscillation result the KARMEN experiment has fulfilled its central mission and established the most stringent oscillation limit so far in this important oscillation mode.

Tom Lancaster and Steve Blundell (Oxford) filling the MuSR cryostat during investigations of organic superconductivity (02EC3162).



Pascal Manuel (Leeds) with his GEM sample holder containing amorphous Y_7Fe_3 (01RC4037).



Peter Georgiev, Jian Liu and Manuchehr Babaei-pour (Salford) analysing their OSIRIS data during an in situ study of battery electrode materials (01RC3990).



Pavel Alekseev (Kurchatov Institute, Russia) preparing his sample of $Yb_{0.1}Lu_{0.9}B_{12}$ for HET investigations (01RC3974).



Audrey Dupont (Bristol) and Sam Foster (ISIS) cleaning the LOQ pressure cell (01RC3981).

ISIS Scheduling Panel Meetings

These are held every June and December, in order for panels of external, international experts to review the experimental proposals that have been submitted to the facility.

David Timms (Portsmouth) and Ralph Simmons (Illinois) (02RC2539).



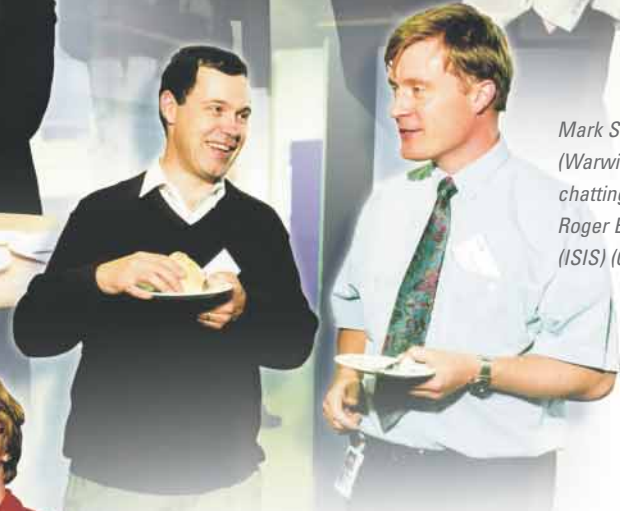
Brian Rainford (Southampton, left), Bob Cywinski (Leeds, centre) and Mike Johnson (Director, RAL Instrumentation Department) (02RC2563).



Nigel Clarke (Durham, left) and Fredrik Tibergh (Oxford) (02RC2541).



Mark Smith (Warwick) chatting with Roger Eccleston (ISIS) (02RC2535).



Albero Albinati (Milan, left) and Marco Zoppi (IFAC-CNR, Italy, centre), discussing ISIS science with Uschi Steigenberger (ISIS) (02RC2547).

The meetings are held together by Paula Woods, Emma Young and Katie Hoggood from the ISIS User Office (02RC2545).



Highlights of ISIS Science

The advanced facilities provided by ISIS enable world-class research to be performed by scientists from around the world, together with facility staff. Academic and industrial applications of the intense neutron and muon beams encompass Physics, Chemistry, Biology, Materials Science, Engineering and Earth Science. The quality and variety of ISIS science is demonstrated by this selection of research summaries.

2

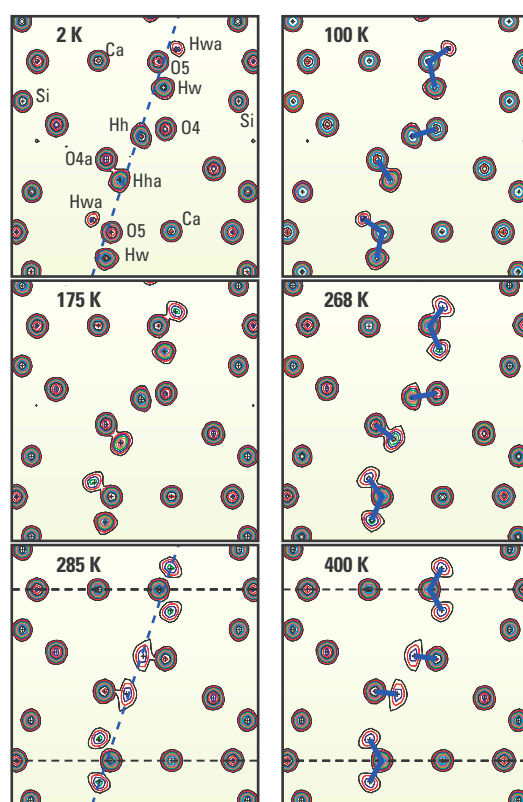
Structural phase transitions in minerals at low temperatures

MA Carpenter, H-W Meyer (University of Cambridge), KS Knight (ISIS), P Sondergeld (University of Vienna), S Marion (University of Oslo).

Almost any structural change that occurs within a crystal is usually accompanied by a change in lattice parameters. Neutron diffraction using HRPD permits such changes to be determined to high precision and hence yields detailed insights into the mechanisms and thermodynamic character of phase transitions. The mineral lawsonite ($\text{CaAl}_2\text{Si}_2\text{O}_7(\text{OH})_2\cdot\text{H}_2\text{O}$) is representative of a large group of materials in which structural phase transitions occur as a consequence of, or associated with, changes in hydrogen bonding. It has been of interest in a broader geological context because of its roles as an indicator of high pressure, low temperature metamorphism and as a contributor to the water budget at subduction zones in the Earth's crust.

The stability of lawsonite below room temperature has attracted considerable attention since the recent discovery of structural instabilities at ~ 120 K and ~ 271 K. Both transitions involve some combination of proton ordering and framework distortion, while the lower temperature transition is a rare example, among minerals, of a proper ferroelectric transition. Two types of experiment have been undertaken on HRPD at ISIS to shed some light on their driving

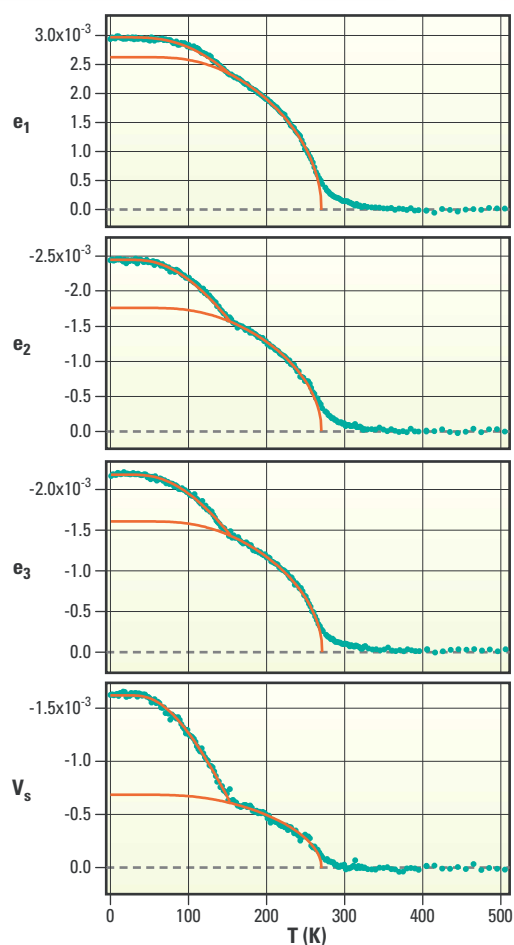
Fig. H1.1. Fourier maps of a section of the lawsonite structure at different temperatures. Inclined dashed lines are shown to draw attention to chains of O–D...O–D sequences through channels in the structure. Individual O–D bonds are indicated by solid lines in some of the diagrams. Horizontal dashed lines represent mirror planes in the $Cmcm$ structure.



mechanisms. Long runs (180 $\mu\text{A}\cdot\text{Hr}$) gave powder diffraction patterns suitable for full Rietveld refinement of the crystal structure at specific temperatures in the stability fields of each structure (space groups $Cmcm$, $Pm\bar{c}n$ and $P2_1cn$). Much shorter runs (7.5 $\mu\text{A}\cdot\text{Hr}$) at many temperatures between 1.6 K and 505 K gave diffraction patterns suitable for the refinement of lattice parameters. Hydrogen atoms in the natural sample were replaced by deuterium atoms, by exchange from D_2O vapour at 425 °C, in order to improve the visibility of proton sites in the structure.

Fig. H1.1 shows Fourier maps (F_{obs}) of a section through the lawsonite structure that contains the crystallographic sites for the D_2O and D–O components. At 400 K ($Cmcm$ structure), there is a horizontal mirror plane (dashed lines) and a mirror plane within the plane of the diagram. At 268 K and 175 K ($Pm\bar{c}n$ structure), the horizontal mirror is lost due to rotation of the D_2O molecules. At 100 K and 2 K ($P2_1cn$ structure), the mirror in the plane of the diagram is lost by out-of-plane tilting of the D_2O molecules. The symmetry breaking mechanism of the two phase transitions appears to involve, primarily, the positions of the D (or H) atoms in the structure, but oxygen atoms of the silicate framework were also found to move significantly from their high symmetry positions.

Spontaneous strains derived from the lattice parameter data are more informative than the lattice parameters themselves. This is because they can be interpreted directly in terms of thermodynamic changes which accompany the phase transitions. In particular, strains parallel to the crystallographic a , b and c -axes (e_1 , e_2 and e_3 , respectively) are expected to vary with the order parameter, Q , as $e \propto Q^2$. Here Q is a measure of the extent of transformation from the high symmetry parent structure. Lines through the data in Fig. H1.2 represent solutions derived from Landau theory for the evolution of the order parameter associated with each transition.



They show the $Cmcm \leftrightarrow Pm\bar{c}n$ transition as being tricritical in character, and the $Pm\bar{c}n \leftrightarrow P2_1cn$ transition as being second order. There is a distinct tail in each of the strains above 271 K, suggestive of dynamical or short range ordering effects ahead of the $Cmcm \leftrightarrow Pm\bar{c}n$ transition, but, otherwise the strain data are superficially consistent with a simple Landau expansion containing one driving order parameter. The exceptionally high resolution of the strain data reveal an additional anomaly at ~ 250 K, which is not consistent with the evolution of a single order parameter, however. It appears that both proton ordering and a structural distortion are important in the 271 K transition.

There are other materials in which phase transitions occur and in which the principal driving mechanism might be proton ordering.

Perhaps the best known of these is KH_2PO_4 (KDP). The general question is: to what extent does proton ordering provide the driving mechanism as opposed to some lattice distortion (soft mode) to which the proton ordering is coupled? This issue can be addressed by comparing the behaviour of samples which have either H or D atoms in an otherwise unchanged structure. For the case of lawsonite, there are dilatation data for natural (hydrogenated) samples against which the new strain data can be contrasted. Replacing H by D causes the low temperature transition point to be increased by ~ 27 K (Fig. H1.3), and the anomaly in the strain evolution of the $Pm\bar{c}n$ structure to increase from ~ 225 K to ~ 250 K. This type of change would be expected if the role of H/D is dominant. The transition temperature for the 271 K transition remains the same within experimental error, however. This implies that proton ordering is not the dominant symmetry breaking process in this transition; a displacive component provides the initial symmetry breaking mechanism, with structural changes which are more dependent on the behaviour of H or D developing ~ 20 – 50 K later. A more complete description of these phase transitions is being achieved by combining the neutron diffraction data with data for the heat capacity, elastic constants and dielectric properties of lawsonite.

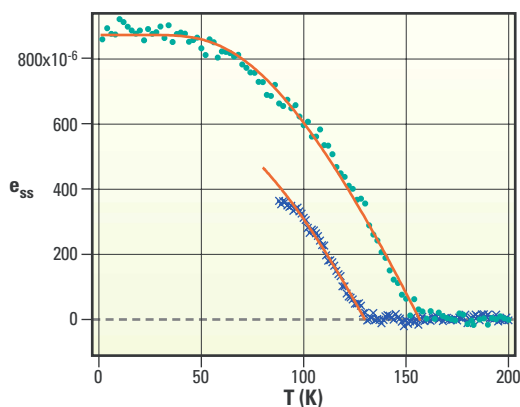


Fig. H1.2.

Spontaneous strains extracted from lattice parameter data, where $e_1 = (a-a_0)/a_0$, $e_2 = (b-b_0)/b_0$, $e_3 = (c-c_0)/c_0$, $V_s = (V-V_0)/V_0$; a , b , c , and V are lattice parameters of the $Pm\bar{c}n$ and $P2_1cn$ structures, a_0 , b_0 , c_0 , V_0 are parameters of the $Cmcm$ structure extrapolated into the stability fields of the $Pm\bar{c}n$ and $P2_1cn$ structures. Curves through the data are solutions to a Landau free energy expansion for each phase transition.

Fig. H1.3.

Variation of the total (scalar) strain for the $Pm\bar{c}n \leftrightarrow P2_1cn$ transition. The transition point (where e_{ss} goes to zero) of the natural hydrogenated sample is ~ 27 K below that of the deuterated sample, implying that the behaviour of the H/D atoms has a large and, perhaps, dominant influence on the transition.

An unusual molecular glue - unconventional di-hydrogen bonds in boraneamines

JAK Howard, AE Goeta (Durham University), M Thornton-Pett (Leeds University), CC Wilson (ISIS)

There has been increasing interest in unconventional hydrogen bonds in recent years. One of the most unconventional of these is the so-called dihydrogen bond. These 'bonds' have the feature that either B-H or M-H (B=boron, M=transition metal) σ bonds are apparently acting as hydrogen-bond acceptors towards proton donors such as O-H and N-H.

Boraneamines are a good example of compounds which tend to have these close B-H δ^- ... δ^+ H-N contacts. The compound 2-amino-4-methylpyridine borane has been fully characterised using SXD, shedding light on the four possible B-H...H-N contacts (1 intramolecular and 3 intermolecular), to help us understand this highly novel bonding and the influence it has on supramolecular architectures.

In addition to the intrinsic interest of these novel interactions, the BH_3 adducts of substituted pyridine molecules are also viewed as possible model systems for the more complex 6,9-disubstituted 'diadducts' of nido-decarborane, which themselves show potential as ceramic precursors – for example in BN or BCN layered ceramics. With an eye on crystal engineering for such favourable physical properties, it is vital to quantify if unconventional interactions can play a significant role in governing crystal packing and overall molecular self-association in the solid state, and hence lead to macroscopic properties. Despite the interest in these materials, to our knowledge only one such

compound, BH_3NH_3 , has been characterised previously using neutron diffraction. Our accurate SXD study of 2-amino-4-methylpyridine borane therefore represents a significant contribution in this area.

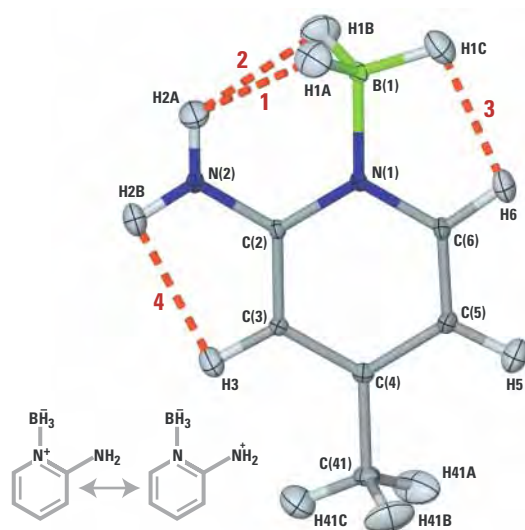
The molecular geometry is summarised in Fig. H2.1. The amino nitrogen atom, N(2), is sp^2 hybridised. The positive charge associated with the nitrogen atom of the B \rightarrow N adduct bond (Fig. H2.1, schematic diagram, left) is therefore somewhat delocalised onto the amino nitrogen atom (schematic diagram, right). Consequently, the C(2)-N(2) distance is comparable with the ring C-N bonds and the B-H bond lengths are significantly longer than both C-H and N-H. The B-H bond lengths are comparable with those determined for the neutron structure of NH_3BH_3 (average 1.17 Å).

There are several potentially significant intramolecular non-bonded contacts, as indicated by the dashed red lines in Fig. H2.1. Even though the molecular geometry imposes constraints on these intramolecular contacts, there are several points worthy of note. Firstly, the amino hydrogen atom H(2a) is asymmetrically positioned between H(1a) and H(1b), a possible consequence of the close approach of H(1c) to H(6) (contact 3), which may lead to a small rotation about the B-N bond. The important factor in terms of hydrogen bonded networking is that these intramolecular contacts effectively block potential sites for intermolecular hydrogen bonds. There are clearly more acceptor hydrogen atom sites (on boron based hydrogen atoms) than there are donor sites (on nitrogen-based hydrogen sites). On this basis one would not expect a three-dimensional H...H network and this is indeed what is observed.

Examining the intermolecular dihydrogen-based contacts, a simple way of visualising the packing of this molecule is provided by a three-stage *aufbau* principle based on Kitaigorodskii's premise that all molecules attempt to close-pack in the

Fig. H2.1.

Molecular geometry of 2-amino-4-methylpyridine borane, as determined from SXD neutron diffraction data. The dashed red lines indicate intramolecular H...H contacts.



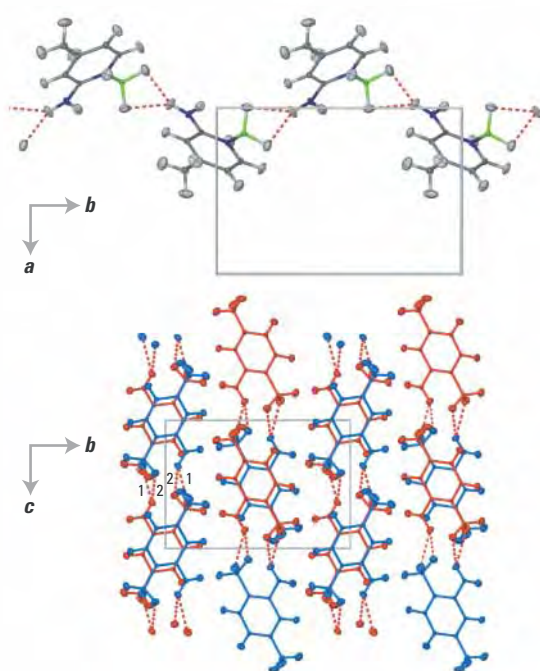


Fig. H2.2. Intermolecular H...H contacts, forming chains of molecules (upper) and further intermolecular H...H contacts involving the formation of dimeric units (lower).

crystalline state. The space group is $P21/c$ and the first stage involves generating a chain structure by successively applying a 2_1 screw operation (Fig. H2.2, upper). It can be clearly seen that bifurcated dihydrogen bonds propagate along the chain, although these contacts are towards the longer end of the observed range for such bonds. However, the contact angular parameters are typical, with N-H...H reminiscent of conventional hydrogen bonds (tending towards linear) whilst the B-H...H angles approach 90° , as this leads to the most favourable alignment of bond dipoles.

The next stage in generating the crystal packing in this material, vital to the underlying aims of crystal engineering, is to generate a sheet structure by applying successive c -glide operations to the chain, as shown in the lower half of Fig. H2.2. It can be seen that pairs of inversion-related bifurcated dihydrogen contacts are generated between chains (one

pair has been labelled), reminiscent of the familiar carboxylic acid dimer. The chains stack on top of each other to give a two molecule thick 'sheet'. The sheet structures then stack on top of one another to form the overall packing motifs in the structure (Fig. H2.3).

In summary, from the SXD structural study we have determined several significant contacts in accordance with the characteristics expected for this kind of dihydrogen bond; i.e. $d_{\text{HH}} < 2.2 \text{ \AA}$, N-H...H within 150° - 170° and B-H...H within 95° - 115° . Further characterisation of these interactions will follow once we complete complementary charge density refinements. Yet it is already clear that these contacts play a key role in determining the packing of molecules into the crystal structure. The use of weak or unconventional hydrogen bonds in this way offers another potential 'molecular glue' to chemists involved in the expanding areas of molecular design, supramolecular chemistry and crystal engineering.

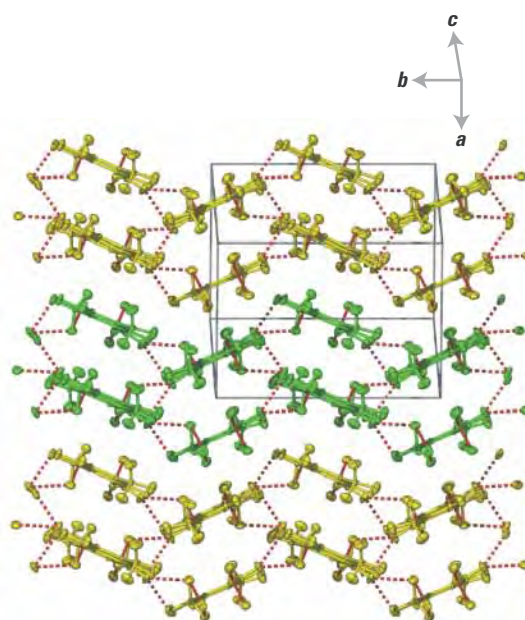


Fig. H2.3. Stacking of the sheets to form the overall packing motif.

Location of hydrogen in ternary transition metal hydrides

G Auffermann (MPI CPfS Dresden), W Bronger (TH Aachen), RM Ibberson, S Hull (ISIS)

Ternary transition metal hydrides are a comparatively new class of solid state compounds, the first and, for a long period, the only fully characterised example of which was K_2ReH_9 . The 1980's saw a marked increase of interest in these materials due to their potential technological use in hydrogen storage applications. However, syntheses by solid state reactions invariably result only in powder samples. Progress in the structural chemistry of the new metal hydrides has therefore been closely connected with the development of high intensity or high resolution powder diffractometers such as POLARIS and HRPD, respectively, and the progressive optimisation of the computer analysis process.

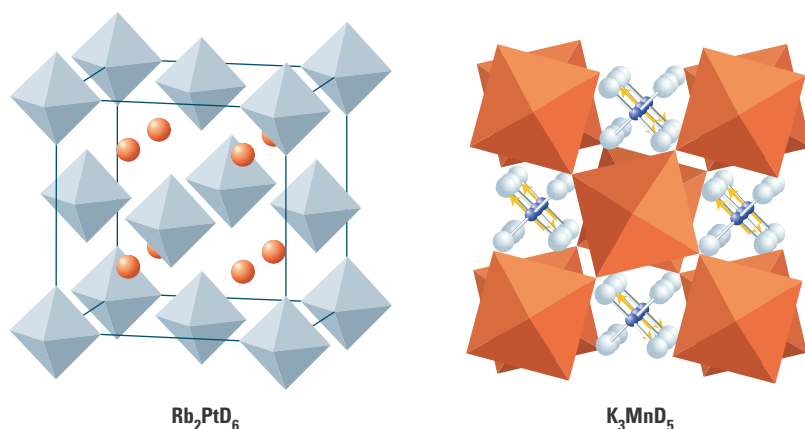


Fig. H3.1.
The crystal structures of Rb_2PtD_6 (left) and K_3MnD_5 (right), the latter also showing the ordered spin structure observed for $T < 28$ K.

Ternary metal hydrides of the general formula $A_xM_yH_z$ – where A is either an alkali metal or an alkaline earth metal and M a transition metal – can be synthesised by the reaction of a mixture of a binary alkali or alkaline earth metal hydride and the transition metal in an atmosphere of hydrogen at temperatures ranging from 500 K to 800 K. Over the past decade, the development of high pressure equipment permitting the use of hydrogen pressures up to 6000 bar has made possible the synthesis of hydrogen-rich compounds containing transition metals in a relatively high oxidation state. Previously, it was only possible to prepare hydrides containing transition metals from subgroup eight in low oxidation states.

In the alkali metal-platinum-hydrogen system the new high pressure synthesis method led to the colourless hydrides Rb_2PtD_6 and Cs_2PtD_6 – formerly we only obtained Rb_2PtD_4 or Cs_2PtD_4 . X-ray investigations showed the

atomic arrangement of the metal atoms, which was confirmed by subsequent neutron diffraction studies on the deuterated compounds. The latter also identified the deuterium atom positions, resulting in a full structure determination and showing that all four structures belong to the K_2PtCl_6 structure type (Fig. H3.1, left). In the two deuterium-rich compounds, which were intensively studied on POLARIS, the vertices of the octahedra are completely occupied. In the low pressure modification only a statistical 2/3 occupation of the octahedral positions was observed. The analysis of the neutron diffraction data revealed clearly the stoichiometric composition of the deuterium rich compounds, showing that, under the synthesis reaction conditions, an elemental platinum oxidation state of up to +4 is possible in a hydrogen atmosphere!

With the next example, we addressed the fundamental question as to whether it is possible to synthesise a ternary hydride containing a *d* transition metal from outside subgroup eight. The rose-coloured product K_3MnD_5 exhibits a tetragonal I-centred structure, which can be described in terms of a framework structure with vertex-sharing alkali metal octahedra, with deuterium atoms located at the octahedra centres. Due to the space occupied by the accompanying chains of $[MnD_4]^{2-}$ tetrahedra, the alkali metal octahedra are twisted along the *c*-axis (Fig. H3.1, right). This atomic arrangement is identical to that of the Cs_3CoCl_5 structure type, once again highlighting the fundamental structural similarity between hydrides and halides. Magnetic susceptibility measurements exhibit Curie-Weiss behaviour over a large temperature range, with a magnetic moment magnitude consistent with that expected for Mn^{2+} . Long range antiferromagnetic ordering is observed for $T < 28$ K and the low-temperature neutron diffraction data were of sufficient quality to determine the overall magnetic structure. The Mn^{2+} spins are oriented perpendicular to the *c*-axis. Although

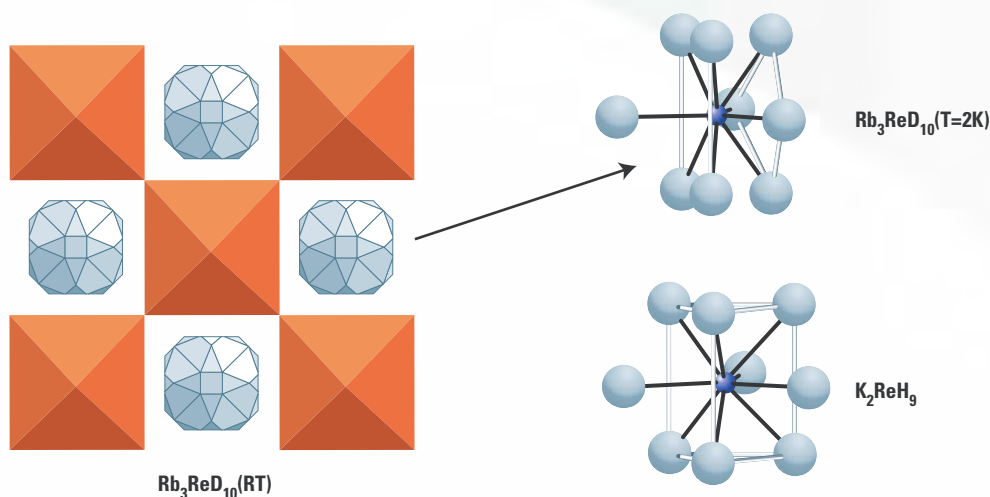


Fig. H3.2.

The crystal structure of Rb_3ReD_{10} at room temperature (left) and the Re coordination observed at 2 K (right, upper) compared with that reported for K_2ReH_9 (right, lower).

the Mn-Mn distances are comparatively long the polarizability of the hydrogen ligands promotes super-exchange interactions, a previously unobserved phenomenon in alkali metal transition metal hydrides.

The extraordinary behaviour of hydrogen ligands is also evident in the dynamic properties and is responsible for numerous phase transitions. In the high temperature modifications the mobility of hydrogen leads to a statistical occupation of the ligand positions, whereas in the low temperature modifications these motions are frozen out and an ordered arrangement occurs. This is shown in the final example. In the alkali metal-rhenium-hydrogen system, neutron diffraction experiments revealed the composition and structure of K_3ReD_{10} , Rb_3ReD_{10} and Cs_3ReD_{10} . At room temperature these three hydrides exhibit a primitive cubic structure which – as with the manganese hydride – contains vertex sharing alkali metal octahedra centred by hydrogen ions. The $[ReD_9]^{2-}$ units are incorporated within this framework. The coordination polyhedron of deuterium atoms surrounding each rhenium atom can be described crystallographically as a statistical occupation of two 24-fold sites (Fig. H3.2, left). At low temperature the hydrides undergo phase transitions, in which the hydrogen mobility is frozen out. The low temperature structure could only be solved from high-resolution HRPD data collected

owing to the small distortions of the alkali metal octahedra resulting from the altered configuration of the now ordered $[ReD_9]^{2-}$ groups – see Fig. H3.3. Here the hydrogen ligands form monocapped square antiprisms, similar to tricapped trigonal prisms found in K_2ReH_9 (Fig. H3.2, right).

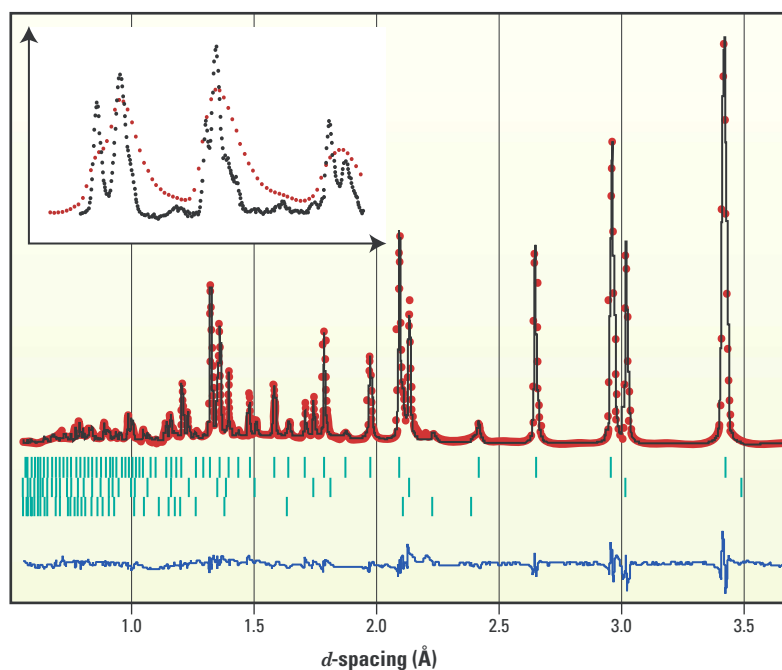


Fig. H3.3. Powder diffraction profile for Rb_3ReD_{10} at room temperature, showing the observed data (red dots), calculated profile (black line), and difference plot (blue line). The vertical tick marks are the calculated Bragg peak positions of Rb_3ReD_{10} , RbD & Re (top to bottom). The inset illustrates the differing resolutions of HRPD (black) and LAD (red) for the case of the low temperature phase of Rb_3ReD_{10} .

Isotopic substitution with combined Rietveld analysis methods for definitive structural information from powder neutron diffraction

PF Henry, MT Weller (Southampton University), CC Wilson (ISIS).

Why bother determining the structure of a material using powder diffraction? The usual answer is that structure is key in deciding the properties of the material and that powder techniques allow rapid assessment of readily available polycrystalline materials. However, small differences in structural features, such as the level and distribution of dopants, changes in bond lengths/angles as a function of temperature and thermal displacements of atoms, all influence properties and, hence, applications. Using isotopically substituted samples and combined data-set analysis we have been able to extract structural information of unprecedented quality from polycrystalline samples of systems covering a wide range of interest in solid state chemistry.

Fig. H4.1. Periodic table showing elements with isotopes with > 20 % scattering length contrast (orange), 5 - 20 % contrast (blue), mono-isotopic, lack of scattering length contrast or prohibitively expensive isotopes (grey), elements with high absorption coefficients where non-absorbing isotopes are available (green), elements with isotopes to overcome incoherent scattering effects (yellow) and radioactive elements (red).

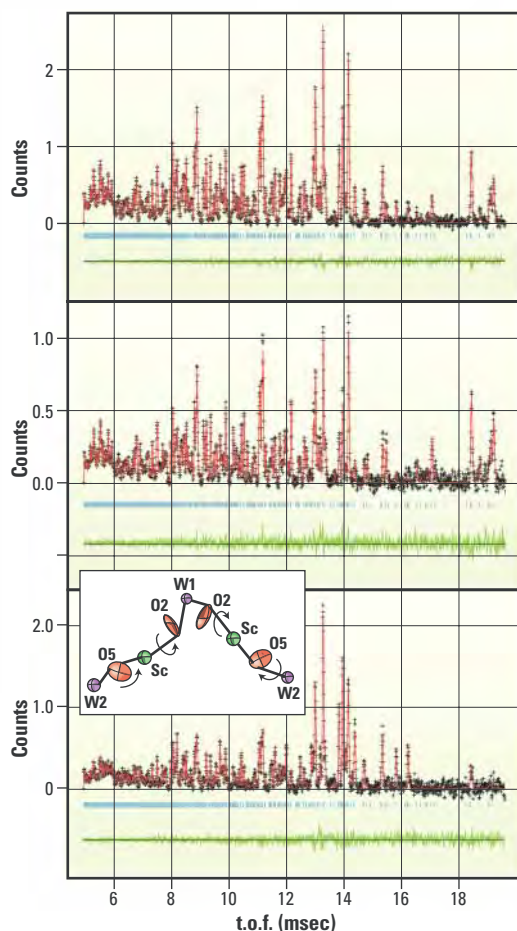
The use of isotopic substitution in powder neutron diffraction (ISND) to overcome absorption effects (e.g. ^7Li , ^{11}B , ^{154}Sm and ^{160}Gd) and incoherent scattering problems (e.g. ^2H) is well established. However, using the contrast in the scattering lengths of isotopes of a particular element to obtain enhanced structural information from powder neutron diffraction data has been almost exclusively restricted to local structure investigations of non-crystalline materials and liquids. The potential of isotopes in neutron diffraction of crystalline materials can be seen by considering Fig. H4.1 where for over half of elements there exist, at reasonable cost (between \$1 and \$5 per mg), two or more isotopes with strongly contrasting scattering length.

H																	He																												
Li	Be											B	C	N	O	F	Ne																												
Na	Mg											Al	Si	P	S	Cl	Ar																												
K	Ca	Sc	Ti	V	Cr	Mn	Fe	Co	Ni	Cu	Zn	Ga	Ge	As	Se	Br	Kr																												
Rb	Sr	Y	Zr	Nb	Mo	Tc	Ru	Rh	Pd	Ag	Cd	In	Sn	Sb	Te	I	Xe																												
Cs	Ba	La	Hf	Ta	W	Re	Os	Ir	Pt	Au	Hg	Tl	Pb	Bi	Po	At	Rn																												
Fr	Ra	Ac																																											
<table border="1"> <tbody> <tr> <td>Ce</td> <td>Pr</td> <td>Nd</td> <td>Pm</td> <td>Sm</td> <td>Eu</td> <td>Gd</td> <td>Tb</td> <td>Dy</td> <td>Ho</td> <td>Er</td> <td>Tm</td> <td>Yb</td> <td>Lu</td> </tr> <tr> <td>Th</td> <td>Pa</td> <td>U</td> <td>Np</td> <td>Pu</td> <td>Am</td> <td>Cm</td> <td>Bk</td> <td>Cf</td> <td>Es</td> <td>Fm</td> <td>Md</td> <td>No</td> <td>Lr</td> </tr> </tbody> </table>																		Ce	Pr	Nd	Pm	Sm	Eu	Gd	Tb	Dy	Ho	Er	Tm	Yb	Lu	Th	Pa	U	Np	Pu	Am	Cm	Bk	Cf	Es	Fm	Md	No	Lr
Ce	Pr	Nd	Pm	Sm	Eu	Gd	Tb	Dy	Ho	Er	Tm	Yb	Lu																																
Th	Pa	U	Np	Pu	Am	Cm	Bk	Cf	Es	Fm	Md	No	Lr																																

The basis of the technique derives from the fact that the structure factor, and therefore intensity, of a general reflection is dependent on the scattering length, position, occupancy and thermal displacement of the component atoms of the material in question (see Fig. H4.2). The data from a series of such isotopically substituted samples are then analysed simultaneously by Rietveld refinement using a *single crystallographic model* for all data-sets. The advantages of the technique over single data-set Rietveld analysis are significant. Where reflections overlap significantly, typical for most powder diffraction data-sets, the isotope substitution technique allows apportioning of the observed intensity between the background and each contributing reflection to be done more accurately, which leads to a decoupling of refined parameter correlations.

Potential disadvantages of the technique are that sample homogeneity and equivalence are essential for the combined data-set analysis approach to hold. However, the use of relatively small samples (50 - 500 mg), simultaneous synthetic techniques and thorough pre-characterisation have been successful in overcoming these problems. The result is that using the ISND technique structures are determined to a much higher level of precision and accuracy, which allow details to be extracted that are impossible to obtain from single data-set analysis. This can be illustrated through the following examples.

Accurate determination of thermal displacement parameters was illustrated by a study on $\text{Sc}_2(\text{WO}_4)_3$ – a negative thermal expansion (NTE) material. Much recent work has focussed on structural investigations to determine the origin of the NTE effect. However, structural analysis has until now been restricted by the complexity of the relatively low symmetry crystal structures, requiring the use of rigid body constraints in all but the simplest cases. Using tungsten isotopic substitution, full, unconstrained Rietveld analysis was performed allowing the structural



origin of the NTE effect to be determined – see inset to Fig. H4.2.

Improved accuracy in the determination of fractional site occupancies was illustrated by a study on $\text{Ni}_x\text{Mg}_{1-x}\text{O}$ ($x = 0.005 - 0.1$) using nickel isotopes. Here it was possible to determine accurately the dopant concentration down to the 0.5 % level, a significant improvement on the best results from single data-set analysis (approximately 2%) – see Fig. H4.3.

BaTiO_3 is an important ferroelectric material used as an electroceramic in capacitors, thermistors and electro-optic devices. The ferroelectricity arises from very small deviations from an ideal cubic perovskite structure and three separate ferroelectric phases are known, depending on temperature: rhombohedral, orthorhombic and tetragonal.

The exact nature of the titanium displacements in each of these phases are not well understood because the structural distortions are small, resulting in correlation of the titanium atomic positions with the thermal parameters of oxygen and titanium. Using barium and titanium isotopic substitution, it was possible to de-couple the highly correlated structural parameters and quantify the titanium displacements in each of the ferroelectric phases below room temperature.

These initial studies amply demonstrate that the use of isotopic substitution and combined data-set analysis to reduce parameter correlation and probe subtle structural effects with unprecedented accuracy is a significant advance. With ongoing developments in diffraction instrumentation (e.g. GEM), neutron sources and fluxes (e.g. the 300 μA ISIS upgrade) it will become possible to extend the method routinely to a wider range of materials. In conclusion, a small investment in sample preparation cost, through the use of isotopes, has significant benefits in determining structure and understanding the associated material properties.

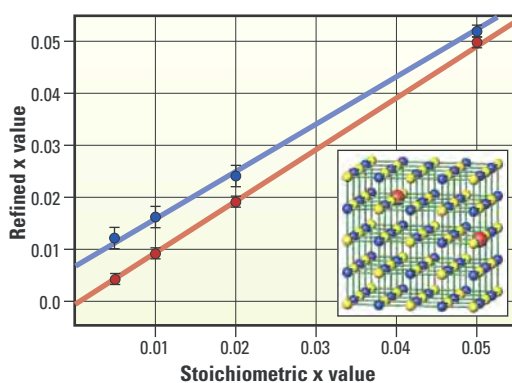


Fig. H4.2. Observed (black), calculated (red) and difference (green) patterns of $\text{Sc}_2(\text{Nat}\text{WO}_4)_3$ (top), $\text{Sc}_2(^{184}\text{WO}_4)_3$ (middle) and $\text{Sc}_2(^{186}\text{WO}_4)_3$ (bottom) collected using the backscattering bank of POLARIS at 50 K. The inset shows the section of the structure containing the bridging oxygen atoms O2 and O5 illustrating a likely local rotational motion of the oxygen atoms leading to negative thermal expansion.

Fig. H4.3. Theoretical versus refined x values in $\text{Ni}_x\text{Mg}_{1-x}\text{O}$ for ^{62}Ni single data-set (blue circles) and combined data-set – ^{62}Ni , ^{60}Ni , ^{58}Ni and $^{\text{Nat}}\text{Ni}$ – (red circles) refinements with error bars and calculated best-fits using linear regression (solid lines). Combined data-set refinements are significantly better at low doping levels shown by the intercept of the best-fit line being much closer to 0,0. The inset shows a pictorial representation of nickel doping (red spheres) into MgO (blue and yellow spheres respectively).

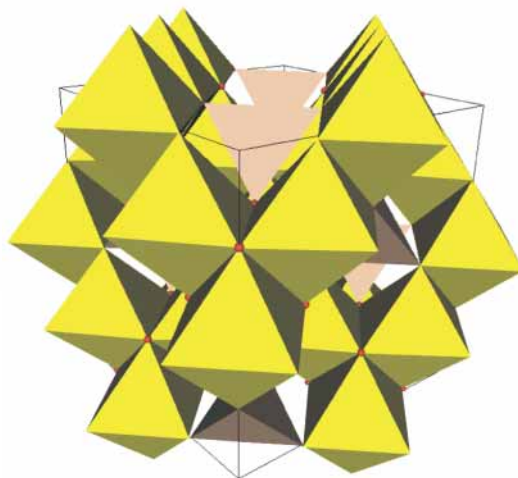
Formation of isomorphous Ir^{3+} and Ir^{4+} octamers and spin dimerization in the spinel CuIr_2S_4

PG Radaelli, MJ Gutmann, RM Ibberson (ISIS)

Inorganic compounds with the AB_2X_4 spinel structure have fascinated physicists for many years, because the topology of their B-site network frustrates the tendency for charge and spin ordering. The thiospinel CuIr_2S_4 is a recent example, well known for the presence of a metal-insulator transition at 230 K which is accompanied by a loss of localized magnetic moments. We have determined the low-temperature crystallographic structure of CuIr_2S_4 and have shown that this system undergoes a simultaneous charge-ordering and spin-dimerization transition – a unique phenomenon in three-dimensional compounds.

Fig. H5.1.

Three-dimensional view of the spinel crystal structure. The A-site cations are bonded with four anions, forming isolated tetrahedra (shown in grey). The B-site cations are bonded with six anions, forming chains of edge-sharing octahedra (yellow). The prototypical spinel is MgAl_2O_4 , a well-known red gemstone with a cubic crystal structure.



The spinel crystallographic structure (Fig. H5.1) – first solved by Bragg in 1915 – has cations occupying both tetrahedral (A) and octahedral (B) sites. As shown by P.W. Anderson in 1956, interesting physics arises when the B-site cations either become mixed in valence or carry a magnetic moment with antiferromagnetic coupling. In fact, Coulomb or magnetic interactions are prevented from being simultaneously satisfied for all sites and bonds by the geometry of the B-site network, which is said to be ‘frustrated’. The most famous example of this behaviour is magnetite (Fe_3O_4), the oldest magnetic material known to mankind, which undergoes a metal-insulator transition near 120 K, due to a presumed ordering of Fe^{2+} and Fe^{3+} on the B-site lattice.

Only discovered in the late eighties, the thiospinel CuIr_2S_4 shares some phenomenology with its much older relative (it also undergoes a metal-insulator transition, near 230 K), but with a very unique ‘twist’. In the metallic, high-temperature phase, CuIr_2S_4 is paramagnetic, as expected; however, in the insulating, low-temperature phase, all traces of magnetism are lost, with the exception of the negative susceptibility from the filled electronic shells (Larmor diamagnetism). The metal-insulator transition in CuIr_2S_4 could be explained with the same charge-ordering mechanism as in magnetite, since iridium is also thought to be in an intermediate valence state between Ir^{3+} (with a spin value of $S=0$) and Ir^{4+} ($S=1/2$). However, the ‘case of the disappearing spins’ in the thiospinel has taunted researchers for many years.

One possible explanation, put forth in the mid nineties, is that the spins may ‘pair up’ in two-atom quantum states known as ‘singlets’, which have zero net magnetic moment. Although a variety of materials containing one-dimensional atomic chains are known to display this ‘spin dimerization’ effect, this phenomenon was neither observed nor expected in a three-dimensional material such as the spinel. Since both charge ordering and spin dimerization should yield a distinct structural signature, a complete structural solution was required to confirm or contradict this model.

We have recently solved the low-temperature crystal structure of CuIr_2S_4 by a combination of electron, synchrotron X-ray and neutron diffraction data. Temperature-dependent data from the medium-resolution GEM diffractometer (Fig. H5.2), as well as high-resolution data collected on HRPD at selected temperatures, were employed to determine the general pattern of atomic displacements, and were ultimately combined with the synchrotron X-ray data for the final structural refinement in the triclinic space group $P\bar{1}$.

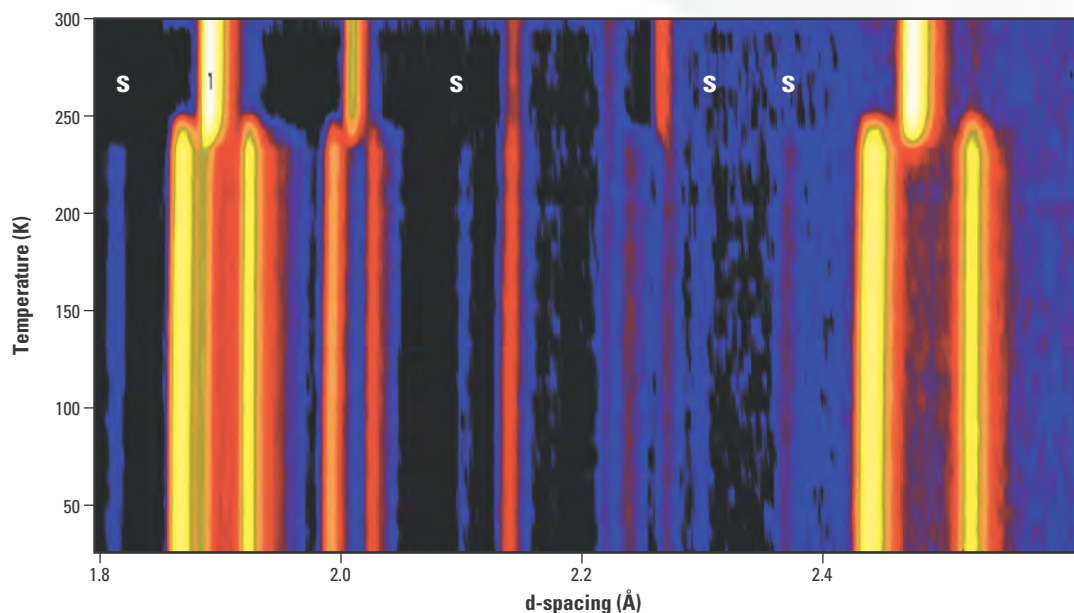


Fig H5.2. GEM neutron powder diffraction data for CuIr_2S_4 , collected as a function of temperature. The 230 K structural transition from cubic to triclinic is apparent in the data. The large lattice distortion is accompanied by the appearance of superlattice peaks (marked with an 'S'), which are mainly due to the formation of Ir-Ir dimers.

The triclinic unit cell of the low-temperature structure (Fig. H5.3) contains 16 iridium atoms. Of these, eight (shown in blue) form very short pair-wise bonds with each other (~ 3.1 Å) and, we believe, accommodate the spin-dimerized Ir^{4+} . The other eight sites (shown in red) display regular metal-metal distances (~ 3.5 Å), and naturally accommodate the non-magnetic Ir^{3+} species. In this scenario, below the metal-insulator transition, the iridium charges would order and self-assemble into eight-site nanoscopic objects that we dubbed 'octamers'. The two types of octamer ('blue' and 'red') are topologically identical (except for the internal dimerization pattern) but have different spatial orientations. The driving force for the creation of such unique arrangement is unknown; nevertheless, the combination of charge ordering and spin dimerization accounts well for the observed transport and magnetic properties. Furthermore, the elegant and previously unnoticed decomposition of the spinel structure in terms of octamers is in itself remarkable, and represents a significant increase in complexity with respect to all other known charge-ordered structures.

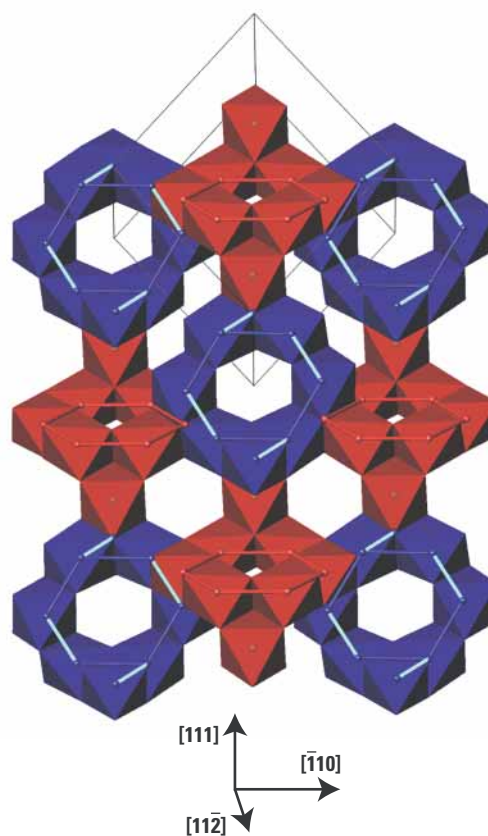


Fig. H5.3. The low-temperature crystal structure of CuIr_2S_4 . Red and blue octahedra have Ir^{3+} and Ir^{4+} , respectively, at the centres, and S at the corners, and form eight-atom 'octamers'. The dimerized Ir^{4+} - Ir^{4+} bonds are indicated with light-blue cylinders. The copper atoms (not shown) are in the tetrahedral holes of the octahedral framework. The triclinic unit cell is also shown.

The structures of high and low density amorphous ice

A Hallbrucker, I Kohl (Innsbruck), J Finney (UCL), D Bowron, A Soper (ISIS)

Within the past decade, in an effort to understand the well-known anomalous properties of water, it has been conjectured that water has a liquid-liquid critical point. If this were true it would mean that two distinct forms of water should exist at low temperature. It has been proposed that high and low density amorphous ice (HDA and LDA) are the physical manifestations of these two forms of water. The aim of the work described here was to determine the detailed structure of HDA and LDA, and hence assess whether these materials constitute the sufficiently distinct forms that are required by the second critical point scenario.

There is therefore a fundamental question at stake here: is there a genuine phase transition between HDA and LDA, as would be expected if these materials represent two physically distinct liquid structures? The importance of settling this point has been emphasised by the world's leading expert in metastable liquids, Pablo Debenedetti, who has commented that 'the relationship between LDA and HDA is of fundamental importance, not just for understanding the phase behaviour of water, but for the physics of disordered systems in general'. Identifying their relationship requires detailed structural data on the two structures. This was achieved

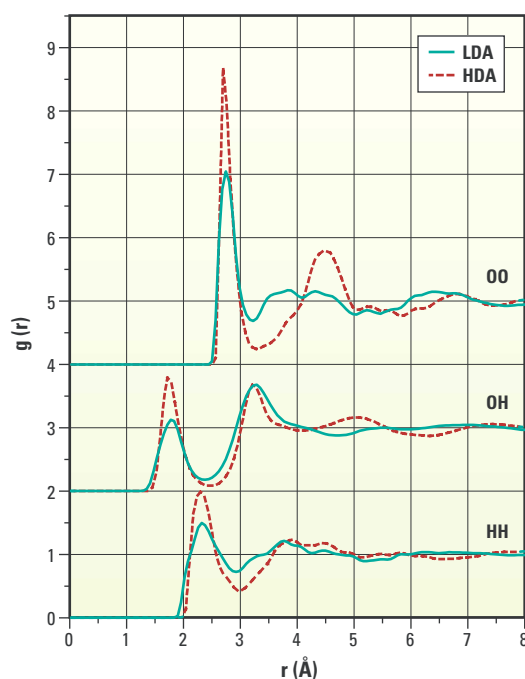
recently in a series of isotope substitution measurements on SANDALS which determined for the first time the partial radial distribution functions (rdfs) of both HDA and LDA.

Fig. H6.1 shows the three partial radial distribution functions for the two structures, which clearly are very different. However, coordination number analysis of these curves shows both structures to be 4-coordinated hydrogen bonded networks, as are liquid water and all known ices. The most obvious difference between the two structures is in the OO radial distribution function. If we calculate the first neighbour OO coordination number, we interestingly find a value of $5.0(\pm 0.1)$ for HDA, significantly greater than the more 'normal' $3.9(\pm 0.1)$ for LDA. This tells us that there is on average one more water molecule within the first co-ordination shell in HDA – yet we know that it is still a 4-coordinated hydrogen bonded network. How can we resolve this apparent contradiction? How does this extra molecule interact with the molecule at the centre of the coordination shell?

The answer is very interesting. It can be deduced from considering the spatial density functions (SDFs) in Fig. H6.2, which show the distribution of first and second neighbour waters around a central water for LDA at 80 K, liquid water at 298 K and HDA at 80 K. In essence, these plots give directional information about the pair correlations. Focusing first on the first shell features for liquid water and LDA, the two lobes above the central water indicate the location of neighbouring molecules that accept hydrogen bonds from the central water. The broad lobe beneath the central molecule corresponds to hydrogen bonded neighbours that interact with the central molecule's lone pairs of electrons.

The strong similarity of these plots indicates very similar first neighbour structures for LDA and liquid water. For HDA we note an additional close in feature: there are two additional lobes that indicate the directions in

Fig. H6.1.
Intermolecular radial distribution functions of HDA and LDA at 80 K.



which the additional ‘first neighbour’ water molecules approach the central water. Yet we know from the OH coordination numbers – and a more detailed look at orientational correlation functions obtained from the data – that this fifth molecule is not hydrogen bonded to the central molecule. Although it is linked to other molecules by hydrogen bonds, it is not so linked to the central molecule. It can perhaps be considered as some kind of ‘interstitial’ molecule that has been forced into the first coordination shell.

This interstitial molecule is very important. In LDA where there are no such interstitials, the hydrogen bonded first shell waters are freer to rotate about their water-water hydrogen bonds, resulting in the spatially diffuse second shell of the SDF in Fig. H6.2. In contrast, in HDA, the presence of this interstitial pins the possible orientations of first shell waters, and forces the spatial structure on the second shell as seen in Fig. H6.2.

So what do we conclude from this concerning the nature of the HDA to LDA transition? The transformation is observed to be relatively sudden, and can be triggered only by raising the temperature. The picture implied by this work is that the HDA-LDA transition cannot occur at low temperature because the molecular kinetic energy is insufficient to let the interstitial molecules move out of their first shell positions. These interstitial molecules therefore act as the lynch pin which keep the HDA structure intact. This implies that the HDA to LDA transition is prevented from occurring for kinetic, rather than thermodynamic reasons, and thus suggests that it is probably not the true phase transition that might be expected on the basis of the ‘two fluid’ scenario.

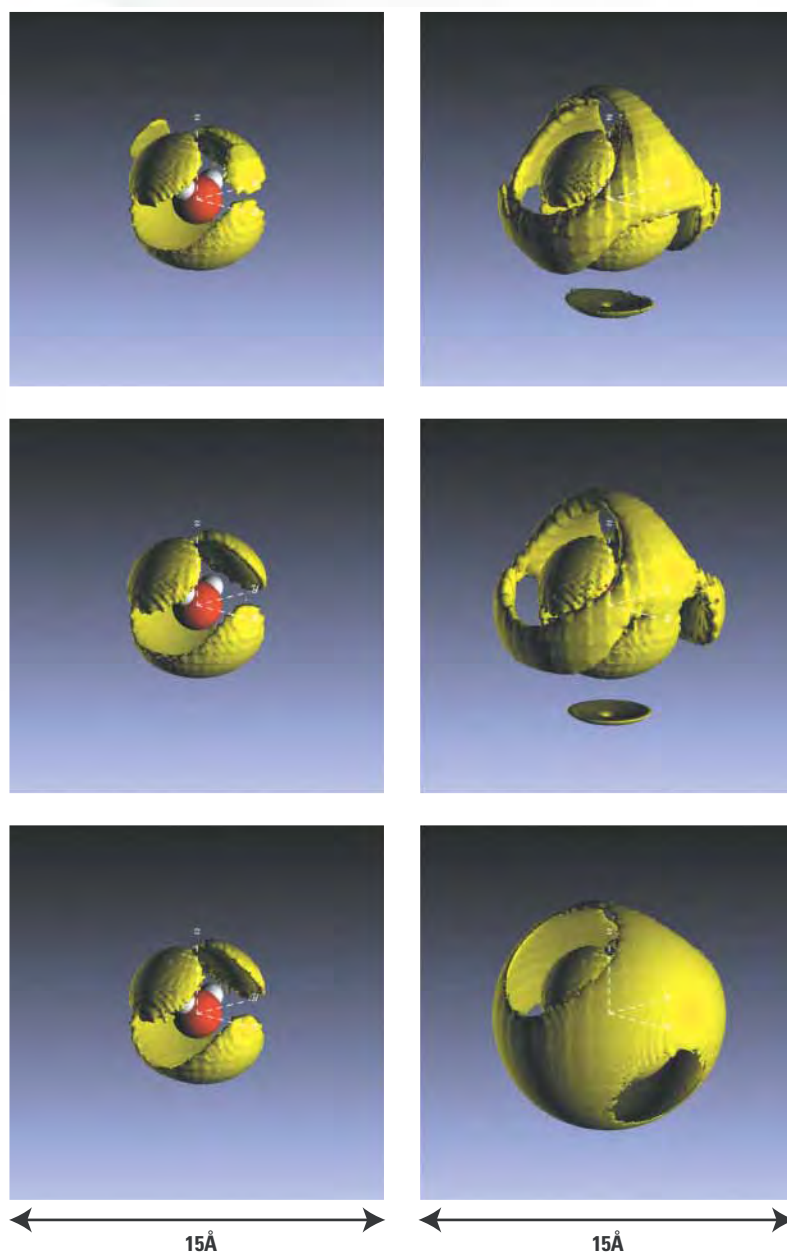


Fig. H6.2. Spatial density functions showing the distribution of the (left) first and (right) second neighbour water molecules around a central water for (bottom to top) LDA at 80 K, liquid water at 298 K, and HDA at 80 K.

Acetylcholine in water

E Hulme (MRC Mill Hill), A Soper (ISIS), J Finney (UCL)

Acetylcholine (ACh) is a molecule of great importance in the function of the central and peripheral nervous systems, and on stimulation by an action potential at the synaptic terminal is released into the synaptic fluid, where it can excite or inhibit a neighbouring neuron. There has been much progress in recent years in understanding this process, but exactly how the acetylcholine ion sheds its water of hydration as it enters the receptor protein is not understood. Here we use neutron diffraction with hydrogen isotope substitution on both the water and ACh to identify the key elements of this hydration shell.

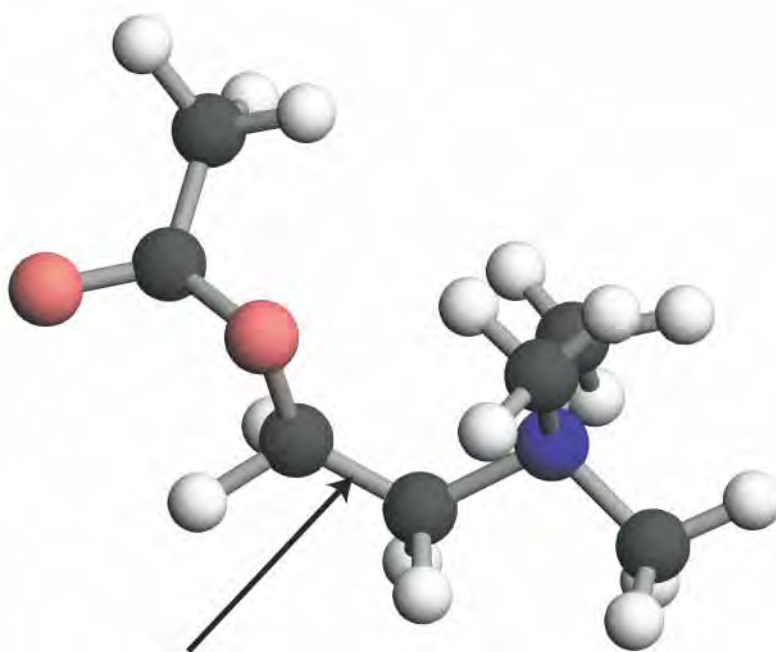


Fig. H7.1. Possible conformation of the acetylcholine molecule in solution. A crucial factor is the torsional angle along the C-C bond (arrowed) between the nitrogen (blue) and first oxygen (pink). In the conformation shown this angle is about 50°. Our simulations indicate that in fact most of the time this angle adopts values in the range 60-180°, forcing the tail to extend into the surrounding water.

The activation of neuron receptors requires the transmitter molecule to make specific bonds with amino acid side chains in the receptor molecule. The channel that ACh has to fit into is believed to be quite small, which means that any water of hydration that exists around ACh in the synaptic fluid has to be shed on entering the channel. In addition the conformation of the molecule in solution is probably important in defining its readiness to be accepted by the receptor.

There are therefore several questions of interest concerning this molecule in solution, and although other techniques such as NMR may provide some of the answers, there has so far been no definitive measurement of the

molecular conformation and of the hydration shell in solution.

ACh is of course a cation, and any solution must include a counter ion, in this case bromide. There are a total of 26 atoms on the ACh molecule, with at least 7 distinct atomic sites. Thus together with the counter ion and the water there is a total of 55 site-site pair correlation functions required to describe the structure of this solution! There is no possibility of measuring all of these functions, so interpretation of the diffraction data relies heavily on a computer simulation of the system run in parallel with the experiment. Hydrogen isotope substitution is performed on the water protons and on the methyl protons on the choline headgroup, to give a total of 6 sets of diffraction data to compare with the simulation. These data are used to constrain the conformation and determine the most likely configurations of molecules in the simulation.

The nature of the conformation of ACh in solution is probably fundamental to its function. The structure of the trimethyl choline headgroup is well defined by tetrahedral angles, but in the acetoxy tail, twisting about three sets of atom-atom bonds gives rise to a broad range of possible conformations. Fig. H7.1 shows one possible conformation but there are many others. In our simulation no constraint on torsional angles is made – they are allowed to take on any values allowed by the diffraction data and atomic overlap constraints, and therefore give the most disordered conformation consistent with the experiment. In fact, although the oxygen atoms in this tail are negatively charged and the choline headgroup is positive, the acetoxy tail is invariably found to be extended, indicating that the interaction of the tail with the surrounding water is much stronger than any tendency it might have to curl back towards the headgroup.

A second major finding is that the water shell is almost entirely hydrophobic, that is the water molecules tend to lie with their planes

tangential to the ACh-water axis in any direction that you look (Fig. H7.2). With one exception, all the water molecules shown form hydrogen bonds with each other (or with others not shown outside this region), and do not appear to interact with choline headgroup, in spite of its charge. Thus the water-water hydrogen bonding is taking precedence over the interaction of the water molecule lone pairs with the charged ion.

The exception to the above rule is the bonding of one or more water molecules to the C=O radical at the end of the tail (arrowed in Fig. H7.2). This apparently quite strong interaction with the surrounding water is no doubt one factor which helps to keep the tail extended.

We have therefore quite a detailed view of the hydration shell of ACh and the molecular conformation. The tail is almost certainly extended, due in part to a specific interaction with the surrounding water at the C=O site. At the same time the hydration shell itself is hydrophobic, which may explain how ACh can shed its water with relative ease in spite of being charged. Such a loosely bonded cage around the ion could easily be opened up at the receptor surface allowing the ion to pass into the receptor, while the water bonding to the tail would serve to ensure the molecule enters the receptor head first.

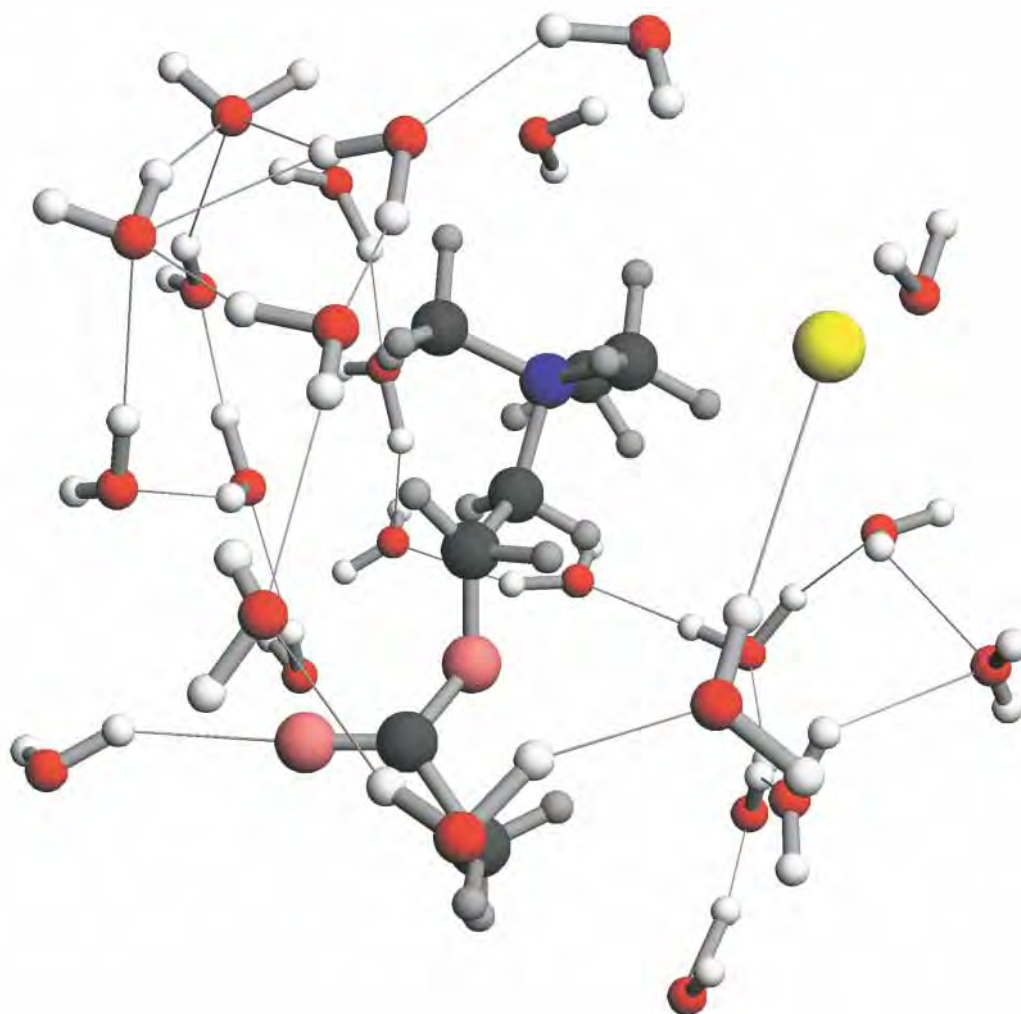


Fig. H7.2.

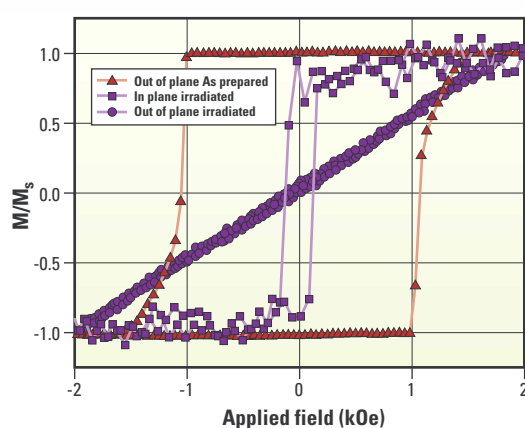
Partly cut-away view of the hydration shell of one ACh molecule out to a distance of 6.5 Å from the centre of the molecule. One bromide ion (yellow) can be seen near the molecule: all of these ions are found to be separated from the cation by at least one shell of water molecules. Hydrogen bonding between water molecules is shown as the narrow lines.

Observing magnetically patterned structures on CRISP

ND Telling, PJ Grundy, VM Vishnyakov, MJ Bonder (University of Salford),
RM Dalgliesh, S Langridge (ISIS).

Magnetic patterning is a process in which the lateral magnetic structure of a thin film is defined without the physical removal of material by, for example, lithographic techniques. Ion-beam induced magnetic patterning of Co/Pt multilayer films is currently under investigation for possible applications in magnetic recording media. Off-specular polarised neutron reflectivity measurements were performed on such structures, enabling the observation of the long-range lateral magnetic structure created in the films.

Fig. H8.1.
The observed magnetisation loops for the as-deposited (red) sample and the ion beam irradiated sample (lilac).



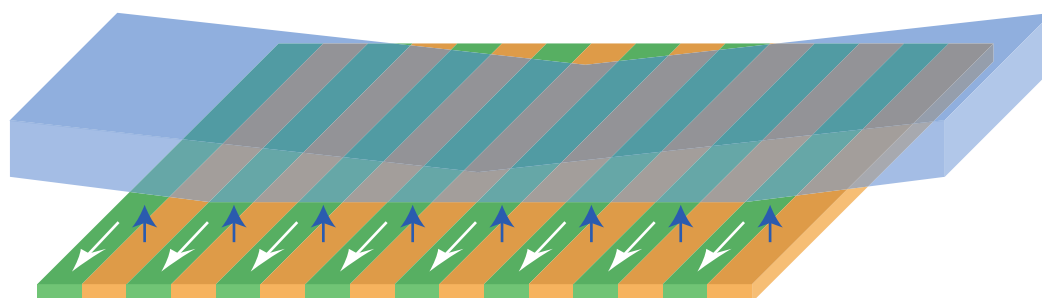
The drive to obtain higher density magnetic recording media has generated a growing interest in laterally patterned magnetic films as a possible solution to the thermally excited, spontaneous reversal of small magnetic grains (the so-called superparamagnetic limit). However, practical difficulties arising from the rough surface created by *physical* patterning have led recently to the study of possible mechanisms for *magnetically* patterning films. One approach, adopted here, is to ion-beam irradiate a Co/Pt multilayer film through a stencil, creating localised in-plane magnetisation regions in the otherwise perpendicularly magnetised film. Off-specular polarised neutron reflectivity is an ideal probe

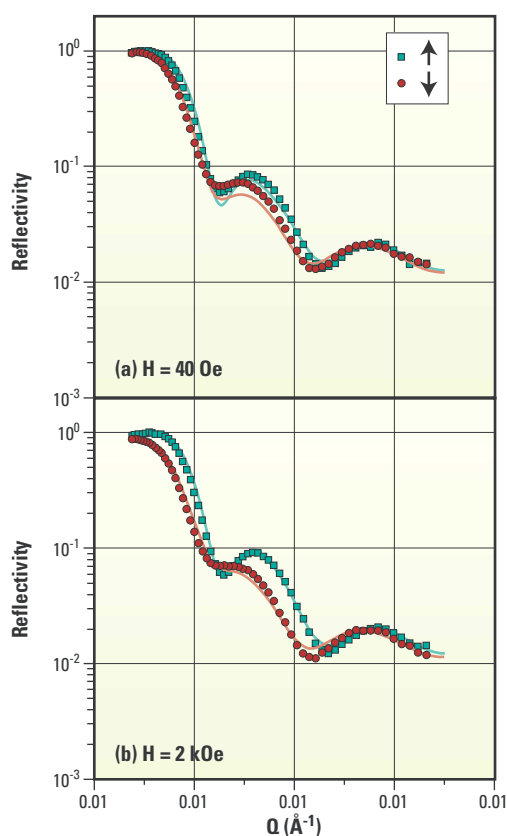
of such structures as it can reveal the *lateral* long-range artificial magnetic structure created in the film.

Co/Pt multilayers showing strong perpendicular anisotropy and with coercive fields of ~ 1 kOe were prepared using a conventional magnetron sputtering technique. The nominal structure of these films was $\text{Si}(100)/\text{Pt}(250 \text{ \AA})/[\text{Co}(4 \text{ \AA})/\text{Pt}(13 \text{ \AA})]_{10}$, confirmed by X-ray reflectivity measurements with a r.m.s. interface width between the Co and Pt layers of $\sim 4 \text{ \AA}$. Ion-beam irradiation using a dose of 10^{15} Ar ions/cm² at 80 keV was then performed simultaneously for larger areas of film and through a grid stencil with a period of $13 \mu\text{m}$. The effect of the ion irradiation was to rotate the easy magnetisation axis into the film plane as shown in Fig. H8.1. X-ray reflectivity measurements suggest that the origin of this effect is the disordering of the buried interfaces by ion irradiation, eradicating the interface anisotropy.

The area irradiated through the grid contains adjacent regions where the interfacial structure is disordered and where the interfaces remain intact, arranged in a periodic fashion. From Fig. H8.1 it is clear that in the remanent state, after applying a saturating field in the film plane, the irradiated regions will remain saturated in the film plane. However, the as-deposited regions will be magnetised perpendicularly to the film plane. Since the interaction cross-section between the neutron moment and the perpendicular film moments is zero, in the remanent state the film will thus appear as an in-plane magnetic diffraction

Fig. H8.2.
A schematic view of the ion-beam synthesised magnetic grating in the Co/Pt multilayer.





grating as illustrated in Fig. H8.2. In order to measure this lateral (in-plane) periodicity, a component of the scattering vector parallel to the surface is required. Thus the periodicity can only be seen in the diffusely scattered intensity. X-ray reflectivity further showed that for the ion dose used here the interface disorder is confined to the buried periodic interfaces in the multilayers. Therefore, at grazing angles close to the critical angle for total external reflection (i.e. far away from the multilayer Bragg reflection) resonant features in the off-specular reflectivity will arise from magnetic rather than structural ion-beam induced periodicity.

Polarised neutron reflectivity (PNR) measurements were performed on the multilayer film irradiated through the grid (Fig. H8.3). Fits to the data show that the effective moment increases from $0.6 \mu_B$ to $1.9 \pm 0.15 \mu_B$ when the out-of-plane moments are forced into the plane at saturation.

Generally, the off-specular reflectivity measurements (Fig. H8.4) indicated very little correlated structural interface roughness in the multilayers. A resonant stripe can, however, be seen running almost parallel to the specular direction when the film is in its remanent state. These resonant off-specular reflections are weak and can be seen more clearly in the wavelength integrated cross-section shown in the figure. They reveal the artificial lateral magnetic periodicity induced by the ion irradiation. The purely magnetic nature of these reflections was confirmed by saturating in the film plane. At saturation the out-of-plane magnetisation in the as-deposited regions is rotated into the plane and the apparent magnetic diffraction grating is lost. Thus the resonant reflections in the off-specular intensity should disappear, as indeed is seen in Fig. H8.4.

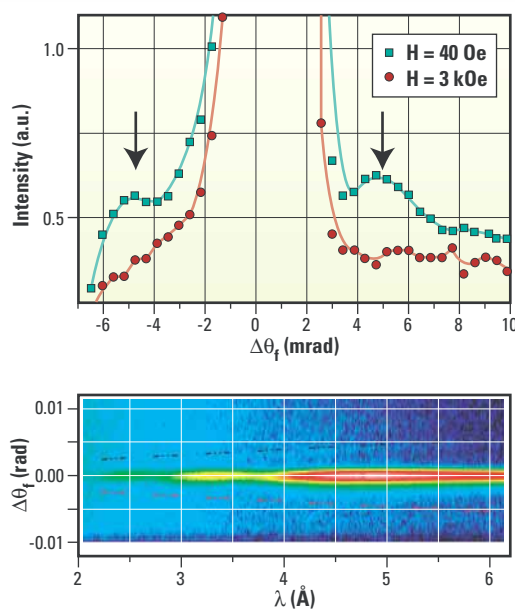


Fig. H8.3.

The specular reflectivity measured at remanence (40 Oe) and at saturation (2 kOe). The large splitting at 2 kOe is indicative of a large in-plane moment whilst in the reduced field of 40 Oe the moments relax out of plane to form the magnetic grating.

Fig. H8.4.

The magnetic grating results in diffraction peaks around the specularly reflected beam at remanence (top panel, green curve). Applying a saturating field forces the moment in-plane and the grating is erased (top panel, red curve). The dashed lines (lower panel) indicate the calculated diffraction peak position.

These measurements demonstrate the possibility of using off-specular PNR to probe magnetically patterned films. Further experiments are proposed in which spin-resolved off-specular PNR could be used to determine the reversal mechanism in magnetically patterned films containing magnetic and nonmagnetic regions.

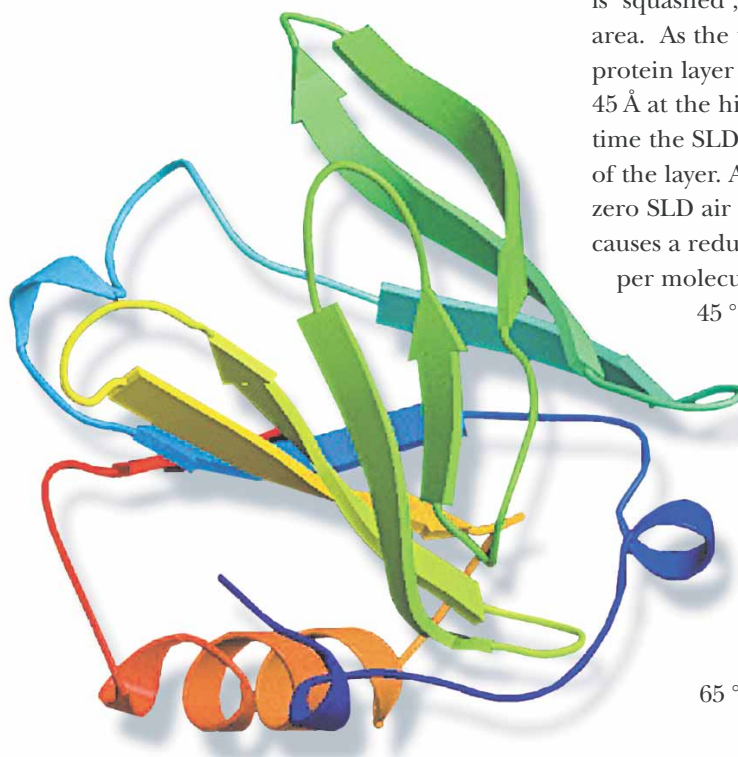
Thermal denaturation of interfacial protein layers

SA Holt (ISIS), MJ Henderson, JW White (Australian National University).

For many proteins it is not only the chemistry but also the 3-dimensional conformation that is crucial to determining the functionality. Indeed many amyloid-related diseases are considered to be related to an irreversible change in the tertiary structure of proteins in vivo. In this work we use neutron reflectometry to investigate temperature induced changes in the interfacial structure of β -lactoglobulin and hen egg white lysozyme which is compared to denaturation within that bulk solution. The key question is the impact that adsorption to an interface has on the protein stability.

Lysozyme and β -lactoglobulin (β -lg) are globular proteins, which, unlike random coil proteins, have strong tertiary structure related primarily to disulfide bonds within the protein. They therefore show little deformation from the protein solution dimensions when adsorbed to the air/liquid interface at room temperature. We have used the CRISP reflectometer to study the surface excess at the air/liquid interface of solutions of these proteins from 25 to 75 °C. The most important qualitative result from this work is that it is possible to measure the reflectivity from the air/liquid interface at temperatures up to 75 °C with high precision.

Fig. H9.1. Representation of the globular β -lg crystal structure, dimensions 35.8 x 35.8 x 35.8 Å³, showing the secondary structure of α -helices and β -sheets.



Similar trends were observed for both the β -lg and lysozyme systems as a function of temperature; we concentrate on the behaviour of β -lg (see Fig. H9.1) here. The reflectivity data were fitted adequately with a one layer model at room temperature, with some systems requiring a two layer model at high temperatures. In all cases the fitted structure at the highest temperatures was significantly different to the room temperature structure and the changes were irreversible upon cooling.

At pH = 7.0 β -lg exists in a dimerised state in solution. The effect of temperature upon the scattering length density (SLD) and layer thickness can be seen in Fig. H9.2. The layer thickness at time zero for β -lg was 35 Å, identical to the crystal structure dimensions. After a number of hours incubation at 25 °C the final surface conformation is reached where the layer thickness has reduced to 28 Å, and an area/molecule of ca 1900 Å² (compared with 1281 Å² from crystal dimensions) is reached. The protein has therefore adopted a conformation in which it is 'squashed', resulting in an increased surface area. As the temperature is increased the protein layer thickness reaches a maximum of 45 Å at the highest temperature. At the same time the SLD initially indicates a densification of the layer. At higher temperature ingress of zero SLD air contrast matched water (ACMW) causes a reduction in SLD. The smallest area per molecule, 1400 Å², was calculated at 45 °C, increasing to 1700 Å² at 65 °C.

These results are consistent with at least a partial unravelling of the protein structure above 55 °C. Calculations of the volume per molecule compared to the crystal structure volume reveal the following ratios for the surface conformation of 1.2:1, 1.0:1 and 1.7:1 for 25, 45 and 65 °C respectively.

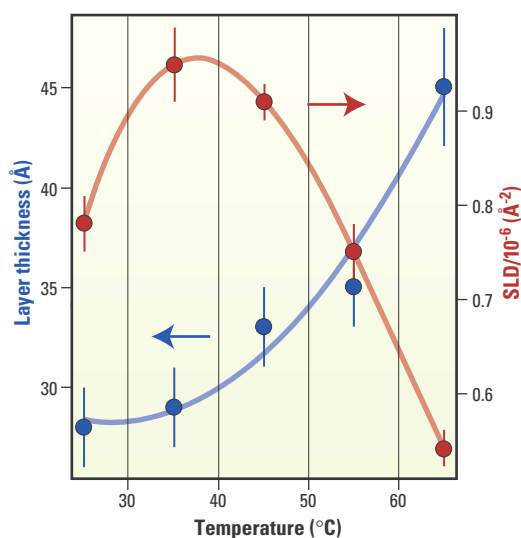


Fig. H9.2. Model parameters from fits to β -lg pH = 7.0 in ACMW as a function of temperature. (Line is a guide to the eye).

Denaturation experiments carried out on bulk solutions of β -lg have shown an inflection point in the denaturation curve at temperatures ranging from 72 to 76 °C. We have used the approach of assuming a two state model and calculating the fraction of unfolded protein (F_u) from the thickness versus temperature data for the proteins (Fig. H9.3). Limited datasets did cause some uncertainties in the fit; however the simulated profile does provide a reasonable guide to the energetics of denaturation.

An analytical protocol involving the fraction of unfolded protein as a function of temperature (T), determined from the layer thickness measurements for both lysozyme and β -lg, has been developed. For each case, a plot of F_u vs. T shows a sigmoidal behaviour. The profiles can be simulated by a model in which denaturation is considered to be an equilibrium between two states only, whose proportions change between the extremes of the temperatures studied. From these simulations we derive the enthalpy of unfolding (ΔH) and midpoint of unfolding (T_m) of 50 kcal mol⁻¹ and 52 °C respectively for β -lg. For lysozyme the figures are 70 kcal mol⁻¹ and 40 °C respectively.

This experiment has demonstrated that it is possible using neutron reflectometry to follow *in situ* the temperature induced denaturation of a single layer of protein molecules at the air/solution interface. The data has then been analysed and simulation of the unfolding curve has enabled the calculation of ΔH and T_m , both of which are lower than expected for the proteins in the bulk solution. This may indicate that using this methodology the enthalpy contribution of the surface towards protein denaturation can be determined.

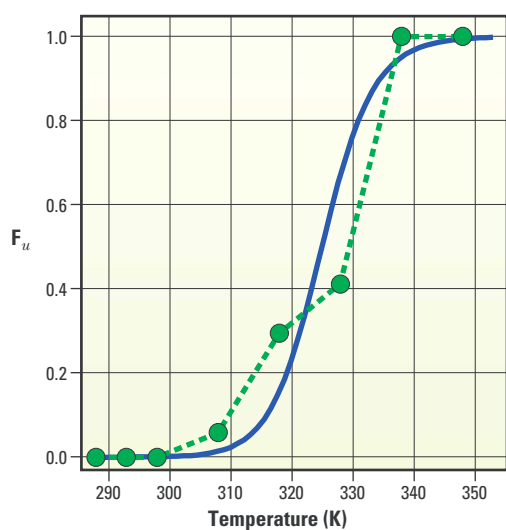


Fig. H9.3. F_u for 1 mg mL⁻¹ (pH=7.0) β -lg as a function temperature. The solid blue line is the simulated curve.

Combining small-angle X-ray and neutron scattering to elucidate complex layer structures in model polymers

XB Zeng, G Ungar (University of Sheffield), SJ Spells (Sheffield Hallam University).

Thermoplastics like polyethylene, polypropylene and nylon are semicrystalline, with alternating crystalline and amorphous layers 10-50 nm in thickness. This basic structure is crucial in determining mechanical and other polymer properties and is thought to be driven by the kinetics of crystallisation during processing. Understanding the complex crystallisation mechanism and morphology has been hindered by the molecular weights spread of commercial polymers. Here we study a binary mixture of two model polyethylenes with strictly uniform molecular weights and a deuterium label. We find that semicrystalline structures are not necessarily metastable. We also find that simple model polyethylenes can produce complex superlattices.

Very long normal alkanes (*n*-paraffins), with several hundred carbons, are ideal models for studying polymer crystallisation, morphology and conformation. They enter the molecular weight range of polymers, yet have completely uniform molecular weight. Like their shorter-chain homologues, long alkanes can crystallize as extended chains but, like polymers, they can also form folded-chain lamellar crystals. These have been studied in recent years in order to understand the complexities of semicrystalline polymers. Small-angle X-ray scattering (SAXS) has been useful, but a much more detailed picture is obtained using a combination of SAXS and small-angle neutron scattering (SANS) on selectively deuterated compounds.

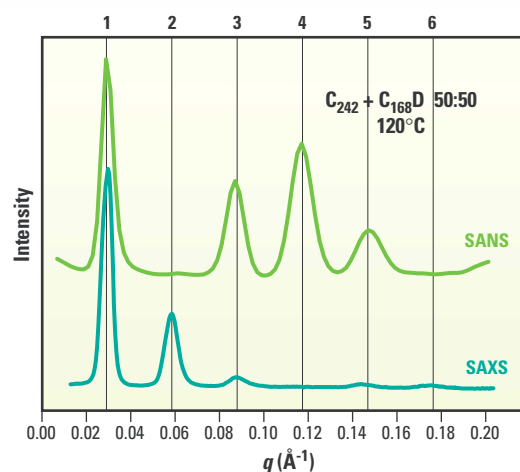
Here we describe some unusual layer structures in binary mixtures of long alkanes. While shorter crystalline binary paraffins tend to phase separate, surprisingly, long paraffins with up to 100 carbons difference mix in the solid state. Two solid solution phases are observed, one at high and one at low temperatures.

In a combined SAXS and SANS study we have examined a mixture of *n*-alkane $C_{242}H_{486}$ and a shorter alkane $C_{12}D_{25}C_{144}H_{288}CHDC_{11}D_{23}$ with a total of 168 carbons of which 12 at each end are perdeuterated. The compounds were synthesised by Drs. G.M. Brooke, C. Farren and A. Harden of Durham University.

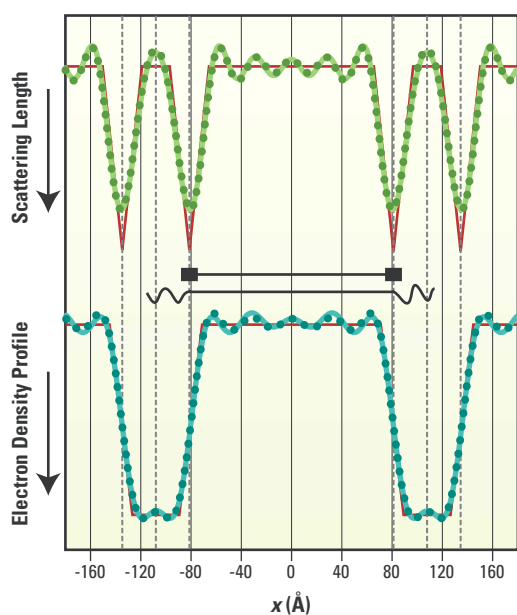
SANS and SAXS were recorded in both the high temperature ($T > 100$ °C) and the low

temperature phase ($T < 100$ °C). Fig. H10.1 shows a comparison of SANS and SAXS spectra both recorded at 120 °C. The scattering functions show the same Bragg periodicity but different intensity distributions among diffraction orders. The 1-dimensional scattering length profile (SLP) and the electron density profile (EDP) of the lamellar structure are reconstructed from the recorded SANS and SAXS intensities, respectively, via Fourier transformation and shown in Fig. H10.2. The higher frequency oscillations arise from Fourier truncation, due to the finite range of Q measured. The SLP and EDP were reconstructed from the best-fit models using the same number of Fourier terms as in the experiment, thus re-introducing the truncation 'wiggles'.

Fig. H10.1. Experimental SAXS and SANS curves for the 1:1 mixture of $C_{242}H_{486}$ and $C_{12}D_{25}C_{144}H_{288}CHDC_{11}D_{23}$ at 120 °C.



The model profiles suggest the structure of the high-temperature phase schematically depicted in Fig. H10.3a. The structure is made up of alternating crystalline and amorphous layers. The thickness of the crystal layers is close to the length of the shorter chains, corrected for the usual 35° chain tilt with respect to the layer normal. The longer chains co-crystallise, but their surplus length remains outside the crystalline layers as loose tails, or *cilia*, which make up the amorphous layer. Hence the alternating crystalline-amorphous layer structure of this unique thermodynamically stable semi-crystalline phase.



The broad dip in the EDP reflects the dip in mass density and corresponds to the amorphous layers. The peaks in neutron scattering length (SLP) show the position of deuterated ends of the shorter alkane. The combination of EDP and SLP shows that the crystalline-amorphous interphase spans approximately 12 end carbons of the shorter alkane. Thus the chain ends of the shorter alkanes are in fact disordered. This provides new evidence for the phenomena of surface roughening and ‘premelting’ in semicrystalline polymers.

Similar analysis of SAXS and SANS data for the low-temperature phase results in the structural model represented in Fig. H10.3b. The structure is a superlattice containing a triple-layer repeat unit. This phase is highly crystalline and its ideal molar composition is 1:1. The transition mechanism leading to the superlattice phase is intriguing. Two adjacent crystal layers of the high-temperature phase act in tandem, with all long chains in the top layer moving down, and all long chains in the bottom layer moving up. This results in a smooth top and bottom surface of aligned chain ends and in a third thinner crystalline middle layer made up of former amorphous cilia. Such triple-layer superlattices occur in all long alkane pairs with a chain length ratio between 1.3 and 2.

In summary, this work has shown that a phase consisting of alternating crystalline and amorphous regions can be thermodynamically stable even though its constituent chain molecules are fully crystallisable and well below their respective melting points. Semicrystalline polymers may thus be closer to equilibrium than it is normally assumed. The low-temperature superlattice structure illustrates an ingenious way for such molecules to maintain low energy (high crystallinity) while maximising the entropy of mixing.

Fig. H10.2.

Fourier reconstruction of the SLP from SANS (top) and EDP from SAXS (bottom). Wavy line: direct reconstruction from experimental intensities; straight lines: best-fit trapezoidal model; dots: Fourier reconstruction from the model. A molecule each of $C_{12}D_{25}C_{144}H_{288}CHDC_{11}D_{23}$ and $C_{242}H_{486}$ is shown to scale.

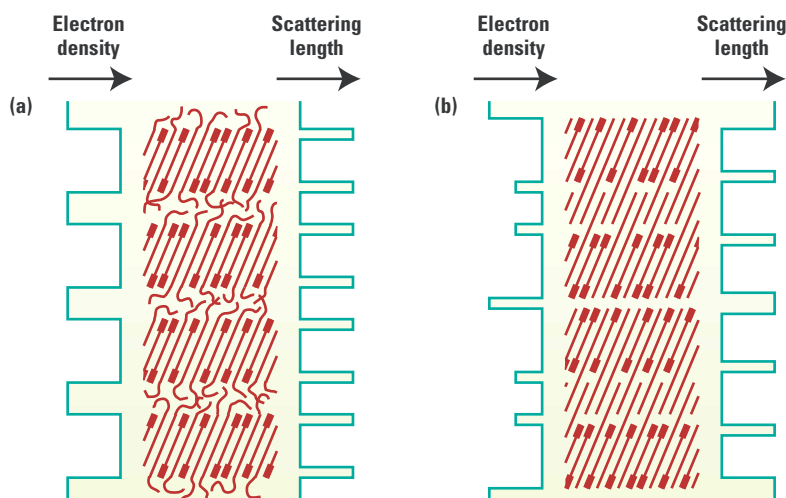


Fig. H10.3.

Structural models of the alkane mixture and the related schematic SLP and EDP: (a) Semicrystalline Form (high temperature phase), (b) Triple Layer Superlattice (low temperature phase).

Formation mechanisms in surfactant templated films

KJ Edler, T Brennan (Bath University).

Controlling the size, shape and orientation of structures on the nanometer size range is a central goal of modern materials chemistry. We are currently working on understanding the formation mechanisms of materials that spontaneously self-assemble over both nanometer and macroscopic length scales, using a combination of X-ray reflectivity and contrast variation SANS.

Thin films of hexagonally packed hollow cylinders of silica (~ 45 Å in diameter) have been synthesised with their long axes aligned parallel to the surface of the film. These films have potential applications as membranes for catalysis or separations, or as surface coatings in which the channels encapsulate dyes or sensor molecules. The films grow spontaneously at the solution/air interface from acidic solutions containing an inorganic precursor (here tetramethoxysilane), and a surfactant micelle as 'template' (cetyltrimethylammonium bromide, CTAB). The size, packing and uniformity of cylindrical surfactant micelles controls the ordering, connectivity and dimensions of channels in the hybrid film. Porosity may then be created by removal of the surfactant from the core of the cylinders. Film formation occurs after a lengthy induction period and has been followed using both X-rays and neutrons. Off-specular X-ray reflectivity provides information on film development at the solution/air interface, whilst small angle neutron scattering follows structure evolution in the bulk solution.

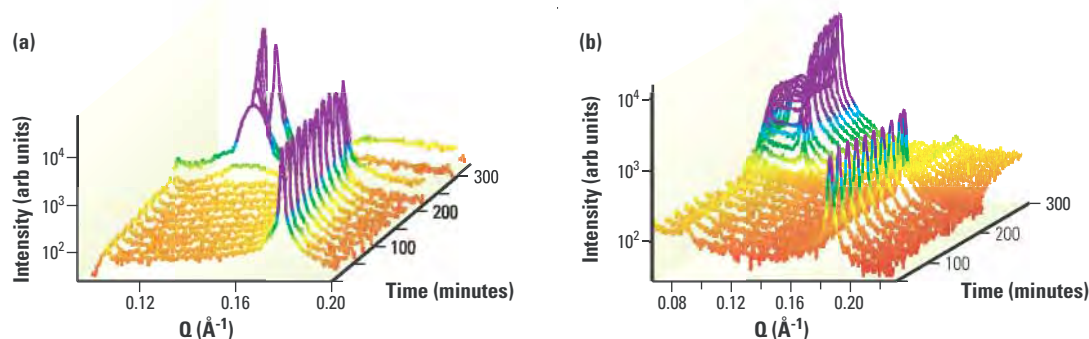
X-ray reflectivity experiments, in 60 second time frames, were made on the Tröika II beamline at the ESRF. Surprisingly the observed film formation mechanism varied

with silica concentration. At low and high silica concentrations (TMOS/CTAB < 3.6 or > 10.7), at the point of film formation, a broad diffraction peak grew next to the sharp specular reflectivity peak (Fig. H11.1a). This peak increased in intensity and became narrower with time. The width of diffraction peaks is inversely proportional to the number of repeat units, so this peak development indicates film formation from nanostructured domains, which nucleate at the surface and grow down into the solution. However at intermediate silica concentrations, the diffraction peak appearing at the end of the induction period is narrow, and has constant peak width (Fig. H11.1b). In this case the nanostructured aggregates appearing at the surface are sufficiently large that the diffraction peak width is defined by the resolution of the reflectometer (*ca.* 40 repeat units), even at the first moment they are visible. At intermediate concentrations therefore, the nanostructure forms first in solution and the film grows through packing of these pre-formed aggregates at the interface.

To investigate this unexpected result we used small angle neutron scattering on LOQ at ISIS to examine the subphase during the induction period. Using synthesis solutions prepared with varying proportions of H₂O and D₂O, the contrast was changed without altering the chemistry. At the intermediate silica concentration, the development of a diffraction peak is clearly observed (Fig. H11.2b) at the same spacing as observed in the films, indicating that particles related to

Fig. H11.1.

X-ray reflectivity: evolution of the specular reflection, first order diffraction peak and Yoneda wing as a function of time for (a) high silica TMOS/CTAB=10.7, and (b) intermediate silica TMOS/CTAB=7-10 concentrations. The Yoneda wing (small peak at far left) increases in intensity as the specular reflection (at the right) decreases due to increasing surface roughness as the films grow. The diffraction peak later grows in between the Yoneda wing and the specular reflection, it is initially broad in (a) but sharp in (b).



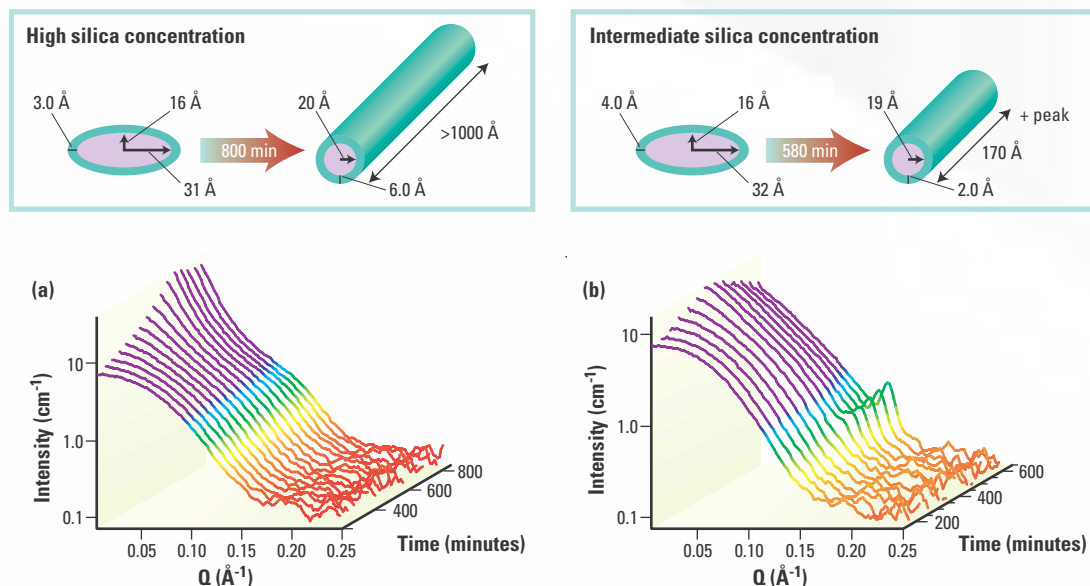


Fig. H11.2.

SANS: from CTABr/TMOS solutions in D_2O at 20 minute intervals, until precipitate is formed at (a) high, and (b) intermediate silica concentrations. The schematic diagrams (not to scale) represent the changes in silica structure around the surfactant micelles in solution, based on fits to the data.

the film exist in the subphase. At a higher silica concentration no diffraction peak develops, although the shape of the scattering curves evolves with time (Fig. H11.2a).

By contrast matching either the silica or surfactant the changes in SANS signal allow an unambiguous determination of the structures present. Simultaneous fits to three contrasts used cylindrical or elliptical form factors and also allowed for interparticle interactions via a Hayter-Penfold charged particle $S(Q)$ function. Initially the structures in both systems were elliptical core-shell particles with a CTAB micellar core and a thin silica shell. At the end of the experiment, indicated by precipitation, the solutions contained cylindrical core-shell structures but the intermediate concentration also contained aggregates producing the diffraction peak. At high silica concentrations the templated silica cylinders are much longer and have a thicker silica shell than at the intermediate concentration.

These observations can be explained by considering the polymerising silica as a growing polyelectrolyte chain interacting with the surfactant micelles. However both the surfactant and silica are positively charged so

they interact through the mediating Br⁻ counterion. At intermediate silica concentrations the micelles are completely coated with the polyelectrolyte, charge matching occurs and they no longer repel each other. This allows a liquid-liquid phase separation (coacervation) to occur, as more concentrated droplets of silica and surfactant separate from the less concentrated bulk solution. The nanostructure responsible for the SANS peak in the subphase and the constant width diffraction peak at the surface develops within these phase separated droplets. At higher silica concentrations the micelles become encapsulated in excess silica polymer, resulting in elongated micelles with a thicker shell which remain in dilute solution. The excess charge on the shell combined with entropic constraints means the cylinders do not phase separate in the bulk, but coalesce into an ordered structure at the air/interface.

A combination of X-ray reflectivity and contrast variation SANS has provided a detailed picture of the mechanism of formation of these novel silica films.

Polymer diffusion in supercritical fluids

TP Russell, R Gupta, J Watkins, K Lavery (University of Massachusetts, USA).

Supercritical fluids (SCFs) are emerging as industrially important solvents for polymer synthesis and processing. SCFs provide a 'solventless route' to processing since CO₂ can plasticize the polymer, thus imparting enhanced mobility to the polymer chains, improving chain diffusivity and providing a means for overcoming kinetic barriers in high molecular weight polymer processing. In addition, the 'solvent' is fully removed by simply depressurising the system. Here we study the effect of SC CO₂ on the mobility or diffusivity of polymer chains in CO₂-dilated polymers using high-pressure Neutron Reflectivity.

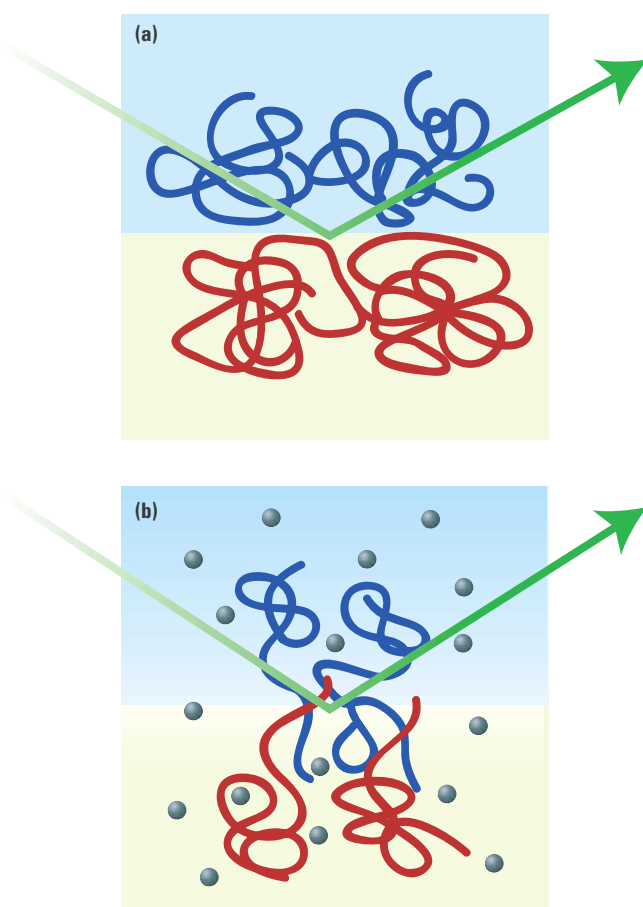


Fig. H12.1. Schematic of the sample a) prior to annealing, and b) after the incorporation of CO₂ (grey spheres) at a particular temperature and pressure.

Neutron Reflectivity (NR) has emerged as a simple yet powerful tool to probe polymer interfaces. With a depth resolution of ~ 1 nm NR has been quite effective for the investigation of polymer/polymer interdiffusion in stopped time experiments. For thermally annealed samples this is fine; however, experimental difficulties arise when working with CO₂-pressurised systems. Cavitation of the polymer film upon depressurisation leads to porous films and distortions of the polymer-polymer interface, leading to erroneous values for the diffusion constant. In studying CO₂-dilated polymers it is, therefore, imperative that the measurements be made *in situ*, in real time, at a particular temperature and pressure of CO₂. This, however, places severe demands on the source, detection system and experimental geometry. Full reflectivity profiles must be obtained in minutes to follow the interdiffusion quantitatively.

Using the SURF reflectometer it has been possible to study the interfacial broadening of CO₂ polymer systems as a function of pressure and temperature on the minute timescale. Fig. H12.1 displays a representation of the system under study, where the two colours represent different polymer films. A chain for each polymer is shown to illustrate the interfacial broadening from initial sharp interfacial structure to that showing a gradual interface from one system to the other. After pressurisation the neutron beam is reflected from the top, bottom and the interfacial region of the sample. The film dimensions increase upon addition of CO₂ due to the swelling of the film by the sorbed CO₂.

Samples consisting of layers of protonated and deuterated polystyrene (PSH and PSD) were prepared on a silicon substrate with the deuterated layer placed adjacent to the substrate. Samples were mounted in the pressure cell and heated to 62 °C. At this temperature PSH and PSD do not interdiffuse. CO₂ was then rapidly introduced to 83 bar and

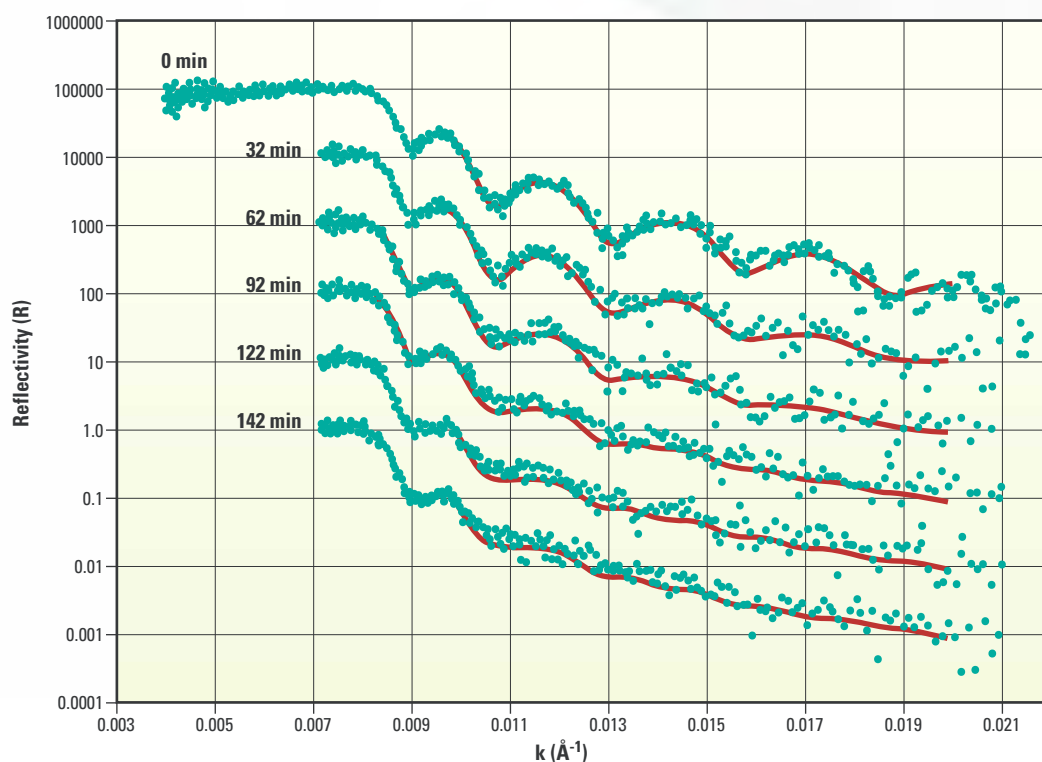


Fig. H12.2.
Reflectivity profile and fit for the PSH/PSD bilayer. Counting time 5 min at the indicated time.

reflectivity curves were collected at a single incident angle. The data, seen in Fig. H12.2, show that the amplitude of the fringes, resulting essentially from the thickness of the PSD layer, decays with time as the interface broadens due to interdiffusion.

The polystyrene self-diffusion coefficient can be calculated from the interfacial broadening as a function of time and is shown in Fig. H12.3 as a function of CO₂ weight fraction. The diffusivity of the PS chain in CO₂ diluted PS shows nearly an order of magnitude increase in mobility upon sorption of CO₂ from 8.8 to 11% by weight (6 to 10% by volume). These diffusivity values are several orders of magnitude larger than those seen for the interdiffusion of PS chains in the absence of CO₂ under similar conditions. In Fig. H12.3 the diffusivity data is fitted to the Vrentas and Duda free volume theory (solid line), which describes the mobility of chains in polymers as a function of the free volume present in the system.

These results show that SC CO₂ is an effective plasticizer since it enhances the diffusivity of chains by several orders of magnitude under moderate temperatures and pressures. Removal of the pressure removes this solvent. These studies have laid the ground work for the study of time-resolved ordering in high molecular weight copolymers, a precursor of photonic bandgap materials.

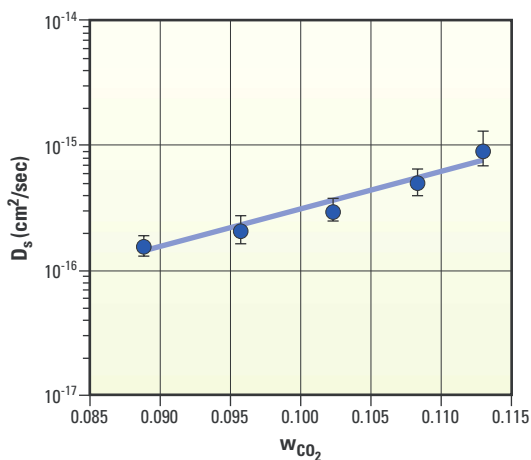


Fig. H12.3.
Diffusivity of PS chains in CO₂-diluted PS at 62 °C. The pressure in the CO₂ fluid phase ranges from 76 bar to 104 bar.

Bose-Einstein condensation in disorder

H Glyde (University of Delaware), R Azuah, (NIST),
R Scherm, (Physikalisch-Technische Bundesanstalt, Braunschweig), B Fåk, (ISIS).

The Bose-Einstein condensation (BEC) is of great interest in a wide variety of systems. It was proposed by Einstein in 1924 and is the microscopic origin of the remarkable superfluid properties of liquid ^4He . More recently in some amazing experiments BEC has been realized in dilute gases of alkali atoms confined in magnetic traps. Here 100% of the atoms condense into a single quantum state opening the door to creation of 'atom lasers'. The BEC of 'Cooper pairs' of electrons (Bosons) is the origin of superconductivity, and in the high temperature superconductors, this BEC takes place in doped and disordered materials. Our goal is to observe BEC directly in disorder on the MARI spectrometer.

Liquid ^4He confined in porous media is the most flexible example of 'Bosons in disorder' in nature. In addition, the superfluid properties of ^4He in several porous media such as Vycor and aerogel have been extensively investigated. Confinement lowers the transition temperature, T_c , to superfluidity below the bulk value ($T_\lambda = 2.17\text{ K}$). Measurement of elementary excitations of liquid ^4He in porous media using low energy transfer neutron scattering techniques has also recently begun. Among many interesting findings, we observe well-defined phonon-ron excitations above T_c in Vycor and Geltech silica. Since well-defined excitations

are associated with BEC, this suggests that there is BEC above T_c in Vycor. Above T_c , this BEC is probably localized to favourable regions in the media (a Bose glass).

The atomic momentum distribution, $n(y)$ folded with final state effects, is observed directly on MARI, and is shown in Fig H13.1 for superfluid and normal bulk ^4He . The BEC, a macroscopic occupation of the zero momentum state ($y=0$), appears predominantly as additional intensity at $y=0$ at $T=0.5\text{ K}$ (below T_λ) compared to that in the normal phase at $T=2.3\text{ K}$ (above T_λ). Fig H13.2 shows the condensate fraction, $n_0(T)$, in bulk superfluid ^4He obtained from data as in Fig. H13.1.

The corresponding atomic momentum distribution of liquid ^4He in Vycor above and below $T_c = 1.95\text{ K}$ are shown in figure H13.3. As before additional intensity at $y=0$ below T_c signals a condensate. The statistical precision of the data is not, however, so good because the volume of liquid ^4He in Vycor is necessarily small and significant background subtractions are necessary. Because of the poorer statistics, we are able to extract only 'one parameter' reliably in a fit to data, the

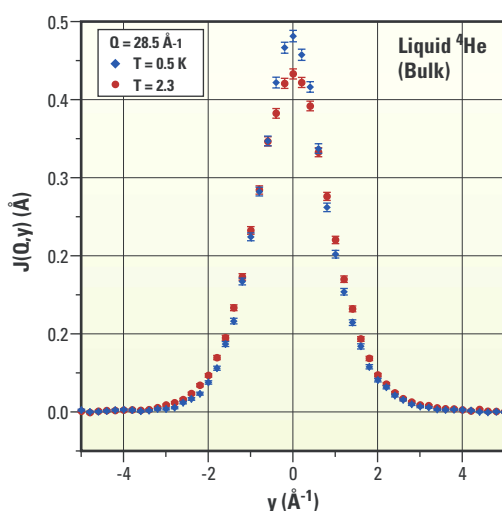


Fig. H13.1. Dynamic structure factor, $J(Q,y)$, of bulk normal (red) and superfluid (blue) ^4He observed on MARI.

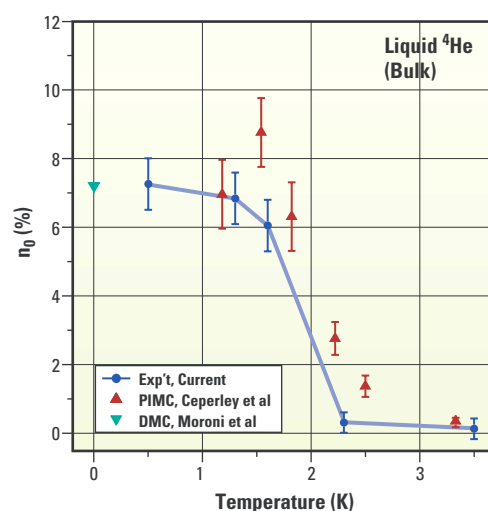


Fig. H13.2. Bose-Einstein Condensate fraction, $n_0(T)$, in bulk liquid ^4He observed on MARI (solid circles) compared with Monte Carlo calculations (PIMC, DMC).

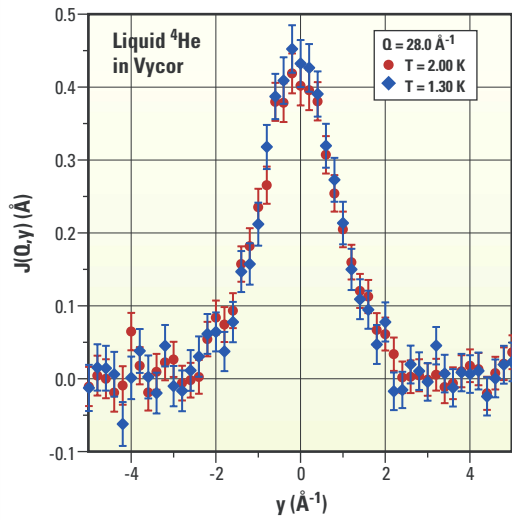


Fig.H13.3. $J(Q,y)$ of liquid ^4He in Vycor in the normal (red) and superfluid (blue) phases.

The condensate fraction, $n_0(T)$, both in Vycor and in the bulk are finally obtained from the drop in the kinetic energy in the Bose condensed phase using a well known expression. This approximate expression overestimates $n_0(T)$ somewhat. The resulting condensate fraction in Vycor and in the bulk (see Fig. H13.5) are the same, both overestimated in the same way. Also shown is the accurate value of $n_0(T)$ for the bulk for comparison.

Our pioneering measurements show that there is definitely a condensate in superfluid ^4He in Vycor. As in the bulk, BEC accompanies superfluidity in disorder. Within current precision, the condensate fraction is the same in Vycor and in the bulk at low temperature and as a function of temperature. We have not been able to determine whether T_c for BEC in Vycor differs from T_c for superfluidity or not; a challenge for the future.

atomic kinetic energy, $\langle K \rangle$. Fig H13.4 shows $\langle K \rangle$ of ^4He in Vycor and in the bulk obtained using the ‘one parameter’ fit. The two are the same within precision. In the bulk there is good agreement between the ‘one parameter’ and an accurate kinetic energy.

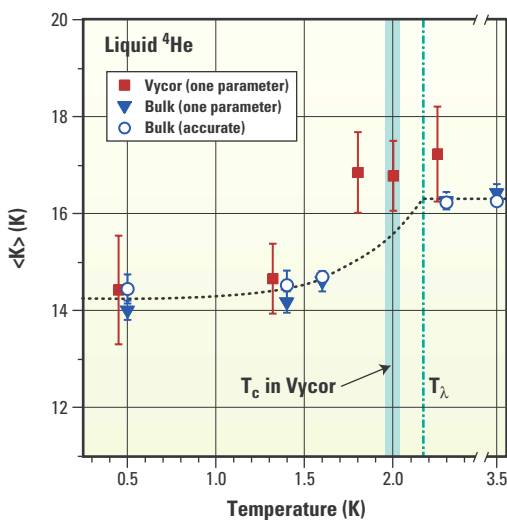


Fig. H13.4. Atomic kinetic energy $\langle K \rangle$ of liquid ^4He obtained from data as in Figs. H15.1 and H15.3. The shaded region shows the superfluid-normal transition temperature of ^4He in Vycor.

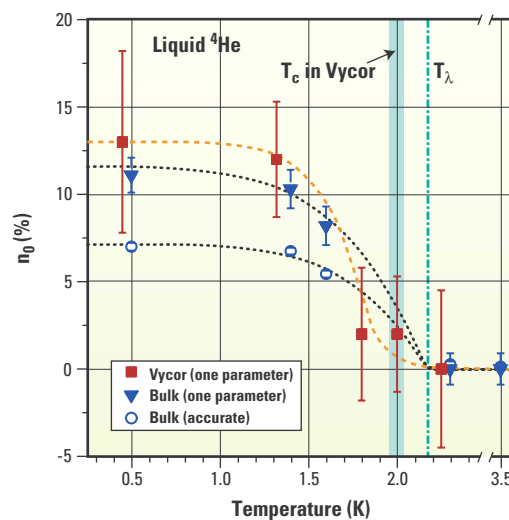


Fig. H13.5. Condensate fraction, $n_0(T)$, of liquid ^4He in Vycor and in bulk. One parameter values uses $\langle K \rangle$.

Understanding the origin of non-Fermi liquid behaviour in doped Kondo insulators

DT Adroja (ISIS), J-G Park, (Sung Kyun Kwan University, Korea), KA McEwen (UCL), J-Y So (Seoul National University, Korea), AP Murani (ILL).

Recently there has been considerable interest in the non-Fermi liquid (NFL) behaviour of heavy fermion systems. Although some compounds show NFL behaviour without external perturbations, most have to be tuned to exhibit NFL behaviour by doping, or by applying pressures or magnetic fields. Recent efforts have focused on finding the origins of such NFL behaviour. In this report, we have used inelastic neutron scattering techniques to investigate the dynamical susceptibility and high-energy spin dynamics of $\text{CeRh}_{0.8}\text{Pd}_{0.2}\text{Sb}$ and $\text{Ce}_{0.7}\text{Th}_{0.3}\text{RhSb}$. In particular we have examined the so-called E/T scaling behaviour in an attempt to understand the origins of NFL behaviour reported for these two systems.

Theories based on the Fermi liquid (FL) quasiparticle concept have been very successful over the last forty years in describing the low temperature properties of metals, including strongly correlated electron systems. The main predictions of these theories are that well below the characteristic Fermi temperature, T_F , the resistivity should exhibit quadratic temperature dependence, the heat capacity should show linear temperature dependence and the magnetic susceptibility should be temperature independent. These predictions have been borne out in many metals and seemed to allow no exception until

recent experiments demonstrated that such exceptions indeed exist in some heavy fermion compounds. These growing numbers of systems show physical properties significantly deviating from the predictions of FL theories at low temperatures, the so-called non-Fermi liquids (NFL).

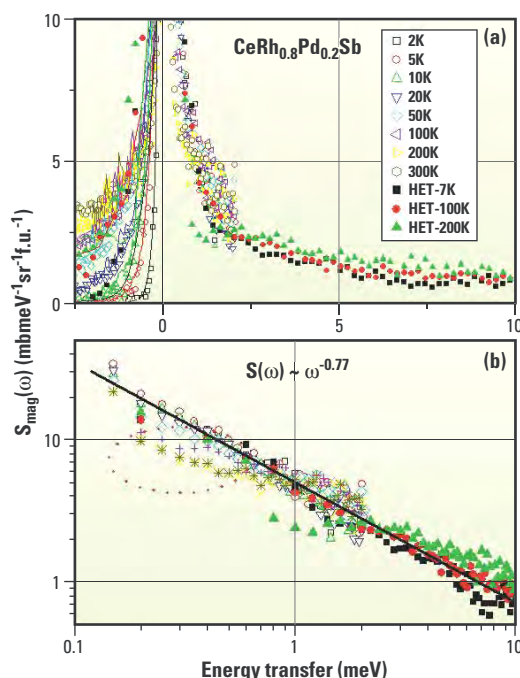
Another interesting feature of the NFL systems is that they show unusual E/T scaling behaviour in the dynamical susceptibility, $\chi''(\omega, T)$ measured using the inelastic neutron scattering technique. This then implies that the temperature itself is the energy scale governing the spin fluctuations. This E/T scaling behaviour has been observed in $\text{U}(\text{Cu},\text{Pd})_5$ by Aronson and $\text{Ce}(\text{Cu},\text{Au})_6$ by Schröder. We note that the two groups' experimental results produced different scaling exponents in the dynamical susceptibility (0.33 and 0.77 respectively). These different scaling exponents, we believe, are deeply related to the underlying microscopic mechanism of NFL behaviour. Theoretical scenarios proposed for the NFL behaviour include the $T=0$ quantum phase transition theory (QPT), the two-channel Kondo model, and the disordered Kondo model.

CeRhSb is a Kondo insulator with a small energy gap ($\sim 4\text{K}$) at E_F . With Pd doping on the Rh site, the gap is rapidly suppressed and, at $x = 0.2$, it exhibits NFL behaviour in the heat capacity. Furthermore, a new antiferromagnetic state develops for higher Pd concentration up to $x = 0.4$. A very similar phase diagram was also observed for Th doped CeRhSb , where NFL behaviour is found at $x = 0.3$. The aim of the present study was to investigate whether $\text{CeRh}_{0.8}\text{Pd}_{0.2}\text{Sb}$ and $\text{Ce}_{0.7}\text{Th}_{0.3}\text{RhSb}$ show E/T scaling in $\chi''(\omega, T)$ and to determine the scaling exponent.

We performed inelastic neutron scattering measurements on $\text{Ce}_{0.7}\text{Th}_{0.3}\text{RhSb}$ and $\text{CeRh}_{0.8}\text{Pd}_{0.2}\text{Sb}$ using the HET spectrometer, extending the study on the latter to lower energies than HET on IN6, at the ILL.

Fig. H14.1.

(a) Magnetic scattering measured on HET (low energy data from IN6). The solid line shows that spectra obey the detailed balance factor. (b) Log-log plot of magnetic scattering. The dotted ellipse indicates a region where the scaling breaks down at high temperatures.



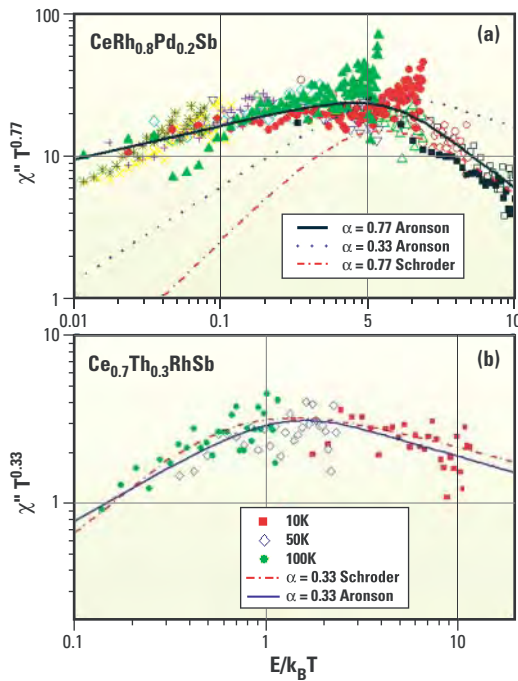


Fig. H14.1a shows that the data for $\text{CeRh}_{0.8}\text{Pd}_{0.2}\text{Sb}$. On the energy loss side, the data collapse on top of each other giving rise to scaling behaviour of $S(\omega, T) \approx \omega^{-\alpha}$ with $\alpha = 0.77$ (see Fig. H14.1b) in the energy range of 0.1 to 10 meV. On the energy gain side the scattering remains temperature dependent in accordance with the detailed balance principle (solid line in Fig.H14.1a). We note that the data above 200 K and 15 meV deviate from the scaling behaviour. Furthermore the NFL scaling behaviour has not been observed in $\text{CeRh}_{0.9}\text{Pd}_{0.1}\text{Sb}$, implying a $T = 0$, QPT in $\text{CeRh}_{0.8}\text{Pd}_{0.2}\text{Sb}$.

A similar response is also observed for $\text{Ce}_{0.7}\text{Th}_{0.3}\text{RhSb}$, but with a different scaling exponent $\alpha = 0.33$. Figs.H14.2a and H14.2b show the E/T scaling of $\chi''(\omega, T)$ for both compounds using the aforementioned α values. We analysed the E/T scaling behaviour shown in Fig. H14.2 using two functions, which were previously employed for the analysis of $\text{U}(\text{Cu},\text{Pd})_5$ by Aronson and $\text{Ce}(\text{Cu},\text{Au})_6$ by Schröder, to find that for the data of $\text{CeRh}_{0.8}\text{Pd}_{0.2}\text{Sb}$ Aronson's function fits better with $\alpha = 0.77$ whereas both functions fit

the data of $\text{Ce}_{0.7}\text{Th}_{0.3}\text{RhSb}$ with $\alpha = 0.33$ equally well.

A further interesting point is the presence of crystal field (CF) excitations in our data. As shown in Figs. H14.3a and H14.3b, two well-defined CF excitations are observed for $\text{CeRh}_{0.8}\text{Pd}_{0.2}\text{Sb}$ while much broader CF excitations are present in $\text{Ce}_{0.7}\text{Th}_{0.3}\text{RhSb}$. This observation, we argue, indicates the extent of disorder of Ce neighbour, and that apparently disorder is less important in $\text{CeRh}_{0.8}\text{Pd}_{0.2}\text{Sb}$ than in $\text{Ce}_{0.7}\text{Th}_{0.3}\text{RhSb}$.

In summary, we have observed clear E/T scaling behaviour in the dynamical susceptibility of $\text{CeRh}_{0.8}\text{Pd}_{0.2}\text{Sb}$ and $\text{Ce}_{0.7}\text{Th}_{0.3}\text{RhSb}$. We also demonstrated that the measurements of CEF can be used as an experimental indicator of the degree of disorder on the Ce sites and hence whether the Kondo disorder model can be applicable to a specific system. Based on our measurements, we think that the NFL behaviour in $\text{CeRh}_{0.8}\text{Pd}_{0.2}\text{Sb}$ originates from a $T = 0$ QPT whilst the NFL behaviour in $\text{Ce}_{0.7}\text{Th}_{0.3}\text{RhSb}$ is more likely to be due to the Kondo disorder model.

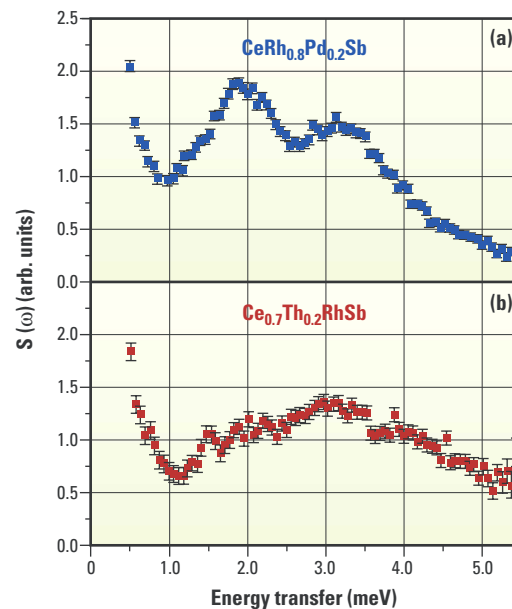


Fig. H14.2.

$\chi'' T^\alpha$ versus E/T plot (a) for $\text{CeRh}_{0.8}\text{Pd}_{0.2}\text{Sb}$ (the same symbols for each temperature as in Fig. H14.1) and (b) for $\text{Ce}_{0.7}\text{Th}_{0.3}\text{RhSb}$. The lines represent fit to the model functions (see the text).

Fig.H14.3.

Magnetic scattering obtained with $E_i = 60$ meV at 7K from (a) $\text{CeRh}_{0.8}\text{Pd}_{0.2}\text{Sb}$ and (b) $\text{Ce}_{0.7}\text{Th}_{0.3}\text{RhSb}$.

Vibrational studies on disaccharide/H₂O systems

C Branca, S Magazù, G Maisano, (Univ. Di Messina, Italy),
SM Bennington, B Fåk (ISIS).

The structure and dynamics of hydrated disaccharides are currently the subject of intense research effort due to fundamental physiochemical reasons as well as to important biomedical and biotechnological applications whose underlying molecular mechanisms have not yet been entirely understood. The MARI spectrometer allows us to get information on the hydrogen bond structural network in homologous disaccharide-water solutions by analysing the structural modifications induced by the presence of trehalose and sucrose on the main spectral features of pure water. These measurements show that the great bioprotective effectiveness of trehalose is related to the nanoscale biostructures becoming more rigid.

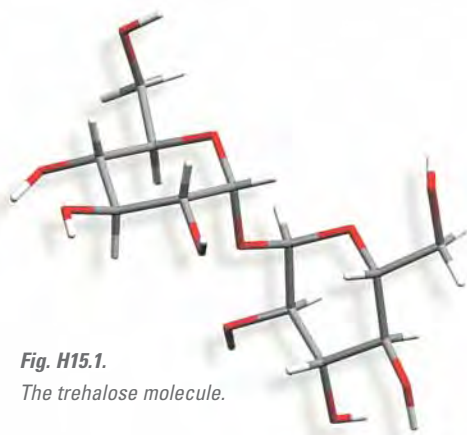


Fig. H15.1.
The trehalose molecule.

In nature the disaccharide trehalose seems to provide many living organisms with the ability to survive under extreme conditions of dehydration and in a freezing environment without cumulating effects of functional stress. Even where disaccharides such as maltose and sucrose have shown similar properties, trehalose is significantly the most effective as a bioprotector.

Notwithstanding that many of the mechanisms are not well understood, it is clear that they involve interactions that derive from the unique properties of the water molecules.

Here we focus on the structural modifications induced on water by homologous disaccharides, such as trehalose and sucrose, to look for different structural arrangements that can account for their different effectiveness as bioprotectors.

Inelastic neutron scattering (INS) measurements have been performed on pure water and on sucrose/H₂O and trehalose/H₂O solutions at different molar fractions with the MARI spectrometer. Data were collected at T = 293 K with an incident energy of 750 meV. Special emphasis was addressed to the intramolecular stretching and bending spectral contributions and to the intermolecular librational mode. A

comparison of the INS spectra from pure water with those of homologous disaccharide/water mixtures showed the same peculiar behaviour as found in Raman scattering, infrared spectroscopy and computational results derived from Density Functional Theory (DFT). In particular, by comparing the INS spectra of pure water with those of the trehalose and sucrose/H₂O mixtures, at $\phi = 0.09$ and at T = 293 K (see Fig. H15.2) a more marked downshift of the OH intramolecular stretching mode and a greater narrowing of the bandwidth for the trehalose/H₂O mixture than for the sucrose/H₂O mixture is observed. These changes can be interpreted in terms of different structural arrangements present in the two disaccharide/H₂O mixtures. More specifically, the lower frequency peak position of the trehalose/H₂O mixture can be justified by the highest value of its hydration number in comparison with that of the sucrose/H₂O, as

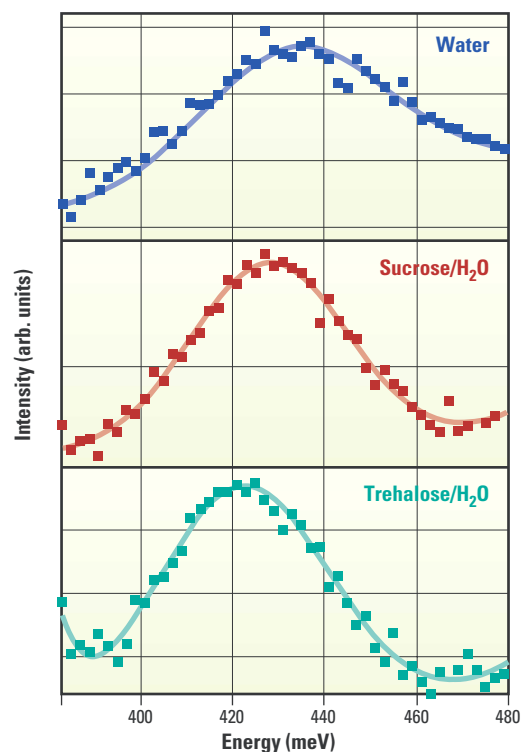
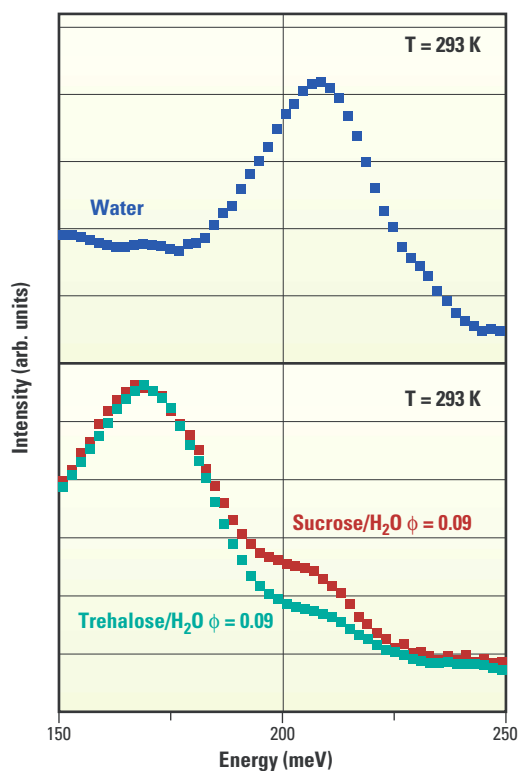


Fig. H15.2. INS spectra of water, trehalose/H₂O and sucrose/H₂O mixtures, $\phi = 0.09$, at T = 293 K and $\langle Q \rangle = 0.745 \text{ \AA}^{-1}$.



mixture. This hypothesis is supported by previous quasi-elastic neutron scattering measurements which have allowed us to recognize the trehalose/ H_2O mixture as the ‘strongest’ system compared to the sucrose/ H_2O mixture at the same concentration. Moreover, comparison of the spectral features of the two disaccharide/ H_2O mixtures suggests the presence in the trehalose/ H_2O mixture of highly symmetric in-phase oscillations indicative of a greater degree of crystallinity of this system at high concentration (from 2 to 20 water molecules for each disaccharide molecule). All these findings, supported by similar results obtained by Raman, infrared and DFT techniques, evidence the presence in the trehalose/ H_2O mixture of a more ordered nanoscale structure which, although able to adapt the trehalose/water complex to the irregular surface of the bio-structures, encapsulates them into more ‘rigid’ structures. This, in our opinion, accounts for the greater bioprotective effectiveness of trehalose.

has been inferred also from density and ultrasonic velocity findings. The analysis of the intramolecular HOH bending mode (see Fig. H15.3) supports this hypothesis. The presence of trehalose tends to modify more markedly the spectral mode of pure water which results in less intensity for the trehalose/ H_2O mixture in comparison with the sucrose/ H_2O mixture.

Evidence of a relevant modification in the hydrogen bond network of pure water emerged also by analysing the INS intermolecular librational band (see Fig. H15.4). The analysis of these spectra shows the presence of a more marked upshift in the position of the librational band of the trehalose/ H_2O mixture compared to that of the sucrose/ H_2O mixture at the same concentration. Due to the intermolecular nature of the vibrational properties observed, this upshift can be explained by hypothesising a stronger hydrogen-bond interaction in the trehalose mixture than in the sucrose/water

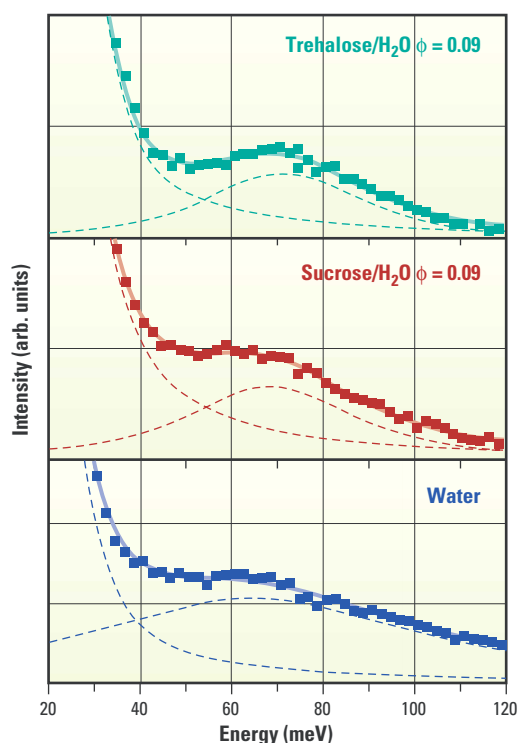


Fig. H15.4. Comparison of the intermolecular librational band of water, trehalose/ H_2O and sucrose/ H_2O mixtures at $\phi = 0.09$ at $T = 293 \text{ K}$. The Gaussian components and the resulting fitting functions are also shown.

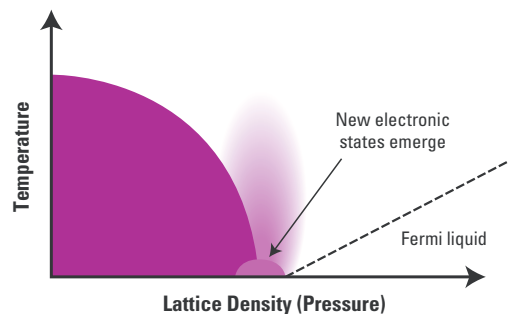
Quantum melting in magnetic metals

MJ Bull (ISIS), SS Saxena (University of Cambridge),
RA Sadykov (Institute for High Pressure Physics, Troitsk, Russia), CD Frost (ISIS)

A physical system that crosses the boundary between two phases changes its properties in a fundamental way, for example, it may melt or freeze. This macroscopic change is driven by microscopic fluctuations, but when the temperature of the system approaches absolute zero, all thermal fluctuations die out, prohibiting phase transitions in classical systems. However, their quantum-mechanical counterparts can show fundamentally different behaviour. Accessing the region in which these phase transitions can be studied is not trivial, requiring a combination of ultra-low temperatures and high pressures. Recent experiments on Prisma at ISIS have successfully begun to explore the quantum critical regime.

Classical phase transitions bring with them a change in entropy associated with the move from some state of order to one of less or more order when an external variable, such as temperature, is changed. The steam-water-ice phase transitions are a familiar example. By reducing the temperature of a system to absolute zero, and varying a second external parameter, a phase transition can be made to occur that does not involve a change of entropy (Fig. H16.1). The phase transition is from one ordered state to another ordered state and is driven by quantum rather than thermal fluctuations. Consequently, these quantum phase transitions have quite unusual characteristics, and represent an entirely new situation in the history of physics and science in general.

Fig. H16.1. Schematic illustration of a quantum critical point. As the lattice density is increased, either by external pressure or chemical substitutions, the system is driven from the magnetically ordered phase into the paramagnetic phase. If the ordering temperature is driven to zero, new physics is expected as quantum fluctuations become dominant in the vicinity of the critical point.



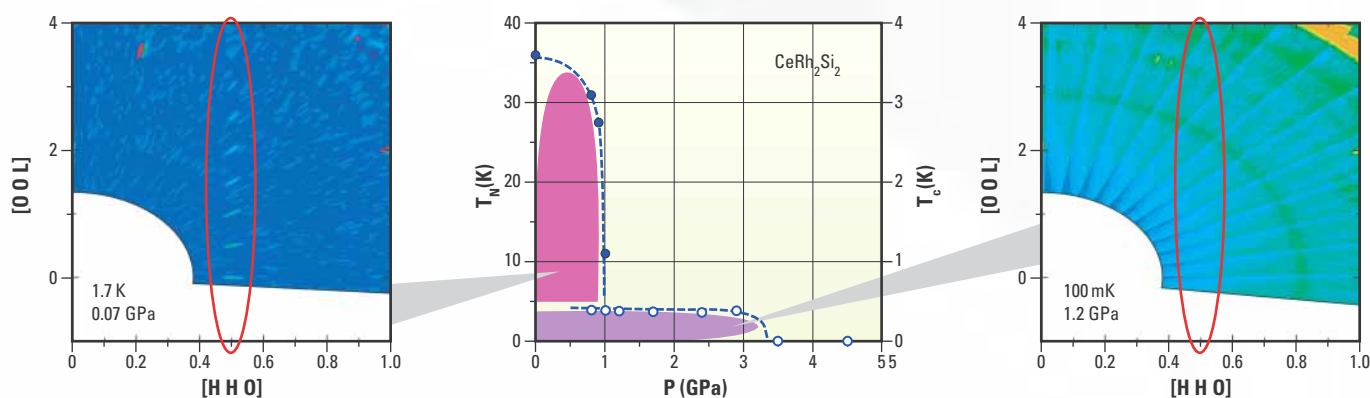
In classical systems, as the material passes into the ordered state, it goes through a remarkable stage known as the critical point, at which interactions with infinite range develop within the material. At a quantum critical point, the interactions have,

additionally, infinite range in time (the influence of one particle on another is felt long after it has passed), or may have infinite range in time and be localised in space – the exact opposite to what happens at a classical critical point.

It is therefore imperative to find examples in which this new paradigm can be explored and tested. Magnets offer an excellent testing ground as they are simple natural models, where we see nature finding its way to reduce entropy by ordering atomic spins into regular periodic structures below a characteristic temperature. If we increase the lattice density in the ordered state and lower the entropy of the system, the characteristic ordering temperature can be tuned continuously to zero, causing the quantum melting of the spin structure.

In the vicinity of the quantum critical region, it has been found that a number of well-understood physical models no longer apply. For example, in magnetic metals, low-temperature thermodynamic properties like resistivity (ρ), magnetic susceptibility (χ) and heat capacity (C) no longer seem to conform to the so-far extremely successful Fermi liquid description. This theory predicts convergence of thermodynamic parameters at low temperatures, eg. $C/T \propto \gamma$, $\rho = \rho_0 + AT^2$, $\chi^{-1} = \chi_0^{-1} + cT$. However, in the critical regime measurements of these thermodynamic parameters seem to diverge with $C/T \propto \ln T$, $\rho \propto T^{1+\epsilon}$ and $\chi^{-1} \propto T^\alpha$.

The phenomena driving these divergent properties in magnetic metals seems to be related to spin fluctuations which are brought about by a quenching of magnetic order. Apart from these divergent characteristics, a host of novel electronic states, including magnetically-mediated superconductivity, emerge. Here the hypothesis is that at low temperatures where the phonon modes are frozen out, and in clean samples where impurities are minimal, the 'glue' that binds conduction electrons into Cooper pairs is likely to be mediated by the magnetic fluctuations that are dominant in the vicinity of the quantum critical point.



Resistivity, magnetisation, heat capacity and related measurements, whilst extremely powerful, offer only an indirect probe of the microscopic quantum states, and are incapable of easily determining the magnetic properties within the superconducting state. Neutron scattering then becomes a powerful complementary technique, directly probing structural and spectroscopic properties of the microscopic quantum states, enabling us to measure the magnetic properties even when they seem to have been terminated by the onset of superconductivity.

We have begun our investigations of the quantum critical phase diagram in the superconducting region by using single crystal neutron diffraction. Measurements of resistivity and susceptibility under pressure have shown that when the antiferromagnetic transitions in CeRh_2Si_2 are tuned to zero by application of external pressure, the sample becomes superconducting (Fig. H16.2). However these measurements are not able to comment on the nature of the magnetic state within the superconducting bubble.

Recent upgrades to Prisma giving enhanced long wavelength flux, high signal-to-noise ratio and flexibility in controlling the incident beam optics to match the sample size, make it ideal for these measurements. Technical complications arise for the pressure cell design, since it must reach the high pressures required for a small but reasonably sized crystal in the

limited space of the inner vacuum jacket of the dilution refrigerator (Fig. H16.3).

Our measurements have been able to confirm that the magnetic state remains in tact below the superconducting transition below the critical pressure, whilst we find that the material loses magnetic order but remains superconducting above the critical pressure. The success of this international collaboration means that we are now well-placed to tackle inelastic measurements of the spin fluctuation spectrum in the quantum critical regime.

Fig. H16.2.

Reciprocal space maps of the (hhl) plane in single crystal CeRh_2Si_2 below and above P_c . The phase diagram is determined from resistivity and susceptibility measurements and combines data from the literature with our own measurements. T_c is around 400 mK; T_N is reduced from 36 K with increasing pressure.

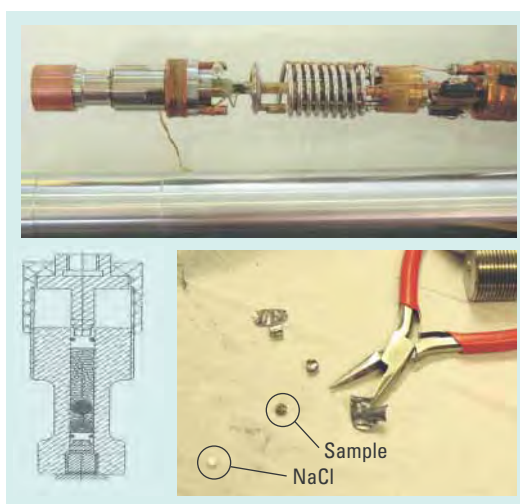


Fig. H16.3.

The large bore Ti/Zr + NiCrAl-alloys piston cell mounted on the dilution fridge insert. The cell can accept a crystal up to 4 mm in diameter and operates at pressures up to 1.5 GPa at low temperature.

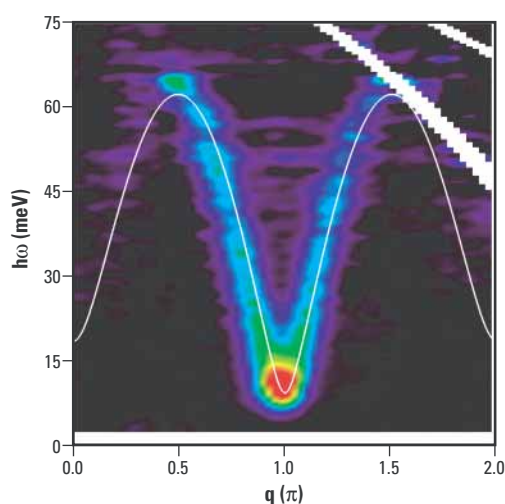
Spin polaron in a quantum spin liquid

Y Chen, C Broholm (Johns Hopkins University, USA), G Aeppli (NEC Research Institute, Princeton, USA), JF DiTusa (Louisiana State University, USA), TG Perring, CD Frost (ISIS), T Ito, K Oka (Electrotechnical Laboratory, Tsukuba, Japan), H Takagi (University of Tokyo Hongo, Japan)

Charge carriers doped into insulating transition metal oxides have interesting and potentially useful properties. Examples range from colossal magneto-resistance in manganites to high temperature superconductivity in cuprates. We have used neutron scattering to provide a detailed picture of magnetism around a charge carrier in a transition metal oxide. The hole nucleates an antiferromagnetic droplet with a central phase shift of π . Characteristic energy levels allow tentative identification of intra-polaron exchange interactions.

Rather than doping an antiferromagnetically ordered transition metal oxide, this experiment started from a quasi-one-dimensional material where quantum fluctuations produce a cooperative singlet ground state. The excitation spectrum of $Y_2\text{BaNiO}_5$ as measured on MAPS is shown in Fig. H17.1. Instead of gapless spin waves, there is evidence for an exciton that propagates coherently along spin chains. The threshold energy of 9 meV for exciton creation in the bulk leaves a clean spectral range to probe impurity dynamics.

Fig. H17.1. False colour image of the low temperature magnetic neutron scattering cross section from the antiferromagnetic spin-1 chain $Y_2\text{BaNiO}_5$. The solid line shows a fitted variational dispersion relation.



Holes are introduced by substituting Ca^{2+} for Y^{3+} in $Y_{2-x}\text{Ca}_x\text{BaNiO}_5$. While the material remains an insulator, the conductivity at any finite temperature increases dramatically indicating loosely bound holes. Reflectivity measurements show that holes populate super-exchange mediating oxygen atoms on NiO_6 octahedra. We have probed the spin structure of such holes through magnetic neutron

scattering using the MAPS spectrometer. A comparison of the low energy excitation spectrum for pure and doped $Y_{2-x}\text{Ca}_x\text{BaNiO}_5$ is shown in Fig. H17.2. Perpendicular cuts through the sub-gap feature in the doped spectrum are shown in Fig. H17.3. While the doubly peaked structure factor could indicate incommensurate correlations from partial hole ordering, samples with varying hole concentrations show no change in the location of the peaks, which indicates a single impurity effect. The energy spectrum is broad, indicating interactions between impurities, but there are also distinct maxima in the spectrum associated with intra-polaron excitations.

Analysis of the data starts from the valence bond solid model for the Haldane spin-1 chain. It breaks spin-1 degrees of freedom into two spin- $\frac{1}{2}$ degrees of freedom and pairs each of them into singlets with their counterparts on the nearest two neighbors. Consider the consequence of a defect that breaks a spin-chain in two. At the ends of the chain are un-paired spin- $\frac{1}{2}$ degrees of freedom. These have been observed through various experiments in spin-1 chain systems where magnetic ions are replaced by non-magnetic defects. Holes on super-exchange mediating oxygen atoms carry a spin- $\frac{1}{2}$ degree of freedom that re-links the chain end segments. Thus the minimal model is one of three spin- $\frac{1}{2}$ degrees of freedom that interact with each other. For an isolated hole the inversion symmetry about the hole ensures that there can be no scattering from the chain end spins for $q=\pi/d$, d being the Ni-spin spacing. This accounts for the dip in the scattering at this value of wave vector transfer. Finite spin polarization of a well localized hole would produce asymmetry between the two peaks, which is not observed. The finite scattering at $q=\pi/d$ is thus most likely associated with the lifting of inversion symmetry due to the finite density of randomly placed neighboring holes.

The proposed spin structure around a hole is indicated in Fig. H17.3. The corresponding scattering can be calculated

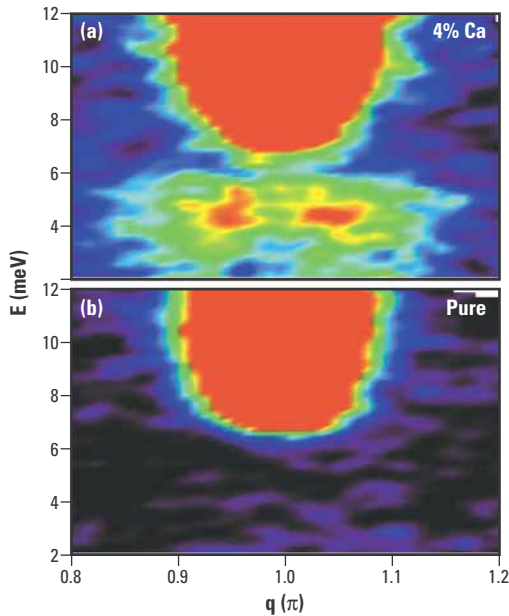


Fig. H17.2. Comparison of the low energy part of the magnetic excitation spectrum for pure and doped $Y_{2-x}Ca_xBaNiO_5$.

analytically and is in perfect agreement with the measured intensity distribution with the spatial extent of the antiferromagnetic spin-polarization cloud as the only non-trivial adjustable parameter. Holding this parameter fixed at a value close to the Haldane length, produces excellent fits for the samples studied so far, which cover the range from 4% to 14% calcium doping.

While the excellent agreement for the q -dependence cements the case for the spin-polaron structure, only the energy spectrum can provide details of intra-polaron energetics. Compared to Y_2BaNiO_5 , the 4% Ca doped sample shows spectral features at 4.5 meV and possibly 12.5 meV. Three spin- $\frac{1}{2}$ degrees of freedom with bilinear interactions have three levels: a ferromagnetic quartet and two antiferromagnetic doublets. If we neglect spin-space anisotropy, which is known to be small in this compound, there should be exactly two transitions from the ground state to excited states. All transition energies involve the exchange interaction energy between the hole and the chain-end spin, which is expected to

be of order the parent compound exchange energy of 25 meV. A possible assignment puts the ferromagnetic quartet lowest with a hole to chain-end exchange constant of $J=9$ meV and a chain-end to chain-end interaction constant, J' , less than 1 meV. Other assignments that do not involve spin space anisotropy seem unlikely as they imply a smaller value of J and a larger value of J' .

There are many similarities between the

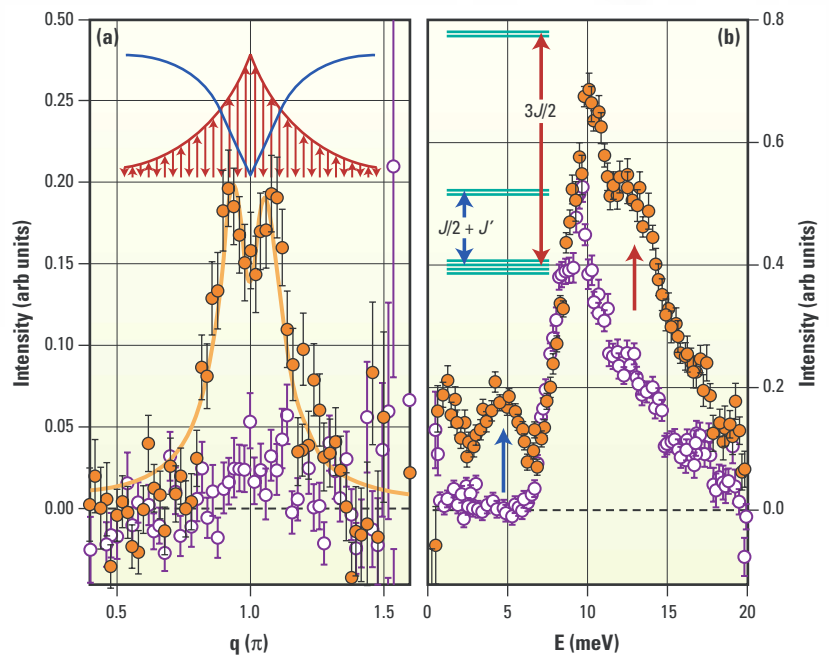


Fig. H17.3.

Perpendicular cuts along the (a) wave vector and (b) energy directions for pure (open circles) and doped (filled circles) $Y_{2-x}Ca_xBaNiO_5$. The line through the data in (a) corresponds to the model described in the text and the sketch shows the corresponding spin structure. The sketch in frame (b) shows the proposed impurity level scheme.

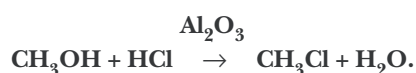
results derived here for a quasi-one-dimensional spin-1 chain through neutron scattering and those derived through NMR for the vacancy induced spin-polaron in high temperature superconductors. While it is unclear to what extent specific details of the spin-polaron in $Y_{2-x}Ca_xBaNiO_5$ can be generalized to other compounds, the experimental technique of neutron scattering that was used to analyze impurity structure and dynamics is applicable to many other systems, in particular when the impurity response lies within a gap in the bulk excitation spectrum.

The application of INS spectroscopy in heterogeneous catalysis: methyl chloride synthesis

D Lennon, DT Lundie (University of Glasgow), P Jones, CC Dudman (INEOS Chlor Ltd.), SM Bennington, SF Parker (ISIS)

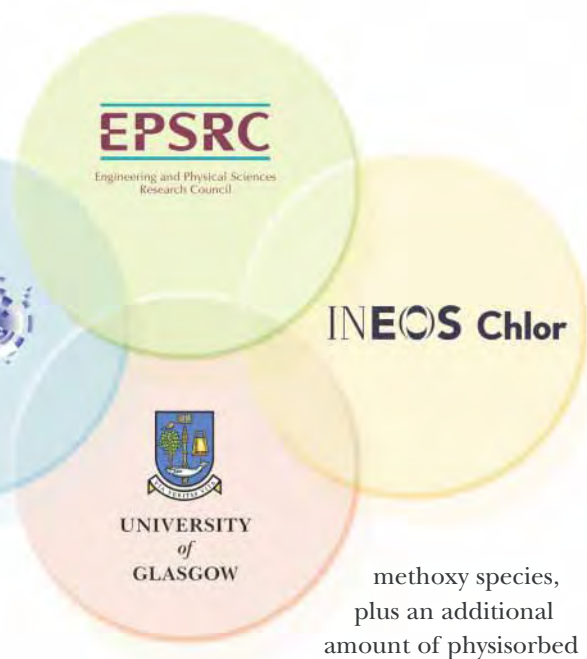
High selectivity heterogeneous catalysis is one of the tools available to the chemicals industry to reduce waste and minimise costs: Sustainable Development. An important part of the catalyst development cycle is confident identification of the molecular species present at the catalyst surface. This report describes a novel procedure of combining information from TOSCA and MARI to assist in the assignment of a surface species active in the production of methyl chloride.

Methyl chloride is an important industrial product, having a global annual capacity of ca. 900 ktonne. Its primary use is for the manufacture of more highly chlorinated materials such as dichloromethane and chloroform, which are used as solvents and reaction components, and it is also used in the production of silicone fluids and elastomers. It is usually manufactured by the reaction of methanol with hydrogen chloride over a suitable acid catalyst, such as alumina.



INEOS Chlor Ltd. produce methyl chloride at their Runcorn complex and are currently examining ways of optimising their methyl chloride synthesis catalysts.

In order to develop a site-specific reaction mechanism and a kinetic model for the overall process, one first needs to identify *all* the reagents present at the catalyst surface and the nature of their interactions with that surface. This information can be gleaned via *in situ* infrared spectroscopy. Fig. H18.1 shows the diffuse reflectance infrared spectrum that results from saturation of an activated alumina catalyst (surface area 235 m²g⁻¹) with methanol at 293 K. No features below 1400 cm⁻¹ are visible because of strong absorption by substrate phonon modes. The vibrational modes observed indicate the presence of the expected chemisorbed



methoxy species, plus an additional amount of physisorbed methanol. The latter occurs as a result of capillary condensation in the pore structure of the high surface area alumina. However, the origins of the strong band centred about 2600 cm⁻¹ (indicated with a question mark in Fig. H18.1), with features just resolvable at 2560 and 2610 cm⁻¹, was originally unknown. Despite a considerable literature of methanol adsorption on alumina, no definitive assignment for this feature could be found.

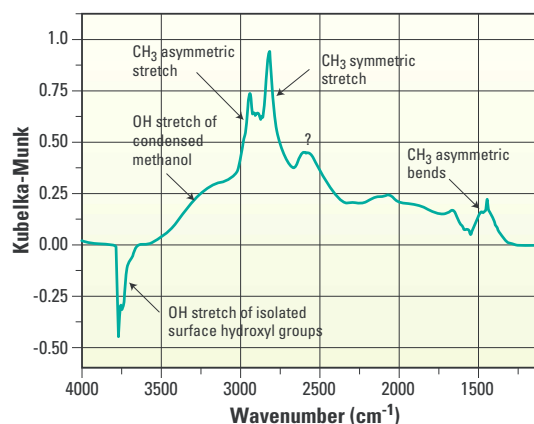


Fig. H18.1. Diffuse reflectance infrared spectrum of activated alumina saturated with methanol by sequential pulsing of methanol vapour at 293 K.

Fig. H18.2a shows the INS spectrum for a chemisorbed overlayer of methanol recorded using TOSCA. Extensive purging with helium ensured no presence of physisorbed methanol. The spectrum is characterised by the normally unseen CH_3 rocking mode at 1170 cm^{-1} and a CH_3 deformation mode at 1460 cm^{-1} . Fig H18.2a is assigned to chemisorbed methoxy species, formed from the dissociative adsorption of methanol with coordinatively unsaturated surface aluminum atoms. In order to confirm this assignment, the spectrum of $\text{Al}(\text{OCH}_3)_3$ was also recorded and this is shown in Fig. H18.2b. There is reasonable agreement with Fig. H18.2a, in particular the coincidence of bands at 90 , 1170 and 1460 cm^{-1} .

Was it possible that the unassigned 2600 cm^{-1} doublet in Fig. H18.1 might not be a fundamental of an unidentified species but, instead, arose as a combination of low frequency modes not accessible via optical spectroscopy? Unfortunately the resolution of the TOSCA spectrometer about 1500 cm^{-1} is insufficient to determine the fine structure of the methyl deformation at 1460 cm^{-1} . The issue was eventually resolved by application of the MARI neutron spectrometer. Fig. H18.3a shows the vibrational spectrum for the same coverage of methanol on alumina as presented in Fig. H18.2 recorded with an incident energy of 4034 cm^{-1} . The C-H stretching region is observed about 3000 cm^{-1} and the unidentified band seen in the infrared spectrum (Fig. H18.1) is reproduced at 2592 cm^{-1} . In order to optimise the resolution about the crucial methyl deformation/rock region of the spectrum, the incident energy was then changed to 1613 cm^{-1} and the resulting spectrum is presented in Fig. H18.3b. The methyl rocking mode is detected at 1165 cm^{-1} and the antisymmetric and symmetric methyl deformations are seen at 1460 and 1520 cm^{-1} respectively.

The surface species is now confirmed as adsorbed methoxy, with the 2560 cm^{-1} band assigned to a combination of the methyl rock

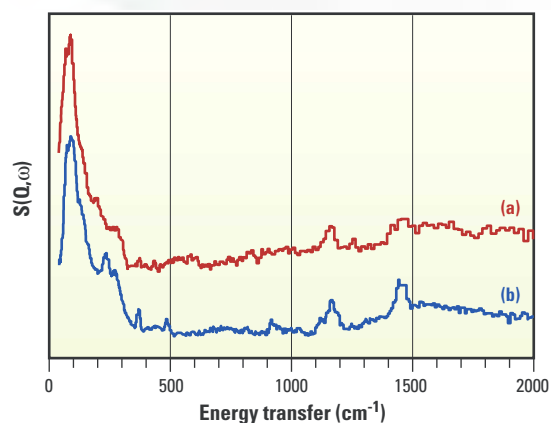


Fig. H18.2. INS spectra (TOSCA) recorded at 20 K of (a) activated $\text{Al}_2\text{O}_3 + 1.12\text{ mmol CH}_3\text{OH g}^{-1}$ adsorbed at 300 K and (b) $\text{Al}(\text{OCH}_3)_3$

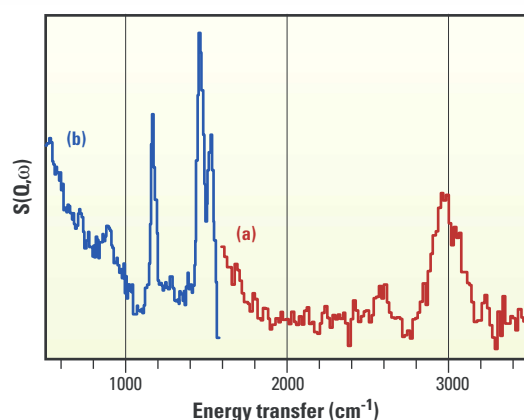


Fig. H18.3. The INS spectrum at 20 K of activated $\text{Al}_2\text{O}_3 + 1.12\text{ mmol CH}_3\text{OH g}^{-1}$ adsorbed at 300 K recorded using MARI. (a) $1600 - 3500\text{ cm}^{-1}$, incident energy 4034 cm^{-1} (red); (b) $500 - 1600\text{ cm}^{-1}$, incident energy 1613 cm^{-1} (blue).

(1165 cm^{-1}) with the antisymmetric methyl deformation (E mode, 1460 cm^{-1}). Likewise, the 2610 cm^{-1} band is assigned to a combination of the methyl rock (1165 cm^{-1}) and the symmetric methyl deformation (A mode, 1520 cm^{-1}).

This approach of combining information from the TOSCA and MARI neutron scattering spectrometers to solve problems in surface chemistry is novel. The resulting spectra have been used to understand the complex *in situ* infrared spectrum of the reaction of a reagent over a high surface area industrial grade catalyst. It is through an improved awareness of reagent-catalyst interactions that increased efficiencies of industrial chemical processes can be recognized and realised.

Hydrogen spillover on carbon-supported metal catalysts

PCH Mitchell (Reading University), AJ Ramirez-Cuesta, SF Parker, J Tomkinson (ISIS)

Inelastic neutron scattering (INS) on TOSCA provides unique information on hydrogenic species in catalysts. Spillover hydrogen consists of hydrogen atoms diffused on to a catalyst support following dissociation of adsorbed dihydrogen at a metal centre. For the first time, spillover hydrogen atoms on carbon-supported catalysts have been detected directly. Surface vibrational modes of the substrate are amplified by H atoms and are observed as H riding modes in the INS spectra of the H-dosed catalysts. Spillover H atoms can be exploited as surface probes of dispersed catalyst particles, the H monitored by INS.

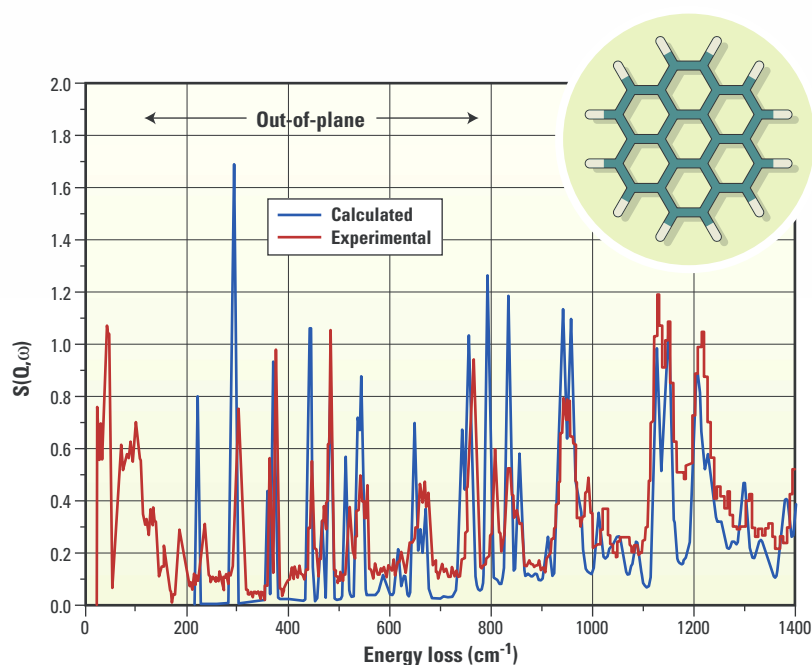


Fig. H19.1. INS spectrum of coronene, a planar polycyclic hydrocarbon (structure shown in the inset) used as a model for a graphite layer.

Hydrogen spillover arises in hydrogen-catalysed reactions on supported metal catalysts. Dihydrogen molecules dissociate on the metal part of the catalyst. Some hydrogen atoms remain attached to the metal, whilst others diffuse to the support and are said to *spillover*. Spillover hydrogen has often been inferred from hydrogen adsorption and reactivity studies. Now, using inelastic neutron scattering on TOSCA, we have observed directly, for the first time, spillover hydrogen atoms on Pt, Ru and PtRu carbon-supported catalysts. These are fuel-cell catalysts made and provided by Johnson Matthey.

We carried out three sets of experiments on TOSCA. First coronene, used as a molecular model of a graphite layer (Fig. H19.1). The coronene INS spectrum was measured and calculated, and the vibrational modes identifying atomic displacements were assigned. Secondly, fast hydrogen uptake at 293 K. In this case, the catalysts were loaded into a circular steel sample cell and dosed with dihydrogen at 293 K. Uptake was fast and complete after 10 - 30 min. Thirdly, slow hydrogen uptake and diffusion at 500 K. The catalysts were heated to 500 K and dosed with dihydrogen over a period of days. Extra dihydrogen was taken up as spillover hydrogen diffused over the carbon support. We used a specially designed annular cell, which was loaded with graphite. Pelletted catalyst was added around the inside edge of the cell which was outside of the neutron beam. Thus, neutrons were scattered from graphite in the centre of the cell but not from the outer ring of catalyst.

Coronene INS spectra are shown in Fig. H19.1. The vibrational modes were calculated *ab initio* with GAUSSIAN 98. The eigenvalues and eigenvectors were input to the a-CLIMAX program to generate the INS spectrum.

INS spectra of the fast-H-dosed catalysts and of H-free graphite (Fig.19.2) show the scattering due only to the H dosing. The patterns of scattering peaks from the catalysts and the graphite are remarkably similar; see the vertical lines labelled HRC. We interpret these peaks as riding modes of H on carbon. The H atoms move in time with the vibrations of the surface carbon atoms (as a rider moves with her horse); they are said to ride on the support. The surface modes, displacements of the carbon atoms, are amplified by neutrons scattered by surface-bound H atoms. The presence of these riding modes is direct, unequivocal evidence for spillover H on the carbon support. By analogy with the coronene INS spectrum, we can identify these modes as

out-of-plane displacements, representing H atoms bound at the edges of graphitic regions of the carbon particles of the catalysts. There is no amplification of the higher wavenumber in-plane ring nodes, demonstrating that H is absent from the basal plane. Additionally we observe H-Pt (or H-Ru) riding modes (Fig. H19.2) at wavenumbers close to the lattice vibrations of Pt metal and Pt black. Thus through the H-amplification of the riding modes we can observe H on the metal part and spillover H on the carbon support part of the catalysts.

Fig. H19.3. shows the INS spectra of spillover H on graphite after slow H-dosing. Again we observe H-C riding modes. But, in addition, we observe a stepwise increase of scattering intensity between 500 and 1000 cm^{-1} leading to a continuum at energy transfer greater than 1000 cm^{-1} typical of scattering from a layer of weakly bound, mobile H atoms. Evidently, as a result of the slow, higher temperature H-dosing of the catalyst, spillover H atoms have diffused over the carbon support forming a layer of H atoms.

These experiments have directly shown the presence of spillover hydrogen on the carbon support of these fuel cell catalysts but they are likely to have a wider, more general impact on surface science. We can study surface vibrational states through the H riding modes – the H-amplification effect. We can thus exploit H atoms, generated, for example, by spillover, as surface probes of dispersed catalyst particles, monitoring the H by INS. We are pursuing this theme.

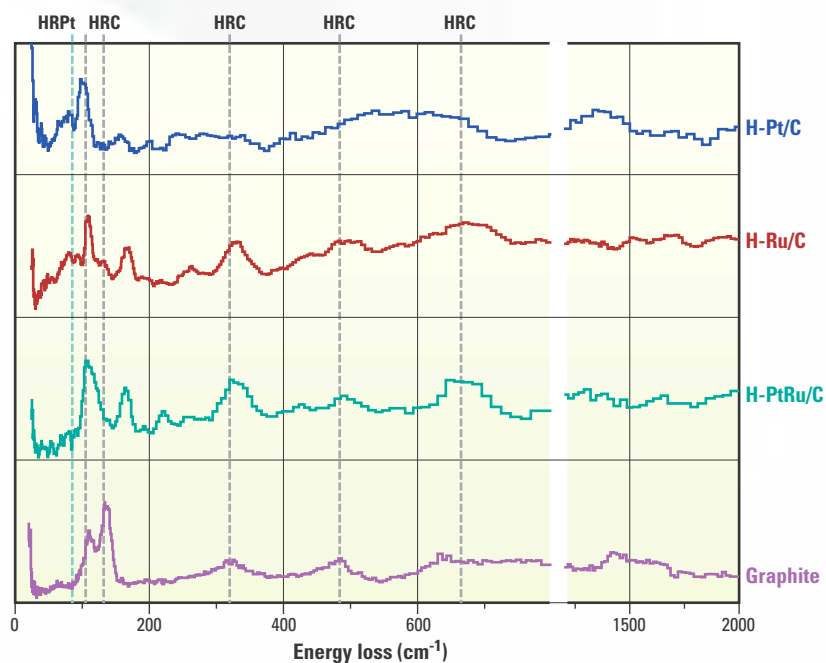


Fig. H19.2. INS spectra of graphite and of H on the carbon-supported catalysts after dosing with H_2 for no more than 30 min (background – steel container plus catalyst before hydrogen dosing – subtracted) showing peak positions and principal assignments: HRPt, H riding on Pt; HRC, H riding on carbon.

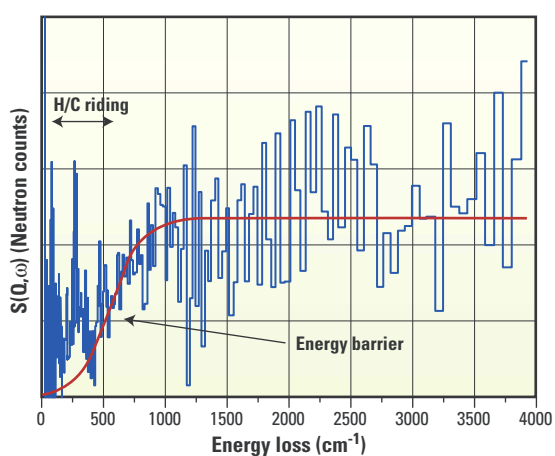


Fig. H19.3. INS of spillover H diffused to the carbon support following H_2 dissociation on a Pt/C catalyst. Neutron scattering vs energy loss from carbon in the central region of the annular cell: difference spectrum (INS of after H_2 dosing with hydrogen at 500 K for 36 h less INS before dosing).

Pressure effect on water dynamics in TBA-water mixtures

V Calandrini, A Deriu (University of Parma and INFM, Italy),
G Onori, A Paciaroni (University of Perugia and INFM, Italy)

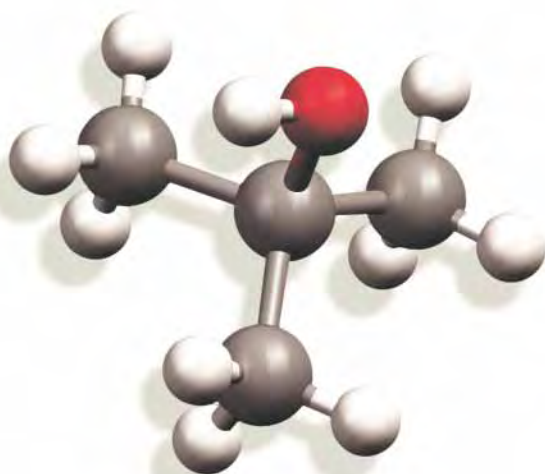
Thermodynamic and spectroscopic results, along with simulation studies, suggest that the solvation of a-polar groups (hydrophobic hydration) increases the amount of order in the random, transient H-bond network of the coordinated water molecules, and reduces their mobility. Such hydrophobic effects are of wide interest, water being the basis of all biologically important fluids. Following our earlier work on hydrophobic hydration and interaction in water/alcohol mixtures, we report here a QENS investigation, carried out on IRIS, on the effect of pressure on water diffusivity in a dilute solution of tert-butyl alcohol. The observed behaviour is described in terms of pressure-induced distortions of the H-bonded network of liquid water, whose structure is enhanced in the presence of TBA molecules.

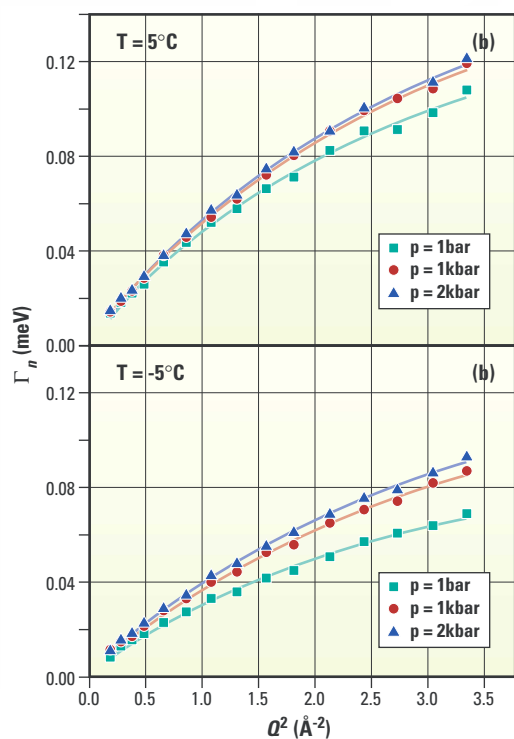
In recent years there has been an increasing interest in the study of hydrophobic effects in connection to the very important role they play in protein folding, micelle formation and in the stability of biological membranes. Hydrophobic effects arise from basic interactions between hydrophobic species and water molecules (hydrophobic hydration), as well as from the solvent-mediated interactions among hydrophobic groups (hydrophobic interactions). The series of monohydric alcohols is the most commonly investigated among the systems featuring hydrophobic effects. Within this series, the tert-butyl alcohol (TBA, Fig. H20.1) has the largest hydrophobic group, i.e., it is the most hydrophobic molecule

among the low-weight water-soluble alcohols. For these reasons, TBA appears to be the ideal candidate to investigate possible variations in the structural and dynamical properties of water near a-polar solutes.

Simulation studies indicate that the structure of water is significantly enhanced in the presence of TBA, particularly as the concentration is increased. However, the interpretation of experimental data in terms of water structure is a frequent and controversial question. Consistent with the indication of the increase in structure, computer simulation results suggest also a retarded solvent molecular mobility in the water shell affected by hydrophobic interactions. Despite much thermodynamic data, only very few investigations of the diffusive dynamics in TBA/water systems exist. Dielectric and NMR data have shown, in agreement with simulation results, that the diffusion coefficient of water molecules decreases with the addition of TBA molecules. We have carried out a QENS investigation on the pressure dependence of water diffusivity in TBA/water mixture at a 0.02 molar fraction of TBA. Among the most pronounced anomalies in the dynamic properties of liquid water, there is an increase of the translational mobility with initial compression that is observed as an increase in the self-diffusion coefficient especially in the supercooled regime. Since this anomaly is commonly associated with a pressure-induced decrease in the structural association of water molecules, high-pressure diffusion studies in dilute solutions of TBA can give information about hydrophobic hydration in this system. The aim of our study is to investigate how pressure affects hydrophobic hydration by comparing the pressure dependence of water diffusivity in the TBA/water solutions to that of pure water. The QENS experiment on TBA/water solution was performed at fixed solute concentration (0.02 molar fraction) and varying the pressure from 1 to 2000 bar at two temperatures ($T = -5$ and $T = 5$ °C). To this purpose we built a special cell, made up from

Fig. H20.1.
The TBA molecule.



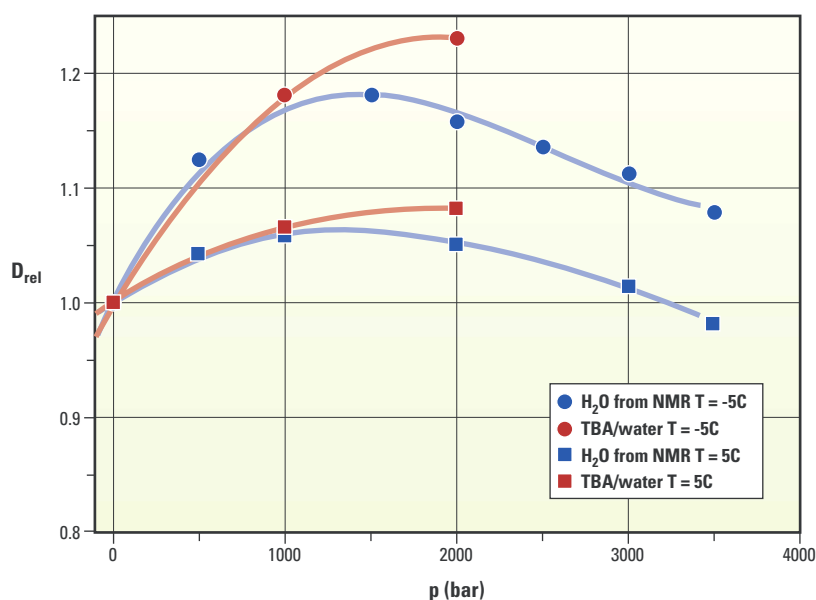


stainless-steel capillaries (inner diameter 0.4 mm), capable of withstanding pressures up to ~4 kbar. We made use of perdeuterated solutes in order to minimise the incoherent scattering from TBA. The QENS spectra can therefore be related to the self-dynamic structure factor of water protons. The simplest approach to the analysis of incoherent QENS spectra of H_2O is to assume a scattering law with two Lorentzian contributions: a narrower one (with width Γ_n) describing the diffusive motion of the water centre of mass and a broader one (with width Γ_b) describing the 'local' proton dynamics within subsequent diffusive steps. The Q -dependence of the Γ_n can be described by a random jump model ($\Gamma_n = (DQ^2/(1 + D\tau_0 Q^2))$). In this framework, the width Γ_n depends on two microscopic parameters: the translational diffusion coefficient, D , and the residence time, t_0 , between subsequent jumps. The dependence of Γ_n on Q^2 is shown in Fig. H20.2. For both temperatures the diffusion coefficient, D , increases with increasing pressure and this

effect becomes more relevant at the lowest temperature. Fig. H20.3 shows the relative diffusion coefficients. The corresponding values for pure water, derived from NMR experiments, are also shown for comparison. The maxima found in the self-diffusion coefficient for water at low temperature ($T = 300$ K) are well known. This phenomenon is due to a competition between compression, which generally slows down translational motion, and the effect of pressure on the random, transient hydrogen-bonded network of liquid water, which increases water mobility. Our data indicate that, on increasing pressure, the diffusion coefficient of the TBA/water mixture exhibits a larger relative increase than that of pure water under the same conditions. The extent of this effect increases on decreasing temperature. This is consistent with the concept that water is more structured in the TBA solutions at this composition and that this structural effect is more important at low temperatures.

Fig. H20.2. Q -dependence of the width, Γ_n , of the narrow Lorentzian component measured at $T = 5^\circ\text{C}$ (a) and $T = -5^\circ\text{C}$ (b) at different pressures. The solid lines are fits to a random jump model.

Fig. H20.3. Relative diffusion coefficients $D_{\text{rel}} = D(p)/D(1 \text{ bar})$ for water in water-TBA solutions compared with those for pure water at $T = 5^\circ\text{C}$ and -5°C , vs. pressure.



Measurement of the proton wave function in hydrogen bonds by eV neutron scattering

GF Reiter (University of Houston, USA), J Mayers (ISIS), P Platzman (Bell Labs, New Jersey, USA)

The motion of the proton in hydrogen bonds is known primarily from theoretical calculations, although the anharmonicity and the effects of surrounding ions, critical for the configurational changes of large molecules that are essential for biological processes, is difficult to calculate reliably. Experimental information on the anharmonicity of the motion has previously come primarily from the measurement of deviations in vibrational spectra from harmonic series, and does not provide a stringent test of the theories. Recent progress in instrumentation and data analysis on the VESUVIO spectrometer has made possible direct measurement of the momentum distribution of the proton using neutron Compton scattering (NCS).

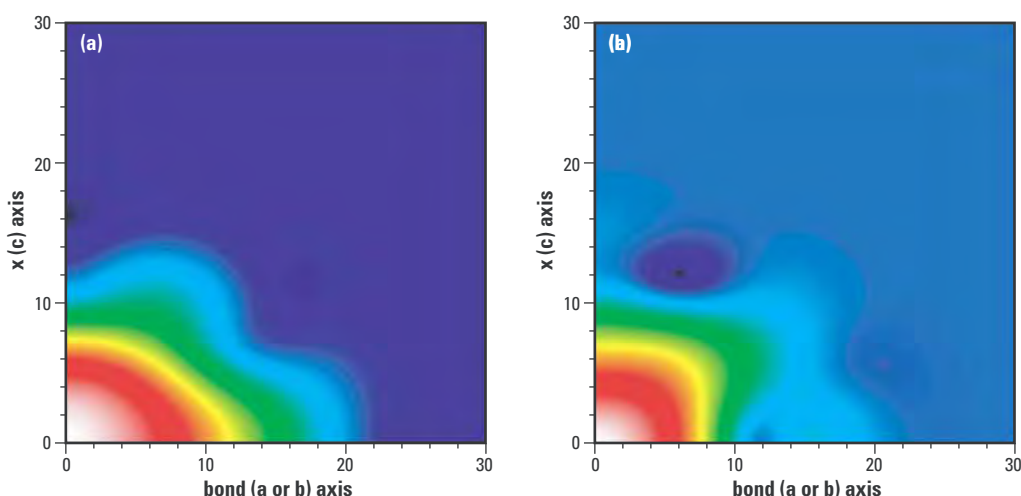
The measurement of proton momentum distributions by neutron scattering is analogous to the measurement of electron momentum distributions by Compton scattering and relies upon the fact that if the momentum transfer is large the neutron interacts with a single atom, with conservation of momentum and kinetic energy. Thus from a measurement of the momentum and energy change of the neutron, the momentum of the proton before the collision can be determined. The momentum distribution $n(\vec{p})$ of the proton is directly related to its wave function $\Psi(\vec{r})$ by standard quantum mechanics, and the determination of $\Psi(\vec{r})$ from $n(\vec{p})$ is a formally identical problem to the determination of real space structure from a diffraction pattern. If $n(\vec{p})$ is known for a

symmetric potential, then the phase problem is trivial and in principle both the proton wave function and the exact form of the potential energy well in which the proton sits can be directly reconstructed in a model independent way.

The method has been applied to the study of the ferroelectric transition in KH_2PO_4 which occurs at $T_c=124$ K. It is known from neutron diffraction measurements that the protons are equally likely to be in either of two positions in the hydrogen bond above the ferroelectric phase transition, where the structure is tetragonal, and are nearly entirely in one site below T_c , where the structure is orthorhombic. What has not been known is whether they are tunnelling between the two equivalent sites, or are localised in one or the other of the two sites and simply disordered, above the transition. The data collected on VESUVIO provides strong evidence that tunnelling is occurring. Fig. H21.1 shows the momentum distribution of the proton in a single plane below (90 K) and just above (130 K) the ferroelectric transition, whilst Fig. H21.2 shows a section through this distribution along the bond axis at the two temperatures. We see that overall, there is considerable narrowing of the distribution in the high temperature phase, indicating an increase in the length along the bond over

Fig. H21.1.

The momentum distribution in the xz plane for a single hydrogen bond below ($T=90$ K) and just above ($T=130$ K) the ferroelectric transition at $T=124$ K. Note the overall narrowing of the distribution in the $T=130$ K data, and the additional structure along the hydrogen bond (z axis) where the distribution has a zero. There is very little change along the x axis.



which the spatial wave function is coherent. The prominent feature of the high temperature distribution, the zero and the subsequent oscillation, is precisely what one would expect for a spatial wave-function that was coherent over both sites, with the position of the zero being determined by the separation of the sites.

The effective Born-Oppenheimer potential that corresponds to the measured momentum distribution along the bond at $T=130$ K is shown in Fig. H21.3 and is consistent with previous measurements using other techniques. For example neutron diffraction gives a separation of the minima of the potential as 0.36 Å, whereas we find 0.31 Å. The horizontal lines give the first four energy levels for the measured potential. Although this potential is quite different from that inferred from infrared absorption data, the transition energies obtained from the potential reconstructed from the VESUVIO data are substantially the same. For example the 0 - 3 transition has an energy measured by infrared spectroscopy as 4600 cm^{-1} , whereas we obtain 5088 cm^{-1} . For the 1 - 2 transition, infrared measurements give 2260 cm^{-1} while we obtain 2039 cm^{-1} .

The measurements show that neutron Compton scattering is now sufficiently sensitive to provide a detailed measurement of the proton momentum distribution. This sensitivity opens up the possibility of studying the effect of the systematic variation of the surrounding ligands on the dynamics of hydrogen bonds. The knowledge gained could then be used to identify the best models and ab-initio approximation schemes, and to infer the behaviour of the bonds in environments where the measurements can not be done because there are too many inequivalent protons, such as in DNA or proteins

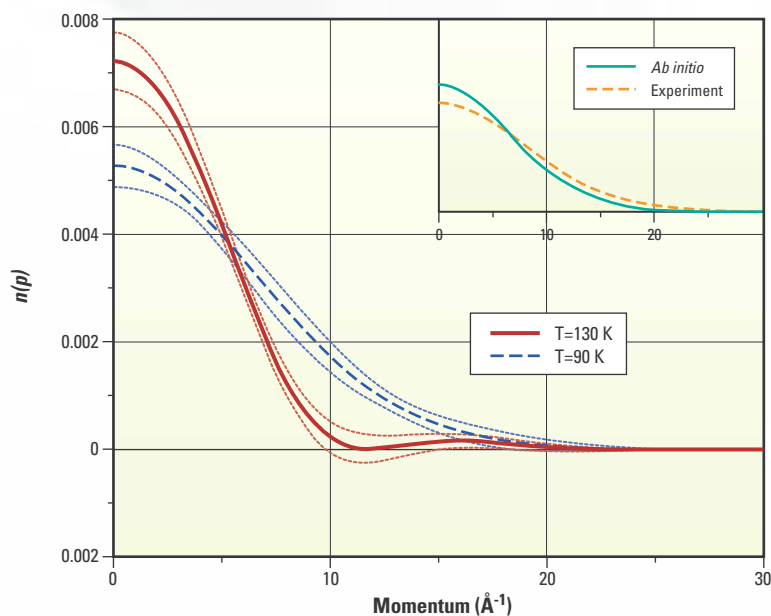


Fig. H21.2. The momentum distribution along the bond axis for temperatures just above and below the structural phase transition at 124 K. The dotted curves surrounding the heavy lines are one standard deviation error markers. The inset is a comparison of the measured momentum distribution at $T=90$ K with a recent calculation in which an ab-initio one particle potential along the bond was used to calculate the momentum distribution from the one dimensional Schrödinger equation.

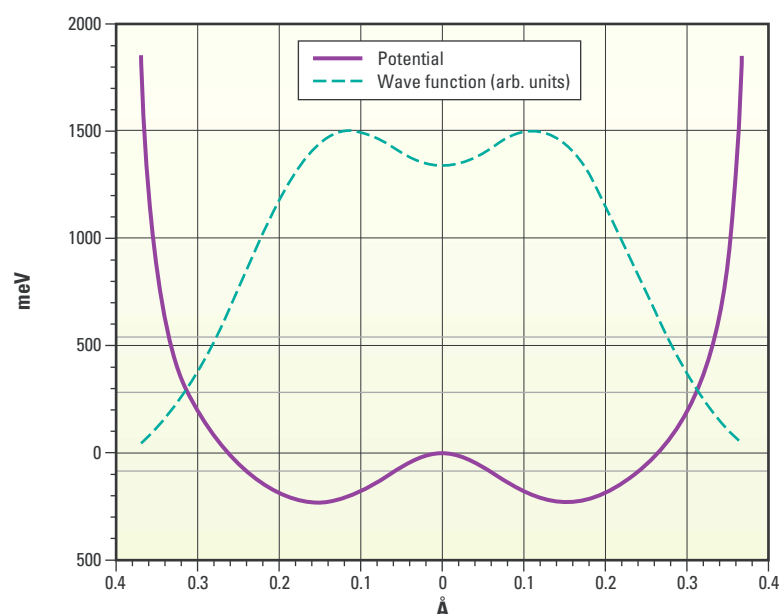


Fig. H21.3. The effective Born-Oppenheimer potential that corresponds to the measured momentum distribution along the bond at $T=130$ K.

Magnetic correlations vs anisotropic Kondo fluctuations

EA Goremychkin, R Osborn (Argonne National Laboratory),
BD Rainford, CA Scott (Southampton University), PJC King (ISIS).

Heavy fermions are metals whose conduction electrons are so strongly hybridized with the more localised f-electrons that they appear to have an extremely high effective mass. They are normally unstable at low temperature to the development of long-range order, either superconducting or magnetic. However, it is unclear what happens in CeAl₃, one of the canonical heavy fermion compounds. Muon spin relaxation (μ SR) shows evidence of static magnetic correlations, but they do not undergo a conventional magnetic phase transition with increasing temperature. Instead, they are washed out by the collapse of a spin gap, a single-ion effect predicted by the Anisotropic Kondo Model.

Although it is nearly thirty years since CeAl₃ was identified as the first heavy fermion compound, its low-temperature state is still not established. When a peak was observed in the specific heat and magnetic susceptibility of CeAl₃, magnetic order was strongly suspected.

The peaks become even stronger with lanthanum doping (see the inset to Fig. 22.1), and it was natural to assume that magnetism was being stabilized by the reduced hybridisation resulting from the expansion of the lattice, although neutron diffraction has never shown evidence of magnetic Bragg peaks in any of these compounds.

Muon spin relaxation measurements do indeed show clear evidence of static magnetic correlations in both pure CeAl₃ and compounds with less than 10% lanthanum-doping. In a magnetically ordered phase, muons precess in the static internal field of the sample. In zero-field μ SR, this leads to well-defined oscillations of the muon spin depolarisation with a frequency that is proportional to the ordered moment, in addition to the exponential relaxation caused by spin fluctuations. We modelled the muon depolarization by the sum of two components, one magnetic and the other nuclear. The need for two components could mean either that there are two muon sites in these samples, one dominated by nuclear and the other by magnetic relaxation, or that the samples are magnetically inhomogeneous. At least 70% of each sample shows oscillatory behaviour.

Fig. H22.1 shows that muon oscillations can be seen for lanthanum concentrations of 0, 5% and 10%, but they could not be resolved in a 20%-doped sample. Note that, whereas the specific heat peaks become stronger and sharper with increasing lanthanum content, the magnetic oscillations become more strongly damped. However, it is the temperature dependence that shows the most striking anomalies. Fig. H22.2 shows that the oscillation frequency is nearly temperature-independent in the 5%-doped compound up to 1.5 K even though the specific heat peak is at 1.3 K. In a conventional magnet, the frequency should fall to zero, in a manner similar to the mean field curve shown as the dotted line. Instead, the specific heat peak marks the temperature at which the transverse damping diverges, suggesting an increasing spread of magnetic

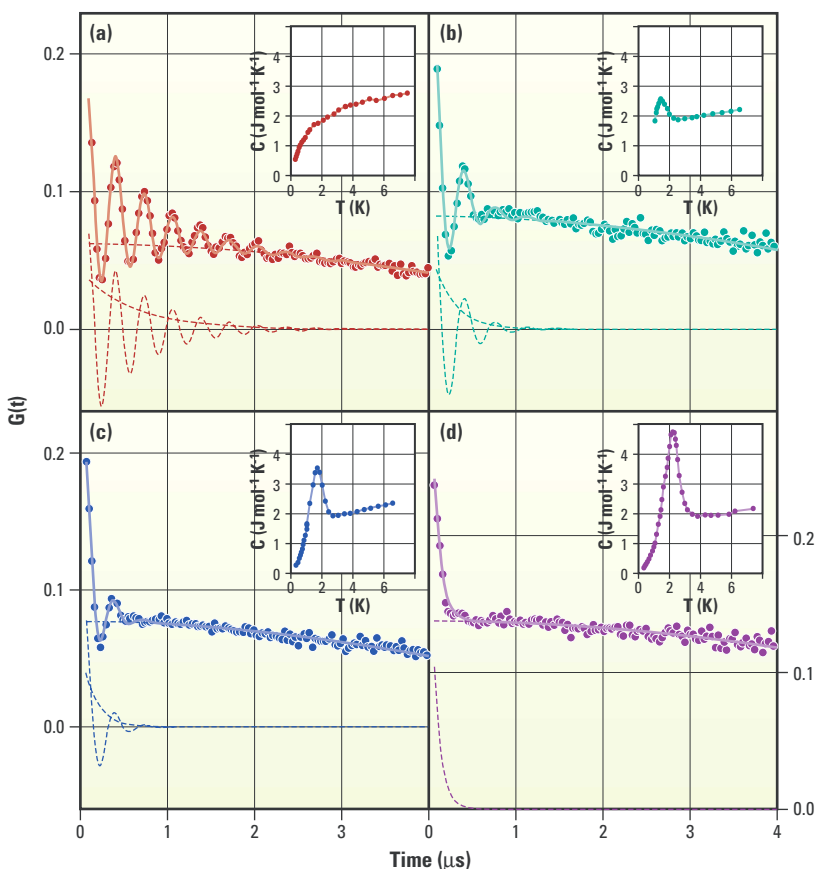


Fig. H22.1. Zero field muon spin depolarisation in Ce_{1-x}La_xAl₃ with (a) $x = 0$ at 50 mK, (b) $x = 0.05$ at 100 mK, (c) $x = 0.1$ at 50 mK, and (d) $x = 0.2$ at 1.6 K. The solid lines are fits whose three components (transverse and longitudinal magnetic, and nuclear) are shown as dashed lines. The insets show the specific heat data from B. Andraka et al Phys. Rev. B **52**, 9462 (1995).

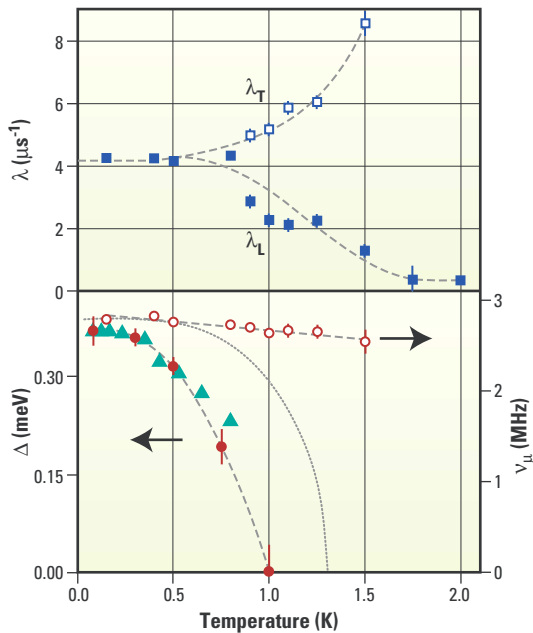


Fig. H22.2. Temperature dependence of the muon spin depolarisation and the excitation energy measured with inelastic neutron scattering. The open and filled squares denote the transverse and longitudinal muon damping coefficients λ_T , λ_L (below 1 K, $\lambda_T = \lambda_L$), the open circles denote the muon precession frequency and the filled circles denote the excitation energy of the magnetic response, Δ . The triangles are the theoretical values of Δ derived from an inelastic Lorentzian fit to the NRG calculations of $S(\omega)$. The dashed lines are guides to the eye. The dotted line shows the mean field behaviour of an ordered moment with a critical temperature of 1.3 K.

moments, and the longitudinal damping falls to zero. At higher temperatures, the hybridization-induced, or Kondo, spin fluctuations are too rapid for the muons to follow.

We have proposed that the resolution to this discrepant behaviour is provided by the Anisotropic Kondo Model (AKM). The strong magnetic anisotropy of CeAl_3 causes the hybridization interactions that lead to Kondo spin fluctuations to be very anisotropic. It has been shown theoretically that this can lead to a splitting of the magnetic doublet ground state into two non-magnetic singlets. At high temperature, they cannot be resolved because of the strong Kondo damping, so the magnetic fluctuations, observed by inelastic neutron scattering, are quasielastic. However, at low

temperature, the AKM predicts that a gap opens up in the magnetic spectrum, and that neutron scattering can resolve the tunneling transitions between the two singlet levels (Fig. H22.3). This is what we have observed in measurements on IN6 at the ILL.

Within this model, the static magnetic correlations could result from weak intersite coupling inducing a small magnetic moment in the singlet ground state. However, when the spin gap falls to zero, the low-frequency spin fluctuations are too strong to sustain magnetic order, and the static moments become washed out. Although strong, sharp specific heat peaks normally denote a cooperative phase transition, it appears that, in this case at least, the physics is purely local.

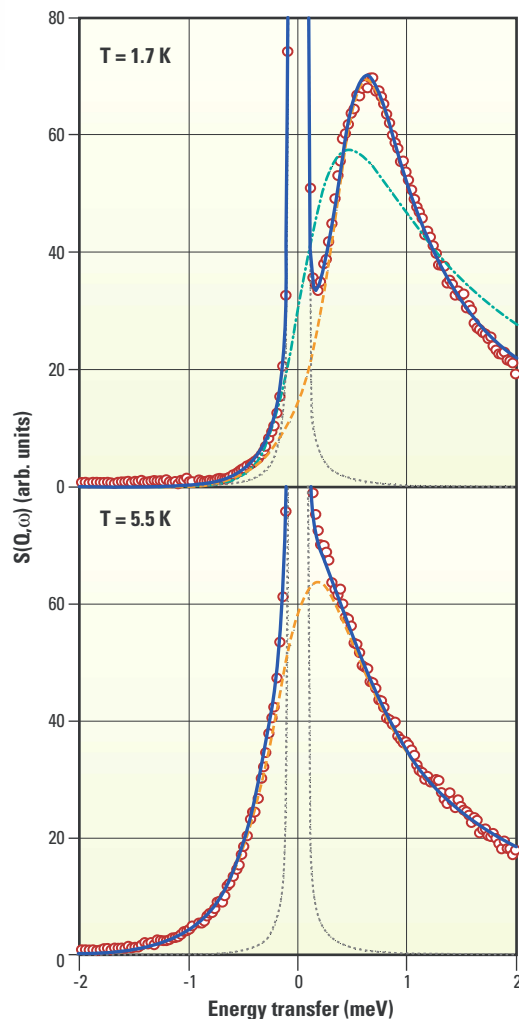


Fig. H22.3. Inelastic neutron scattering data (open circles) from $\text{Ce}_{0.2}\text{La}_{0.8}\text{Al}_3$ measured on the IN6 spectrometer. The solid line is the sum of the magnetic response (dashed line) and the elastic nuclear scattering (dotted line). The dash-dotted line is the best fit at $T = 1.7$ K to a quasielastic line shape.

Vortex motion in type-II superconductors probed by Muon Spin Rotation

D Charalambous, PG Kealey, EM Forgan, MW Long, D Fort, D Ucko (*Birmingham University*), TM Riseman (*NIST, USA*), AJ Drew, UK Divakar, SL Lee (*St. Andrews University*), F Ogrin (*Exeter University*), R. Khasanov (*PSI & Zürich, Switzerland*), C Goupil (*Caen, France*), PJC King, AD Hillier, SP Cottrell (*ISIS*), R Cubitt, CD Dewhurst (*ILL*).

The vortex lattice in type-II superconductors provides an ideal system for the study of the dynamics of interacting systems in the presence of disorder. The phase diagram of this system can be explored by changing the applied magnetic field, temperature, driving force or by using different samples with different degrees of pinning. The underlying physics of vortex motion is thus very rich, and brings together many diverse concepts from almost all branches of Physics. We have carried out detailed muon spin rotation (μ SR) measurements on the moving vortex lattice (VL) in Pb-In superconducting alloys. We observe motional narrowing of the μ SR lineshape $p(B)$ which is consistent with a range of orientations of the moving VL. Small-Angle Neutron Scattering (SANS) results confirm our observations.

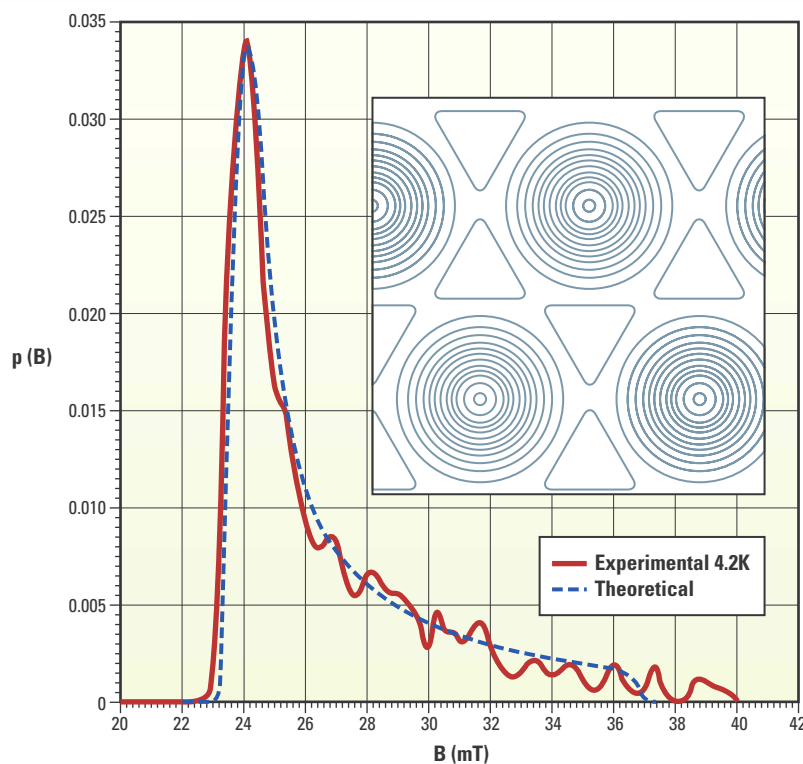


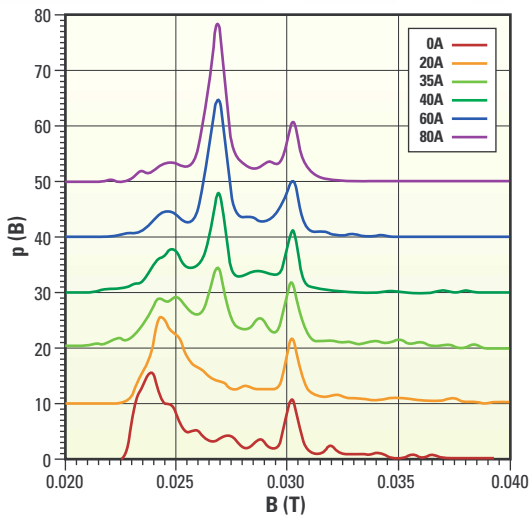
Fig H23.1. Experimental and theoretical $p(B)$ lineshapes for a stationary VL, with field contours as shown in the inset. The calculated $p(B)$ was obtained from a solution to the Ginzburg-Landau equations for $\kappa = 5.2$ and an average field of 27 mT.

When an electric current is applied to a type-II superconductor in the mixed state, the vortices experience a Lorentz force proportional to the applied magnetic field and the current density. In a typical superconducting sample, vortices are pinned by various forms of disorder, such as sample inhomogeneities and dislocations. Hence, no vortex motion takes place until the Lorentz force is large enough to exceed the pinning force. When this happens, the vortices flow and a flux-flow voltage appears across the sample, perpendicular to the direction of vortex motion. Energy dissipation then arises from relaxation of the order parameter as well as from the presence of normal currents.

We have carried out detailed μ SR measurements from the moving VL in Pb-In superconducting alloys. Pb-In provides an ideal system for studying the dynamics of the mixed state: its critical temperature is 7 K and it has an upper critical field of just 0.27 T at liquid helium temperature. These alloys can be ‘engineered’ to give low pinning and hence a low critical current (the current required to overcome the pinning force and set the vortices in motion).

Our measurements were performed at ISIS, where the μ SR beamline provides short pulses of longitudinally polarised muons to which the transport current was synchronised. The use of pulsed currents reduced ohmic heating as well as enabling us to check that there was negligible heating of the sample during the current pulse, which we could shift relative to the muon pulse. Changes in the μ SR lineshape were observed only when the muons were in the sample at the same time as the current pulse, implying that these changes were due to vortex motion alone.

The VL gives rise to a characteristic distribution of values of field $p(B)$ within the sample, which is detected as a distribution of muon precession frequencies. Fig. H23.1 shows the $p(B)$ lineshape obtained from μ SR



measurements in a stationary VL, along with a theoretical lineshape calculated from a solution to the Ginzburg-Landau equations. The inset shows a contour map of the theoretical field distribution for a triangular vortex lattice. Fig. H23.2 shows maximum entropy fits to μ SR spectra for a range of applied currents. For large driving currents, the $p(B)$ lineshapes exhibit motional narrowing, i.e. the muons experience an effective magnetic field close to the average field.

We have also calculated the expected $p(B)$ lineshape corresponding to a moving VL with a range of orientations with respect to the direction of motion (Fig. H23.3). Although these lineshapes were obtained by assuming a uniformly distributed set of VL orientations, they remain essentially unchanged when a 0.2 radian (RMS) distribution of VL orientations is assumed, as obtained from our recent SANS measurements on the same sample under similar experimental conditions. When a single orientation of the moving VL is present, the expected $p(B)$ lineshape should only have two peaks, one at low and the other at high field. This behaviour is clearly not present in our data, and we can therefore rule out the possibility of vortex motion along a single, well-defined direction.

The above μ SR results, when combined with SANS measurements, lead to the conclusion that the vortices flow by following each other along well-defined static ‘channels’, which are elastically coupled. The topological order of the moving VL, as seen from the μ SR lineshapes and SANS diffraction patterns, depends on the ‘roughness’ of these channels. On the timescale of the muon lifetime, a muon samples the channel roughness as multiple orientations of the flowing VL.

There exist a number of theoretical calculations and computer simulations on (mainly 2D) vortex systems in motion, which require microscopic experimental investigation. The above system is 3D but we are planning to extend our technique to study thin superconducting films using low-energy muons, where one can adjust the implantation depth of the muon. These experiments form part of a large research program, which combines various microscopic experimental techniques, such as SANS, neutron spin-echo, μ SR and possibly low-energy μ SR, to study the static and dynamic properties of vortex matter in type-II superconductors. All the above techniques are complementary to each other: SANS is ideal for probing the *structure* of the VL, μ SR is most suitable for studying the microscopic field distribution in the sample and neutron spin-echo can be used to measure the velocity distribution of the vortices in the flux-flow state.

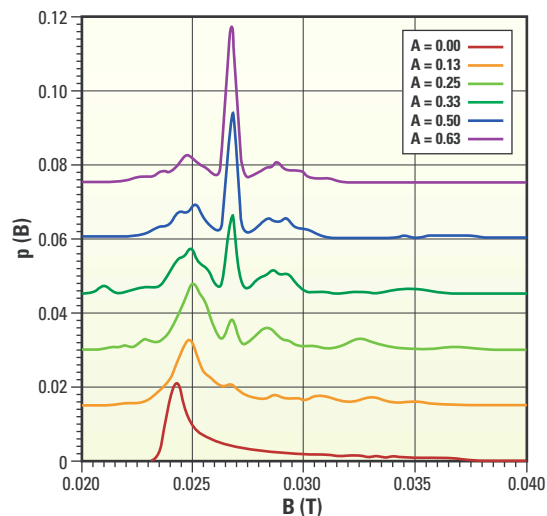


Fig. H23.2. μ SR lineshapes for a range of applied currents at 30 mT and 4.2 K. The peak at approximately 30 mT corresponds to muons stopping in the sample cryostat.

Fig. H23.3. Calculated $p(B)$ lineshapes for a moving VL, assuming a uniformly distributed range of orientations of the moving VL. R is a dimensionless measure of vortex velocity (and hence of applied current).

Very low-frequency excitations in frustrated antiferromagnets

P Carretta, R Melzi and N Papinutto (*Dipartimento di Fisica 'A Volta' e Unità INFM di Pavia, Italy*).

Study of the crossover among the ground-states of low-dimensional antiferromagnets has recently attracted much interest. In a two-dimensional $S=1/2$ Heisenberg antiferromagnet the Néel order can be suppressed, with no generation of any topological disorder, by frustration arising from competing exchange interactions. Frustration yields a phase transition to strongly degenerate ground-states, characterised by very low-frequency spin fluctuations which can be investigated with μ SR. Longitudinal field μ SR measurements performed at ISIS have allowed, for the first time, the characteristic correlation times to be derived for these very low-frequency motions in a frustrated two-dimensional $S=1/2$ Heisenberg antiferromagnet.

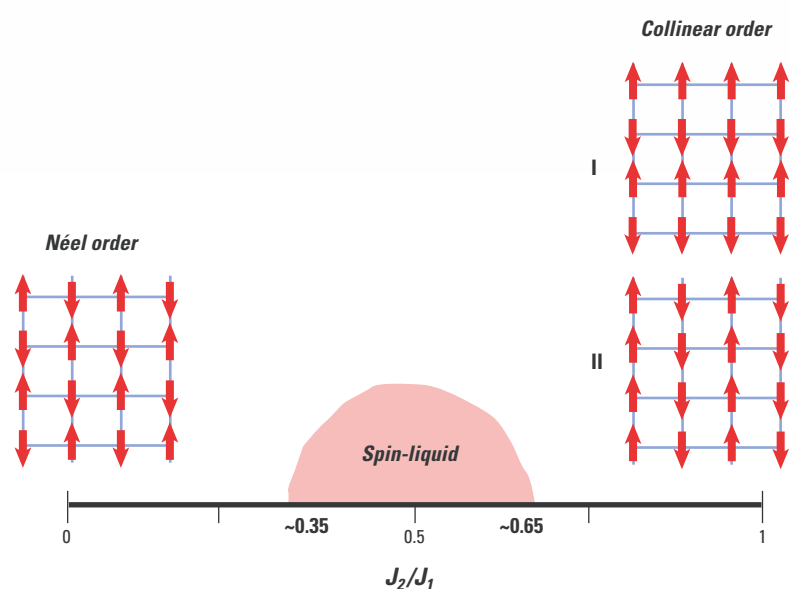


Fig. H24.1
Schematic zero temperature phase diagram of a frustrated $S=1/2$ Heisenberg antiferromagnet on a square lattice, as a function of the ratio J_2/J_1 between the exchange couplings.

The two-dimensional $S=1/2$ Heisenberg antiferromagnets (2DQHAF) are characterized by strong quantum fluctuations owing to the reduced dimensionality and low spin value, with long range order taking place, in principle, only at zero temperature. It is possible to enhance quantum fluctuations by frustrating the antiferromagnetic exchange interactions. This situation is encountered in the $J_1 - J_2$ systems on a square lattice, where the next nearest neighbour interaction J_2 , along the diagonal of the square, competes with the nearest neighbour interaction J_1 , along the

side of the square. On increasing J_2 one expects first a quantum phase transition from a Néel ordered phase to a non-magnetic ground state and then another transition to a collinear ground state. The collinear phase can be considered as formed by two interpenetrating sublattices with a reciprocal orientation of the Néel vectors which classically can assume any orientation. This infinite degeneracy is lifted by quantum fluctuations and just two collinear ground-states are realised: collinear I, with magnetic wave-vector $Q = (q_x = \pi/a, q_y = 0)$, and collinear II, with $Q = (0, \pi/a)$ (see Fig. H24.1). These two ground states are degenerate and it is not possible to say *a priori* which one will be realized, in the absence of other interactions. At a certain temperature an Ising transition should take place and the system collapses into either one of the two ground-states.

Recently a prototype of a frustrated 2DQHAF with $J_2/J_1 \approx 1$ was discovered, $\text{Li}_2\text{VO}_2\text{SiO}_4$. In this compound the V^{4+} ($S = 1/2$) magnetic ions are coupled by J_1 and J_2 superexchange interactions through the oxygens at the corners of regular SiO_4 tetrahedra (see Fig. H24.2). $\text{Li}_2\text{VO}_2\text{SiO}_4$, which has $J_1 + J_2 \approx 8.5$ K, always shows a collinear ground state of type I, with the spins pointing along the x direction. The degeneracy among the two ground-states is relieved by a lattice distortion occurring just above the transition to the collinear phase at T_N . For $J_1 + J_2 \geq T > T_N$ the system is characterised by a correlated spin dynamics with domains of type I and II extending over a length of the order of the in-plane correlation length.

μ SR is a powerful tool for investigating the low-frequency spin dynamics in these systems and, unlike NMR, does not require the application of strong magnetic fields which could affect the effective exchange interactions. Measurement of the time evolution of the muon polarisation for different values of the applied longitudinal field has allowed both the amplitude and the

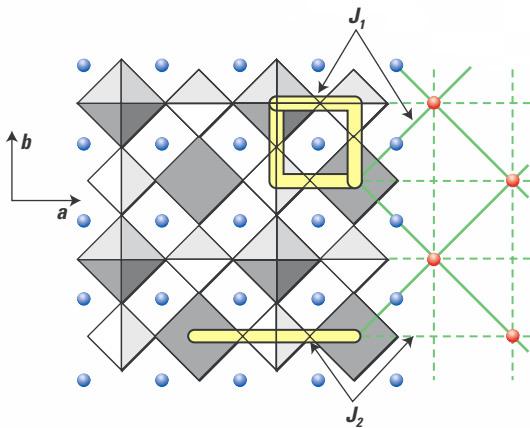


Fig. H24.2. (Left) $\text{Li}_2\text{VOSiO}_4$ structure projected along $[001]$. VO_5 pyramids are in black, SiO_4 tetrahedra in gray and the circles indicate Lithium ions. The two superexchange channels for J_1 and the one for J_2 are also shown. (right) schematic view of the exchange interactions J_1 (solid line) and J_2 (dashed line) among V^{4+} $S=1/2$ ions (red circles).

characteristic correlation time τ_c of the field fluctuations at the muon to be derived. In a 2DQHAF the frequency of the spin fluctuations is expected to be of the order of the Heisenberg exchange frequency $\nu_E = (J_1 + J_2)k_B/h \approx 2 \times 10^{11}$ Hz, for $T \approx J_1 + J_2$. However, the μSR measurements in $\text{Li}_2\text{VOSiO}_4$ reveal the presence of a spin dynamic at frequencies $\nu_c \equiv 1/(2\pi\tau_c)$, orders of magnitude below ν_E (see Fig. H24.3).

What is the origin of this very low-frequency dynamics not observed in non-frustrated 2DQHAF? In $\text{Li}_2\text{VOSiO}_4$ domains of type I and II coexist down to temperatures $T \approx E(T)$, the energy barrier separating the two collinear phases. The magnitude of this barrier is temperature dependent and is related to the degree of frustration, namely to the ratio J_2/J_1 . The motions of the domain walls yield a rotation of the magnetic wave-vector from $Q = (\pi/a, 0)$ to $Q = (0, \pi/a)$, causing a phase shift of V^{4+} spins, as in presence of soliton modes. These motions are at very low-frequencies because they are activated over a barrier $E(T)$, which

increases on cooling. Moreover, the phase fluctuations will be detected by a muon at a given lattice site only after the domain walls have spanned through all the entire domain. The temperature dependence of τ_c derived from longitudinal field μSR measurements in $\text{Li}_2\text{VOSiO}_4$ is in good agreement with the one theoretically predicted for such a dynamic. At lower temperatures a lattice distortion, which relieves the degeneracy among the two collinear states, takes place and yields a progressive increase in the size of the collinear I domains on cooling.

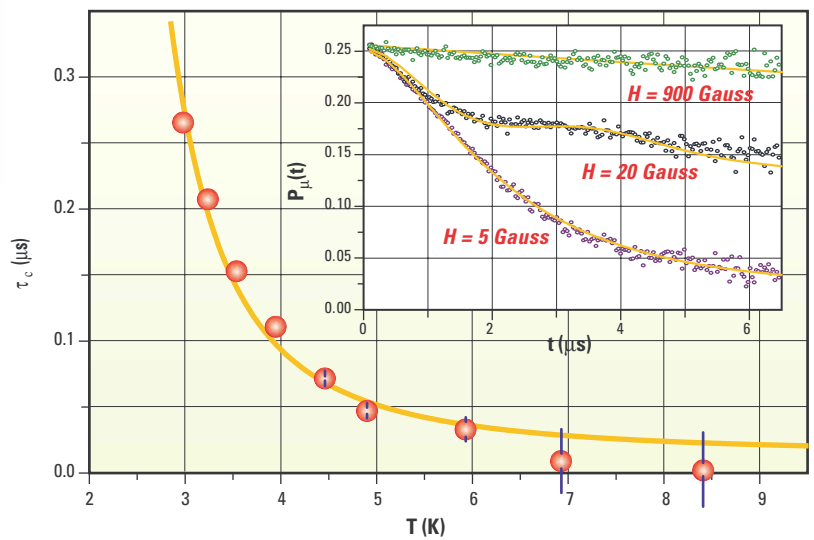


Fig. H24.3 Temperature dependence of the correlation time for the low-frequency spin dynamics in $\text{Li}_2\text{VOSiO}_4$, derived from the fit of the time evolution of the muon polarization for different intensities of the longitudinal magnetic field (see the inset).

Internal strain and texture evolution in piezoelectric ceramics

R Rogan, E Üstündag, B Clausen (California Institute of Technology), M R Daymond (ISIS), V Knoblauch (Robert Bosch GmbH).

Piezoelectric materials exhibit a coupling between applied stress and electric field. This property allows their use as both sensors and micromechanical actuators (also called ‘smart’ materials). Unfortunately, most piezoelectrics are often susceptible to fatigue and premature failure, thus limiting their usefulness as micromachines and memory devices. The roots of fatigue lie in the micromechanical interaction of crystallites within the piezoelectric material. Until recently, there has been no extensive *in situ* data that described the evolution of internal strain and texture during the electro-mechanical loading of piezoelectrics. The deep penetration of neutrons has allowed the collection of such data on the ENGIN instrument for the first time.

Piezoelectric ceramics are widely used in a diverse set of devices including sensors, actuators, transducers, micromachines and ultrasonic motors. In these applications, they exhibit a complicated behavior as they respond to both electrical and mechanical loading. During this process large internal stresses are generated which eventually lead to failure. Efforts to model and predict the behavior of piezoelectrics have often been hindered by the lack of *in-situ* data that accurately describe the electro-mechanical response of these materials.

microstructural interactions of individual phases and crystallites in piezoelectric materials before their performance can be improved.

Because PZTs possess relatively large amounts of lead, bulk studies of these materials can only be performed with neutron diffraction techniques which offer full sample penetration. Through the use of the optimized diffraction geometry of the ENGIN instrument on the PEARL beam line at ISIS, crystal lattice strain and texture can be measured simultaneously. Different detectors observe different sample directions, providing information on both the axial and transverse behavior. For the first time, bulk characterization of a dual phase, axially poled piezoelectric sample was performed using neutron diffraction.

After subjection to a high electric field (the poling field), randomly distributed domains with individual dipole moments are aligned, producing a macroscopic remnant electric field, much the way a bar magnet possesses a permanent magnetic field (Fig. H25.1). As mechanical stress is applied,

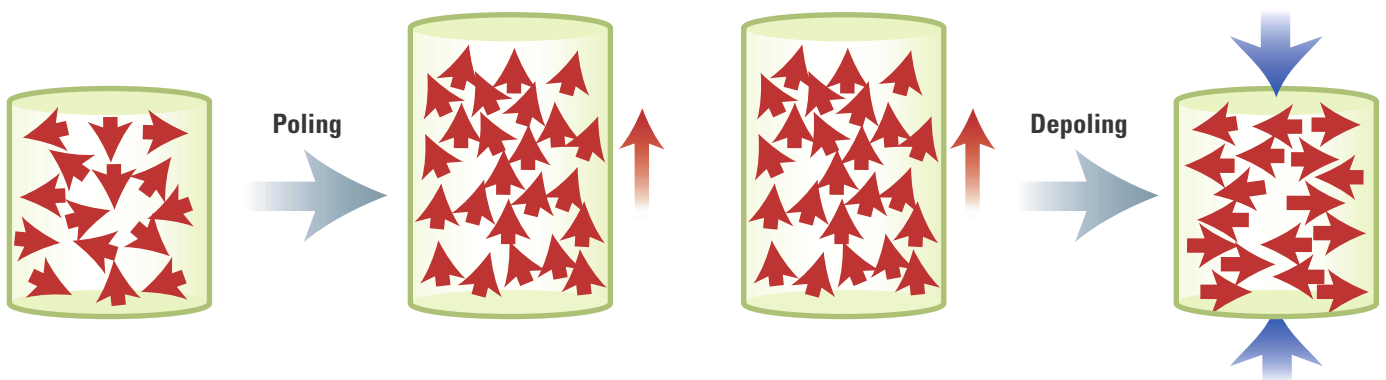


Fig. H25.1. Effects of poling and depoling on a PZT sample. Red arrows indicate direction of electric dipoles, and blue arrows direction of applied stress.

Some of the most technologically important piezoelectrics are two phase mixtures of lead zirconate titanate ($\text{Pb}(\text{Zr,Ti})\text{O}_3$ -PZT). While these two phase mixtures perform far better than their single phase constituents, the interaction between these phases is not well understood, and there is an urgent need to comprehend the

these domains are forced to ‘switch’ to the direction transverse to the applied uniaxial stress in order to relax internal stresses. This process is known as depoling. Studying the effects of domain switching and the lattice strain *for both phases simultaneously* during the depoling process has not previously been accomplished in the bulk scale.

The sample was placed under successively higher levels of applied load using the ENGIN load frame. At each stress level, diffraction patterns were taken and analysed to determine lattice strain and texture. Texture was modeled using the March model, whose characteristic variable is the March coefficient. This single number characterises the relative strength of the texture for a given detector; a value less than one indicates a high level of alignment with the axial direction (parallel to the applied load), a number greater than one implies alignment with the transverse direction.

In Fig. H25.2 we can clearly observe the onset of domain switching around -25 MPa as evidenced by the large change in the March coefficient. By the time we reach -150 MPa, the process has been exhausted and no further texture evolution occurs. Because there is no impetus for the domains to switch back to their original configuration (i.e., no poling field), they remain aligned in the transverse direction during unloading. The fact that the extreme values for the rhombohedral phase March coefficient span a greater range than those of the tetragonal phase indicates that the rhombohedral phase is more strongly textured during both poling and depoling.

The large anisotropy in the tetragonal lattice strain points to a complicated internal stress state (Fig. H25.3). Domains aligned with their c axis parallel to the sample axis (the expected result of poling) deform greatly between -25 and -150 MPa because they relieve the internal stresses by switching. Beyond -150 MPa, all those domains are locked and can only deform in a linear elastic manner. Domains which were not initially poled successfully have their a axis aligned in the axial direction and those, too, deform elastically since they cannot switch. The opposite associated crystal axes in each case above (i.e., a - and c -normal in Fig. H25.3) display tensile lattice strains in accordance with the Poisson effect.

With the ability to separate strain and texture effects, these experiments offer theorists direct evidence for comparison with their models. In the future, these models and simulations will supplant empirical knowledge of piezoelectric materials processing and allow for the production of custom materials 'tuned' to exhibit desirable properties for specific applications.

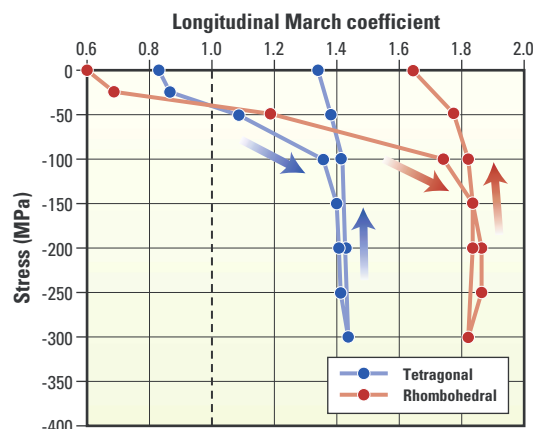


Fig. H25.2. March coefficients of each phase, arrows indicate order of applied stress.

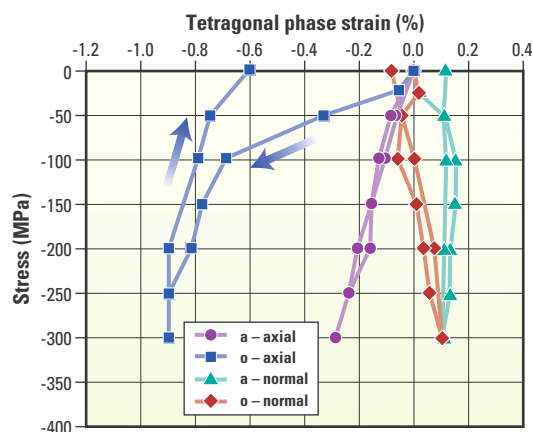


Fig. H25.3. Lattice strains in the tetragonal phase, arrows indicate order of applied stress.

Revealing the missing-link with Bayes and MaxEnt

DS Sivia, S Hull, DA Keen (ISIS), P Berastegui (Stockholm University)

The traditional heavy-atom method for structure completion encounters awkward conceptual and practical difficulties when faced with powder diffraction data; these are naturally circumvented when the problem is formulated within a Bayesian framework. This leads to a significant improvement in the analysis as the limitations of both the experimental measurements and the partially-known structure are taken into account, and because weak additional prior knowledge can also be encoded. The procedure has proved to be very useful in recent studies of some superionic conductors.

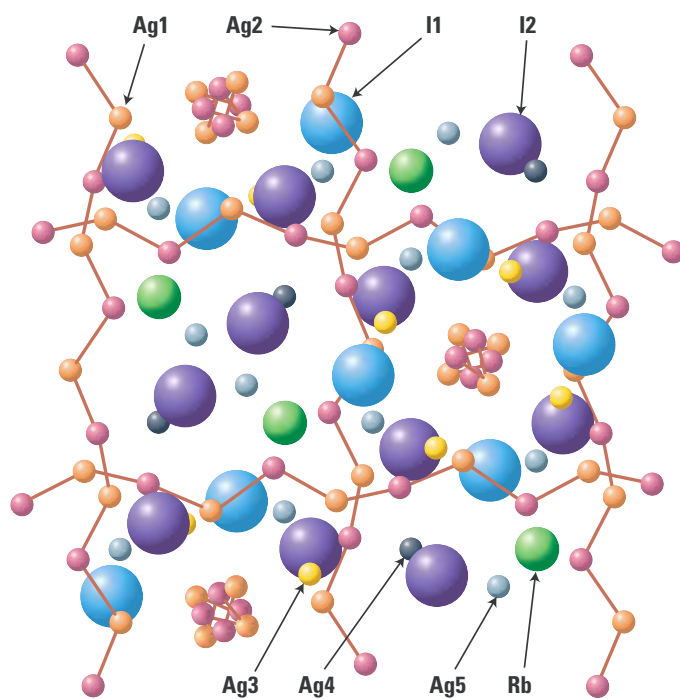


Fig. H26.1.
The crystal structure of Ag_4RbI_9 , showing the locations of the two symmetry independent I^- (I1 and I2) and the immobile cations (Rb), plus the five proposed sites for the mobile cations (Ag1 , Ag2 , Ag3 , Ag4 and Ag5). The red lines joining the Ag1 and Ag2 sites illustrate the probable diffusion pathways along one-dimensional channels parallel to the three cubic axes.

The lack of phase information in diffraction data has always made the solution of crystal structures a challenging problem. While the difficulty can often be reduced by having several sets of measurements related by known changes, as in isomorphous replacement, most experiments consist of a single data-set. The successful solution of a crystal structure then hinges on the use of additional information; this can range from a good initial estimate of the answer, or a general knowledge of the atomic connectivity, to just the physical positivity of the scattering density distribution. The case of interest here concerns the situation where part of the structure is known,

such as the location of the heavier atoms or a ring-fragment, and the remainder needs to be solved.

The basic idea behind Fourier recycling, or the heavy-atom method, is straightforward, and often very effective. In the simplest procedure, the phases yielded by the known fragment are assigned to the measured reflection amplitudes and these hybrid complex structure factors Fourier transformed. The resultant real-space scattering density distribution is then interpreted in the hope of recognising more of the crystal structure. Improvements to this elementary scheme have been put forward over the last fifty years, and the encoding of additional prior knowledge, such as the positivity of a scattering density distribution through the use of maximum entropy, also helps. The limitations of the simplest procedure with regard to partial phase information and noisy amplitudes come to a head when dealing with powder data, for the overlap of the Bragg peaks means that the extracted amplitudes are entangled, making the assignment of phases to individual reflections awkward to say the least.

The conceptual difficulty with powder diffraction disappears once we realise that the task is not one of *inverting* the reciprocal data through a Fourier transform, but of making the best *inference* of the scattering density given the limited information available. The intensity-data from the Bragg peaks, whether correlated or not, form only one constraint on the nature of the permissible scattering density; knowledge of both the located atoms and the characteristics of the unlocated ones also play a role in our best estimate of the crystal structure, as does the encoding of any other cogent prior information. The benefits of adopting such a Bayesian and maximum entropy approach have been illustrated earlier (ISIS 99 page 24) with the pharmaceutical molecule chlorothiazide, and have again been demonstrated in recent studies of superionic conductors.

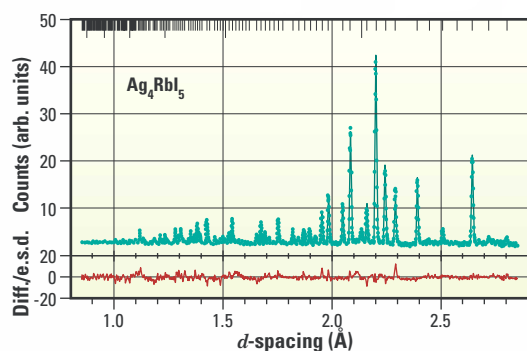


Fig. H26.2. Least-squares fit to powder diffraction data for Ag_4RbI_5 collected on POLARIS. The two rows of ticks along the top of plot denote the calculated positions of the reflections for Ag_4RbI_5 and for the vanadium sample can.

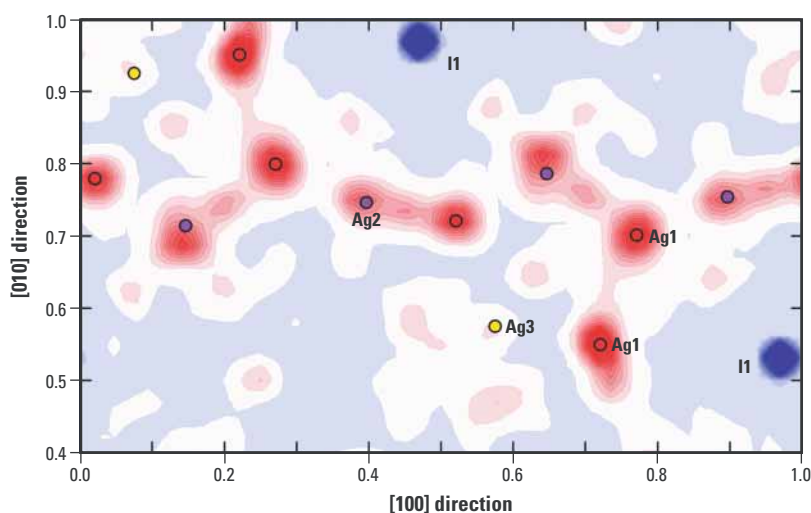
Superionic conductors are materials which exhibit exceptionally high values of ionic conductivity whilst in the solid state. Typically, the crystal structure of such a compound can be described in terms of rapid diffusion of one (or more) of the constituent ionic species between the cavities formed by the essentially immobile sublattice of the remaining ions. However, modelling of the time-averaged distribution of the diffusion ions often requires rather complex constructs, and it can be difficult to derive an unambiguous description.

A typical example is the case of Ag_4RbI_5 . Whilst the high cost of silver has limited its commercial application in, for example, solid state batteries, it has been widely studied because it possesses one of the highest values of room temperature ionic conductivity ($\sigma \sim 0.2 \Omega^{-1} \text{cm}^{-1}$). Ag_4RbI_5 adopts a cubic crystal structure in space group $P4_132$, with $a \approx 11.24 \text{Å}$ and four formula units per unit cell. The two symmetry independent Γ ions (labelled I1 and I2) form a sublattice with the so-called ‘ β -Mn’ structure. Within this anion array there are four distorted octahedral interstices which are all filled by immobile Rb^+ . In addition, there are 5 sets of sites (labelled Ag1, Ag2, Ag3, Ag4 and Ag5) which are plausible locations for the mobile cations, since their surrounding anion polyhedra approximate to the tetrahedral environment

favoured by Ag^+ (see Fig. H26.1). The multiplicities of these sites are $24\times$, $24\times$, $8\times$, $4\times$ and $12\times$, giving a total of 72 possible locations for the $16\times\text{Ag}^+$ in the unit cell.

Rietveld refinement of powder diffraction data collected on POLARIS (Fig. H26.2) indicate that the Ag1 and Ag2 sites are those predominantly occupied, suggesting that diffusion of Ag^+ takes place between these sites to form one-dimensional channels parallel to the three cubic axes (see Fig. H26.1). Whilst this accounts for the high observed ionic conductivity it raises the question of whether Ag^+ hop between these (non-intersecting) channels. On purely geometric grounds, three plausible routes are direct Ag1-Ag1 hops or indirect Ag1-Ag1 and Ag2-Ag2 paths via Ag3 and Ag5 sites, respectively. Unfortunately, correlation between the fitted parameters (particularly the thermal vibrations and occupancies of the cation sites) does not give a reliable estimate of the mean occupancies of the Ag3 and Ag5 positions. Instead, we have constructed MaxEnt maps of the Ag^+ density within the unit cell, using the positions of the Γ and Rb^+ as the ‘known’ fragment of the structure. The resultant distribution (Fig. H26.3) shows evidence of direct hops between the channels at their positions of closest approach but no indication of the alternative ‘indirect’ mechanisms.

Fig. H26.3. MaxEnt reconstruction of the scattering (ionic) density with a (001) section shown as a slice with $0.45 \leq z \leq 0.55$. Blue and red coloured regions represent Γ^- and Ag^+ densities, respectively. The conduction between the Ag1 and Ag2 sites is apparent and there is evidence of hopping between Ag1 sites. The Ag3 site does not appear to be a significant conduction route.



Successful operation of the ISIS radio frequency quadrupole

CP Bailey, CJ Barton, MH Bates, RA Corderoy, JP Duke, DJS Findlay, PA Harper, JA Hirst, S Hughes, M Keelan, JC Kerr, P Knight, M Krendler, CR Lambourne, AP Letchford, JP Loughrey, LJ Pearce, M Perkins, J Saunders, R Sidlow, AF Stevens, JWG Thomason, MO Whitehead (ISIS)

Following many months of dedicated effort by members of ISIS staff, the ISIS radio frequency quadrupole (RFQ) accelerator successfully accelerated its first beam in October 2001. An extensive experimental programme undertaken since then has shown the RFQ performance to be in very close agreement with the design specification.

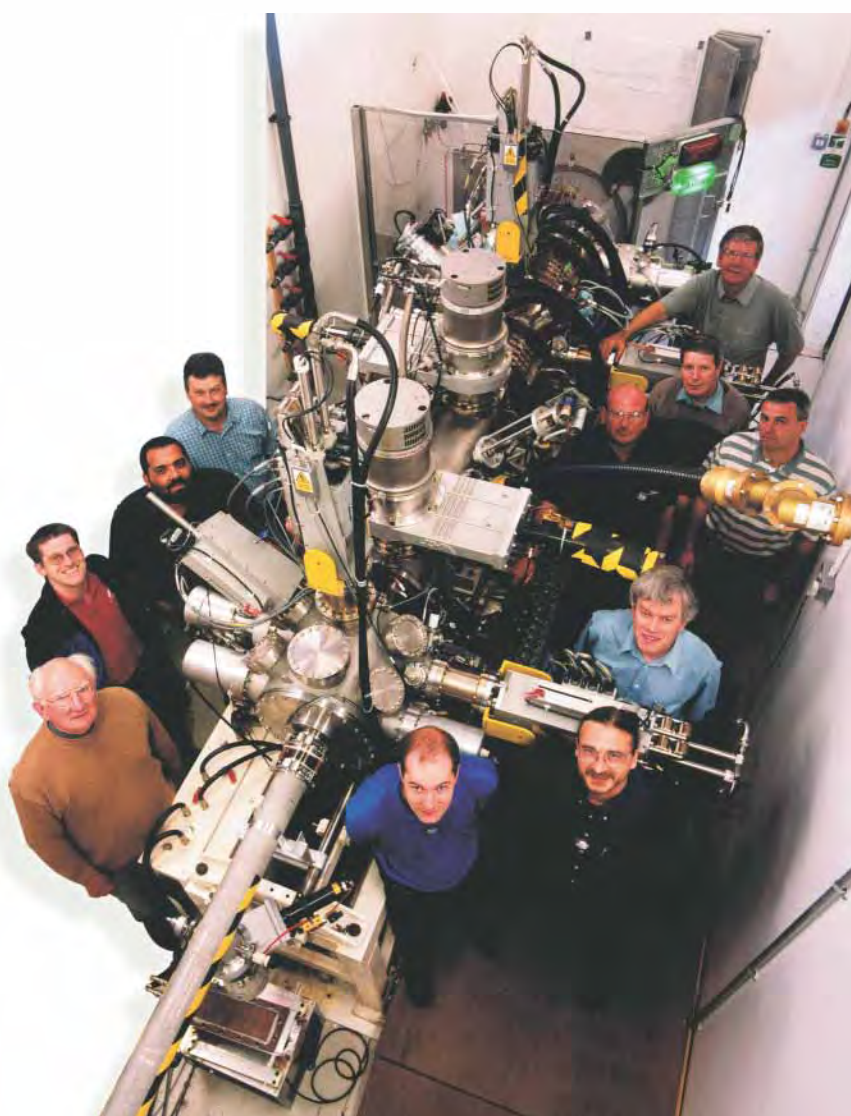


Fig. H27.1. The RFQ test facility and some of the team who made it all possible (02RC2523).

The RFQ is intended as a pre-injector upgrade for ISIS. On ISIS, before injection into the 800 MeV synchrotron, the beam is raised to 70 MeV by an injector drift tube linac (DTL). However, mechanical constraints on the DTL structure set a lower limit on the velocity of particles which can be accepted for acceleration by the DTL. Consequently, a pre-injector stage is necessary to raise the energy at which particles from the H⁻ ion source can be accepted by the DTL. On ISIS this pre-injector stage currently consists of a 665 kV DC accelerating column connected to an EHT platform which houses the Penning H⁻ ion source and its associated power supplies. The platform is raised to a potential of -665 kV via a Cockcroft-Walton multiplier stack. Between the accelerating column and the DTL are magnetic quadrupoles for focusing and a two-gap buncher cavity. The latter bunches the DC beam from the accelerating column to facilitate capture by the DTL, but the bunching is not complete so that not all of the beam produced by the ion source is captured by the DTL and delivered to the synchrotron.

RFQs use intense radio frequency (RF) electric fields to focus, bunch and accelerate particles, and are particularly well suited for use with low velocity ions where electric focusing is stronger than magnetic focusing. Inside the ISIS RFQ four specially shaped electrodes produce an alternating gradient quadrupole electric field with an axial component for bunching and acceleration. By the time the beam reaches the end of the RFQ at 665 keV it is so well bunched and tightly focused that nearly all of it would be accepted by the ISIS DTL. There are therefore substantial efficiency gains to be made by substituting this RFQ pre-injector for the Cockcroft-Walton pre-injector.

The ISIS RFQ is the result of collaboration between RAL and the Institute of Applied Physics at the J W Goethe University, Frankfurt, Germany. Electrode design, beam dynamics simulations, thermal modeling and the design of the water cooling

circuits were carried out at RAL, whilst the resonator design, manufacturing, alignment and initial testing were carried out in Frankfurt.

A full-scale test facility, see Fig. H27.1, has been built at RAL for evaluating the RFQ pre-injector before installation on ISIS. The complete facility consists of the H^- ion source, a 35 kV post-accelerator, three solenoids for beam matching, the RFQ itself, and diagnostics. Using a peak RF power of ~ 200 kW, beam currents of up to 35 mA peak (400 μA mean) have been accelerated with transmission efficiencies of $>95\%$, in excellent agreement with computer simulations carried out using codes developed at RAL. If this level of performance can be maintained after installation, the ISIS 300 μA upgrade should be possible with no additional beam required from the ion source. The final energy of the beam has been measured and is within ± 1 keV of the design value. The test facility has allowed the beam emittance from the ion source to be measured at low energy for the first time. Beam emittances at the output of the RFQ have also been measured and are again in very good agreement with the design. Fig. H27.2 shows typical measurements.

Installation of the RFQ on ISIS is scheduled at present for 2003. Between now and then the experimental programme will continue together with long term reliability testing, vital if the present high availability of ISIS is to be maintained.

In addition to being an upgrade for ISIS, the RFQ forms part of CLRC's contribution to the R&D programme for the European Spallation Source (ESS) project, in which CLRC is a major player. The ESS will require two 2.5 MeV RFQs, each 4.2 m long and capable of accelerating peak beam currents of 60 mA at $>90\%$ efficiency with a duty cycle of up to 10%. Much is being learnt about the design and operation of such high power, high current RFQs from our experiences at ISIS before construction of a full size prototype begins.

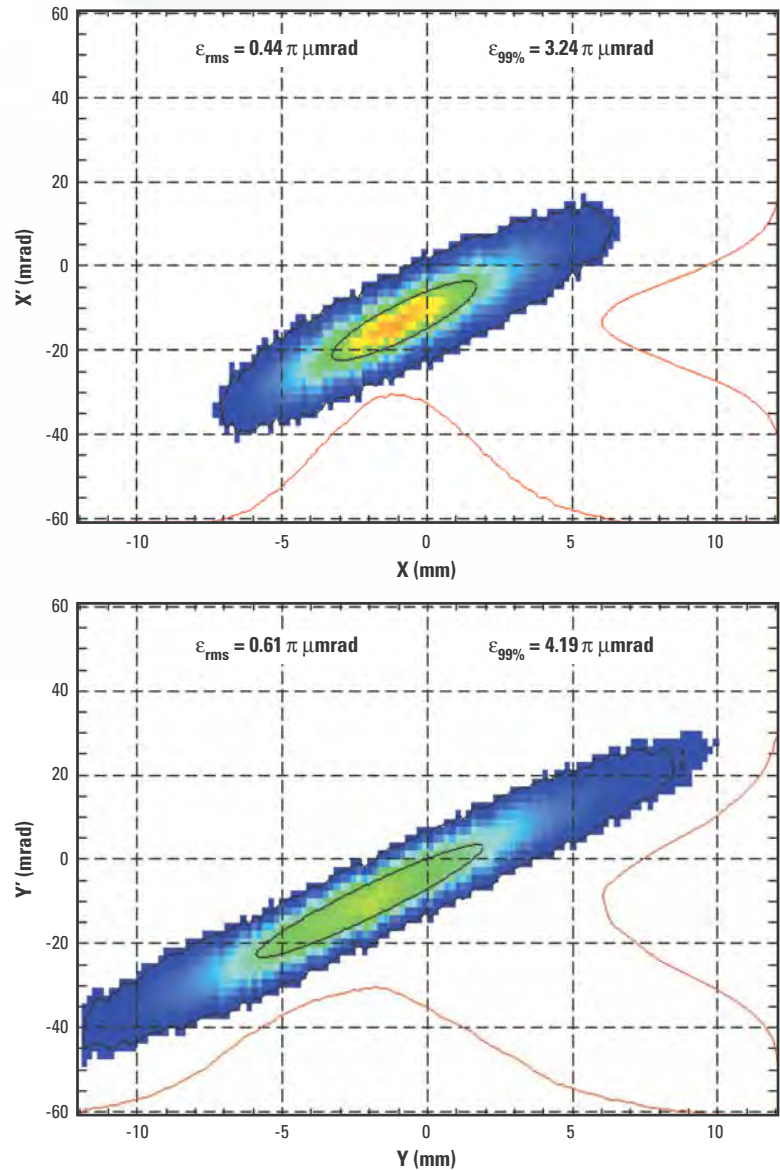


Fig. H27.2. Typical horizontal (a) and vertical (b) emittance measurements at the RFQ output for a 35 mA, 665 keV beam.

A fast beam chopper for the ESS

MA Clarke-Gayther (ISIS)

The European Spallation Source (ESS) is the most ambitious of the existing proposals for the next generation of accelerator-driven pulsed neutron sources, and is 'pushing the envelope' in many areas of accelerator design. The ESS H⁻ linac fast beam choppers in the 2.5 MeV medium energy transport lines must produce the precisely defined gaps in the 280 MHz bunched beam that will enable low beam loss operation during accumulator ring injection and extraction.

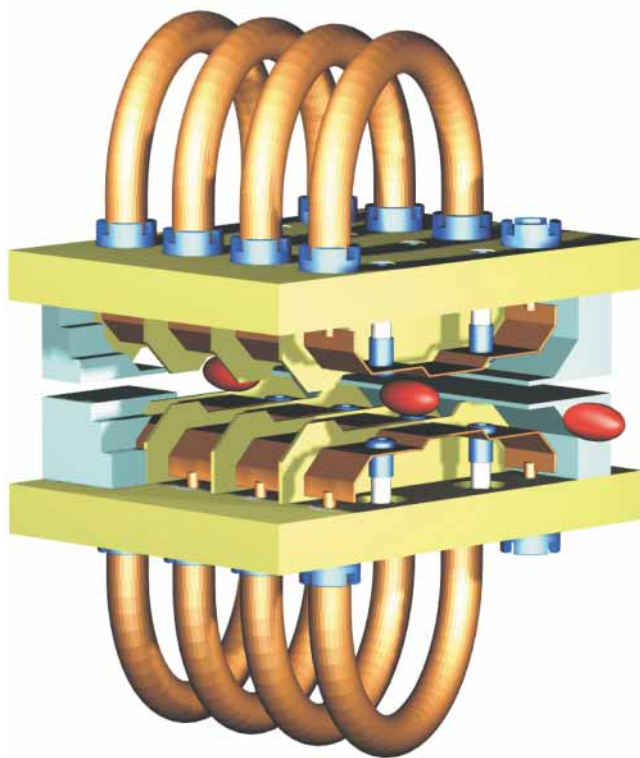


Fig. H28.1. Cut-away view of a helical slow-wave structure.

Stringent beam loss requirements in the ESS linacs and accumulator rings dictate that the chopping fields should rise and fall within the beam bunch interval of 2.9 ns, to eliminate the possibility of acceleration and subsequent loss of partially chopped beam. Slow-wave (E-field) transmission line structures have demonstrated field transition times in the ~ 10 ns regime, and ESS chopping schemes utilising these structures have been identified and refined.

Slow-wave electrode design

Slow-wave (E-field) transmission line structures have been designed using finite element field modelling codes, where complex geometry,

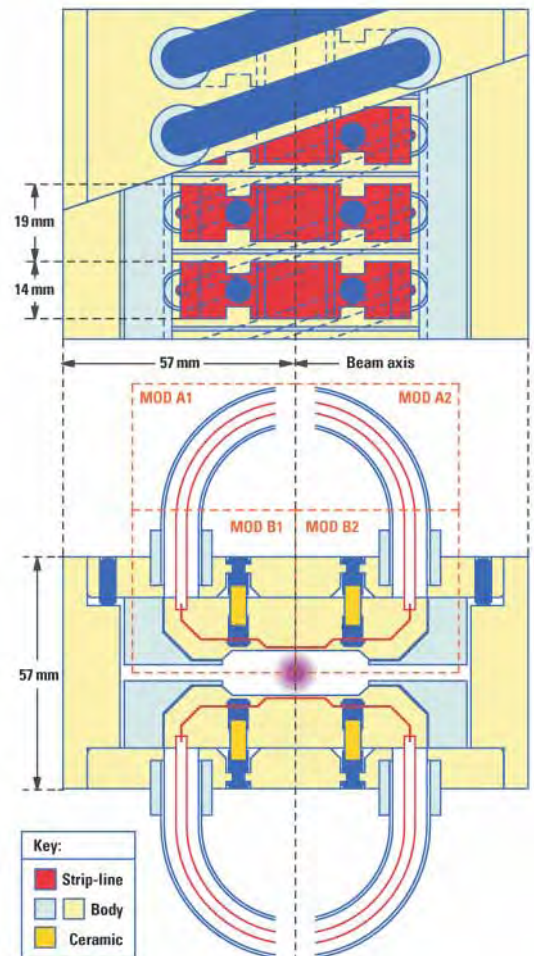


Fig. H28.2. Helical electrode structure.

electrical length, and inter-electrode coupling set a practical limit on the computational accuracy of the broad-band properties. Speed of computation and /or accuracy of the computed properties for the proposed structures have been enhanced by identifying small repetitive modules, and modelling their properties in the three dimensional finite element frequency domain (FEFD) HFSS and MAFIA codes, and the finite difference time domain (FDTD) CONCERTO code. Time domain characteristics for the complete structures were analysed in a SPICE-based circuit simulator where the complete structures were modelled by linking the repetitive two-port modules in large series arrays.

A helical electrode structure

Planar and helical slow-wave structures have been analysed. The compact helical structure shown in Fig. H28.1 and H28.2 is formed by strip-line sections near the beam axis, linked to semi-circular sections of semi-rigid coaxial cable. Coaxial to strip-line transitions, and ceramic strip-line supports, are capacitively compensated by structure and notch dimensioning, respectively.

Finite element models for two modules, identified as A1/A2 and B1/B2 in Fig. H28.2, were analysed (Fig. H28.3). Simulated S-parameters for the modules are shown in Fig. H28.4, where the S21/A1/A2 for the coaxial cable shows good agreement with manufacturer’s data. Frequency and time domain characteristics for the complete structure were computed by circuit simulation of the series-connected two-port modules and lumped element inter-electrode coupling capacitors, as shown in Fig. H28.5. The simulated transmission characteristics in the frequency and time domain are shown in Figs. H28.6 and H28.7, respectively.



Fig. H28.3.
Finite element mesh for module B1/B2.

Summary

Computed frequency and time domain characteristics indicate that the helical slow-wave structure will meet the stringent ESS specifications for chopper pulse fidelity. Prototype planar and helical structures will be manufactured and tested in the near future.

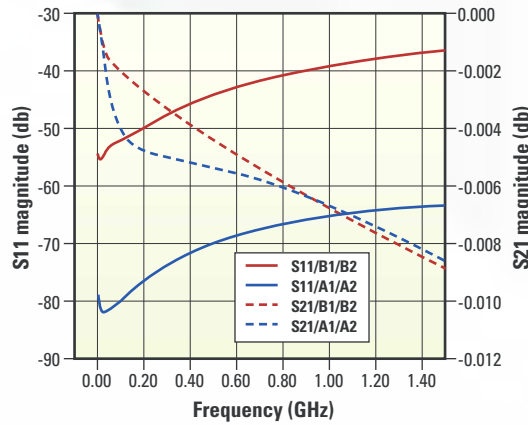


Fig. H28.4.
The plot of S21 for module A1/A2 (UT390 coaxial cable) is in good agreement with manufacturer’s data and provides a check on the computational accuracy of the finite element field modelling code

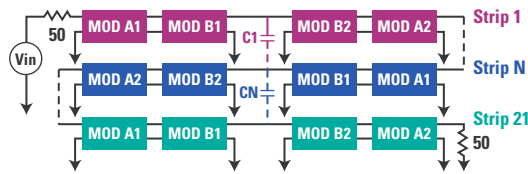


Fig. H28.5.
SPICE model of the complete structure. This method of analysis is computationally efficient for large repetitive structures.

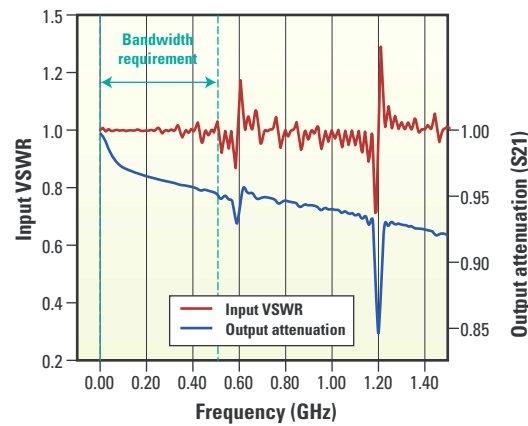


Fig. H28.6.
Simulated reflection and transmission characteristics in the frequency domain show that the resonant frequencies of the structure are safely above the upper limit of the required bandwidth.

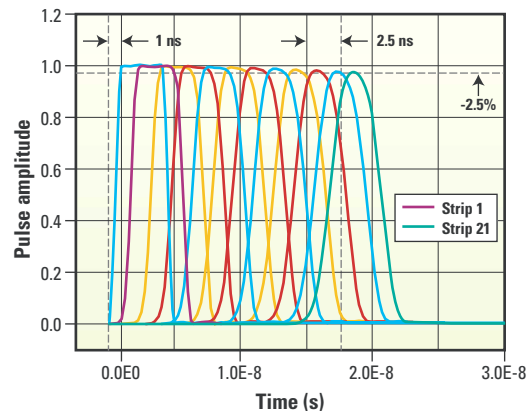
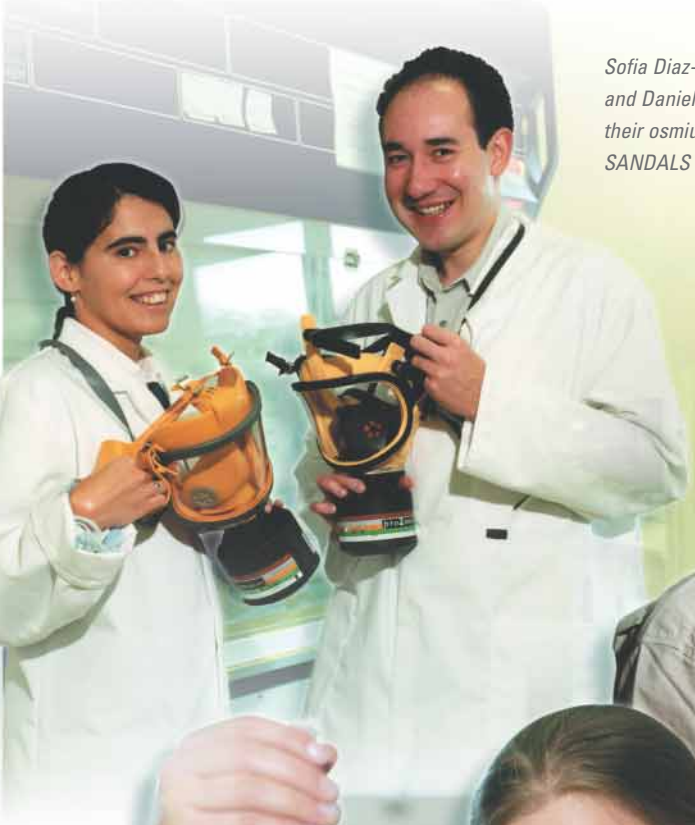
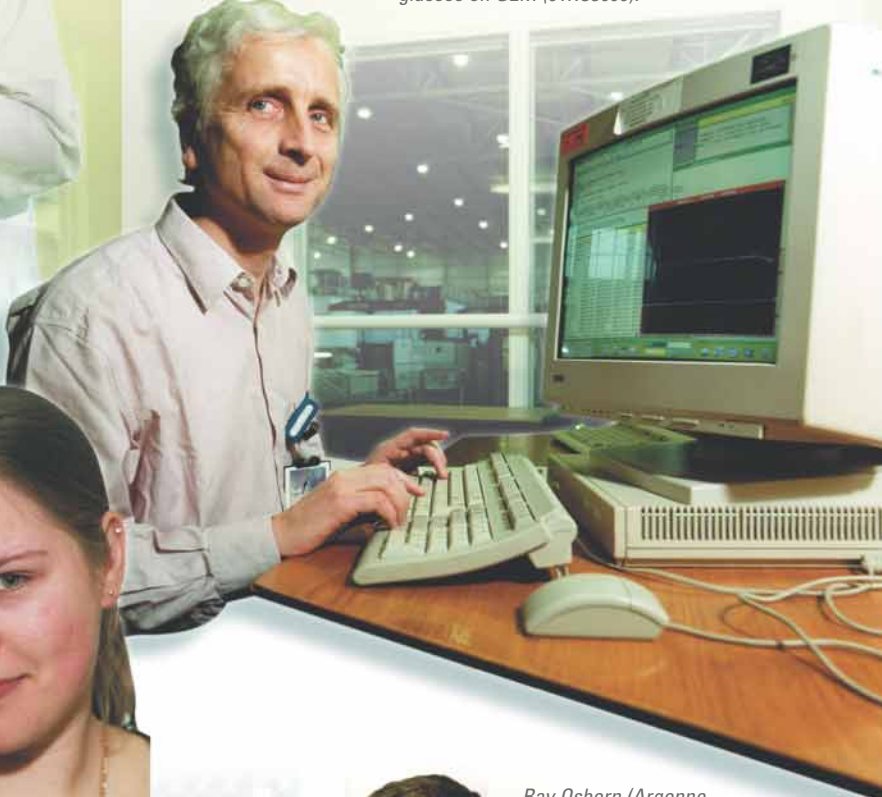



Fig. H28.7.
Simulated characteristics in the time domain indicate that the structure should meet the stringent ESS specifications for chopper pulse fidelity.



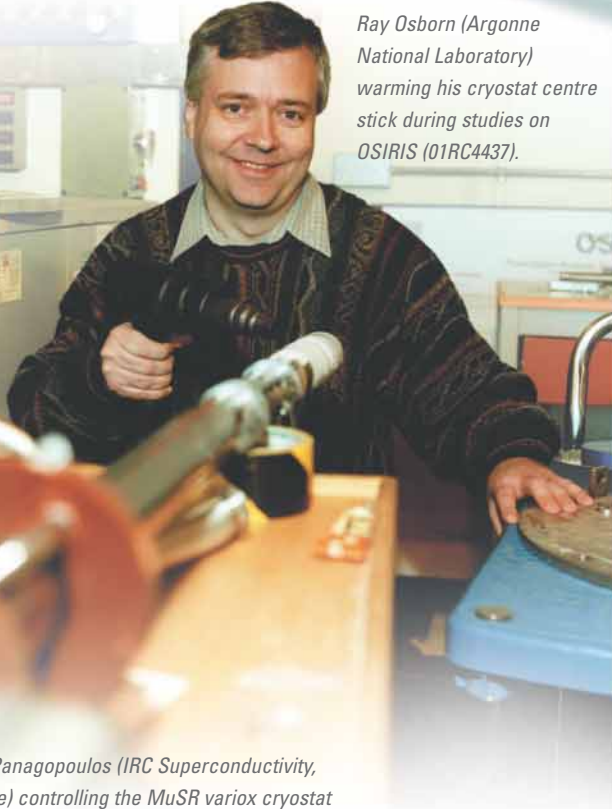
Sofia Diaz-Moreno (ESRF, Grenoble) and Daniel Bowron (ISIS) preparing their osmium tetroxide sample for SANDALS (01RC4020).




Uwe Hoppe (Universitat Rostock, Germany) studying short-range order of tellurite glasses on GEM (01RC3966).



Danusia Grzeszczak (UMIST) preparing her anionic surfactant solution for CRISP investigation (01RC4414).



Ray Osborn (Argonne National Laboratory) warming his cryostat centre stick during studies on OSIRIS (01RC4437).



Christos Panagopoulos (IRC Superconductivity, Cambridge) controlling the MuSR variox cryostat during studies of quantum criticality in the $\text{Bi}_2\text{Sr}_2\text{CaCu}_2\text{O}_{8+\delta}$ superconductor (01RC4398).

Instrument Developments

Development at ISIS is a continuous process, driven both in response to the changing needs of the user community and to maintain the facility as a world-class neutron and muon source. Evolution of existing instruments, and design and construction of new ones, open up fresh opportunities for condensed matter investigations. Some of the major improvements over the past year are described here.

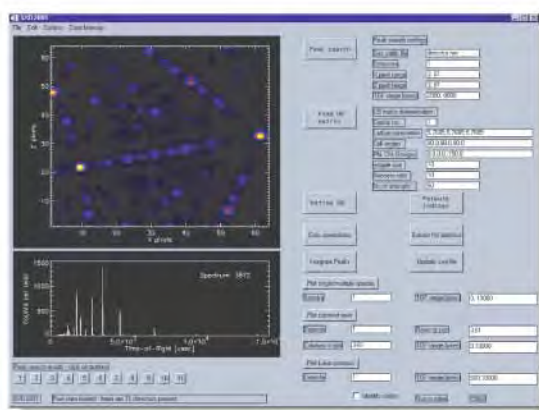
3

Progression of the ISIS instrument suite has been constant since the Facility began operations. Described in this chapter are the ongoing, major instrument developments over the past year.

SXD-II

The new SXD single crystal diffractometer, funded by EPSRC, took its first neutrons on May 11th 2001, as reported in ISIS 2001. In September 2001 the complete DAE-II system became available allowing full operation to commence, with all 11 detectors available through the enhanced electronics. These position-sensitive detectors (offering 2π detector solid angle coverage) provide over 45,000 detector elements and around 2000 time channels; a typical data frame contains around ~360 Mbyte of data. With data frame collection times as short as 15-20 minutes, this represents a major data processing challenge. To meet this challenge, a new software suite has been devised. The IDL-based SXD2001 program suite (Fig. 3.1) is developing well and will be available for routine use by the end of the 2002 long shutdown. Recent developments allow for the correction of diffuse scattering patterns and display of cuts through reciprocal space.

Fig. 3.1
SXD2001 initial Laue and time of flight visualisation.



The scientific possibilities of the new instrument are already being realised in, for example, the study of smaller crystals, in rapid structure determinations and in more parametric (e.g. T, p) single crystal

investigations. The latter also use the recently upgraded 5 kbar He pressure cell, the open-geometry of this device being vital in allowing exploitation of the large detector solid angle. An early example of this has been the study of low symmetry hydrogen bonded systems under pressure. The potassium hydrogen maleate system has a short, symmetric, intramolecular O-H...O hydrogen bond (O...O separation ~2.43 Å), with the H atom located on a mirror plane. The p/T phase diagram of this material has been mapped out at 8 points from single crystal neutron diffraction data, rarely achieved before for molecular systems (Fig. 3.2).

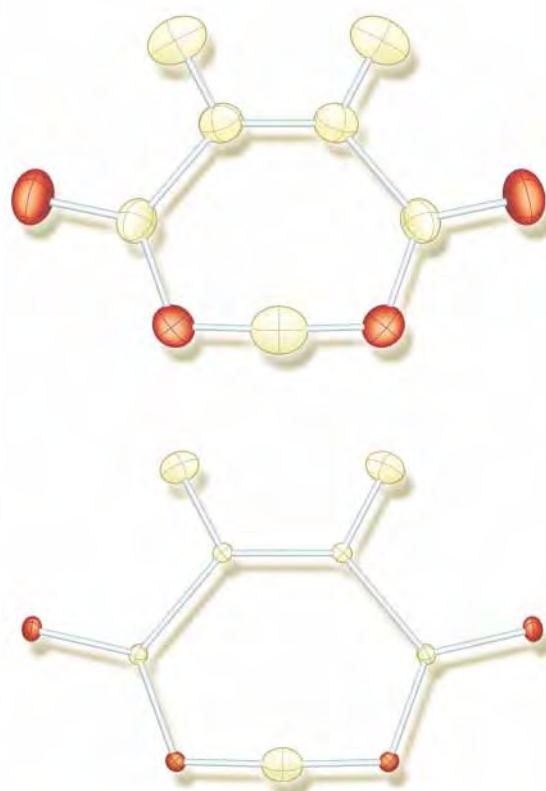


Fig. 3.2. Typical refinements of potassium hydrogen maleate from SXD pressure cell data at room temperature (top) and 30 K (bottom).

The final stage of the SXD upgrade project, to improve the beamline optics including both collimation and focusing options along with laser-assisted sample

alignment, is nearing completion. A 400 mm-long 2D supermirror focusing device ('Trompette') has been obtained and is ready for mounting for tests on the instrument.

HRPD

The upgrade of the HRPD 90° detector bank, reported in detail in ISIS 2001, has been completed in the past year. Following the initial demonstrations of the effectiveness of the new bank, it has been fully commissioned both technically and scientifically as part of the upgrade grant. The upgraded instrument has substantially improved capability in the areas of small molecular systems, magnetic diffraction and high pressure studies.

GEM

The programme to complete the GEM detector array, as funded by EPSRC, is proceeding very close to schedule. At the present time the full complement of Bank 4 detectors is available, and Bank 3 detector modules are arriving steadily and are being tested as they come in. The low angle bank, Bank 0, is in manufacture, and is expected to be delivered in time for testing and installation before the end of 2002. At that stage the GEM detector array will be complete with more than 6500 elements.

The other main item covered by the current development programme is the oscillating radial collimator, designed to reduce background scattering from sample environment equipment like pressure cells and cryostats. The collimator itself was delivered last year, but after extensive testing the oscillating mechanism was found to be faulty and failed after relatively short service. This delayed the installation in the previous year until a new and robust oscillating mechanism had been developed. After a few final adjustments the collimator is now installed and operating, and although there has so far been very little experience with it, initial results look extremely exciting (Fig. 3.3).

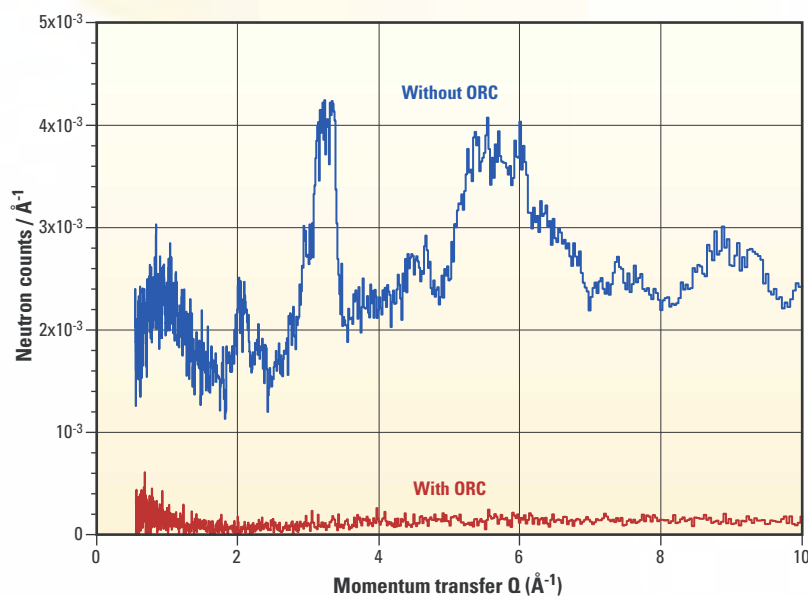


Fig. 3.3.

Initial experiments with the GEM oscillating radial collimator. The empty instrument background on GEM is shown with (red) and without (blue) the collimator in place for the low angle detector modules Bank 2. The structure in the background without the collimator arises from scattering from the beam scraper which is viewed by the low angle detectors on GEM. The collimator has removed this background completely.

VESUVIO

The eVS instrument has undergone significant modification over the past year, and has been re-inaugurated as VESUVIO. Resolution improvements have been obtained by a new filter consisting of six 60° segments each containing either a thick, thin or no uranium foil. By oscillating the device by $\pm 60^\circ$ about the vertical position, each detector at back-scattering is covered by one of these options and the double difference technique is then used to eliminate the Lorentzian tails in the resolution function. Further improvement in resolution is obtained by cooling the foils to 30 K, thereby eliminating thermal broadening of the uranium resonance line-shape, which defines the resolution function. The device has been tested using the original detector modules at back scattering and has performed according to expectations. The first 60° segment of the new ^6Li doped glass scintillator back-scattering detector, with optimised geometry, was installed during August 2001 and should lead to a further improvement in resolution and also in count rate.

IRIS and OSIRIS

Installation of the OSIRIS spectroscopy detectors took place in June 2002, immediately followed by the start-up of the user programme for inelastic measurements. Optimisation will be gradual, with installation of the radial collimator for the spectroscopy section scheduled for September, and cryogenic cooling of the analysers to be installed during the long shutdown in 2003.

A new CCR-based cooling system for the graphite analyser has been installed on IRIS and is now operational. This has led to significant cost savings compared to the original liquid helium

cooling system, whilst maintaining all of the advantages gained from the enlarged IRIS graphite analyser.

Engineering

Major developments have been made in the availability of sample environment equipment for the Engineering programme, in response to demands from users. Facilities now available *in situ* on the beamline include high voltage (≤ 20 kV) and a wide range of temperatures (-30 °C $\leq T \leq 1000$ °C) using the dedicated furnace and cooling grips. Additionally, gas flow equipment allows for controlled temperature excursions and stroboscopic capabilities, enabling examination of cyclic material behaviour on a much smaller time scale than that achieved generally at neutron laboratories. Most importantly, these facilities are all available concurrently with the existing 50 kN uniaxial stress rig, allowing for investigations of material behaviour under a broader range of realistic engineering conditions than ever before (Fig. 3.4).

Fig. 3.4. Jude Dann (ISIS) by the new gas flow tube coupled with the furnace and stress rig allowing for controlled temperature excursions for engineering measurements (01RC3885).

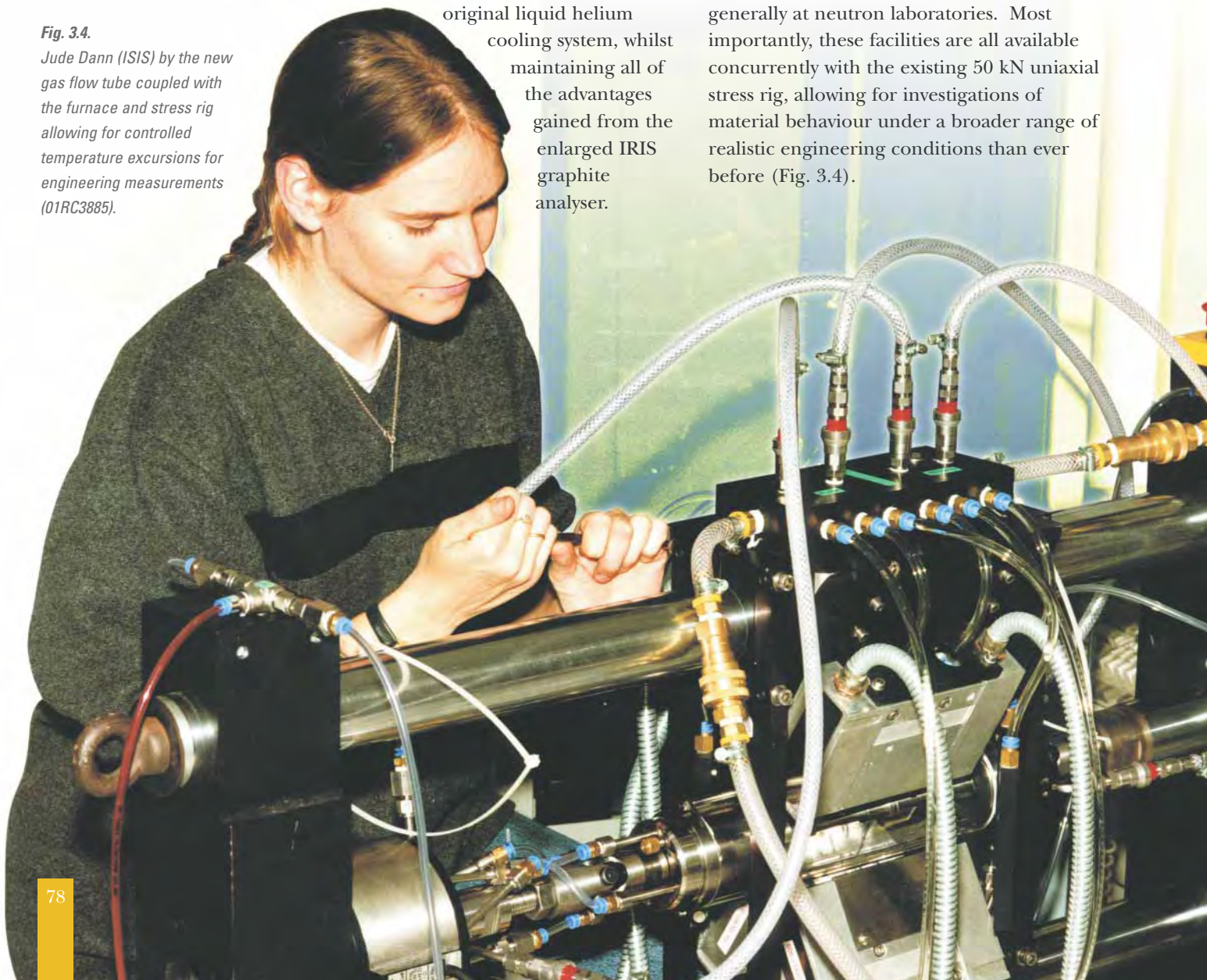




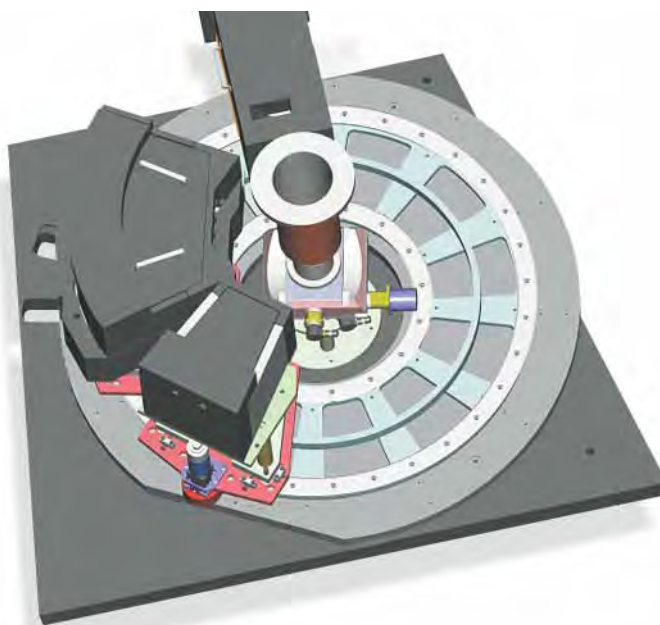
Fig. 3.5. Installation of the ENGIN-X guide by the team from Swiss Neutronics (02RC2110).

The installation of the new engineering beamline, ENGIN-X, is in its final stages, with commissioning scheduled to be completed this year (Fig. 3.5). The full Engineering user program will be delivered on this beamline from January 2003, while the PEARL beamline will see increased use for the High Pressure programme. ENGIN-X was designed as a dedicated beamline for engineering requirements, providing an order of magnitude increase in performance compared with ENGIN, as well as an increase in the days of beam time available, to meet the increasing demand from the user community. Major effort is also being put into software development to enable highly automated sample alignment and data reduction routines, allowing for increased accuracy in sample alignment and real time analysis of data.

PRISMA

PRISMA has seen a sustained programme of investment over the last few years; with the investment in the primary spectrometer complete and the new guides delivering greatly enhanced flux, we are now concentrating on improving the reliability and ease of use of the secondary spectrometer. The PRISMA dual detector operation project has made good progress during the shutdown. The existing rotating table for changing the scattering angles of the PRISMA detector modules has now been replaced by a high precision concentric rail system centred on the sample position (Fig. 3.6). This makes it possible to position the detectors in two-theta well within the angular resolution of the instrument. The new system has the added advantage that both inelastic and elastic detector modules can be operated simultaneously and kept permanently installed on the instrument, enabling experiments to easily switch between data collection modes. The new system was commissioned during the last two run cycles.

Fig. 3.6. The new PRISMA detector rail system.



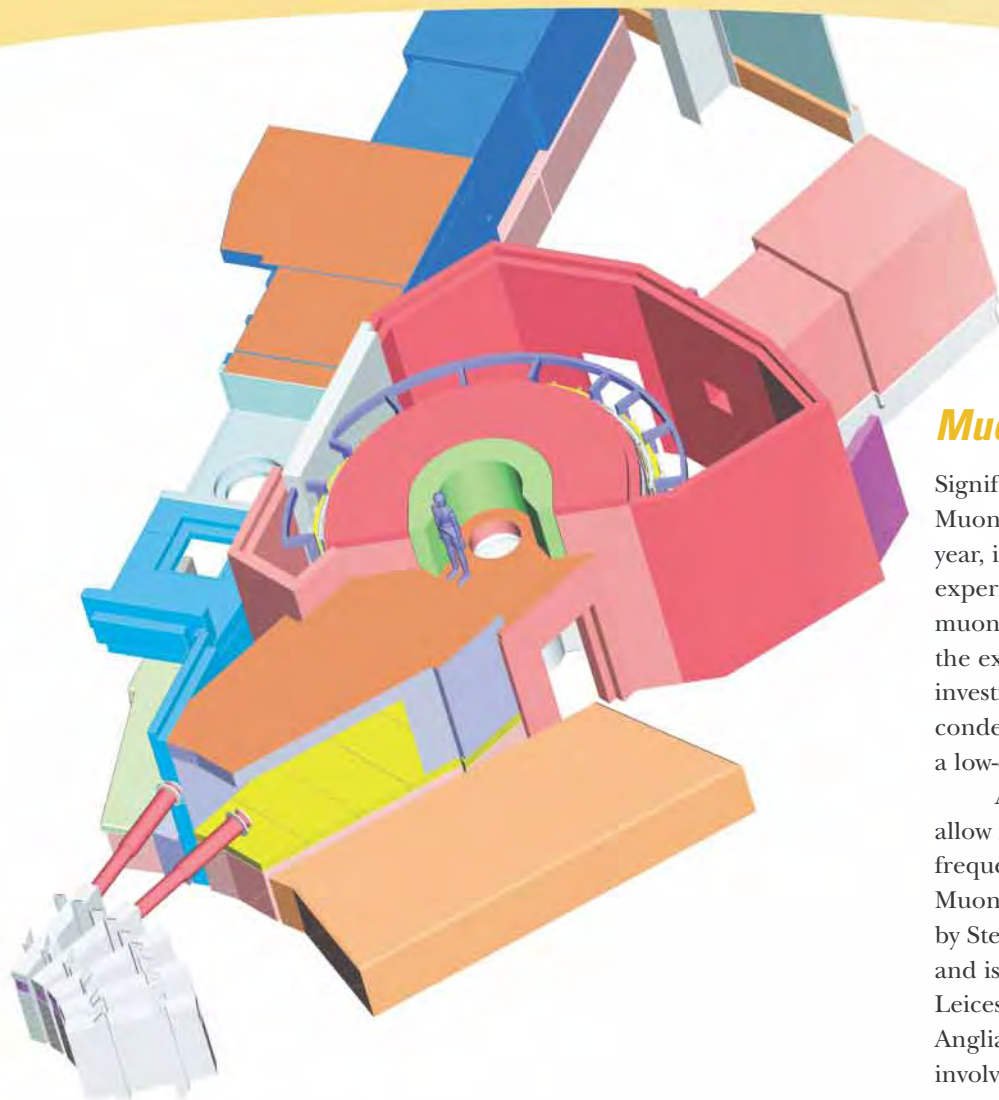


Fig. 3.7.
Schematic of the MERLIN instrument.

MERLIN

In February EPSRC announced that it was to fund the MERLIN project. The three grant holders are Keith McEwen (UCL), Stephen Hayden (Bristol) and Martin Dove (Cambridge). MERLIN is designed to be a high intensity, medium energy resolution spectrometer, and will utilise all the latest advances in technology: a super-mirror guide to enhance flux, as well as MAPS style position sensitive detectors making it ideal for single crystal studies. The detector bank will cover a massive π steradians of solid angle with an angular range from -45° to 135° in the horizontal plane and $\pm 30^\circ$ in the vertical plane. This will allow large swathes of (q, ω) space to be accessed in a single run.

The spectrometer will be positioned on the S4 neutron port between MARI and SXD, viewing an ambient water moderator (Fig. 3.7). This port has recently become available with the removal of the KARMEN bunker. The instrument build is a three year project, with a commissioning phase anticipated for June 2005.

Muons

Significant development of the RIKEN-RAL Muon Facility has taken place over the past year, including the addition of a fourth experimental port to be used for the study of muonic atoms (Fig. 3.8). This complements the existing areas, which are used for investigation of muon catalysed fusion, condensed matter studies and development of a low-energy muon source.

An EPSRC grant was awarded this year to allow further development of the radio-frequency μ SR technique on the European Muon Facility. This work is being co-ordinated by Steve Cottrell from the ISIS Muon Group, and is a collaboration between researchers at Leicester, Manchester, University of East Anglia and ISIS (Fig. 3.9). The work will involve application of the technique in the areas of gas phase reactions, ionic conductors, radical reactions and semiconductors.

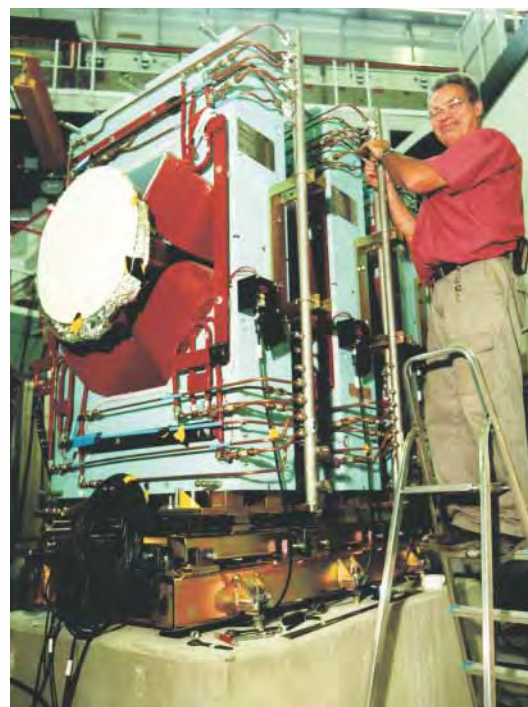


Fig. 3.8. Bill Breton examines the cooling water plumbing on a new quadrupole magnet for the RIKEN-RAL Muon Facility fourth beamline (01RC3968).

Polarising Filter Development

Work continues on ^3He -based polarising filters with the parallel development of two techniques for the polarisation of ^3He by optical pumping. Central to this work is the new polarising filters laboratory in which the technology can be developed before being implemented on ISIS instruments (Fig. 3.10). The laboratory is now fully operational; ^3He polarisation using the metastable method was achieved in November 2001 and in August 2002 using the spin-exchange method.

Polarisation work is continuing on OSIRIS with the development of a continuously pumped circulating system using the metastable method in order to provide a continuously high level of ^3He polarisation. The principle objective is the realisation of a compact compressor which does not depolarise the ^3He – a number are currently being investigated. In addition, detailed modelling of the magnetic environment in OSIRIS has been performed in order to minimise ^3He depolarisation due to inhomogeneities in the magnetic field.

The spin-exchange programme has progressed in collaboration with NIST. Test experiments will soon be performed on CRISP, in which the filter will provide polarisation analysis of the off-specular scattering.



Fig. 3.9. Participants at RAL for the first meeting of the RF- μ SR collaboration (02EC3141).

Fig. 3.10. Kathryn Baker and Steven Parnell setting up the spin-exchange apparatus in the new optical pumping laboratory at ISIS (02EC3168).



Andrew McDowall and Paz Vaqueriro (Heriot-Watt University) having just finished their POLARIS experiment (02EC3144).



Bettina Lotsch (Munich) preparing to use ROTAX (02EC3148).

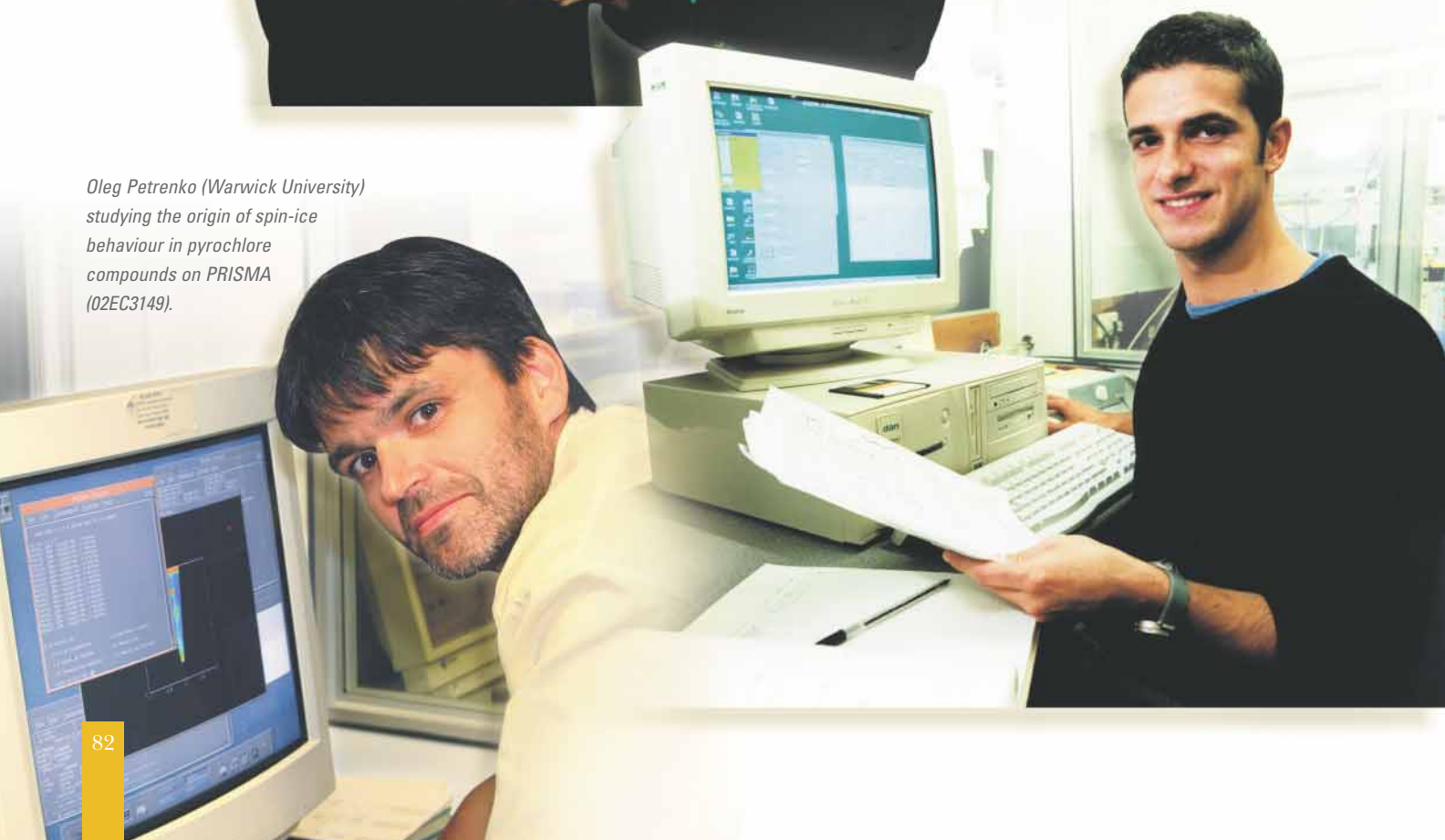


Fabrizio Cavatorta and Vania Calandrini (Universita di Parma) studying restricted water dynamics in hydrated polysaccharides on TOSCA (01RC4409).



Jordan Sarica (Durham) investigating the effects of molecular weight on end-tethered polymers at a fluid interface using SURF (01RC4430).

Oleg Petrenko (Warwick University) studying the origin of spin-ice behaviour in pyrochlore compounds on PRISMA (02EC3149).



Accelerator and Target

Studies of the accelerator and target characteristics, and modifications to the accelerator equipment, enable continual improvements to be made to the proton beam intensity and stability. This chapter outlines the performance of the accelerator and target over the past year, and describes some of the main developments designed to improve the machine reliability and performance.

4

ISIS Beam Statistics 2001 – 2002

ISIS continues to be the world's most intense pulsed spallation neutron source and for the first time exceeded 700 mA.hrs of proton current. For the period of this report and during scheduled operating cycles, ISIS delivered a total of 725 mA.hrs of proton beam to the muon and neutron targets at an average current of 192 μ A.

Table 4.1 gives beam statistics for the individual cycles in the year 2001-2002. Year-on-year statistics for ISIS performance are given in Table 4.2. Fig. 4.1 shows the total integrated current for each year since 1987 and Fig. 4.2 indicates the improvement in operational efficiency since 1987.

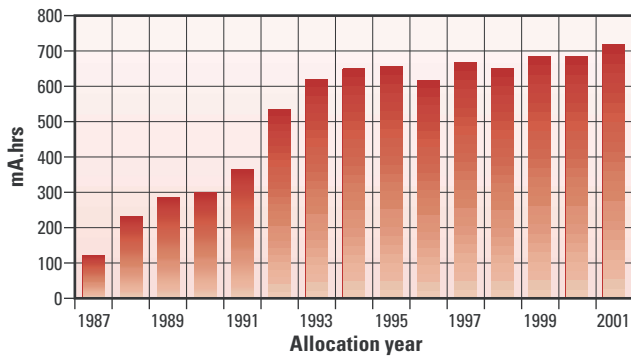


Fig. 4.1. Total integrated ISIS current.

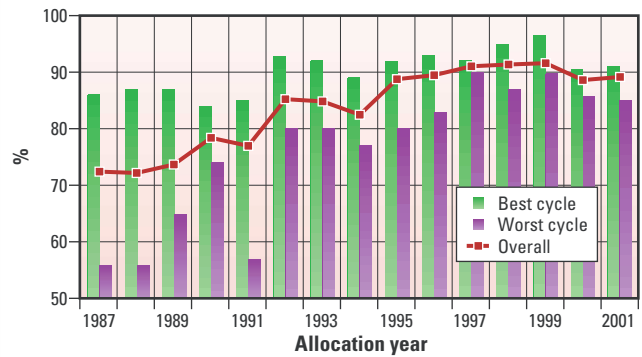


Fig. 4.2. Improvements to operational efficiency since 1987.

Cycle	01/1	01/2	01/3	01/4
Beam on target (hrs)	891	947	937	1008
Total beam current (mA.hr)	168	181	185	190
Average beam current on target (μ A)	189	191	197	189
Peak beam current (μ A, averaged over 24 hrs)	192	195	200	189
Current averaged over cycle (μ A)	161	173	177	172
Average beam trips per day	27	19	25	44

Table 4.1. ISIS operational statistics for year 2001-2002.

Year	1995	1996	1997	1998	1999	2000	2001
Total scheduled user time (days)	168	168	168	175	168	168	168
Total time on target (days)	151	152	153	160	153	154	158
Total integrated current (mA.hrs)	661	621	672	656	687	687	725
Average current on target (μ A)	182	171	183	171	187	186	192
Peak current averaged over 24 hours (μ A)	201	204	197	193	198	194	200
Current averaged over year (μ A)	162	153	167	156	171	165	180
μ A.hrs per trip	80	115	81	72	106	120	141
Total power consumption (GWh)	46	47	47	42	52	46	46
Energy efficiency (mA.hr/GWh)	14.4	13.1	14.9	14.9	13.2	14.9	15.7

Table 4.2. Year-on-year ISIS performance summary.

Accelerator and Target Developments

Efforts are continually made to maintain and advance the ISIS accelerator and target reliability. Old and obsolete equipment is being replaced and systems improved to keep ISIS at the forefront of pulsed neutron sources. Significant progress has been made in a number of areas, including work on the new radio-frequency quadrupole preinjector, new RF cavities for the synchrotron and replacement of the synchrotron extraction straight.

Injector Group

The Injector Group is responsible for maintaining and developing the H⁻ ion source, the 665 keV Cockcroft-Walton preinjector and the 70 MeV drift tube linear accelerator (linac). In the past year this has included significant work on the 665 keV 202.5 MHz 4-rod RFQ accelerator intended as a replacement for the present ISIS Cockcroft-Walton preinjector, and acceleration of the first beam through the RFQ was achieved on 4 October 2001 (Fig. 4.3). Since then the beam characteristics at the output and input of the RFQ have been measured, and in all cases the measurements agree well with the predictions of the RAL computer codes on which the RFQ design was based. This paves the way for future RFQ development work, for example for the proposed European Spallation Source (ESS).

Fig. 4.3.
First beam from the new RFQ
(01RC3905).



The ion source development rig has been commissioned, and measurements have already begun. In particular, beam emittances

have been measured directly at the output of the ISIS ion source for the first time (hitherto measurements have been possible only after the beam has passed through the Cockcroft-Walton accelerating column). The measurements can be reproduced using electromagnetic design and particle tracking codes, and this provides a good basis for future programmes on high current ion source development to be carried out on the rig.

Synchrotron and Electrical Engineering Group

Group activities have concentrated on continual monitoring, refurbishing, redesigning and replacing of equipment as necessary to achieve optimum performance of ISIS. This has included preparations for the ISIS 300 μ A upgrade which will involve installation of four new dual harmonic RF cavities in the synchrotron. Two of these cavities have been installed during the 2002 shutdown (Fig. 4.4) with a further two planned for installation in 2003.

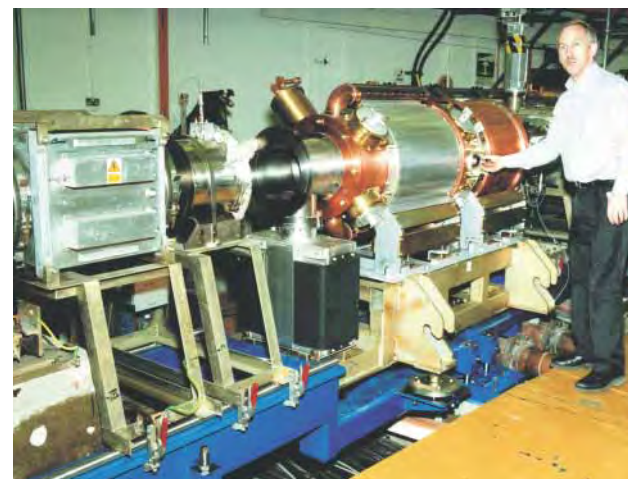


Fig. 4.4. Mike Crendler aligning the second-harmonic cavity installed in super period 6 (02RC1874).

Under the obsolescence programme the synchrotron main magnet power supply is undergoing major changes. During the 2002 long shutdown the 40-year-old capacitor bank



Fig. 4.5.
Neil Meadowcroft inspects
the new main magnet power
supply capacitor bank
(02EC3184).

has been replaced with modern low-loss dielectric capacitors (Fig. 4.5). Estimated power saving will be approximately 150 kW.

Target Group

Operation of the present target station has been reliable through the year. Some problems have been encountered by the users of the methane moderator due to temperature variations. Work is in progress to investigate how best to improve the temperature stability of the moderator.

Work to replace obsolete equipment on the control systems has continued successfully. Equipment installed includes a new control system for the cryogenic chillers, a new dynamic interlock interface for the critical parameters system and the first stage of a new intrinsically safe cabling system and its associated hardware for the hydrogen and methane moderators.

Work on the proposal for a Second Target Station has continued. Emphasis has been on optimisation of neutron output from the target, moderator and reflector assembly, and on the site layout (see pages 94-95 for more details).

Controls Group

The Group provides computer control and monitoring for accelerator and target systems using the Vsystem package, and a variety of custom and industrial control hardware and software. This includes the integration of new equipment as obsolescent components are replaced on the accelerator.

This year has seen the stripping out of all the old control system hardware from the target control room, replacement of the target critical parameter and scanner systems, and the addition of a system for the target chillers. Unattended running of the RFQ system using the extension of the control system to the test rig has now commenced. Control desk displays have moved on to faster and more easily maintainable NCD X-terminals and the controls network has been migrated to optical fibre. We have played a major role in implementing new software for the synchrotron straight one replacement, supporting the work of the beam diagnostics and accelerator physics staff, in addition to upgrading and developing software for the injector, synchrotron RF systems and magnet control. Work has started on a replacement for the existing Analogue Waveform Switching system (AWS) which routes oscilloscope signals from round the machine to the MCR control desk.

Operations and Installations Group

The Group is responsible for co-ordinating a Facility-wide installation service through its electrical, mechanical, ancillary plant and vacuum sections. It is also responsible for the correct operation of the Facility during user cycles. In addition to participation in a wide range of activities involving other groups, in particular the synchrotron straight one replacement project, the Group's own work programmes this year have included updating the main ring vacuum system and replacement

of the fire alarm system in the R55 experimental hall. Much effort has also gone into the pre-build and testing of components to replace the beam collection and extraction straight section in the synchrotron (Figs. 4.6, 4.7). This was completed during the 2002 long shutdown.



Fig. 4.6. Ian Gardner and Mike Krendler watch during the installation of new beam collectors and monitors in super period 1.

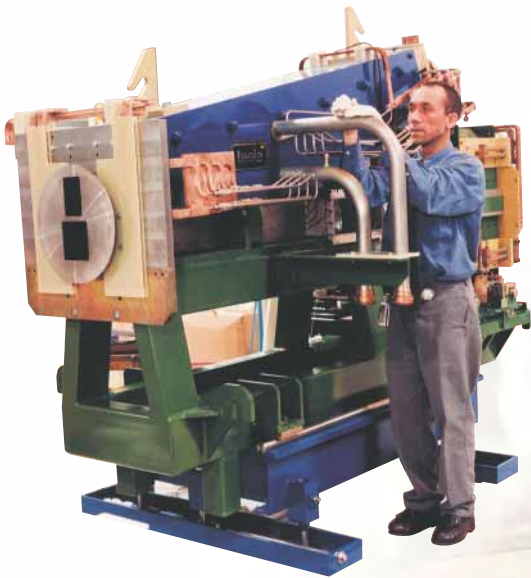


Fig. 4.7. David Jenkins with the new extraction septum magnet (02RC2336).

Project Engineering Group

The PE Group provides mechanical engineering support to the ISIS facility. Significant effort has gone into preparing the proposal for the Second Target Station, and

work on the R&D phase of the ESS case has also been undertaken.

Projects over the past year have included the preparatory design for the installation of the new RFQ on the linac. All of the main cooling water systems are also under review with the aim of updating and developing a controllable distribution system. The linac cooling plant has been extended to facilitate independent operation; additional water-cooling has been added for the RFQ and the 2nd harmonic accelerating cavities. A prototype oil-cooling package has also been produced which will accommodate the increased heat load on the six thyatron kicker switches for 300 μ A operation. Additionally, the dismantling of the KARMEN equipment has commenced, thus increasing the number of available neutron ports by opening up the south side upper rear ambient water moderator.

The SXD-II beam line has been commissioned and other improvements aimed at increasing reliability have been provided. The numerous projects for sample environment equipment included the challenging design and manufacture of 28 mm diameter sapphire beam windows for a CO₂ gas container at a pressure of 1200 bar and temperature of 120 °C for the LOQ beam line.

Fig. 4.8.

Hanna Firkremariam, a Kingston University placement student with the Project Engineering Group, looks at the 100 kW water cooled resistive load which she helped to design. The load will be used for development of the new main magnet power supply (02RC2797).



Ion Beams Group

Studies into targets for a neutrino factory (NF) have concentrated on the problems associated with shock waves induced by short proton pulses, namely material strength and fatigue. Finite element modelling of thin sections of the target material have shown that the stress experienced by a target under beam bombardment can be reproduced (albeit in small volumes) by intense high power electron beams such as those used in large volume welding facilities. Experiments are underway which subject candidate materials to typical high levels of stress with the additional advantage that the effects on the target materials due to many cycles of shock can be studied – essentially a lifetime test. These studies should prove invaluable in assessing the practicality of a solid target for a NF.

A proposal to build a muon beam facility suitable for proof-of-principle experiments for a neutrino factory has been investigated, and if built this would be the focus of an international collaboration for a Muon Ionisation Cooling Experiment (MICE). The study would involve the installation of a short linac section, superconducting solenoids and special liquid hydrogen absorbers. This will replace the existing high-energy physics test facility on ISIS, but should still be able to cater for those needs.

Accelerator Theory and Future Projects Group

New blood has been injected into the group with the arrival of Frank Gerigk from CERN and the conversion of Giulia Bellodi from Particle Physics at QMC to accelerator research (Fig. 4.9). The increased manpower has enabled work to progress on the European Spallation Source with many loose ends being tidied up. Parallel studies have produced a new design for a synchrotron that could be used both for an upgrade of ISIS to 1 MW and as a test-bed for the proton driver for a neutrino factory.



Fig. 4.9. New recruits to the Accelerator Theory and Future Projects Group, (clockwise from the bottom right) Giulia Bellodi, Stephen Brooks (summer student, Trinity College, Oxford), Frank Gerigk and group leader, Chris Prior (02RC3049).

Much of the Group's mandate relates to collaboration with laboratories overseas. In this respect, work has been carried out with CERN on neutrino factory rings, one of which might be a possible replacement for the ageing PS; with Fermilab on an 8 GeV synchrotron-based proton driver; and in a preliminary way, with the KEK group designing JHF at Tokai-mura in Japan. Other activities by group members include a series of lectures at the CERN Accelerator School in Seville, involvement with the accelerator board of the European Physical Society, and preparation of a successful bid by the U.K. to host the European Particle Accelerator Conference (EPAC) in 2006 in Edinburgh, Scotland.

A year around ISIS



John Thomason (ISIS) explains the workings of the Cockcroft-Walton pre-injector to A-level students attending the Oxford Particle Physics Masterclass (02RC1583).



ISIS instrument scientists Chris Frost and Martyn Bull organised a two-day event for teachers in February, to build links between the science done at ISIS, and the national curriculum. Here, Martyn is explaining the workings of the accelerator in the extracted proton beamline (02EC1218).



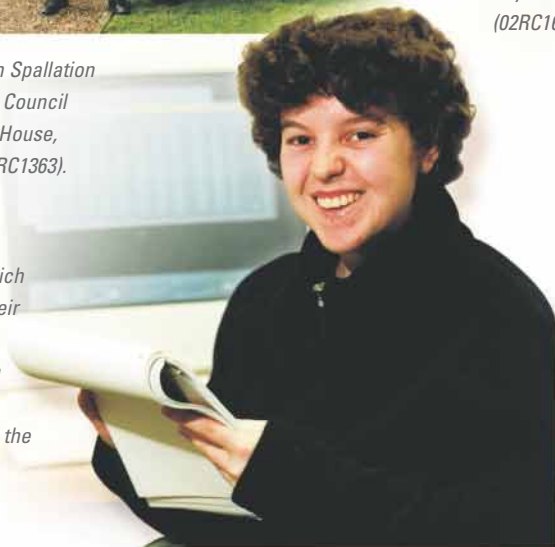
Members of the European Spallation Source Science Advisory Council meeting at the Cosener's House, Abingdon in February (02RC1363).

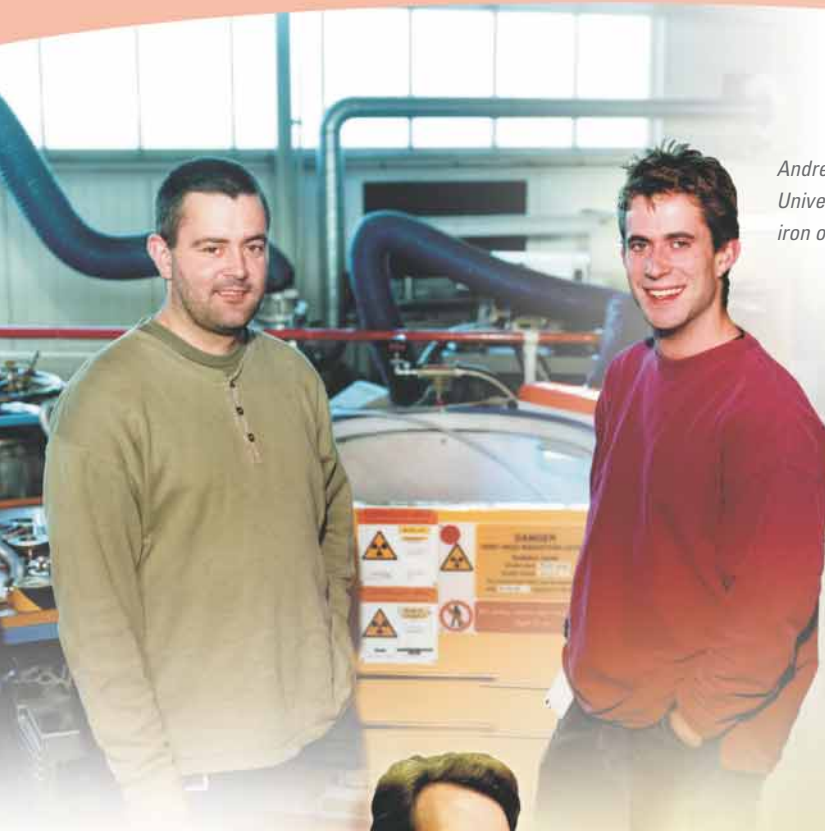


Chris Frost (ISIS) showing the wonders of superconductivity to young folks at a Laboratory day for 'exploring particles' (02RC1615).

Uschi Steigenberger shows ISIS to visitors from the Korean Atomic Energy Research Institute in December (01RC5551).

ISIS takes several sandwich students each year for their mid-university placement time. Lynne Thomas from Edinburgh University has spent her time working in the Crystallography Group (01RC4405).

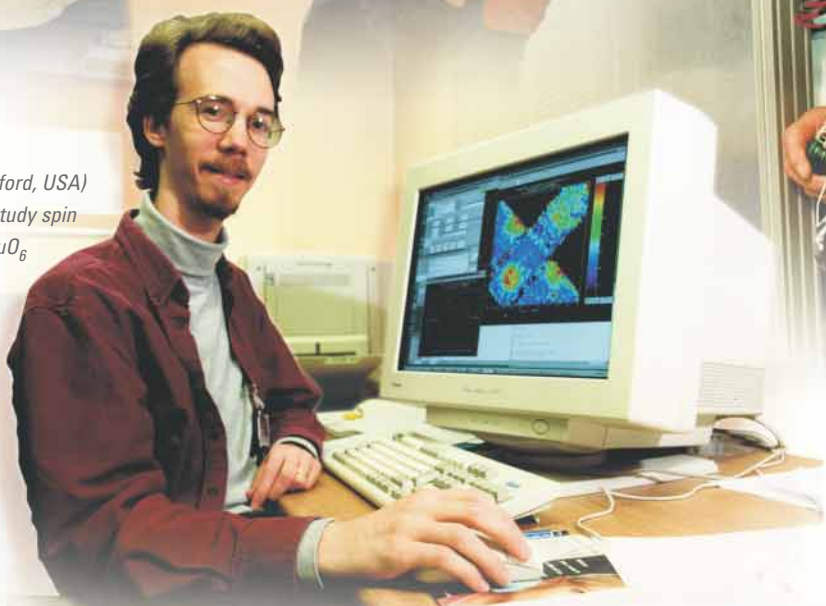




Andrew Hector and Alex MacDonald (Southampton University) during their experiment studying layered iron oxide halides on OSIRIS (01RC4416).

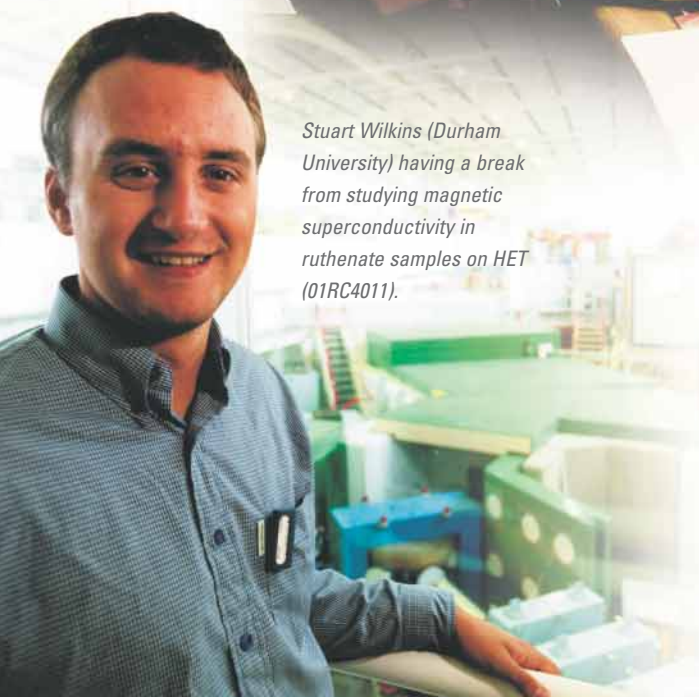


Raymond Moreh (Ben Gurion University of the Negev) measuring the kinetic energy of H₂ molecules adsorbed on active carbon fibre using TOSCA (01RC4015).

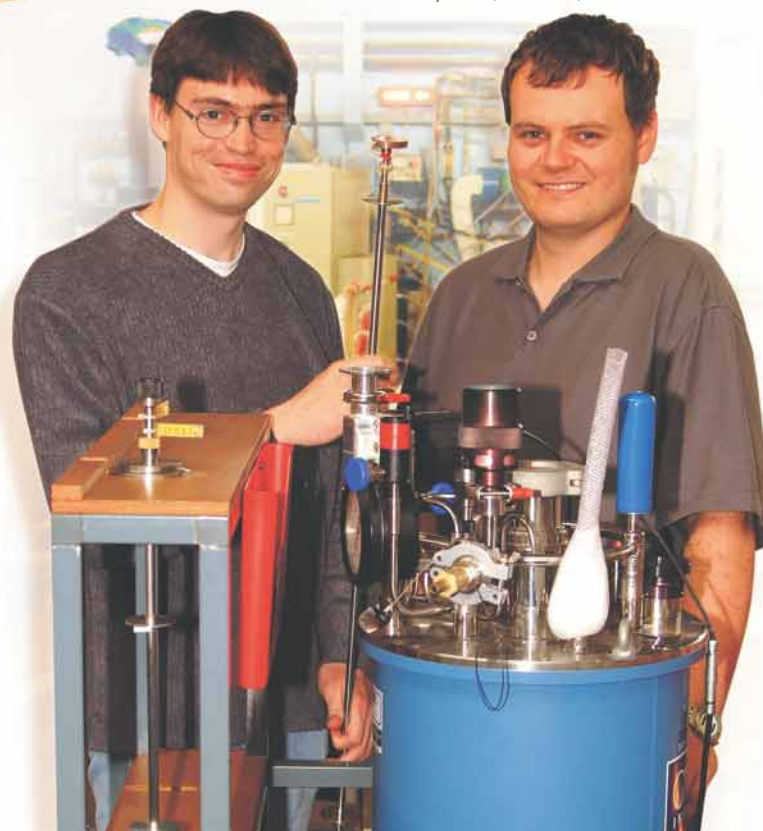


Owen Vajk (Stanford, USA) using MAPS to study spin dynamics in SrCuO₆ (01RC4010).

Marek Schmidt and Graeme Blake (ISIS post-docs) working on a GEM cryostat (02EC3157).



Stuart Wilkins (Durham University) having a break from studying magnetic superconductivity in ruthenate samples on HET (01RC4011).



User Interaction and Support

Essential for the successful operation of ISIS are the specialised teams responsible for maintaining and developing experimental and computing facilities. The technical support given by these groups is complemented by the organisational and administrative services provided by the User Office, which oversees the arrangements for the 1600 scientists who visit annually.

5

Organisation and User Interaction

The ISIS User Office is responsible for the travel and accommodation arrangements for the 1600 researchers who visit the Facility each year. The Office also collates and records the 1000 or so proposals for beamtime on ISIS instruments received annually; these proposals are reviewed by international scientists who make up the Instrument Scheduling Panels.

Each year there are two calls for experimental proposals, with deadlines on 16th April and 16th October. Following these deadlines the ISIS Scheduling Panels (ISPs) meet early in June and December. The seven ISPs comprise ~70 international scientists (see Table 5.1) who have the job of assessing the scientific quality and timeliness of proposals submitted to individual instruments, and to advise on the allocation of beamtime.

User Liaison

The ISIS User Office plays a central role in user reception and programme organisation. The information entered into the ISIS integrated database system by the ISIS User Office forms the first stage in the scheduling of the instruments and the sample environment equipment which is carried out by the instrument scientists and the user support group.

Information about ISIS, the ISIS instruments and how to apply for beamtime is available on the World Wide Web (<http://www.isis.rl.ac.uk>). This site also includes electronic versions of the ISIS beamtime application forms; electronic submission is very popular and about 90% of the applications are received via this route.

ISIS User Committee

The ISIS user community is represented by the ISIS User Committee (IUC) which draws its membership from the seven ISIS Instrument User Groups. The chairman from each group plus an elected representative attend, together with the Division Heads of the ISIS Science Divisions and the Leader of the User Support Group. The committee reports to the Director of ISIS. The present committee membership is shown in Table 5.2. The Chairman of the committee can act as Ombudsman in cases of unresolved disagreement between ISIS and members of the community. The group meets twice a year immediately following the ISP's. Its terms of reference are: to address all aspects of user satisfaction at the facility, including scientific and technical support, source reliability, instruments, sample

Table 5.1.
ISIS Scheduling Panel
Membership.

ISP-1 Diffraction	ISP-2 Liquids	ISP3 Large Scale Structures	ISP4 Excitations	ISP5 Molecular Spectroscopy	ISP 6 Muons	ISP7 Engineering
A Albinati G Artioli W Clegg J A Hriljac P. Lightfoot A Powell G D Price P R Raithby C Ritter P Stephens P Thomas	P Madden T. Fukunaga R McGreevy K Seddon N Skipper M E Smith J Swenson	J Andrews N Clarke I Gentle J Lawrence F Leermakers A Rennie R Richardson S Thompson R Triolo	A Boothroyd C Broholm R Cowley D Edwards M Gunn S Julian A Krimmel D Noreus K Yamada	J Bradshaw S Kilcoyne J Larese D O'Hare C Rhodes R Simmons D Timms	S Blundell J Campos-Gil P Carretta A Fisher R Lichti P Mitchell E Morenzoni M Iwasaki	J Bouchard M Fitzpatrick M Johnson R Peng D Smith G Swallowe
RM Ibberson CC Wilson	D Bowron AK Soper	J Webster J Penfold	TG Perring S Bennington	J Mayers J Tomkinson	S Cottrell P King	J Dann M Daymond

environment, detectors, electronics, data acquisition, instrument control, computing, data analysis, safety, security, food, accommodation, transport and claims. The group provides input and advice on the development of new instruments, sample environment and associated equipment. It also serves as co-ordinator for the User Groups and their meetings and it recommends specific training courses for the wider community.

User Satisfaction

ISIS values the opinions of its users and solicits them openly – all visiting scientists are asked to complete a satisfaction survey after each experiment. The Facility scores consistently highly in areas of scientific and technical support, and instrument performance (Fig. 5.1). Areas where improvements are needed are acted upon – as an example, last year’s efforts to increase the restaurant’s opening hours were very successful.

Chairman	R J Stewart, University of Reading
IUG1 Crystallography	P Battle, University of Oxford R J Nelmes, University of Edinburgh
IUG2 Liquids and Amorphous	A Barnes, University of Bristol N Skipper, University College London
IUG3 Large Scale Structures	R J Stewart, University of Reading R Thomas, University of Oxford
IUG4 Excitations	D McK Paul, University of Warwick
IUG5 Molecular Science	K Ross, University of Salford
IUG6 Muons	U Jayasooriya, University of East Anglia S Kilcoyne, University of Leeds
IUG7 Engineering	G Swallowe, Open University M Fitzpatrick, Open University
A D Taylor	Director, ISIS
J Green	EPSRC
U Steigenberger	ISIS Spectroscopy and Support Division Head
J Tomkinson	ISIS User Office Co-ordinator
R S Eccleston	ISIS Instrumentation Division Head
R L McGreevy	ISIS Diffraction and Muon Division Head
Z A Bowden	ISIS User Support Group Leader

Table 5.2. ISIS User Committee Membership.

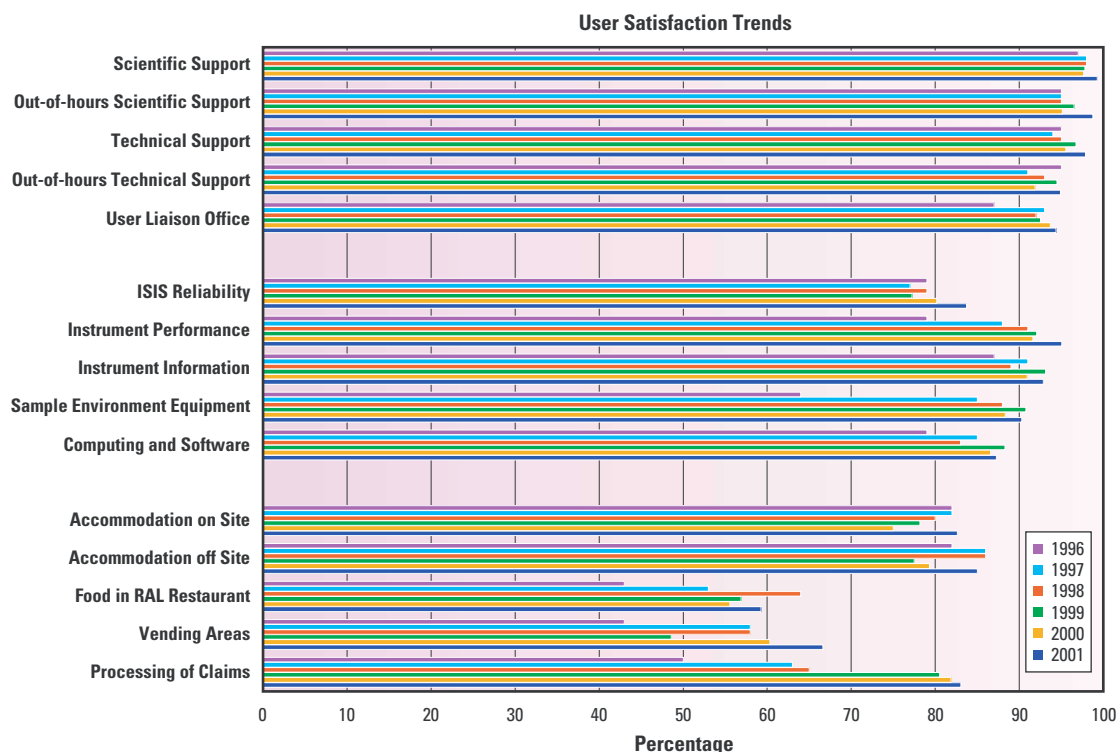


Fig. 5.1. ISIS user survey results 1996 – 2001.

News and Events

A round-up of news and events from the Facility, including an update on the ISIS Second Target Station, new arrangements for access to the Facility for UK researchers and funding for European scientists, the Neutron Training Course, workshops on stress and spintronics, and the dismantling of KARMEN.

The Second Target Station

The ISIS Second Target Station is a new major development at ISIS. It will provide a considerable enhancement in the area of cold neutrons, providing significant new opportunities for the development of studies in Soft Matter, Advanced Materials and Bio-Materials. Taking one pulse in five from ISIS, the 60 kW target station can be optimised for the production of cold neutrons in a way not possible on higher power target stations, giving a performance for cold neutrons equivalent to that expected of a 600 kW source. Detailed simulations and calculations carried over the last year during the feasibility phase of the project confirm those expectations.

Good progress has been made towards securing a start to the project. The Business Case has been reviewed and accepted, in line with the Government requirements – the

Gateway process. Funds have now been released to enable site preparation work to start in early 2003, and work is now underway in order to confirm detailed planning authority in late autumn this year. This will ensure that the major civil engineering work takes place at the same time as that for Diamond.

A Scientific Advisory Committee has been set up to represent the broad scientific interests of the major project stakeholders, the UK user community; its membership is listed below.

Scientific Advisory Committee

R K Thomas	(Chairman, Oxford)
J A C Bland	(Cambridge)
A Donald	(Cambridge)
M Dove	(Cambridge)
P Edwards	(Birmingham)
M Gunn	(Birmingham)
A Harrison	(Edinburgh)
R A L Jones	(Sheffield)
R W Richards	(Durham)
D Tildesley	(Unilever)
P Madden	(Oxford)
A Watts	(Oxford)

Fig. 5.2.
Members of the Second Target Station Scientific Advisory Committee during the inaugural meeting in July (02RC2819).



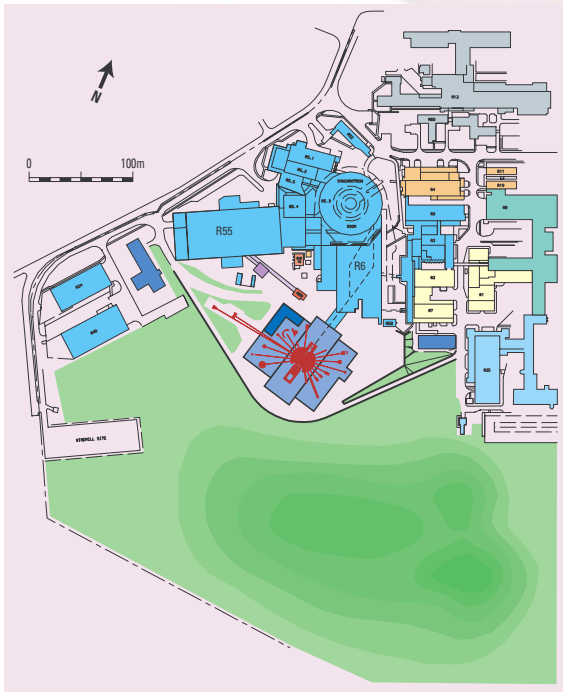


Fig. 5.3.
Plan and 3-dimensional view of the proposed layout for the ISIS Second Target Station.

To proceed to the detailed planning stage of the project, the overall site layout is required, and advice was sought from the Scientific Advisory Committee at its inaugural meeting in July (Fig. 5.2). The layout (Fig. 5.3) was chosen to provide the optimal solution to accommodate the reference instrument suite, provide minimal disruption to the ongoing ISIS programme, and be consistent with future MW developments of ISIS.

The reference instrument suite developed in conjunction with the user community in 1999 is shown in Fig. 5.4.

In the coming months the user community and the Scientific Advisory Committee will be invited to reconsider and update the reference instrument suite, and progress towards deciding the ‘day one’ instruments.

The project is on schedule for neutron production in 2006/07.

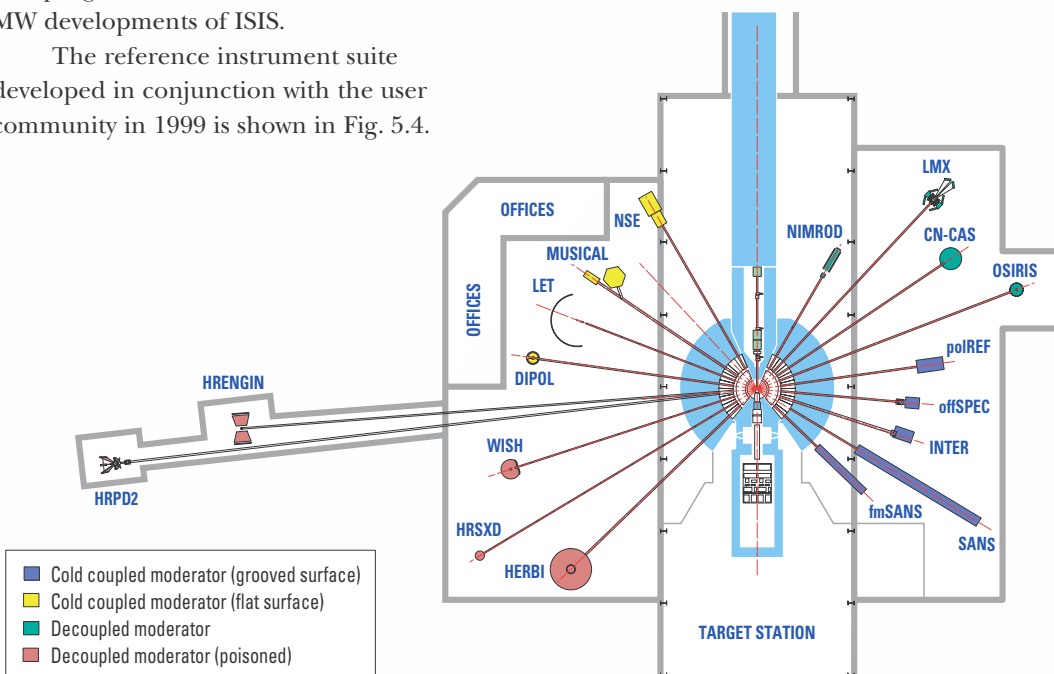


Fig. 5.4.
Current reference instrument suite for the Second Target Station.



Fig. 5.5. ISIS scientists have been involved with various events to explain the Laboratory's work to children and the public. Here, Jude Dann (ISIS) enthral students from a local school with some practical science demonstrations during a day aimed at encouraging women to enter science (02RC1458).

Access to ISIS and Other CLRC Large Facilities

New arrangements for access to ISIS (and the SRS and Central Laser Facilities) will come into place from April next year, as a result of the second stage of the CCLRC Quinquennial Review (QQR). The CCLRC will then be responsible for the peer review and scheduling of proposals from researchers requesting access – meaning that ISIS will be ‘free at the point of access’ to the UK academic research community.

The CCLRC will be developing the QQR recommendations for the ISIS, SRS and CLF facilities including arrangements for access procedures and the peer review of applications for time on the facilities. In order to do this, the CCLRC will consult with the facility user communities to take into account changes to access mechanisms that facility users might require.

Full details of the changes and their implications can be found at http://www.clrc.ac.uk/QReview/QR_FacilityAccess_07_02.htm and the ISIS contact person with regard to access arrangements is Uschi Steigenberger.

European Access Contracts

ISIS neutrons and muons both have new Access contracts under the EC Framework Programme 5 to provide facility time for European researchers wishing to use ISIS facilities. ISIS is particularly keen to attract new user groups or those wishing to apply neutron or muon techniques to novel scientific areas. Researchers wishing to apply under the EC programme can do so via the normal ISIS

proposal mechanism (see www.isis.rl.ac.uk for details); the scheme will provide travel and subsistence costs for up to two researchers participating in a sponsored experiment.

Both access programmes have just undergone a technical review of their contracts, performed by a panel of independent European experts. The review considered factors such as scientific output, quality of the scientific and technical support, selection procedures etc. Both the neutron and muon programmes were rated highly and received excellent reports.

ESS

The European Spallation Source (ESS) is a proposed accelerator-driven facility for condensed matter research in Europe conceived to complement the ~1 MW facilities being constructed in the USA and Japan. The project builds on the success of the ISIS facility, and is supported by 18 laboratories and organisations from 11 countries in Europe. The technical scope of the ESS has expanded and is now based on a 10 MW proton accelerator feeding 5 MW into a 50 Hz short pulse target and 5 MW into a 16 2/3 Hz long pulse target.

The UK neutron community and ISIS scientists continue to have a strong involvement in the development of the scientific case and in providing advice as members of the ESS Scientific Advisory Committee. At the ESS launch meeting in May 2002 in Bonn (Fig. 5.6) the key note science presentations were given by Phil Withers, Gabriel Aepli and Olwyn Byron. They described the impact of neutron scattering experiments on our understanding of and – ultimately – on our ability to control technologically-relevant materials.

In the technical work, ISIS accelerator experts have a leading role in the development of the linac, especially the crucially important front end, and the compressor ring. ISIS instrument scientists are



Fig. 5.6.
The ESS launch meeting was held at the International Congress Centre of the Former House of Parliament of the Federal Republic of Germany in Bonn in May. Inset: Phil Withers (Manchester) explains how the ESS will benefit the Engineering community.

working closely with colleagues from other neutron laboratories to develop further ideas for the ESS instrument suite.

Discussions about the siting of the ESS project are now underway. The UK academic community has a long and distinguished history and a highly successful track record in developing and utilising neutron sources for condensed matter science. The UK, through the CCLRC, has been strongly engaged in the research and development phase of the ESS project for the past 10 years. Clearly the UK will wish to be actively involved in developing next generation neutron facilities for Europe.

Stress Welds European Partners

The Engineering Group have been collaborating on an EU-funded project, JOIN-DMC, which is considering optimisation of the friction stir welding process for dissimilar materials and composites. One aspect of this work is measurement of the residual stresses left in the welds for different welding parameters. This year saw a productive meeting of the EU partners, hosted at The Cosener's House, to push forward the collaboration and consider the next steps for this venture (Fig. 5.7). The project so far has been highly successful, and has allowed determination of suitable process windows for

welding several new material combinations, expected to prove useful for the industrial partners in the collaboration.



Fig. 5.7.
Participants at the April 2002 meeting collaborating on EU project JOIN-DMC.

Neutron Training Course

September last year saw the first of a new series of neutron training courses hosted at ISIS. Thirty students (Fig. 5.8) from all over Britain, representing a wide variety of scientific disciplines, came to ISIS to learn the practical details of running a neutron scattering experiment. Although courses exist to teach the theoretical aspects of neutron scattering, the ISIS training course is currently the only one where UK students can get hands-on experience of time-of-flight neutron scattering techniques.

Fig. 5.8.
Neutron training course participants and tutors (01RC4509).



The next course will be held in January 2003 and is open to all UK based PhD and Postdoctoral students. The content of the course is broken down into four modules: Basic Principles, Large Scale Structures, Spectroscopy and Diffraction.

Early 2003 will also see a practical course in pulsed muon techniques, also for PhD and post-doctoral students new to the subject. As with the neutron course, the training will include substantial hands-on experience to give young researchers the skills in the technique that they need to best exploit future facility time.

Materials for Spin Electronics Meeting

A two-day international workshop was organised at the Cosener's House in January by Chris Marrows (Leeds University) and Sean Langridge (ISIS) to discuss the use of neutron techniques in the burgeoning field of spin electronics. There is currently an enormous world-wide drive to develop devices where the spin of the electron is used to store or process information, either in addition to, or instead of, the charge. Although many device designs have been put forward, finding materials with which to implement them is a significant experimental challenge. Presentations at the workshop covered such diverse areas as reflectometry in magnetic nanostructures, diffraction, spin-injection studied through

small angle scattering and muon studies of the manganites. There was clearly an increased appreciation for the rôle that neutron and muon techniques can play in unravelling the properties of these technologically important systems as well as posing some important questions about the fundamental properties of the materials involved. The meeting was partly funded by the European Union Neutron and Muon Round Table.

Research Networks

ISIS has been very actively involved in CLRC's Research Networks, established to foster links between the various CLRC facilities, their staff and their users. Steve Bennington (Excitations Group Leader) organised the first meeting of the Centre for Materials Physics and Chemistry, a Workshop on Carbon Polymorphs held at RAL in February (Fig. 5.9). Chick Wilson (Crystallography Group Leader) co-ordinates the Centre for Molecular Structure and Dynamics (CMSD), and the inaugural meeting at the Cosener's House in March is already bearing fruit in terms of new collaborations. Nikitas Gidopoulos of the ISIS Theory Division was co-organiser of the CMSD-sponsored workshop on Density Functional Theory, which brought together leaders in the field for a stimulating long-weekend meeting at Cosener's house.

Fig. 5.9.
The first meeting of the CLRC Centre for Materials Physics and Chemistry brought together a wide range of researchers interested in carbon polymorphs (02RC1388).



KARMEN Dismantling

The 6-month shut-down at the beginning of 2002 saw work start on the dismantling of the KARMEN neutrino experiment bunker in the ISIS hall. Data taking on KARMEN came to an end in July 2001, and removal of the bunker will make additional ports available for neutron instruments. Clearing the 7,000 tonnes of steel shielding plates and blocks (Fig. 5.10) is a major exercise in itself and will continue over coming months.



Fig. 5.10. Dismantling of the KARMEN neutrino bunker (02RC1839).

ISIS People

Congratulations are due to several ISIS staff members who have been recognised during the past year for their scientific achievements. Paolo Radaelli, instrument scientist on GEM, has been appointed Visiting Professor in the Department of Physics and Astronomy, University College London, and Chick Wilson, Crystallography Group Leader, has also been appointed as Visiting Professor, Department of Chemistry, University of Durham. At the Annual Spring Meeting of the British Crystallographic Association, Bill David was selected to receive the inaugural BCA Prize lectureship, one of three senior Prize lectureships awarded by the BCA. At the same BCA meeting, Daniel Bowron,



Fig. 5.11. Jimmy Chauhan and colleagues at his retirement (02RC2353).

a member of the ISIS Disordered Materials Group, was awarded the 2002 Philips Analytical Award of the BCA/IoP for outstanding published work by a young scientist in the field of Physical Crystallography. Very many congratulations to all four! Congratulations too to Steve Bennington, who became Leader of the ISIS Excitations Group during the year. And a stop-press announcement: very many congratulations also to Sean Langridge, of the Large Scale Structures Group, who has just been awarded the prestigious Institute of Physics Charles Vernon Boys Medal and Prize for his contributions to the field of modern magnetism.

ISIS has also seen people coming and going during the past year. Professor Robert McGreevy succeeded Gavin Williams as Head of the ISIS Diffraction and Muon Division on Gavin's retirement in May. Robert had been working at the Studsvik Neutron Research Laboratory (Uppsala University) in Sweden since 1992, becoming head of the laboratory in 1994 and then Professor of Neutron Scattering Physics. Jimmy Chauhan and Hari Shah retired after giving stirring support to ISIS cryogenic facilities and electronics respectively; Mike Armstrong retired from the ISIS Main Control Room and Trevor Cooper from the Chopper Section. David Martin and Ken Anderson have also left ISIS to pursue their neutron careers at other institutes.

Experimental Support

The activities of the Sample Environment, Computing, Electronics and Detector Groups can be divided into three areas: support of the experimental programme; delivery of hardware and software for new projects; and the development of new technologies and capabilities.

Sample Environment

The SE Section provide extensive support for the ISIS experimental programme, including experiments which extend the use of SE equipment beyond their usual working envelope. This has included use of pressures up to 1.0 GPa and provision of gas handling facilities for the cryomagnet. Similarly, the dilution refrigerator has also been used with a user-provided clamped high-pressure cell achieving 1.5 GPa at 150 mK.

Additions to SE equipment during the year included a 25 mK-4 K Kelvinox dilution refrigerator system for the MuSR instrument and a recirculating ^3He ultra-low temperature orange cryostat (OC) insert. A 50 mm bore cryogen-free helium exchange-gas cryostat with base temperature of 3.8 K has also been provided for GEM. Three maxi-OCs have been converted to 50 mm bore variable temperature inserts, so combining the capabilities of rapid temperature changes with an improved liquid

helium hold-time. A new high-precision, 4-position, cryogenic sample changer has been provided for CRISP allowing sample tilts of $\pm 2^\circ$ with 0.01° precision even at 1.5 K in 1.5 Tesla. A 10-12 Tesla cryomagnet intended primarily for the GEM diffraction programme has also been ordered from Oxford Instruments with funds from RIKEN and EPSRC. Standard pressure cells are undergoing testing to assess their use at higher pressures than currently permitted. The 1.6 kbar high pressure SANS cell has been successfully used at up to 60°C for studies of super-critical CO_2 , with future use up to 120°C .

Computing

The Computing Group supports 50 VMS and UNIX workstations and 400+ Windows systems around ISIS as well as the network that glues all these machines together. The Group also develops and supports control and analysis software, maintains and develops the archive of ISIS data, and supports the web and databases.

ENGIN-X will be the first instrument to have control and data acquisition systems based entirely on a PC Windows system running Labview and communicating with the data acquisition (DAE) via a VME interface. Most of the instruments currently rely on the VMS system linked to the DAE via a SCSI interface, with some items of sample environment equipment controlled from a PC running Labview and communicating with the VMS system. The PC instrument control system linked to DAE II offers several distinct advantages: the system is simpler and consequently less prone to communication failures; proprietary software drivers are available; and data transfer rates are an order of magnitude higher, with the possibility of further improvements. The new system was tested on ROTAX in December and the improvement in data transfer rate met expectations. Once ENGIN-X has

Fig. 5.12.

Matthias Guttman (ISIS) preparing the SXD closed cycle refrigerator (01RC3995).



demonstrated the usability of the PC control system it will then be deployed on other instruments. At the same time, a data file format will be introduced based on NeXus, which is gaining popularity at neutron, muon and X-ray facilities.

As instruments are becoming more complex and produce more data, increased demands are placed on data storage. SXD, for example, now produces approximately 7 GBytes per cycle. Overall, ISIS produced 200 Gbytes last year compared to 170 Gbytes in the previous year.

Improved wiring using UTP has been progressing during the six-month shutdown and we hope to complete a re-wire of all the instruments. This will improve connections both in cabins and at the sample position. The backbone of ISIS operates at 1 Gbit/sec with 100 Mbits/sec being available around the instruments.

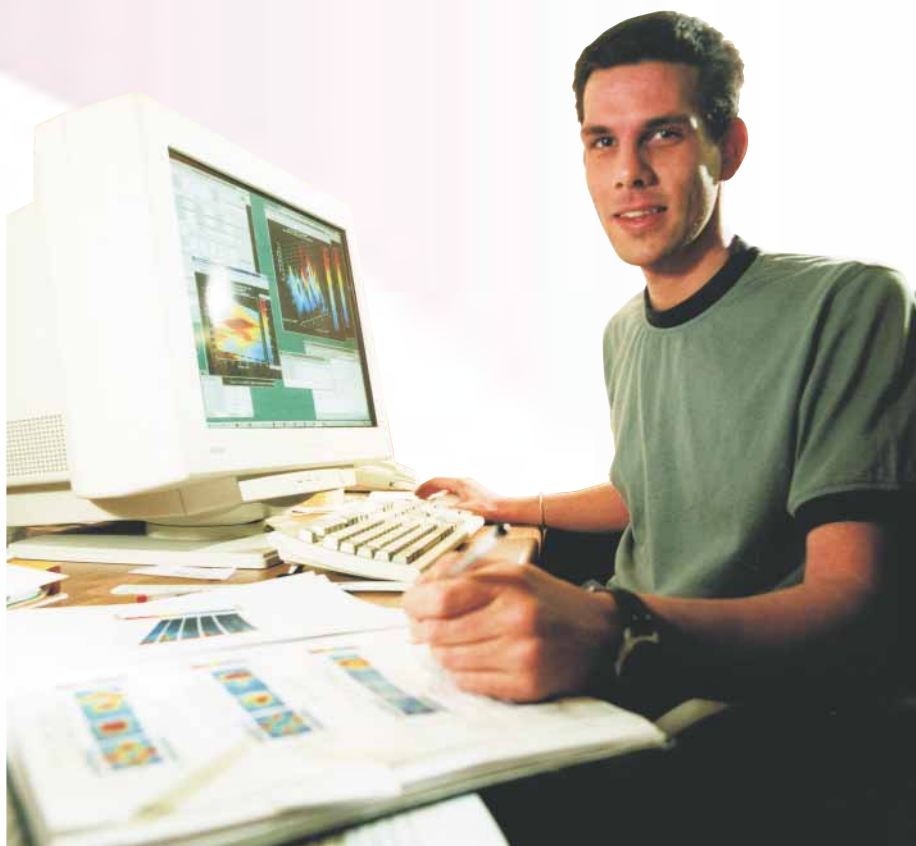


Fig. 5.14.

As data file sizes increase significantly, so must data acquisition, analysis and archiving facilities grow accordingly. Here, Simon Levett (Warwick) is analysing his MAPS data on magnetic correlations in La_2NiO_4 (01RC3998).



Fig. 5.13. *The ISIS Computer Group (02RC2212).*

Detectors

The activities of the Detector Group are divided between implementation of new detector systems, research and development of new materials and techniques, and maintenance of the ever-increasing detector suite.

New detector systems have included the fourteen modules of the 90° detector bank on HRPD, which provide the instrument with 1680 new detector elements and increase the count rate in the 90° region by an order of magnitude. The SXD detector upgrade has

also been completed, consisting of 11 modules comprising 45,000 pixels and covering more than 50% of the solid angle. GEM bank 4 modules have now been installed and the complete bank of 14 detectors comprises 1400 individual elements. A new backscattering detector module, consisting of 44 glass scintillator elements and a newly designed light guide and electronics, has been completed and installed on VESUVIO. It exhibits much better pulse height resolution than the previous VESUVIO detectors and should demonstrate improved detector stability on the instrument. Work has started on the production of a second 44-channel VESUVIO detector.

The 26 position-sensitive gas detectors on the low angle bank of HET have been exchanged for new detectors with a higher ^3He partial pressure, ensuring that all the HET detectors now have the same detector efficiency. The original HET position sensitive detectors are being re-housed to provide a detector array for the crystal alignment facility on ALF.

Detectors for ENGIN-X incorporating a new 3 mm resolution Venetian

Fig. 5.15.

Nigel Rhodes (ISIS detector group) showing GEM detectors to members of the EC COST network on neutron imaging techniques for the detection of defects in materials (02RC1422).



scintillator/reflector geometry have been produced. The Venetian geometry has proved to be a very successful design and there are excellent possibilities for further improving the position resolution of linear position sensitive detectors based on this concept. A scanning transmission detector for MARI is also ready for installation. It consists of 32 linear position sensitive detectors with 1.5 mm^2 pixels, which can be scanned to provide two-dimensional profile measurements of the MARI transmitted beam.

Excellent results have been obtained from the linear position sensitive Gd Borate scintillation detector temporarily installed on HRPD. Gd Borate scintillator offers higher detector count rates and simpler detector construction compared with $\text{ZnS}/^6\text{Li}$ -based detectors, and a programme to explore the potential of Gd Borate for two-dimensional position sensitive detectors has started.

Development of a two-dimensional microstrip gas detector continues in collaboration with the Instrumentation Department. Detector construction is nearing completion and ISIS tests are planned in the summer. Further collaborations with ID and the Centre for Instrumentation include feasibility studies of a scintillation/silicon detector combination for high speed, high position resolution measurements for μSR , and examination of the potential of active pixel sensors for energy resolved neutron radiography.

Under the TECHNI and eVERDI networks collaboration with Rome and Milan has continued on the development of a gamma detector to measure neutrons of energies up to 100 eV using capture resonance techniques. Further tests on VESUVIO are scheduled for the summer and these results will provide important information for designing the very low angle detector for eVERDI.

Electronics

The work of the Electronics Group has focused on producing DAE-II systems both for new instruments and upgrades such as GEM, SXD and ENGIN-X, and for the planned roll-out to existing instruments. DAE-II has been further developed in the light of experience gained on MAPS and changing electronic technologies. The system now has fewer components and is therefore considerably cheaper to make. Thirteen DAE-II boards have been installed on SXD, and systems have also been produced for GEM and ENGIN-X – there is now more data acquisition being performed by DAE-II than DAE-I in the ISIS Hall.

During the last year DAE-I interfaces have been built and commissioned for LOQ's new Ordela multi-wire detector, the OSIRIS diffraction detector and VESUVIO detector modules. Also, a new interface consisting of a proprietary circuit, pulse generators and a LabView setup has been produced for ENGIN-X, allowing a stress rig/Eurotherm combination to control the DAE-I data acquisition process.

Detector electronics have been produced in great numbers for the SXD, HRPD, GEM and ENGIN-X scintillator detectors. Approximately 1000 PMT assemblies and more than 30 integrator/discriminator cards have been produced in the last year.

The ENGIN-X DAE-II will be controlled by a PC through a VME interface, providing faster beginning and ending of runs. Although



Fig. 5.16. Kelvin Gascoyne of the ISIS Electronics Group testing a DAE-II board (02EC3192).

10 Mbytes/sec data transfer is obtainable with the PC interface (a factor of ten better than the SCSI/DAE interface), there is the possibility of doubling this transfer rate by changing the way the histogram memory is read out. This will be investigated during the ENGIN-X commissioning.

Once this ENGIN-X system has been successfully tested, the first phase of its roll-out to established instruments will begin. The first instruments to receive the new system will be SANDALS, VESUVIO, OSIRIS and PRISMA – they have been selected because they experience data-rate problems with DAE-I.

Chopper Section

As well as the usual full chopper maintenance programme, the section successfully completed the development of the counter-rotating double disc chopper. With both discs rotating at 50 Hz, the cut through the neutron beam is faster and the window smaller. Each

disc is driven directly by an on-shaft motor assembly (rather than by a drive belt), offering greater reliability and easier maintenance. Following a lengthy and successful series of trials, two choppers have been built and installed on ENGIN-X.

All choppers on the south side of the experimental hall have been modified for continuous on-line condition monitoring of vibration and temperature. This data is automatically analysed by the monitoring system and any changes considered to be outside the normal operating range reported since they may be indicative of a potential bearing fault. We aim to use the system for predictive maintenance, reducing the frequency of catastrophic failures and hence downtime, as well as reducing the amount of effort dedicated to routine yet unnecessary maintenance.

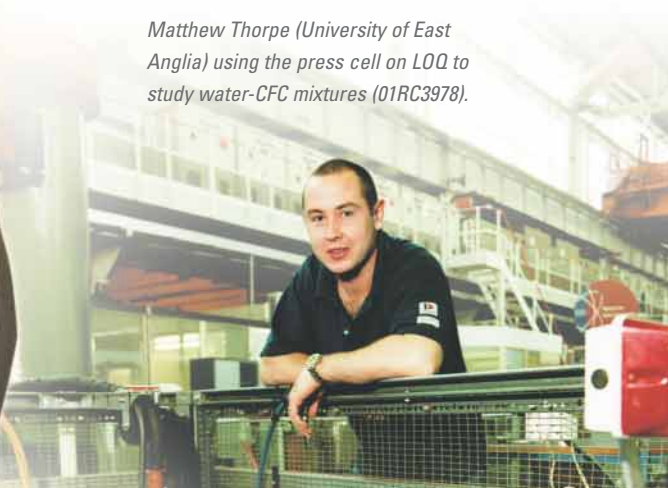


Fig. 5.17. Mike Brind installing the new counter-rotating chopper on ENGIN-X (02RC2729).

*Christophe Houssin (TU-Eindhoven)
reviewing his SANDALS data.
(02EC3143)*



*Matthew Thorpe (University of East
Anglia) using the press cell on LOQ to
study water-CFC mixtures (01RC3978).*



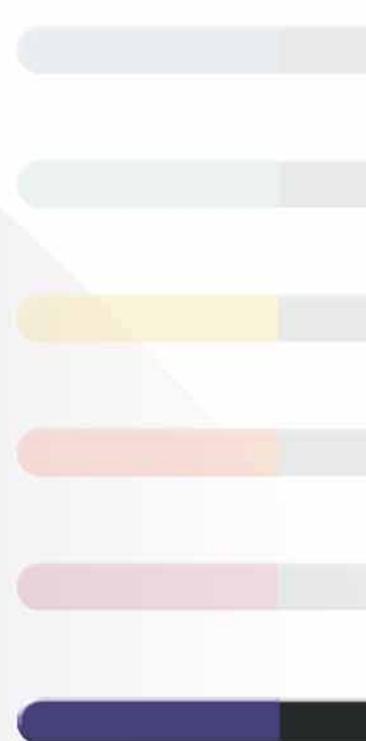
*Daniele Colognesi (INFN, Italy)
and Timmy Ramirez-Cuesta
(ISIS) during investigations
of the vibration spectrum of
alkali hydrides on TOSCA
(02EC3152).*



*Hye Jung Kanguni
(University of Tennessee)
investigating the evolution of
spin-wave excitations in
manganites on HET
(02EC3155).*



*Paul Prince (UCL)
using SXD to explore
novel silicon hydrides
(02EC3159).*



Publications

Publications relate to all work carried out at ISIS. In addition, work performed elsewhere by ISIS staff is included where relevant. Listed here are publications reported for the 2001 – 2002 year, together with an update of the 2000 – 2001 year giving those articles reported after ISIS 2001 was produced and those listed last year as being 'in press'.

6

ISIS Publications 2001 – 2002

- T Abdul-Redah, C A Chatzidimitriou-Dreismann
Decoherence of entangled protons and attosecond dynamics of C-H bond breaking
Appl Phys A (in press 2002)
- I Abrahams, A J Bush, S C M Chan, F Krok, W Wrobel
Stabilisation and characterisation of a new betalll-phase in Zr-doped Bi₂O₃
J Mater Chem 11 1715 (2001)
- I Abrahams, F Krok
A model for the mechanism of low temperature ionic conduction in divalent substituted-bimevoxes
Solid State Ionics (in press 2002)
- St Adams, J Swenson
Pathway models for fast ion conductors by combination of bond volume and reverse Monte Carlo methods
Solid State Ionics (in press 2002)
- H V Alberto, R C Vilao, J Piroto Duarte, J M Gil, N Ayres de Campos, R L Lichti, E A Davis, S P Cottrell, S F J Cox
Powder pattern hyperfine spectroscopy of shallow donor muonium centres
Hyperfine Interact (in press 2002)
- G Allodi, M Cestelli Guidi, R De Renzi, M W Pieper
Inhomogeneous electronic state of low-doped insulating manganites: NMR and μ SR evidence
J Magn Magn Mater (in press 2002)
- G Allodi, M Cestelli Guidi, R De Renzi, A Caneiro, L Pinsard
Evidence of ultra-slow polaron dynamics in low-doped manganites from ⁵⁵La NMR-NQR
Phys Rev Lett 87 127206 (2001)
- S W An, R K Thomas, C Forder, N C Billingham, S P Arnes, J Penfold
The behaviour of nonionic water soluble homopolymers at the air-water interfaces: neutron reflectivity and surface tension results for poly-(vinyl methyl ether)
Langmuir (in press 2001)
- K H Andersen, D Martin, M J Barlow
The OSIRIS diffractometer and polarisation analysis backscattering spectrometer
Appl Phys A (in press 2002)
- C Andreani, D Colognesi, E Degiorgi, M A Ricci
Proton dynamics in supercritical water
J Chem Phys 115 11243 (2001)
- B K Annis, O Borodin, G D Smith, C J Benmore, A K Soper, J D Londono
The structure of a poly(ethylene oxide) melt from neutron scattering and molecular dynamics simulations
J Chem Phys 115 10998 (2001)
- M J Ariza, D J Jones, J Roziere, J S Lord
Muon spin relaxation study of lithium manganese oxides with the spinel structure
Physica B (in press 2002)
- V Arrighi, S Gagliardi, J S Higgins
Restricted dynamics in polymer-filler systems
Mat Res Soc Symp Proc 661 KK4.4.1 (2001)
- M Aslam, S J Perkins
Folded-back solution structure of monomeric Factor H of human complement by synchrotron X-ray and neutron scattering, analytical ultracentrifugation and constrained molecular modelling
J Mol Biol 309 1117 (2001)
- R T Azuah, J V Pearce, W G Stirling, P E Sokol, M A Adams
Microscopic excitations of confined liquid ⁴He
Phys Rev B (in press 2002)
- P D Battle, S J Hartwell, C A Moore
Antimony in the Sr₄PtO₆ structure: a neutron diffraction study of Sr₃NaSbO₆
Inorg Chem 40 1716 (2001)
- P D Battle, A M T Bell, S J Blundell, A I Coldea, E J Cussen, G C Hardy, I M Marshall, M J Rosseinsky, C A Steer
Chemically-induced magnetism and magnetoresistance in La_{0.8}Sr_{1.2}Mn_{0.6}Rh_{0.4}O₄
J Am Chem Soc 123 7610 (2001)
- P D Battle, S J Blundell, J B Claridge, A I Coldea, E J Cussen, L D Noailles, M J Rosseinsky, J Singleton, J Sloan
Spin, charge and orbital ordering in the B-site diluted manganates La_{2-x}Sr_xGaMnO₆
Chem Mater 14 425 (2002)
- A I Becerro, S A T Redfern, M A Carpenter, K S Knight, F Seifert
Neutron diffraction study of displacive phase transitions and strain analysis in Fe-doped CaTiO₃ perovskites at high temperature
J Solid State Chem (in press 2001)
- T G Bellenger, T Cosgrove, A J Goodwin, A Kretschmer, L Marteaux, A J Semlyen, A Dagger
Dynamics and structure of polydimethylsiloxane emulsions studied by pulsed field gradient NMR and small-angle neutron scattering
Polym Prepr (Am Chem Soc, Div Polym Chem) 42 124 (2001)
- P Berastegui, S Hull, S-G Eriksson
A low-temperature structural phase transition in CsPbF₃
J Phys:Condens Matter 13 5077 (2001)
- P Berastegui, S Hull, S-G Eriksson
Oxygen disorder and conductivity in pyrochlore and perovskite-based compounds
Mater Sci Forum 378-381 487 (2001)
- B Berby, J R P Webster
Neutron reflection studies of the composition of interfaces between titanium containing active braze alloys and sapphire
Proc 3rd Int Conf High Temperature Capillarity, Eds N Eustathopoulos, K Nyogi, N Sobczak (Joining and Welding Research Inst, Osaka) p233 (2001)
- G R Blake, T T M Palstra, Y Ren, A A Nugroho, A A Menovsky
Transition between Orbital Orderings in YVO₃
Phys Rev Lett 87 245501 (2001)
- S J Blundell
Muon-spin rotation studies of molecule based magnets
Magnetism: Molecules to Materials, Eds J S Miller, M Drillon (Wiley-VCH, Weinheim) ISBN 3-527-29772-3 p235 (2001)
- S J Blundell, I M Marshall, B W Lovett, F L Pratt, W Hayes, M Kurmoo, S Takagi, T Sugano
Organic magnetic materials studied by positive muons
Hyperfine Interact 133 169 (2001)
- J Bogner, M Reissner, W Steiner, R Cywinski, J A Dann, M T F Telling
Comparison of high-field Mossbauer and μ SR investigations on spin glasses
J Magn Magn Mater 226 1319 (2001)

- A T Boothroyd, J P Barratt, S J S Lister, A R Wildes, P C Canfield, R I Bewley
Magnetic excitations in YbNi₂B₂C
Rare Earth Transition Metal Borocarbides (nitrides): Superconducting, Magnetic and Normal State Properties, Eds K-H Muller, V Narozhnyi (Kluwer Academic Press) 163 (2001)
- A T Boothroyd, S J S Lister, F Dubin, B H Larsen, N H Andersen, A A Zhokhov, A N Christensen, A R Wildes, C D Frost
Dispersive magnetic excitations in non-superconducting PrBa₂Cu₃O_{6.2}
Proc ILL Millennium Symposium, Grenoble, p147 (2001)
- A T Boothroyd, C H Gardiner, S J S Lister, P Santini, B D Rainford, L D Noailles, D B Currie, R S Eccleston, R I Bewley
Localized 4f states and dynamic Jahn-Teller effect in PrO₂
Phys Rev Lett **86** 2082 (2001)
- A Boudjada, J Meinel, A Boucekkine, O J Hernandez, M-T Fernandez-Diaz
Molecular conformation and methyl proton delocalization in triodomesitylene: a combined density functional theory and single-crystal neutron diffraction study
J Chem Phys (in press 2001)
- F Boudjada, J Meinel, A Cousson, W Paulus, M Mani, M Sanquer
Tribromomesitylene structure at 14K: Methyl conformation and tunnelling
Neutrons and Numerical Methods – N2M, Eds M R Johnson, G J Kearley, H G Butner, AIP Conference Proceedings **479** 217
- A Bouzina, M J Balart, M E Fitzpatrick, L Edwards
Measurement of grinding stresses with a combination of neutron and X-ray diffraction
J N Res **9** 167 (2001)
- E Bovell, T St Pierre, W Chua-anusorn, C E Buckley
Iron oxide particle size distribution during iron loading and deloading in rat tissue measured by small angle neutron scattering
BIOIRON 2001 (Cairns, Australia) pP65 (2001)
- A Bowman, P V Mason, D H Gregory
Heteroanionic intercalation into positively charged inorganic hosts: the first nitride mixed halides
Chem Commun 1650 (2001)
- G J Bown, R W Richards, R K Heenan
Organisation and interactions in aqueous dispersions of polystyrene-polyethylene oxide block copolymer micelles
Polymer **42** 7663 (2001)
- S T Bramwell, M J Harris, B C den Hertog, M J P Gingras, J S Gardner, D F McMorrow, A R Wildes et al
Spin correlations in Ho₂Ti₂O₇: A dipolar spin ice system
Phys Rev Lett **87** 047205 (2001)
- C Branca, S Magazu, F Migliardo, G Romeo, V Villari, U Wanderlingh, D Colognesi
Neutron scattering study on the vibrational behaviour of disaccharide aqueous solutions
Appl Phys A (in press 2002)
- C Branca, S Magazu, F Migliardo, P Migliardo
Destructuring effect of trehalose on the tetrahedral network of water: a Raman and neutron diffraction comparison
Physica A **304** 314 (2002)
- C Branca, S Magazu, F Migliardo, P Migliardo, S Coppolino, A Villari, N Micali
Quasielastic and inelastic neutron scattering study of vitamin C aqueous solutions
Physica A **304** 294 (2002)
- C Branca, S Magazu, G Maisano, F Migliardo, A K Soper
Study on destructuring effect of trehalose on water by neutron diffraction
App Phys A (in press 2002)
- C Branca, S Magazu, F Migliardo
New perspectives on bioprotectant complex molecules: spectroscopic findings
Recent Research Developments in Physical Chemistry (in press 2002)
- H Brequel, S Enzo, G Gregori, H-J Kleebe, A C Hannon
Structural investigation of silicon carbonitride glasses by neutron diffraction
Mater Sci Forum **386-388** 365 (2002)
- H Brequel, S Enzo, F Babonneau, P G Radaelli
Neutron diffraction study of nanocrystalline oxycarbonate glasses prepared by sol-gel
Materials Science Forum **386-388** 275 (2002)
- F Bruni, M A Ricci, A K Soper
Structural characterisation of NaOH aqueous solution in the glass and liquid state
J Chem Phys **114** 8056 (2001)
- D G Bucknall, J S Higgins, S A Butler
Early stages of oligomer-polymer diffusion
Chemical Engineering Science **56** 5473 (2001)
- S A Butler, J S Higgins, D G Bucknall, M Sferrazza
Effect of mechanical confinement on an immiscible polymer-polymer interface
Macromol Chem Phys **202** 2275 (2001)
- E Bychkov, M Fourmentin, M Miloshova, D L Price, C J Benmore, A Lorriaux
New structural features and trends in binary chalcogenide glasses
XIII Inter Symp On Non-Oxide Glasses (Pardubice, Czech Republic) (in press 2002)
- C Cabrillo, F J Bermejo, M Jimenez-Ruiz, M T Fernandez-Diaz, M A Gonzalez, D Martin
Partial ordering of supercooled liquid ethanol into a rotator-phase crystal as an example of entropy-driven transitions
J Non-Cryst Solids **287** 252 (2001)
- S J Campbell, V Ksenofontov, Y Garcia, J S Lord, S Reiman, P Gutlich
Spin crossover transitions in Fe(II) molecular compounds – Mossbauer and μ SR investigations
Hyperfine Interact (in press 2002)
- P Carretta, R Melzi, N Papinutto, P Millet
Very-low-frequency excitations in frustrated two-dimensional S = 1/2 Heisenberg antiferromagnets
Phys Rev Lett **88** 047601 (2002)
- M Catti
A mixed a/b superstructure in NASICON ionic conductors: neutron diffraction study of Li₂FeTi(PO₄)₃ and Li₂FeZr(PO₄)₃
J Solid State Chem **156** 305 (2001)

- M Celli, F Cilloco, D Colognesi, R J Newport, S F Parker, V Rossi-Albertini, F Sacchetti, J Tomkinson, M Zoppi
The final configuration of TOSCA neutron spectrometer
Notiziario Neutrone e Luce di Sincrotrone 6 33 (2001)
- G Chaboussant, M T F Telling et al
Low energy spin excitation in the molecular magnet V15
Europhys Lett (in press 2002)
- J D M Champion, A S Wills, T Fennell, S T Bramwell, J S Gardner, M A Green
Order in the Heisenberg pyrochlore: The magnetic structure of $Gd_2Ti_2O_7$
Phys Rev B 64 140407 (2001)
- C A Chatzidimitriou-Dreismann, T Abdul-Redah
Sub-femtosecond quantum entanglement of protons and dissociation of C-H bonds in condensed matter – A new effect
Proc ISQM - Tokyo '01 (in press 2002)
- C A Chatzidimitriou-Dreismann, T Abdul-Redah, J Mayers
Experimental test of a theoretical analysis of deep inelastic neutron scattering experiments for H and D nuclei
Physica B 315 281 (2002)
- C A Chatzidimitriou-Dreismann, T Abdul-Redah, J Sperling
Short lived 'Schrodinger's cat' states of protons in metal-hydrogen systems: A new effect
Compounds & Alloys 330-332 414 (2002)
- C A Chatzidimitriou-Dreismann, T Abdul-Redah, R M F Streffer, J Mayers
Sub-femtosecond dynamics and dissociation of C-H bonds in solid polystyrene and liquid benzene
J Chem Phys 116 1511 (2002)
- C A Chatzidimitriou-Dreismann, T Abdul-Redah, B Kolaric
Entanglement of protons in organic molecules: an attosecond neutron scattering study of C-H bond breaking
J Am Chem Soc 123 11945 (2001)
- C A Chatzidimitriou-Dreismann, T Abdul-Redah
Neutron scattering from short lived quantum entangled protons in condensed matter at T=293 K
Mol Phys Reports 31 34 (2001)
- A Chiba, Y Ohmasa, Y Kawakita, M Yao, H Endo
Neutron scattering experiments of liquid tellurium-selenium mixtures
J Non-Cryst Solids (in press 2002)
- A Chiba, Y Ohmasa, M Yao, O Petrenko, Y Kawakita
Quasielastic neutron scattering of liquid $Te_{50}Se_{50}$ in the semiconductor-to-metal transition range
J Phys Soc Jpn 71 2 (2002)
- J R Cho, D Dye, K T Conlon, M R Daymond, R C Reed
Intergranular strain accumulation in a near-alpha titanium alloy during plastic deformation
Acta Mat (in press 2002)
- S J Clarke, B P Guinot, C W Michie, M J C Calmont, M J Rosseinsky
Oxynitride perovskites: synthesis and structures of $LaZrO_2N$, $NdTiO_2N$ and $LaTiO_2N$, and comparison with oxide perovskites
Chem Materials (in press 2002)
- S J Clarke, P R Chalker, J Holman, C W Michie, M Puyet, M J Rosseinsky
A first transition series pseudo-tetrahedral oxynitride anion – the synthesis and characterisation of Ba_2VO_3N
J Am Chem Soc (in press 2002)
- G Coddens
Comment on 'Atomic motions in the crystalline $Al_{50}Cu_{35}Ni_{15}$ alloy'
J Phys: Condens Matter 13 8869 (2001)
- A I Coldea, S J Blundell, I M Marshall, C A Steer, J Singleton, F L Pratt, L D Noailles, M J Rosseinsky, L E Spring, P D Battle
Evolution of the magnetic and magnetotransport properties of the Ga-substituted manganite compounds $La_{2-x}Sr_xMnGaO_6$
Phys Rev B 65 054402 (2002)
- L Cormier, L Galois, J-M Delage, D Ghaleb, G Calas
Short and medium range structural order around cation in glasses: a multidisciplinary approach
Compte Rendu de l'Academie des Sciences, serie IV 2 249 (2001)
- V Corregidor, D Martin, E Dieguez
Temperature dependence of thermal and lattice parameters of n and p type CdTe
Appl Phys A (in press 2002)
- L Corvazier, L Messe, C L O Salou, R N Young, J P A Fairclough, A J Ryan
Lamellar phases and microemulsions in model ternary blends containing amphiphilic block copolymers
J Mater Chem 11 2864 (2001)
- T Cosgrove, TG Bellenger, A J Goodwin, A Kretschmer, L Marteau
Dynamics and structure of polydimethylsiloxane emulsions studied by pulsed field gradient NMR and small-angle neutron scattering
Abstr Pap - Am Chem Soc POLY-222 (2001)
- S J Covey-Crump, P F Schofield, I C Stretton
Strain partitioning during the elastic deformation of an olivine + magnesiowustite aggregate
Geophys Res Lett 28 4647 (2001)
- S J Covey-Crump, P F Schofield, I C Stretton, K S Knight, W Ben Ismail
Using neutron diffraction to investigate the elastic properties of anisotropic rocks: results from an olivine + orthopyroxene
J Geophys Res (in press 2002)
- S J Covey-Crump, P F Schofield, I C Stretton, M R Daymond, K S Knight
Strain partitioning of two-phase aggregates through the plastic yield point of the constituent phases
Acta Mater (in press 2002)
- R A Cowley, M Kenzelmann, W J L Buyers, D F McMorro, R Coldea, M Enderle
New results on the excitations of an S=1 quantum chain
J Magn Magn Mater 226-230 437 (2001)
- S F J Cox, E A Davis, R L Lichti
Hydrogen in group III nitrides, studied by muon spin resonance
J Phys D: Appl Phys (in press 2002)
- E J Cussen, M J Rosseinsky, P D Battle, J C Burley, L E Spring, J F Vente, S J Blundell, A I Coldea, J Singleton
Control of magnetic ordering by Jahn-Teller distortions in Nd_2GaMnO_6 and La_2GaMnO_6
J Am Chem Soc 123 1111 (2001)
- A C Dagger, V Arrighi, S Gagliardi, M J Shenton, S J Clarson, J A Semlyen
Neutron scattering studies of cyclic and linear poly(dimethyl siloxane)s
Abstr Pap Am Chem Soc 221 – Poly Part 2 225 (2001)

- U Dahlborg, W S Howells, M Calvo-Dahlborg, J Dolinsek, J M Dubois
Reply to Comment on 'Atomic motions in the crystalline Al₅₀Cu₃₅Ni₁₅ alloy'
J Phys: Condens Matter **13** 8873 (2001)
- R M Dalglish
Application of off-specular scattering of X-rays and neutrons to the study of soft matter
Curr Opin Colloid Interface Sci (in press 2002)
- W I F David, K Shankland, J Cole, S Maginn, W D S Motherwell, R Taylor
DASH User Manual (Book) Cambridge Crystallographic Data Centre (2001)
- W I F David, K Shankland, L B McCusker, Ch Baerlocher
Structure Determination from Powder Diffraction Data (Eds) OUP (2002)
- M R Daymond, H G Priesmeyer
Elastoplastic deformation of ferritic steel and cementite studied by neutron diffraction and self-consistent modelling
Acta Mater (in press 2002)
- M R Daymond, N W Bonner
Lattice strain evolution in IM1834 under applied stress
Mat Sci Eng A (in press 2002)
- M R Daymond, M W Johnson
First experimental tests on a neutron silicon lens
Nuc Inst Methods A (in press 2002)
- B de Boer, U Stalmach, P F van Hutten, C Melzer, V V Krasnikov, G Hadziioannou
Supramolecular self-assembly and opto-electronic properties of semiconducting block copolymers
Polymer **42** 9097 (2001)
- S G Denis, S J Clarke
Two alternative products from the intercalation of alkali metals into cation-defective Ruddlesden-Popper oxysulfides
Chem Commun 2356 (2001)
- R Dinnebier, H W Lerner, L Ding, K Shankland, W I F David, P W Stephens, M Wagner
One-dimensional spin chains from Cu-II ions and 2,5-bis(pyrazol-1-yl)-1,4-dihydroxybenzene
Z Anorg Allg Chem **628** 310 (2002)
- S Dixit, W C K Poon, J Crain, J L Finney, A K Soper
Molecular segregation observed in a concentrated alcohol-water solution
Nature **416** 829 (2002)
- S Dixit, A K Soper, J L Finney, J Crain
Water structure and solute association in dilute aqueous methanol
Europhys Lett (in press 2002)
- F T Docherty, A J Craven, D W McComb, J M S Skakle
ELNES investigations of the oxygen K-edge in spinels
Ultramicroscopy **86** 273 (2001)
- J Eastoe, M Summers, R K Heenan, D C Steytler, I Grillo
Polymerisation of cationic surfactant films in microemulsions
J Disp Sci Tech **22** 597 (2001)
- J Eastoe, A Paul, A Rankin, R Wat, J Penfold, J P R Webster
Fluorinated nonionic surfactants bearing either CF₃- or H-CF₂- terminal groups: Adsorption at the surface of aqueous solutions
Langmuir **17** 7873 (2001)
- J Eastoe, A Rankin, R Wat, C D Bain
Surfactant adsorption dynamics
Int Rev Phys Chem **20** 1 (2001)
- L Edwards, J R Santisteban
Improved structural integrity through advances in reliable residual stress measurement; the impact of ENGIN-X
Appl Phys (in press 2002)
- L Edwards
Improved structural integrity through advances in reliable residual stress measurements: the design and implementation of ENGIN-X
Advances in Fracture Research, Proc 10th Int Conf on Fracture (Pergamon) ISBN 0080440428 (2001)
- L Edwards, J R Santisteban, V Stelmukh, P J Bouchard, M R Daymond
Measurement of the residual stresses near a short 20° repair in a 19mm thick stainless steel pipe girth weld
J N Res **9** 173 (2001)
- M Ellerby, K A McEwen, J Jensen, M J Bull
Neutron diffraction study of the P-T phase diagram for erbium
Proc EHPRG39, High Pressure Research (in press 2002)
- D G Eschenko, V G Storchak, J H Brewer, S P Cottrell, S F J Cox, E Karlsson, R W Wappling
Muon diffusion in solid CO₂
Low Temp Phys **27** 527 (2001)
- M P Fernandez-Liencre, A Navarro, J J Lopez-Gonzalez, M Fernandez-Gomez, J Tomkinson, G J Kearley
Measurement and ab initio modeling of the inelastic neutron scattering of solid melamine; Evidence of the anisotropy in the external modes spectrum
Chem Phys **266** 1 (2001)
- A L Fielding, J Mayers
Calibration of the electron volt spectrometer a deep inelastic neutron scattering spectrometer at the ISIS pulsed neutron source
Nucl Inst Meth A (in press 2002)
- F Fillaux, S F Parker, L T Yu
Inelastic neutron scattering studies of polypyrroles and partially deuterated analogues
Solid State Ionics **145** 451 (2001)
- J L Finney
The water molecule and its interactions: the interaction between theory, modelling and experiment
J Mol Liq **90** 303 (2001)
- J L Finney, A Hallbrucker, I Kohl, A K Soper, D T Bowron
The structures of high and low density amorphous ice by neutron diffraction
Phys Rev Lett (in press 2002)
- J L Finney
Ice: Structures
Encyclopedia of Materials Science and Technology, Eds K H J Buschow, R W Cahn, M C Flemings, B Ilshner, E J Kramer, S Mahajan (Elsevier Science) **5** p4018 (2001)
- D Flannery, S P Cottrell, P J C King
The application of the NeXus data format to ISIS muon data
RAL-TR-2001-029 (2001)
- M Fourmentin, M Miloshova, E Bychkov
Ge-S glasses: New structural features from high-resolution neutron diffraction and Raman spectroscopy
ILL Millennium Symposium (Grenoble, France) p 54 (2001)

- J Frantti, S G Eriksson, S Hull, S Ivanov, V Lantto, J Lappalainen, M Kakhana
High resolution neutron powder diffraction study of the microstrain contribution in $\text{Pb}(\text{Zr}_x\text{Ti}_{1-x})\text{O}_3$ ceramic
 Electroceramics VIII conference (in press 2002)
- J Frantti, J Lappalainen, S G Eriksson, S Ivanov, V Lantto, S Nishio, M Kakhana, H Rundlof
Neutron diffraction studies of $\text{Pb}(\text{Zr}_x\text{Ti}_{1-x})\text{O}_3$ ceramics
 Ferroelectrics **261** 193 (2001)
- J Frantti, S Ivanov, J Lappalainen, S G Eriksson, V Lantto, S Nishio, M Kakhana, H Rundlof
Local and average structure of lead titanate based ceramics
 Ferroelectrics **266** (2002)
- A Friedrich, G A Lager, P Ulmer, M Kunz, W G Marshall
High-pressure single-crystal X-ray and powder neutron study of F, OH/OD-chondrodite: Compressibility, structure and hydrogen bonding
 Am Mineral (in press 2002)
- W T Fu, D Visser, D J W IJdo
On the crystal structure of BaTbO_3
 J Solid State Chem **165** 393-396 (2002)
- B J Gabrys, W Zajac, J Mayers, M S Kalhor
Neutron Compton scattering studies of stretched polyethylene
 App Phys A (in press 2002)
- B J Gabrys, A A Bhutto, D G Bucknall, R Braiewa, D Vesely, R A Weiss
Reflectivity studies of ionomer blends
 Appl Phys A (in press 2002)
- Z Gadjourova, Y Andreev, D P Tunstall, P G Bruce
Ionic conductivity in crystalline polymer electrolytes
 Nature **412** 520 (2001)
- C H Gardiner, A T Boothroyd, S J S Lister, M J McKelvy, S Hull, B H Larsen
An investigation of the magnetic structure of PrO_2
 Appl Phys A (in press 2002)
- A Glidle, L Bailey, C S Hadyoon, A R Hillman, A Jackson, K S Ryder, P M Saville, M J Swann, J R P Webster et al
Temporal and spatial profiling of the modification of an electroactive polymeric interface using neutron reflectivity
 Anal Chem **73** 5596 (2001)
- P Gorria, L Fernandez Barquin, V M Prida, W S Howells
Microstructural study of Joule heated nanocrystalline alloys using *in situ* neutron diffraction
 J Magn Magn Mater (in press 2002)
- D Gourdain, Ph Pruzan, J M Besson, S Klotz, J C Chervin, B Canny, W G Marshall, J S Loveday, M Hanfland,
Compression of KNbO_3 up to 30GPa, the transition sequence orthorhombic> tetragonal> cubic
 Phys Rev B (in press 2002)
- R K B Gover, N D Withers, S Allen, R L Withers, J S O Evans
Structure and phase transitions of SnP_2O_7
 J Solid State Chem (in press 2002)
- P C Griffiths, A Y F Cheung, G J Finney, C Farley, A R Pitt, A M Howe, S M King, R K Heenan, B L Bates
Electron paramagnetic resonance and small-angle neutron scattering studies of mixed sodium dodecylsulfate and (tetradecylmalono)bis(N-methylglucamide) surfactant micelles
 Langmuir **18** 1065 (2002)
- P C Griffiths, S M King
Neutron scattering studies of adsorbed polymer layers
Encyclopaedia of Surface and Colloid Science (Marcell Dekker Inc) (in press 2002)
- J Grins, S Esmailzadeh, S Hull
Structure and ionic conductivity of $\text{Bi}_6\text{Cr}_2\text{O}_{15}$, an new structure type containing $(\text{Bi}_{12}\text{O}_{14})_n\text{8n}+$ columns and CrO_4^{2-} tetrahedra
 J Solid State Chem (in press 2002)
- M J Gutmann, E S Bozin, S J L Billinge, N A Babushkina, L M Belova, A R Kaul, O Yu Gorbenko
Temperature evolution of the local atomic structure in oxygen isotope substituted $\text{Pr}_{0.525}\text{La}_{0.175}\text{Ca}_{0.3}\text{MnO}_3$
 Appl Phys A (in press 2002)
- M L Hanham, R F Pettifer
Generalized Ramsauer-Townsend effect in extended x-ray-absorption fine structure
 Phys Rev B **64** 180101 (2001)
- A C Hannon, J M Parker
The use of bond-valence parameters in interpreting glass diffraction results
 Phys Chem Glasses (in press 2002)
- S Hayama, J C Wasse, N T Skipper, J K Walters
The structure of liquid methylamine and solutions of lithium in methylamine
 Mol Phys **99** 779 (2001)
- S Hayama, J C Wasse, N T Skipper, A K Soper
Structure of solutions of lithium in methylamine across the metal-nonmetal transition
 J Phys Chem B **106** 11 (2002)
- A L Hector, J R Owen, G Vitans, E M Raekelboom, M T Weller
Syntheses, structures and preliminary electrochemistry of the layered lithium and sodium manganese(IV) oxides, $\text{A}_2\text{Mn}_3\text{O}_7$
 Chem Mater **13** 4618 (2001)
- R K Heenan, R Cubitt, K Mortensen, D Schwahn, A Wiedenmann, F Mezei
SANS Instruments
Performance of a Suite of Generic Instruments on European Spallation Source, ESS Instrument Group Reports, ESS 115-01-T (2001)
- C H Hervoches, J T S Irvine, P Lightfoot
Two high-temperature paraelectric phases in $\text{Sr}_{0.85}\text{Bi}_{2.1}\text{Ta}_2\text{O}_9$
 Phys Rev B **64** 100102 (2001)
- C H Hervoches, A Sneddon, R Riggs, S H Kilcoyne, P Manuel, P Lightfoot
Structural behaviour of the 4-layer Aurivillius phase ferroelectrics $\text{SrBi}_4\text{Ti}_4\text{O}_{15}$ and $\text{Bi}_5\text{Ti}_3\text{FeO}_{15}$
 J Solid State Chem (in press 2002)
- S J Hibble, S M Cheyne, A C Hannon, S G Eversfield
Beyond Bragg scattering: the structure of AgCN determined from total neutron diffraction
 Inorg Chem **41** 1042 (2002)
- S J Hibble, A C Hannon
Local structure: the realm of the chemist?
From semiconductors to proteins: beyond the average structure, Eds S J L Billinge, M F Thorpe (Kluwer Academic/Plenum Publishers, New York) p129 (2002)
- S J Hibble, S M Cheyne, A C Hannon, S G Eversfield
The structure of CuCN determined from total neutron diffraction
 Chem Commun (in press 2002)

J S Higgins, S A Butler, D G Bucknall

Neutron reflectivity of polymer-plasticiser diffusion
Macromol Symp (in press 2001)

A D Hillier, R Cywinski

A μ SR study of Er spin dynamics in $(Y_{1-x}Er_x)Ni_2B_2C$ superconductors
Hyperfine Interact (in press 2002)

A D Hillier, R I Smith, R Cywinski

Evidence for boron-carbon disorder in $YNi_2^{10}B_2C$
Appl Phys A (in press 2002)

J A Hodges, P Bonville, A Forget, A Yaouanc,
P Dalmas de Reotier et al

First order transition in the spin dynamics of geometrically frustrated $Yb_2Ti_2O_7$
Phys Rev Lett **88** 077204 (2002)

M Hofmann, S J Campbell, W A Kaczmarek, S Welzel

Mechanochemical transformation of $\alpha-Fe_2O_3$ to $Fe_{3-x}O_4$ – Microstructural investigation
Acta Mater (in press 2002)

M Hofmann, S J Campbell, W A Kaczmarek

Mechanochemical treatment of $\alpha-Fe_2O_3$ – Microstructural analysis
Appl Phys A (in press 2002)

M Hofmann, S J Campbell, A V J Edge

Valence and magnetic transitions in $YbMn_2Si_{2-x}Ge_x$
Appl Phys A (in press 2002)

M Hofmann, S J Campbell, K Knorr, S Hull, V Ksenofontov

Pressure-Induced Magnetic Transitions in $LaMn_2Si_2$
J Appl Phys (in press 2002)

M Hofmann, S J Campbell, E Wu, W A Kaczmarek, M Dahlborg,
U Dahlborg

Mechanochemical transformations of $SrFe_{12}O_{19}$ – Microstructural investigation by neutron diffraction
Mater Sci Forum **378-381** 765 (2001)

M Hofmann, S J Campbell, A V J Edge, A J Studer

The magnetic structures of $YbMn_2Si_2$
J Phys:Condens Matter **13** 9773 (2001)

C M Hollinshead, M Hanna, D J Barlow, V De Biasi, D G Bucknall,
P Camilleri, A J Hutt, M J Lawrence, J R Lu, T J Su

Neutron reflection from a dimyristoylphosphatidylcholine monolayer adsorbed on a hydrophobised silicon support
Biochim Biophys Acta **15** 49 (2001)

U Hoppe, R Kranold, A Ghosh, J Neufeind, D T Bowron

X-ray and neutron scattering studies of the structure of strontium vanadate glasses
Phys Chem Glasses (in press 2002)

U Hoppe, E Yousef, C Rüssel, J Neufeind, A C Hannon

Structure of vanadium tellurite glasses studied by neutron and X-ray diffraction
Solid State Commun (in press 2002)

U Hoppe, R Kranold, E Gattef, J Neufeind, D A Keen

An X-ray and neutron scattering study of the structure of zinc vanadate glasses
Z Naturforsch A **56** 478 (2001)

C J Howard, V Luca, K S Knight

High temperature phase transitions in tungsten trioxide - the last word?
J Phys:Condens Matter **14** 377 (2002)

C J Howard, R L Withers, B K Kennedy

Space group and structure for $Ca_{0.5}Sr_{0.5}TiO_3$
J Solid State Chem **160** 8 (2001)

W S Howells, U Dahlborg, M Calvo-Dahlborg, J M Dubois

Reply to Comment on 'Diffusive motions in crystalline AlCuNi by neutron quasielastic scattering'
Physica B **311** 383 (2002)

A Isopo, C Oliva, R Senesi, A K Soper, M A Ricci

Structural study of Ar solvation in supercritical water
J Chem Phys (in press 2002)

S Itoh, Y Kouchi, S Ikeda, K Iwasa, H Ikeda, M A Adams, R Kajimoto

Critical spin dynamics in the two-dimensional percolating Ising antiferromagnet, $Rb_2Co_cMg_{1-c}F_4$
J Phys Soc Jpn **70** 3107 (2001)

M Jung, B H Robinson, D C Steytler, A L German, R K Heenan

Polymerization of styrene in DODAB vesicles: A small-angle neutron scattering study
Langmuir **18** 2873 (2002)

K V Kamenev, W G Marshall, M R Lees, D M Paul, G Balakrishnan,
V G Tissen, M V Nefedova

Pressure effects on the magnetic and structural properties of layered manganites
Mater Sci Forum **373-376** 581 (2001)

T Kanaya, I Tsukushi, K Kaji, B J Gabrys, S M Bennington, H Furuya

Localized picosecond-scale process in glassy poly(methyl methacrylate) far below T_g
Phys Rev B **64** 144202 (2001)

A Kanigel, A Keren, Y Eckstein, A Knizhnik, J S Lord, A Amato

Common energy scale for magnetism and superconductivity in underdoped cuprates: A muon spin resonance investigation of $(Ca_xLa_{1-x})(Ba_{1.752-x}La_{0.251-x})Cu_3O_y$
Phys Rev Lett **88** 137003 (2002)

E B Karlsson, T Abdul-Redah, T J Udovic, B Hjorvasson,
C A Chatzidimitriou-Dreismann

Short-lived proton entanglement in yttrium hydrides
Appl Phys A (in press 2002)

E B Karlsson, C A Chatzidimitriou-Dreismann, T Abdul-Redah

Short-lived proton entanglement in yttrium hydrides, quantum coherence and decoherence
Proc ISQM - Tokyo'01 (in press 2002)

E B Karlsson, S W Lovesey

Scattering by entangled spatial and spin degrees of freedom
Phys Scripta **65** 112 (2002)

E Kemner, C F de Vroege, M T F Telling, I M de Schepper, G J Kearley

Low frequency modes of ferrocene in zeolite Y
Appl Phys A (in press 2002)

A R Kennedy, W E Smith, D R Tackley, W I F David, K Shankland,
B Brown, S J Teat

Tetraaryl biphenyl diamine hole transport materials: a structural study utilizing both single crystal and high resolution powder diffraction
J Mater Chem **12** 168 (2002)

A Keren, G Bazalitsky, I Campbell, J S Lord

Probing exotic spin correlations by muon spin depolarization measurements with applications to spin glass dynamics
Phys Rev B **64** 054403 (2001)

- S M King
New sources – new opportunities
Macromol Symp (in press 2002)
- S M King
Small-Angle Neutron Scattering
Commentary published by Bristol Colloid Centre
(bcc@bris.ac.uk) (2002)
- W Kockelmann, A Meents, A Kirfel
Temperature evolution of the thermal expansion tensors of ammonium Tutton salts
Appl Phys (in press 2002)
- C A Koh, R E Westacott, W Zhang, K Hirachand, J L Creek, A K Soper
Mechanisms of gas hydrate formation and inhibition
Fluid Phase Equilibria 194 143 (2002)
- A I Kolesnikov, J-C Li, S F Parker
Liquid-like dynamical behaviour of water in silica gel at 5K
J Mol Liq 96-7 317 (2002)
- A M Korsunsky, S P Collins, R A Owen, S Achtioui, M R Daymond, K E James
Fast residual stress mapping using energy dispersive synchrotron X-ray diffraction on station 16.3 at the SRS
Scripta Mat (in press 2002)
- A M Kusainova, P Lightfoot, W Zhou, S Yu Stefanovich, A O Mosunov, V A Dolgikh
Ferroelectric properties and crystal structure of the layered intergrowth phase $\text{Bi}_3\text{Pb}_2\text{Nb}_2\text{O}_{11}\text{Cl}$
Chem Mater 13 4731 (2001)
- G A Lager, P Ulmer, R Miletich, W G Marshall
O-D...O bond geometry in OD-chondrodite
Am Mineral 86 176 (2001)
- E Lalik, W I F David, P Barnes, J F C Turner
Mechanisms of reduction of MoO_3 to MoO_2 reconciled?
J Phys Chem B 105 9153 (2001)
- C Lamberti, S Bordiga, A Zecchina, G Artioli, G L Marra, G Spano
Ti location in the MFI framework of Ti-silicalite-1: a neutron powder diffraction study
J Am Chem Soc 123 2204 (2001)
- C Landron, L Hennet, T E Jenkins, G N Greaves, J P Coutures, A K Soper
Molten Alumina: Detailed atomic coordination determined from neutron diffraction data using empirical potential structure refinement
Phys Rev Lett 86 4839 (2001)
- C Landron, A K Soper, T E Jenkins, G N Greaves, L Hennet, J P Coutures
Measuring neutron scattering structure factor for liquid alumina and analysing the radial distribution function by empirical potential structure refinement
J Non-Cryst Solids 293 453 (2001)
- Y Le Godec, M T Dove, D J Francis, S C Kohn, W G Marshall, A R Pawley, G D Price, S A T Redfern, N Rhodes et al
Neutron diffraction at simultaneous high temperatures and pressures, with measurement of temperature by neutron radiography
Mineral Mag 65 737 (2001)
- A Leineweber, H Jacobs, S Hull
Ordering of nitrogen in nickel nitride Ni_3N determined by neutron diffraction
Inorg Chem 40 5818 (2001)
- R L Lichti, S F J Cox, E A Davis, B Hitti, S K L Sjue
Positively charged muonium centers in aluminium and gallium nitrides
Physica B 308-310 73 (2001)
- R L Lichti, K H Chow, B Hitti, E A Davis, S K L Sjue, S F J Cox
Motional properties of positively charges muonium in gallium III—V compounds
Physica B 308-310 862 (2001)
- H Liu, R Harrison, A Putnis
A triclinic phase of relaxor La-modified $\text{Pb}(\text{Zr}_{0.65}\text{Ti}_{0.35})\text{O}_3$ and its structure at 40 K by high-resolution neutron diffraction
J Appl Phys 90 6321 (2001)
- F Lo Celso, A Triolo, F Triolo, J McClain, J M Desimone, R K Heenan, H Amenitsch, R Triolo
Industrial applications of aggregation of block copolymers in supercritical CO_2 : a SANS study
Appl Phys A (in press 2002)
- T Lorentzen, M R Daymond, B Clausen, C N Tomé
Lattice strain evolution during cyclic loading of stainless steel
Acta Mat (in press 2002)
- C Lorenz-Haas, P Muller-Buschbaum, K Kraus, D G Bucknall, M Stamm
Nucleated dewetting of thin polymer films
Applied Physics A (in press 2002)
- J S Loveday, R J Nelmes, M Guthrie, D D Klug, J S Tse
Transition from cage clathrate to filled ice: The structure of methane hydrate III
Phys Rev Lett 87 215501 (2001)
- J S Loveday, R J Nelmes, M Guthrie
High-pressure transitions in methane hydrate
Chem Phys Lett 350 459 (2001)
- J S Loveday, R J Nelmes, M Guthrie, S A Belmonte, D R Allan, D D Klug, J S Tse, Y P Handa
Stable methane hydrate above 2 GPa and the source of Titan's atmospheric methane
Nature 410 661 (2001)
- I M Low, D Lawrence, M Singh
Thermal stability of aluminium-titanate in vacuum
Proc 2001 Joint AXAA/WASEM Conference, Eds M Saunders et al, 188 (2001)
- I M Low, P Manurung, R I Smith, D Lawrence
A novel processing method for the microstructural design of functionally-graded ceramic composites
Proc 2nd China Int Conf on High-Performance Ceramics (CICC-2) (in press 2002)
- I M Low, M Singh, P Manurung, E Wren, D P Sheppard, M W Barsoum
Depth profiling of phase composition and texture in layered-graded Al_2O_3 - & Ti_3SiC_2 - based systems using X-ray and synchrotron radiation diffraction
Proc 2nd China Int Conf on High-Performance Ceramics (CICC-2) (in press 2002)
- S Magazu, F Migliardo, P Migliardo
Analysis of the diffusive properties of vitamin C aqueous solutions by quasielastic neutron scattering. 1.
J Phys Chem B 105 2612 (2001)
- J F Marco, J R Gancedo, M Gracia, J L Gautier, E I Rios, H M Palmer, C Greaves, F J Berry
Cation distribution and magnetic structure of the ferrimagnetic spinel NiCo_2O_4
J Mater Chem 11 3087 (2001)

- S Margadonna, T Muranaka, K Prassides, I Maurin, K Brigatti, R M Ibberson, M Arai, M Takata, J Akimitsu
Phase inhomogeneities and lattice expansion near T_c in the $Mg^{11}B_2$ superconductor
J Phys:Condens Matter **13** L795 (2001)
- M P M Marques, L A E Batista de Carvalho, J Tomkinson
Study of biogenic and α,ω -polyamines by combined INS and Raman spectroscopies
J Phys Chem (in press 2002)
- W G Marshall, D J Francis
Attainment of near-hydrostatic compression conditions using the Paris-Edinburgh cell
J Appl Crystallogr **35** 122 (2002)
- D Martin
Towards high resolution polarisation analysis using double polarisation and ellipsoidal analysers.
Appl Phys A (in press 2002)
- M L Martinez, C R Borlado, F J Mompean, M Garcia-Hernandez, J Gil-Sevillano, J Ruiz, R L Peng, M R Daymond
Neutron strain scanning in eutectoid steel rods
Acta Mat (in press 2002)
- P Mawer, T A Waigh, R Harding, T C B McLeish, S M King, M P Bell, N Boden
Small angle neutron scattering from peptide tapes under shear
Langmuir (in press 2002)
- J Mayers
Microscopic connection between Bose-Einstein condensation and the Two Fluid Model of liquid 4He
 RAL-TR-2001-044 (2001)
- J Mayers, A L Fielding, R Senesi
Multiple scattering in Deep Inelastic Neutron Scattering: Monte Carlo simulations and experiments at the ISIS eVS inverse geometry spectrometer
Nucl Inst Meth A (in press 2002)
- R L McGreevy
Reverse Monte Carlo modelling
J Phys:Condens Matter **13** R877 (2001)
- R L McGreevy, P Zetterstrom
Reverse Monte Carlo modelling of network glasses: useful or useless?
J Non-Cryst Solids **293-295** 297 (2001)
- A C McLaughlin, V Janowitz, J A McAllister, J P Attfield
Doping studies of the ferromagnetic superconductor $RuSr_2GdCu_2O_8$
J Mater Chem **11** 173 (2001)
- R Melzi, S Aldrovandi, F Tedoldi, P C arretta, P Millet, F Mila
Magnetic and thermodynamic properties of Li_2VO_5 : A two-dimensional $S = 1/2$ frustrated antiferromagnet on a square lattice
Phys Rev B **64** 024409 (2001)
- P J Mendes, L P Ferreira, J M Gil, N Ayres de Campos
Muon diffusion in intermetallic compounds of the $MoSi_2$ -type structure
J Phys: Condens Matter **13** 5285 (2001)
- F Mezei, R S Eccleston, T Gutberlet (Eds)
Performance of a Suite of Generic Instruments on ESS
 ISSN 1422-559X, ESS115-01-T (2001)
- I Michalarias, I Beta, R C Ford, S V Ruffe, J-C Li
Inelastic neutron scattering studies of water in DNA
Physica B (in press 2002)
- A F Miller, R W Richards, J R P Webster
Transition in tethered layer thickness induced by concentration changes in a spread film of an amphiphilic graft copolymer
Macromolecules **34** 8361 (2001)
- M C Moron, S Hull
Role of an order-disorder phase transition in increasing the exchange magnetic field in a diluted magnetic semiconductor
Phys Rev B **64** 220402 (2001)
- E G Moshopoulou, J L Sarrao, P G Pagliuso, N O Moreno, J D Thompson, Z Fisk, R M Ibberson
Comparison of the crystal structure of the heavy-Fermion materials $CeCoIn_5$, $CeRhIn_5$ and $CeIrIn_5$
Appl Phys A (in press 2002)
- T Muranaka, T Yokoo, M Arai, I Margiolaki, K Brigatti, K Prassides, O Petrenko, J Akimitsu
Vibrational spectroscopy of MgB_2 by neutron inelastic scattering
J Phys Soc Japan (in press 2002)
- S Nave, J Eastoe, R K Heenan, D C Steytler, I Grillo
What is so special about Aerosol-OT? Part III – glutaconate versus sulfosuccinate headgroups and oil-water interfacial tensions
Langmuir **18** 1505 (2002)
- D Nemirovsky, R Moreh, Y Finkelstein, J Mayers
Study of the anisotropy in the atomic momentum distributions in a Kapton film
J Phys: Condens Matter **13** 5053 (2001)
- J Noreland, J Mayers, G Reiter
Direct measurement of temperature dependent anharmonicity in a hydrogen bond
Phys Rev B (in press 2002)
- H Nowell, J P Attfield, J C Cole, P J Cox, K Shankland, S J Maginn, W D S Motherwell
Structure solution and refinement of tetracaine hydrochloride from X-ray powder diffraction data
New J Chem **26** 469 (2002)
- T Otomo, M Arai, Y Inamura, J-B Suck, S M Bennington
An experimental approach to reveal the origin of collective excitations in $Ni_{33}Zr_{67}$ glass
J Non-Cryst Solids – LAM11 (in press 2002)
- S F Parker
Inelastic neutron scattering spectroscopy
Handbook of Vibrational Spectroscopy, Eds J M Chalmers, P R Griffiths (John Wiley & Sons) 1 838 (2002)
- A Pavese, N Curetti, G Ferraris, G Ivaldi, U Russo
Deprotonation and order-disorder reactions as a function of temperature in a phengite 3T (Cimla Pal, western Alps) by neutron diffraction and Mossbauer spectroscopy
Eur J Miner (in press 2002)
- A Pawlukoic, J Leciejewicz, J Tomkinson, S F Parker
Neutron scattering, infra red, Raman spectroscopy and *ab initio* study of L-threonine
Spectrochim Acta A **57** 2513 (2001)
- J V Pearce, R T Azuah, W G Stirling, R M Dimeo, P E Sokol, M A Adams
High resolution measurements of the temperature dependence of the roton energy of superfluid 4He
J Low Temp Phys **124** (2001)
- J Penfold, E Staples, I Tucker, J D Hines
Effect of solubilised alkane, hexadecane, on micellar growth in the mixed ionic-nonionic surfactant micelles of SDS and $C_{12}E_6$
J Phys Chem B (in press 2001)

- J Penfold, E Staples, I Tucker, R K Thomas
The structure of nonionic surfactant mixtures at the air-water interface: the role of alkyl chain length
Langmuir (in press 2001)
- J Penfold, R K Thomas
Solvent distribution in non-ionic surfactant monolayers
Langmuir (in press 2001)
- J Penfold, E Staples, I Tucker, R K Thomas
The adsorption of mixed anionic and nonionic surfactants at the hydrophilic silicon surface
Langmuir (in press 2001)
- J Penfold, E Staples, I Tucker
On the consequences of surface treatment in the adsorption of non-ionic surfactants at the hydrophilic silica/solution interface
Langmuir (in press 2001)
- S J Perkins
X-ray and neutron scattering analyses of hydration shells: a molecular interpretation based on sequence predictions and modelling fits
Biophys Chem (in press 2001)
- S J Perkins
Applications of highly constrained molecular modelling scattering curve fits to biologically important proteins
Fibre Diffraction Review (in press 2001)
- T G Perring, D T Adroja, G Chaboussant, G Aeppli, T Kimura, Y Tokura
Spectacular doping dependence of interlayer exchange and other results on spin waves in bilayer manganites
Phys Rev Lett **87** 217201 (2001)
- T Pfleiderer, H Bertagnolli, K Todheide, A K Soper
High pressure neutron diffraction on fluid propane and a mixture of propane and methane
J Chem Phys **115** 331 (2001)
- R Pillay, V Arrighi, W Kagunya, J S Higgins
Ester methyl group dynamics in polymethylmethacrylate stereo complex: a neutron scattering study
Macromol Symp **166** 269 (2001)
- M Plazanet, N Fukushima, M R Johnson, A J Horsewill, H P Trommsdorff
The vibrational spectrum of crystalline benzoic acid: inelastic neutron scattering and density functional theory calculations
J Chem Phys **115** 3241 (2001)
- M Prager, H Grimm, S F Parker, R Lechner, A Desmedt, S McGrady, E Koglin
Methyl group rotation in trimethylaluminium
J Phys: Condens Matter **14** 1833 (2002)
- P G Radaelli, R M Ibberson, D N Argyriou, H Casalta, K H Andersen, S-W Cheong, J F Mitchell
Mesoscopic and microscopic phase segregation in manganese perovskites
Phys Rev B **63** 172419 (2001)
- P G Radaelli, Y Horibe, M J Gutmann, H Ishibashi, C H Chen, R M Ibberson, Y Koyama, Y-S Hor, V Kiryukhin, S-W Cheong
Formation of isomorphous Ir³⁺ and Ir⁴⁺ octamers and spin dimerization in the spinel CuIr₂S₄
Nature **416** 155 (2002)
- E A Raekelboom, A L Hector, M T Weller, J R Owen
Electrochemical properties and structures of mixed-valence lithium cuprates Li₂Cu₂O₄ and Li₂NaCu₂O₄
J Power Sources **97-98** 465 (2001)
- A J Ramirez-Cuesta, R A Bennett, P Stone, P C H Mitchell, M Bowker
STM investigation and Monte-Carlo modelling of spillover in a supported metal catalyst
J Mol Catal:A **167** 171 (2001)
- A J Ramirez-Cuesta, P C H Mitchell, S F Parker, J Tomkinson, D Thompsett
Hydrogen spillover on a carbon supported platinum fuel cell catalyst: a computational and inelastic neutron scattering study
Studies in Surface Science and Catalysis **138** 55 (2001)
- J Reading, M T Weller
The structure of Cd₂Os₂O₇ through the metal-semiconductor transition by powder neutron diffraction
J Mater Chem **11** 2373 (2001)
- S A T Redfern
Neutron powder diffraction of minerals at high pressures and temperatures: some recent technical developments and scientific applications
Eur J Mineral (in press 2002)
- P A Reynolds, E P Gilbert, J W White
High internal phase water-in-oil emulsions & related microemulsions studied by small angle neutron scattering. 2. The distribution of the surfactant
J Phys Chem B **105** 6925 (2001)
- C J Rhodes
Muon Spectroscopy
Ann Rep Prog Chem Sect C **97** (in press 2001)
- M A Ricci, A K Soper
Jumping between water polymorphs
Physica A **304** 43 (2002)
- R M Richardson, R M Dalgliesh, T Brennan, M R Lovell, A C Barnes
A neutron reflection study of the effect of water on the surface of float glass
J Non-Cryst Solids **292** 93 (2001)
- I B Rietveld, W G Bouwman, M W P L Baars, R K Heenan
Location of the outer shell and influence of pH on carboxylic-acid functionalised poly(propylene imine) dendrimers
Macromolecules **34** 8380 (2001)
- R Rinaldi
Neutron scattering in mineral sciences
Eur J Mineral **14** 195 (in press 2002)
- R Rinaldi, G Artioli, M T Dove, W Shaefer, P F Schofield, B Winkler
Neutron scattering in mineral science, earth science and related fields with the European Spallation Source (ESS)
Scientific Trends in Condensed Matter Research and Instrumentation Opportunities at ESS, ESS-SAC/ENSA Report 1/01 p91 (2001)
- H M Ronnow, D F McMorrow, A Harrison, I D Youngson, R Coldea, T G Perring, G Aeppli, O Syljuasen
Correlations and fluctuations in the 2D Heisenberg antiferromagnet
J Magn Magn Mater **236** 1 (2001)
- D K Ross, J E Totolici, M Kemali, I Morrison, M Johnson
Proton wave functions in palladium studied by *ab initio* calculations and inelastic neutron scattering methods
Recent Advances in Hydride Chemistry (Elsevier) Ch 17 (in press 2002)
- S V Ruffe, I Michalaris, J-C Li, R C Ford
Inelastic incoherent neutron scattering studies of water interacting with biological macromolecules
J Amer Chem Soc (in press 2002)

- K M Ryan, N R B Coleman, D M Lyons, J P Hanrahan, T R Spalding, M A Morris, D C Steytler, R K Heenan, J D Holmes
Control of pore morphology in mesoporous silicas synthesised from triblock copolymer templates
 Langmuir (in press 2002)
- M-L Saboungi, D L Price, G Mao, R Fernandez-Perea, O Borodin, G D Smith, M Armand, W S Howells
Coherent neutron scattering from PEO and a PEO-based polymer electrolyte
 Solid State Ionics **147** 225 (2002)
- Z Salman, A Keren, P Mendels, A Scuiller, M Verdagner, J S Lord, C Baines
Dynamics at T>0 in half-integer isotropic high spin molecules
 Phys Rev B (in press 2002)
- P S Salmon, S Xin
Chalcohalide glasses: The effect of covalent versus ionic bonding in $(CuI)_{0.6}(Sb_2Se_3)_{0.4}$
 Phys Rev B **65** 064202 (2002)
- J R Santisteban, L Edwards, H G Priesmeyer, S Vogel
Comparison of Bragg edge neutron spectroscopy at ISIS and LANSCE
 Appl Phys (in press 2002)
- J R Santisteban, L Edwards, A Steuwer, P J Withers
Neutron transmission spectroscopy
 J Appl Crystallogr **34** 289 (2001)
- J R Santisteban, L Edwards, A Steuwer, P J Withers, M E Fitzpatrick
Engineering applications of Bragg edge neutron diffraction
 Appl Phys (in press 2002)
- M K Sanyal, M K Mukhopadhyay, M Mukerjee, A Dutta, J K Basa, J Penfold
Role of molecular self-assembly in Langmuir-Blodgett film growth
 Phys Rev B (in press 2001)
- A Schneidewind, W Kockelmann, A Kreyssig, C Ritter, G Behr, M Loewenhaupt
Rietveld refinement of crystalline and magnetic structures of $Tb_{1-x}Pr_xCu_2$ compounds
 Appl Phys (in press 2002)
- P F Schofield, S J Covey-Crump, I C Stretton, M R Daymond, K S Knight, R F Holloway
Using neutron diffraction measurements to characterize the mechanical properties of polymineralic rocks
 Min Mag (in press 2002)
- P F Schofield, K S Knight, S J Covey-Crump, G Cressey, I C Stretton
Accurate quantification of the modal mineralogy of rocks when image analysis is difficult
 Mineral Mag **66** 189 (2002)
- M Sferrazza, S Langridge
Off-specular neutron scattering – exploring in-plane correlations
 Neutron News **12** 15 (2001)
- M Sferrazza, C Xiao, D G Bucknall, R A L Jones
Interface width of low-molecular-weight immiscible polymers
 J Phys: Condens Matter **13** 10269 (2001)
- N Shankland, W I F David, K Shankland, A R Kennedy, C S Frampton, A J Florence
Structural transformations in zopiclone
 Chem Commun **21** 2204 (2001)
- N Shankland, W I F David, K Shankland, A R Kennedy, C S Frampton, A J Florence
Structural transformations and physical properties of zopiclone
 ESRF Scientific Highlight (2001)
- J L Shaw, A C Wright, R N Sinclair, T J Kiczenski, H A Feller, S A Feller, C R Scales
A neutron diffraction investigation of the structure of sodium borosilicate glasses
 Phys Chem Glasses (in press 2002)
- S Siano, W Kockelmann, U Bafille, M Celli, R Pini, R Salimbeni, M Iozzo, M Miccio, O Moze, M Zoppi
Quantitative multiphase analysis of archaeological bronzes by neutron diffraction
 Appl Phys (in press 2002)
- R N Sinclair, C E Stone, A C Wright, S W Martin, M L Royle, A C Hannon
The structure of vitreous boron sulphide
 J Non-Cryst Solids **293-295** 383 (2001)
- R N Sinclair, A C Wright, A G Clare, A C Hannon
An inelastic neutron scattering study of tetrahedral connectivity in vitreous Ge_xSe_{1-x}
 Phys Chem Glasses (in press 2002)
- D S Sivia, W I F David
A Bayesian approach to phase extension
 J Phys Chem Solids **62** 2119 (2001)
- A V Skripov, H Natter, R Hempelmann
Neutron spectroscopic evidence of a low-temperature phase transition in C15-type $ZrCr_2H_x$ ($x=0.2$ and 0.45)
 Solid State Commun **120** 265 (2001)
- D K Smith, G P Tomaino, A C Wright, R N Sinclair
New data on the phases of opal
 Amer Mineral (in press 2002)
- J-Y So, J-G Park, D T Adroja, K A McEwen, S-J Oh
Investigation of the dynamical susceptibility of $Ce_{0.7}Th_{0.3}RhSb$ by inelastic neutron scattering
 Physica B (in press 2002)
- A K Soper
Tests of the empirical potential structure refinement method and a new method of application to neutron diffraction data on water
 Mol Phys **99** 1503 (2001)
- I Sosnowska, W Schafer, W Kockelmann, K H Andersen, I O Troyanchuk
Crystal structure and spiral magnetic ordering of $BiFeO_3$ doped with manganese
 Appl Phys (in press 2002)
- C Stadler, J Daub, J Köhler, R W Saalfrank, V Coropceanu, V Schünemann, C Ober, A X Trautwein, S F Parker et al
Electron transfer in a trinuclear oxo-centred mixed-valence iron complex, in solid and solution states
 J Chem Soc-Dalton Trans 3373 (2001)
- E Staples, I Tucker, J Penfold, N Warren, R K Thomas
The organisation of polymer-surfactant surfaces at the air-water interface: $SDS/C_{12}E_{16}/poly\text{-}dinddac$
 Langmuir (in press 2001)
- E Staples, I Tucker, J Penfold, N Warren, R K Thomas
The organisation of polymer-surfactant surfaces at the air-water interface: $SDS/poly\text{-}dudase$
 Langmuir (in press 2001)

- D Stefanescu, A Bouzina, M Dutta, D Q Wang, L Edwards, M E Fitzpatrick
Comparison of residual stress measurements using neutron and X-ray diffraction around cold expanded holes
J N Res 9 399 (2001)
- A Steuwer, J R Santisteban, P J Withers, L Edwards, M E Fitzpatrick, M R Daymond, M W Johnson
The $\text{Sin}^2\psi$ technique in time-of-flight neutron transmission
J N Res 9 289 (2001)
- D C Steytler, E Rumsey, M Thorpe, J Eastoe, A Paul, R K Heenan
Phosphate surfactants for water in CO_2 microemulsions
Langmuir 17 7948 (2001)
- D C Steytler, A Thorpe, E Rumsey, J Eastoe, R K Heenan
Microemulsions in Suva
Langmuir (in press 2002)
- C E Stone, A C Wright, R N Sinclair, A C Hannon, A Musinu, T P Seward III, H A Feller
Neutron diffraction studies of network glasses
Phys Chem Glasses (in press 2002)
- C E Stone, A C Hannon, T Ishihara, N Kitamura, Y Shirahawa, R N Sinclair, N Umasaki, A C Wright
The structure of pressure-compacted vitreous germania
J Non-Cryst Solids 293-295 769 (2001)
- C E Stone, A C Wright, R N Sinclair, A C Hannon, A Musinu, T P Seward, H A Feller
Neutron diffraction studies of network glasses
Phys Chem Glasses (in press 2002)
- V G Storchak, D G Eshchenko, J H Brewer, S P Cottrell, S F J Cox
Electron transport in condensed rare gases
Phys Rev B (in press 2002)
- V G Storchak, D G Eshchenko, S P Cottrell, S F J Cox, E Karlsson, R Wappling, J M Gil
Landau diamagnetism of a weakly bound muonium atom
Phys Lett A 290 181 (2001)
- I C Stretton, S J Covey-Crump, P F Schofield, M R Daymond, K S Knight
The partitioning of strain during rock deformation
Crystallography News, British Crystallography Association 79 8 (2001)
- T Sugano, S J Blundell, W Hayes, P Day
Magnetism in organic radical ion salts and complexes based on nitronyl nitroxide
Synthetic Met 121 1812 (2001)
- M Summers, J Eastoe, S Davis, Z Du, R M Richardson, R K Heenan, D C Steytler, I Grillo
Polymerization of cationic surfactant phases
Langmuir 17 5388 (2001)
- J Swenson, W S Howells
Quasi-elastic neutron scattering of propylene glycol and its 7-mer confined in clay
J Chem Phys 117 857 (2002)
- J Swenson, C Karlsson, L Borjesson, R K Heenan
Structural inhomogenities in fast conducting glasses
Phys Rev B 64 134201 (2001)
- J Swenson, I Koper, M T F Telling
Dynamics of propylene glycol and its 7-mer by neutron scattering
J Chem Phys 116 5073 (2002)
- J Swenson, R Bergman, D T Bowron, S Longeville
Water structure and dynamics in a fully hydrated Na-vermiculite
Phil Mag B (in press 2002)
- J Swenson, St Adams
Application of the bond valence method to reverse Monte Carlo produced structural models of superionic glasses
Phys Rev B 64 024204 (2001)
- D J F Taylor, R K Thomas, J Penfold
The interaction between dodecyl trimethyl ammonium bromide and sodium poly-(styrene sulphonate) at the air-water interface: a neutron reflection study
Langmuir (in press 2002)
- N D Telling, C A Faunce, M J Bonder, P J Grundy, D G Lord, S Langridge
Interdiffusion in direct ion beam deposited isotopic Fe/Si trilayers
J Appl Phys 89 7074 (2001)
- B Tomberli, P A Egelstaff, C J Benmore, J Neuefeind
Isotopic quantum effects in the structure of liquid methanol: I. Experiments with high-energy photon diffraction
J Phys: Condens Matter 13 11405 (2001)
- B Tomberli, P A Egelstaff, C J Benmore, J Neuefeind
Isotopic effects in the structure of liquid methanol: II. Experimental data in Fourier space
J Phys: Condens Matter 13 11421 (2001)
- J Tomkinson, S F Parker, D A Braden, B S Hudson
Inelastic neutron scattering spectra of the transverse acoustic modes of the normal alkanes from pentane
Phys Chem Chem Phys 4 716 (2002)
- A Triolo, R E Lechner, A Desmedt, M T F Telling, V Arrighi
Complex dynamics in polyisobutylene melts
Macromolecules (in press 2002)
- S C Tsang, C D A Bulpitt, P C H Mitchell, A J Ramirez-Cuesta
Some new insights into the sensing mechanism of palladium promoted tin (IV) oxide sensor
J Phys Chem B 105 5737 (2001)
- D H Ucko, Q A Pankhurst, L Fernandez Barquin, J Rodriguez Fernandez, S F J Cox
Magnetic relaxation in the nanoscale granular alloy $\text{Fe}_{20}\text{Cu}_{20}\text{Ag}_{60}$
Phys Rev B 64 104433 (2001)
- N H van Dijk, S E Offerman, W G Bouwman, M Th Rekveldt, J Sietsma, S van der Zwaag, A Bodin, R K Heenan
SANS experiments on Nb(C,N) and MnS precipitates in HSLA steel
Appl Phys A (in press 2002)
- N H van Dijk, S E Offerman, W G Bouwman, M Th Rekveldt, J Sietsma, S van der Zwaag, A Bodin, R K Heenan
High temperature SANS experiments on Nb(C,N) and MnS precipitates in HSLA steel
Metall Mater Trans A (in press 2002)
- P Vaqueiro, A V Powell, A I Coldea, C A Steer, I M Marshall, S J Blundell, J Singleton, T Ohtani
Colossal magnetoresistance in the layered chromium sulfide $\text{Cr}_2\text{S}_{3-x}$ ($x = 0.08$)
Phys Rev B 64 132402 (2001)
- C A F Vaz, G Lauhoff, J A C Bland, B D Fulthorpe, T P A Hase, B K Tanner, S Langridge, J Penfold
Effect of the Cu capping thickness on the magnetic properties of thin Ni/Cu(001) films
J Magn Magn Mater 226-230 1618 (2001)

- J F Vente, K V Kamenev, D A Sokolov
Structural and magnetic properties of layered Sr₇Mn₄O₁₅
 Phys Rev B **64** 214403 (2001)
- J B Viera, Z X Li, R K Thomas, J Penfold
The structure of triblock copolymers of ethylene oxide and propylene oxide at the air-water interface: neutron reflection data and a reinterpretation of the neutron small angle scattering
 J Phys Chem B (in press 2001)
- P Viklund, S Lidin, P Berastegui, U Haussermann
Variations of the FeGa₃ structure type in the systems CoIn_{3-x}Zn_x and CoGa_{3-x}Zn_x
 J Solid State Chem **164** (in press 2002)
- P Viklund, C Svensson, S Hull, S I Simak, P Berastegui, U Haussermann
From V₈Ga_{36.9}Zn_{4.1} and Cr₈Ga_{29.8}Zn_{11.2} to Mn₈Ga_{27.4}Zn_{13.6}: A remarkable onset of Zn-cluster formation in an intermetallic framework
 Chem-Eur J **7** 5143 (2001)
- G Walter, J Vogel, U Hoppe, P Hartmann
The structure of CaO-Na₂O-MgO-P₂O₅ invert glass
 J Non-Cryst Solids **296** 212 (2001)
- R I Walton, R I Smith, D O'Hare
Following the hydrothermal crystallization of zeolites using time-resolved in situ powder neutron diffraction
 Microporous Mesoporous Mat **48** 79 (2001)
- R I Walton, F Millange, R I Smith, T C Hansen, D O'Hare
Real time observation of the hydrothermal crystallization of barium titanate using in situ neutron powder diffraction
 J Am Chem Soc **123** 12547 (2001)
- D Q Wang, S S Babu, E A Payzant, P G Radaelli, A C Hannon
In situ characterization of γ/γ' lattice stability in a nickel-base superalloy by neutron diffraction
 Metall Mater Trans A **32** 1551 (2001)
- D Q Wang, J R Santisteban, L Edwards
Effect of wavelength-dependent attenuation on strain measurement using pulsed neutron diffraction
 Nucl Instrum Meth A **460** 381 (2001)
- G A Webster, R C Wimpory
Residual stress in weldments
 J N Res **9** 281 (2001)
- G A Webster, A N Ezeilo
Residual stress distributions and their influence on fatigue lifetimes
 Int J Fatigue **23** 375 (2001)
- G A Webster, R C Wimpory
Non-destructive measurement of residual stress by neutron diffraction
 J Mat Processing & Tech **117** 395 (2001)
- G A Webster
A new TTA on measurement of residual stress by neutron diffraction
 ISO Bulletin p22 Aug (2001)
- M D Welch, W G Marshall
High-pressure behavior of clinocllore
 Am Mineral **86** 1380 (2001)
- M D Welch, W G Marshall, N L Ross, K S Knight
Proton positions in leucophoenicite and a comparison with the hydrous B phases
 Am Mineral **87** 154 (2002)
- I G Wood, K S Knight, G D Price, J Stuart
Thermal expansion and atomic displacement parameters of cubic KMgF₃ perovskite determined by high-resolution neutron powder diffraction
 J Appl Cryst (in press 2002)
- K Wozniak, P Mallinson, E Hoverstreyd, C C Wilson, E Grech
Charge density studies of weak interactions in dipicrylamine
 J Phys Chem (in press 2002)
- J P Wright, J P Attfield, P G Radaelli
Long range charge ordering in magnetite below the Verwey transition
 Phys Rev Lett **87** 266401 (2001)
- K Yamada, K Mikawa, T Okuda, K S Knight
Static and dynamic structures of CD₃ND₃GeCl₃ studied by TOF high resolution neutron powder diffraction and solid state NMR
 Dalton Trans Roy Soc Chem (in press 2001)
- O Yamamuro, Y Madokoro, H Obara, K Harabe, T Matsuo, T Kamiyama, H Fukazawa, S Ikeda
Neutron scattering study of protonated and deuterated potassium phosphate glasses
 J Phys Soc Jpn **70** Suppl A 386 (2001)
- M Zoppi, D Colognesi, M Celli
Density dependence of mean kinetic energy in liquid and solid hydrogen at 19.3K
 Eur Phys J B **23** 171 (2001)
- M Zoppi, M Celli, U Bafle, E Guarini, M Neumann
On the microscopic structure of liquid hydrogens
 Condensed Matter Physics **4** 2 (2001)

ISIS 2001 Update

Listed below are publications from the previous reporting year which have been notified to us subsequently or which were 'in press' at the time of last year's report.

- I Abrahams, F Krok, M Malys, A J Bush
Defect structure and ionic conductivity as a function of thermal history in BIMGVOX solid electrolytes
J Mater Sci **36** 1099 (2001)
- P B Aitchison, B Amundsen, T Bell, D J Jones, J Roziere, G R Burns, H Berg, R Tellgren, J Thomas
Proton insertion in spinel lithium manganates and the effect of manganese substitution
Physica B **276-278** 847 (2000)
- P W Albers, J Pietsch, S F Parker
Poisoning and deactivation of palladium catalysts
J Mol Catal:A **173** 275 (2001)
- P W Albers, A Karl, J Mathias, D K Ross, S F Parker
INS-, XPS- and SIMS-investigations on the controlled postoxidation of pigment blacks. Detection of different species of strongly adsorbed water
Carbon **39** 1663 (2001)
- Y Andreev, P G Bruce
Using crystallography to understand polymer electrolytes
J Phys:Condens Matter **13** 8245 (2001)
- R J Angel, U Bismayer, W G Marshall
Renormalisation of the phase transition in lead phosphate, $Pb_3(PO_4)_2$
J Phys:Condens Matter **13** 5353 (2001)
- D J Barlow, M J Lawrence, P A Timmins
Molecular modelling of surfactant vesicles
Synthetic Surfactant Vesicles, Volume II, Ed I Uchegbu (Harwood Academic Press) p9 (2000)
- M K Boehm, S J Perkins
Structural models for carcinoembryonic antigen and its complex with the single-chain Fv antibody molecule MFE23
FEBS Letters **475** 11 (2000)
- C Branca, A Faraone, S Magazu, G Maisano, P Migliardo, V Villari
Polyethylene oxide: a review of experimental findings by spectroscopic techniques
J Mol Liq **87** 21 (2000)
- W Bronger, T Sommer, G Auffermann, P Muller
New alkali metal osmium- and ruthenium-hydrides
J Alloy Compd **330-332** 536 (2002)
- D G Bucknall, S A Butler, J S Higgins
Studying polymer interfaces using neutron reflection
Scattering From Polymers, Eds B S Hsiao, D J Lohse, P Cebe, ACS Symposium Series **739** p57 (2000)
- D J Bull, D K Ross
Monte Carlo simulations of quasi-elastic neutron scattering from lattice gas systems
Physica B **301** 54 (2001)
- E Bychkov, D L Price, A Lapp
Universal trend of the Haven ratio in glasses: Origin and structural evidence from neutron diffraction and small-angle neutron scattering
J Non-Cryst Solids **293-295** 211 (2001)
- J M Cadogan, Suharyana, D H Ryan, O Moze, W Kockelmann
Neutron diffraction and Mössbauer study of the magnetic structure of $HoFe_6Sn_6$
IEEE Transactions on Magnetics **37** 2606 (2001)
- M Catti, S Stratmore
Lithium location in NASICON-type Li^+ conductors by neutron diffraction: II. Rhombohedral $\alpha-LiZr_2(PO_4)_3$ at $T=423$ K
Solid State Ionics **136-137** 489 (2000)
- H Choo, M A M Bourke, P G Nash, M R Daymond
Evolution of thermal residual stress in intermetallic matrix composites during heating
Proc 24th Cocoa Beach meeting, Am Ceram Soc **21** 627 (2000)
- M T Clavaguera-Mora, J Rodriguez-Viejo, D Javokis, J L Touron, N Clavaguera, W S Howells
Neutron diffraction and calorimetric study on Al-based metallic glasses
J Non-Cryst Solids **287** 162 (2001)
- R Coldea, D A Tennant, A M Tsvetlik, Z Tyliczynski
Experimental realization of a 2D fractional quantum spin liquid
Phys Rev Lett **86** 1335 (2001)
- D J Cooke, C C Dong, R K Thomas, A M Howe, E A Simister, J Penfold
The interaction between gelatin and SDS at the air-water interface: a neutron reflection study
J Phys Chem B **16** 6546 (2001)
- S P Cottrell, J S Lord, W G Williams
Proton sites and dynamics in divalent metal hydroxides probed by muon spin relaxation
J Phys Chem Solids **62** 1977 (2001)
- S J Covey-Crump, P F Schofield, I C Stretton, K S Knight
Neutron diffraction measurements of elastic strain partitioning during the experimental deformation of polymineralic geological materials
Eos, Trans Am Geophysical Union **81** supp vol F1210 (2000)
- S F J Cox, E A Davis, P J C King, J M Gil, H V Alberto, R C Vilao, J Piroto Duarte, N Ayres de Campos, R L Lichti
Shallow versus deep hydrogen states in ZnO and HgO
J Phys: Condens Matter **13** 9001 (2001)
- P Dalmas de Reotier, A Yaouanc, P C M Gubbens, C T Kaiser, A M Mulders, F N Gygax, A Schenck et al
Magnetism and superconductivity of UPt_3 by muon spin technique
Physica B **289** 10 (2000)
- M R Daymond, J Schreiber, Yu V Taran
Mechanical characterisation of fatigued austenitic stainless steel under applied loads by *in-situ* neutron diffraction
J N Res **9** 207 (2001)
- M R Daymond, M W Johnson
The determination of d_0 without a reference material
J N Res **9** 469 (2001)
- R Dinnibier, M Schweiger, B Bildstein, K Shankland, W I F David
The disordered structure of tetraferrocenyl-[3]-cumulene $(Fc)_2C=C=C(C(Fc))_2$ by simulated annealing using synchrotron powder diffraction data
J Appl Cryst **33** 1199 (2000)
- R Dinnibier, P Sieger, H Nar, K Shankland, W I F David
Structural characterisation of three crystalline modifications of telmisartan by single crystal and high resolution powder diffraction
J Pharm Sci **89** 1465 (2000)
- R Dinnibier, M Wagner, F Peters, K Shankland, W I F David
Crystal structure of the $(C_2H_4Bme_2)_2Fe-4-4'$ -bipyridine polymer from high resolution X-ray powder diffraction
Z Anorg Allg Chem **626** 1400 (2000)
- A M Donald
Plasticisation and self-assembly in the starch granule
Cereal Chem **78** 307 (2001)

- A M Donald, P A Perry, T A Waigh
The impact of internal granule structure on processing and properties
Starch 2000: Structure and Properties, Eds A M Donald, P J Frazier, T Barnsby (RSC) p45 (2001)
- A M Donald, K L Kato, P A Perry, T A Waigh
Scattering studies of the internal structure of starch granules
Starke **53** 304 (2001)
- J Eastoe, A Bumajdad
Mixed surfactant microemulsions
Recent Research Developments in Physical Chemistry **4** 337 (2000)
- J Eastoe, A M Downer, A Paul, D C Steytler, E Rumsey
Adsorption of fluorosurfactants at air-water and water-CO₂ interfaces
Prog Colloid Polym Sci **115** 214 (2000)
- L Edwards, G Bruno, M Dutta, P J Bouchard, K L Abbott, R L Peng
Validation of residual stress predictions for a 19mm thick J-preparation
Proc 6th Int Conf on Residual Stress (Oxford: Institute of Materials) p1519 (2000)
- J S O Evans, T A Mary
Structural phase transitions and negative thermal expansion in Sc₂(MoO₄)₃
Int J Inorg Mater **2** 143 (2000)
- A N Ezeilo, G A Webster
Neutron diffraction analysis of the residual stress distribution in a bent bar
J Strain Anal Eng Des **35** 235 (2000)
- A N Ezeilo, G A Webster
Residual stresses introduced by electron beam welding
Proc 6th Int Conf on Residual Stress (Oxford: Institute of Materials) p1503 (2000)
- Y Finkelstein, D Nemirovsky, R Moreh, G Kimmel
Study of the papyex structure using neutron Compton scattering
Physica B **291** 213 (2000)
- J Frantti, J Lappalainen, S G Eriksson, V Lantto, S Nishio, M Kakihana, S Ivanov, H Rundlof
Neutron diffraction studies of Pb(Zr_xTi_{1-x})O₃ ceramics
Jpn J Appl Phys **39** 5697 (2000)
- Z Gadjourova, D Martin, K H Andersen, Y G Andreev, P G Bruce
Structure of the polymer electrolyte complexes PEO₆:LiXF₆ (X=P,Sb), determined from neutron powder diffraction data
Chem Mater **13** 1282 (2001)
- J M Gil, H V Alberto, R C Vilao, J Piroto Duarte, N Ayres de Campos, A Weidinger, J Krauser, E A Davis, S P Cottrell, S F J Cox
Shallow donor muonium states in II-VI semiconductor compounds
Phys Rev B **64** 075205 (2001)
- R J Green, T J Su, J R Lu, J R P Webster
The displacement of preadsorbed protein with a cationic surfactant at the hydrophilic SiO₂-water interface
J Phys Chem B **105** 9331 (2001)
- P C Griffiths, P Teerapornchaisit, I A Fallis, I Grillo
Hydrophobically modified gelatin and its interaction with SDS
Langmuir **17** 2594 (2001)
- J Grins, Z Shen, S Esmailzadeh, P Berastegui
The structures of the Ce and La N-phases RE₃Si_{8-x}AlxN_{11-x}O_{4+x} (x= 1.75 for RE = Ce, x = 1.5 for RE = La), determined by single-crystal X-ray and time-of-flight neutron powder diffraction, respectively
J Mater Chem **11** 2358 (2000)
- R J Harrison, S A T Redfern
Short- and long-range ordering in the ilmenite-hematite solid solution
Phys Chem Minerals **28** 399 (2001)
- C M B Henderson, S A T Redfern, R I Smith, K S Knight, J M Charnock
Composition and temperature dependence of cation ordering in Ni-Mg olivine solid solutions: a time-of-flight neutron powder diffraction and EXAFS study
Am Mineral **86** 1170 (2001)
- M Hofmann, S J Campbell, A Szytula
Antiferromagnetism in YbMn₂Ge₂ - Mn magnetic sublattice
J Alloy Compd **311** 137 (2000)
- S A Holt, D J McGillivray, S Poon, J W White
Protein deformation and surfactancy at an interface
J Phys Chem B **104** 7431 (2000)
- U Hoppe, H Ebdorff-Heidepriem, J Neufeind, D T Bowron
A neutron and x-ray diffraction study of the structure of Nd phosphate glasses
Z Naturforsch A **56** 237 (2001)
- U Hoppe, R Kranold, A Barz, D Stachel, J Neufeind, D A Keen
Combined neutron and x-ray scattering study of oxide glasses
J Non-Cryst Solids **293-295** 158 (2001)
- L R Hutchings, R W Richards, R L Thompson, D G Bucknall, A S Clough
Partitioning of a heterotelechelic polystyrene to separate interfaces of thin films
Eur Phys J E **5** 451 (2001)
- T Ikeda, S Mae, O Yamamuro, T Matsuo, S Ikeda, R M Ibberson
Distortion of host lattice in clathrate hydrate as a function of guest molecule and temperature
J Phys Chem A **104** 10623 (2000)
- Y Inamura, M Arai, M Nakamura, T Otomo, N Kitamura, S M Bennington, A C Hannon, U Buchenau
Intermediate range structure and low energy dynamics of densified vitreous silica
J Non-Cryst Solids **293-295** 389 (2001)
- F Juranyi, J-B Suck, O Petrenko
The order-disorder transition in supersaturated Zr_(100-x)Al_(x) studied by inelastic neutron scattering
J Non-Cryst Solids **293-295** 776 (2001)
- M Kenzelmann, R A Cowley, W J L Buyers, R Coldea, J S Gardner, M Enderle, D F McMorrow, S M Bennington
Multiparticle states in the S=1 chain system CsNiCl₃
Phys Rev Lett **87** 017201 (2001)
- A Keren, Y J Uemura, G Luke, P Mendels, M Mekata, T Asano
Magnetic dilution in the geometrically frustrated SrCr_{9p}Ga_{12-9p}O₁₉ and the role of local dynamics: A muon spin relaxation study
Phys Rev Lett **84** 3450 (2000)
- P J C King, I Yonenaga
Low temperature muonium behaviour in Cz-Si and Cz-Si_{0.91}Ge_{0.09}
Physica B **308-310** 546 (2002)
- C S Knee, M T Weller
Temperature dependence of the crystal and magnetic structures of the antiferromagnetic oxides Pb₄Fe₃O₈X, X = Cl and Br
J Mater Chem **11** 2350 (2001)
- K S Knight
Structural phase transitions, oxygen vacancy ordering and protonation in doped BaCeO₃: Results from time-of-flight neutron powder diffraction investigations
Solid State Ionics **145** 275 (2001)

- W Kockelmann, W Schafer, A Kirfel, H Klapper, H Euler
Hydrogen positions in KCo, CsCo, CsNi and CsCu tutton salt compounds determined by neutron powder diffraction
 Mater Sci Forum **378-381** 274 (2001)
- C Kranenberg, D Johrendt, A Mewis, W Kockelmann
Kristall- und elektronische Struktur von LaAlSi₂
 Z Naturforsch A **56** 620 (2001)
- A M Kusainova, S Yu Stefanovich, V A Dolgikh, A O Mosunov, C H Hervoches, P Lightfoot
Dielectric properties and structure of Bi₄NbO₈Cl and Bi₄TaO₈Cl
 J Mater Chem **11** 1141 (2001)
- S Langridge, S W Lovesey
Uses of neutron and x-ray beams to investigate magnetism
 Rad Phys & Chem **61** 235 (2001)
- J Z Larese, D Martin, D S Sivia, C J Carlile
Tracking the evolution of interatomic potentials with high resolution inelastic neutron spectroscopy
 Phys Rev Lett **87** 206102 (2001)
- J M Leger, J Haines, C Chateau, G Gocquillon, M W Schmidt, S Hull, F Gorelli, A Le Sauze, R Marchand
Phosphorous oxynitride PON, a silica analog: structure and compression of the cristobalite-like phase; P-T phase diagram
 Phys Chem Miner **28** 388 (2001)
- Z X Li, J R Lu, R K Thomas, A Weller, J Penfold, J R P Webster, A R Rennie, D S Sivia
Conformal roughness in the adsorbed lamellar phase of aerosol-OT at the air/water and liquid/solid interface
 Langmuir **17** 5858 (2001)
- Y Li, R Xu, S Couderc, D M Bloor, J Warr, J Penfold, J F Holzwarth, E Wyn-Jones
Structure of the complexes formed between sodium dodecyl sulfate and a charged and uncharged ethoxylated polyethyleneimine : small angle neutron scattering, electromotive force and isothermal titration calorimetry measurements
 Langmuir **17** 5657 (2001)
- J S Lord, S P Cottrell, P J C King, H V Alberto, N Ayres de Campos, J Gil, J Piroto Duarte, R C Vilao, R L Lichti et al
Probing the shallow donor muonium wavefunction in ZnO and CdS via transferred hyperfine couplings
 Physica B **308-310** 920 (2001)
- J S Lord, W G Williams
Muon study of proton behaviour in rhenium trioxide
 Solid State Ionics **145** 381 (2001)
- J S Loveday, G Hamel, R J Nelmes, M Guthrie, J M Besson
Neutron diffraction studies of hydrogen bonded ices
 High Pressure Res **17** 149 (2000)
- S W Lovesey, U Staub
Reply to Comment on 'Magneto-elastic model for relaxation of lanthanide ions in YBCO observed by neutron scattering'
 Phys Rev B **64** 066502 (2001)
- S W Lovesey, K S Knight, D S Sivia
Orbital properties of vanadium ions in magnetically ordered V₂O₃
2nd Int Workshop on Electron Correlations and Materials Properties, Eds A Gonis, N Kioussis (Kluwer Academic/Plenum Publishers) (2002)
- S W Lovesey, K S Knight
Calculated X-ray dichroic signals and resonant Bragg diffraction structure factors for dysprosium borocarbide (DyB₂C₂)
 Phys Rev B **64** 094401 (2001)
- W A MacFarlane, P Mendels, J Bobroff, A V Dooglav, A V Egorov, H Alloul et al
Antiferromagnetism in water doped YBa₂Cu₃O_{6+x} for x~0.5
 Physica B **289** 291 (2000)
- S Magazu, V Villari, P Migliardo, G Maisano, M T F Telling
Diffusive dynamics of water in the presence of homologous disaccharides: A comparative study by quasielastic neutron scattering. IV
 J Phys Chem B **105** 1851 (2001)
- S Magazu
NMR, static and dynamic light and neutron scattering investigations on polymeric aqueous solutions
 J Mol Structure **523** 47 (2000)
- A P Maierhofer, D G Bucknall, T M Bayer
Modulation of cytochrome C coupling to anionic lipid monolayers by a change of the phase state: a combined neutron and infrared reflection study
 Biophys J **79** 1428 (2000)
- G Mao, A G Baboul, L A Curtiss, D L Price, M-L Saboungi, M Armand, W S Howells, H E Fischer
Structure and dynamics of lithium polymer electrolytes
Proc Int Symp on Molten Salts XII, Electrochemical Society (Pennington, NJ) 99-41 247 (2000)
- S Matthies, H G Priesmeyer, M R Daymond
On the diffractive determination of elastic single crystal constants using polycrystalline samples
 J Appl Crystallogr **34** 585 (2001)
- P S May, N P O'Dowd, G A Webster
Measurement of residual stress distributions in T-plate joints
Proc 6th Int Conf on Residual Stress (Oxford: Institute of Materials) p1365 (2000)
- D Mazza, S Ronchetti, A Delmastro, M Tribaudino, W Kockelmann
Silica-free mullite structures in the Al₂O₃-B₂O₃-P₂O₅ ternary system
 Chemistry of Minerals **13** 103 (2001)
- G S McGrady, J F C Turner, R M Ibberson, M Prager
Structure of the trimethylaluminium dimer as determined by powder neutron diffraction at low temperature
 Organometallics **19** 4398 (2000)
- J Meinel, M Mani, A Cousson, F Boudjada, W Paulus, M M Johnson
Structure of trihalogenomesitylenes and tunneling of the methyl groups protons II. Protonated tribromomesitylene
 Chem Phys **261** 165 (2000)
- N P O'Dowd, Y Lei, G A Webster
The effect of residual stresses on the fracture behaviour of a ferritic steel
Fracture Mechanics, Applications and Challenges (Eds M Fuentes, M Elices, A Martin-Meizoso, J M Martinez-Esnaola) p1 (2000)
- N Onoda-Yamamuro, O Yamamuro, T Matsuo, M Ichikawa, R M Ibberson, W I F David
Neutron diffraction study on hydrogen bond structure in K₃H(SeO₄)₂ and K₃D(SeO₄)₂ crystals
 J Phys:Condens Matter **12** 8559 (2000)
- C Panagopoulos, B D Rainford, T Xiang, C A Scott, M Kambara, I H Inoue
Penetration depth measurements in MgB₂: Evidence for unconventional superconductivity
 Phys Rev B **64** 4514 (2001)

- J Penfold, E Staples, I Tucker, L Soubiran, R K Thomas
Comparison of the co-adsorption of benzyl alcohol and phenyl ethanol with the cationic surfactant C₁₆TAB at the air-water interface
 J Coll Int Sci **247** 397 (2002)
- J Penfold, E Staples, I Tucker, L Thompson, R K Thomas
Adsorption of non-ionic mixtures at the air-water interface: the effect of temperature and electrolyte
 J Coll Int Sci **247** 404 (2002)
- J Penfold
The structure of the surface of pure liquids
 Rep Prog Phys **64** 777 (2001)
- T G Perring, D T Adroja, G Chaboussant, G A Aeppli, T Kimura
Spin-waves in the bilayer La_{2-2x}Sr_{1+2x}Mn₂O₇ (x=0.35)
 J Magn Magn Mater **226** 860 (2001)
- C Petrillo, F Sacchetti, M Celli, M Zoppi, C A Checchi
An inverse geometry neutron scattering spectrometer with graphite Venetian blind crystal analyser and a para-hydrogen filter
 Nucl Instrum Meth A **441** 494 (2000)
- P Rangaswamy, M R Daymond, M A M Bourke, R Von Dreele, K Bennett, N Jayaraman
Texture and residual strain in two SiC/Ti-6-2-4-2 titanium composites
 Metall Mater Trans A **31** 89 (2000)
- C J Rhodes, T C Dintinger, C A Scott
Dynamics of cyclohexadienyl radicals in zeolite X, by longitudinal field muon relaxation
 Magn Reson Chem **38** 62 (2000)
- C J Rhodes, T C Dintinger, I D Reid, C A Scott
Mobility of dichloroethyl radicals sorbed in kaolin and silica: models of heterogeneous environmental processes
 Magn Reson Chem **38** 281 (2000)
- C J Rhodes, T C Dintinger, I D Reid, C A Scott
Spin-labelling studies of benzene sorbed in carbon particles using muonium: a molecular view of sorption by environmental carbon
 Magn Reson Chem **38** S58 (2000)
- C J Rhodes, T C Dintinger, C A Scott
Sorption of benzene in cation-exchanged zeolite X, as measured by muon spin relaxation (LF-μSR)
 Magn Reson Chem **38** 729 (2000)
- C J Rhodes
Duplicity of thiyl radicals in toxicology: protector and foe
Toxicology of the Human Environment - the Critical Role of Free Radicals, Ed C J Rhodes (Taylor and Francis) p285 (2000)
- C J Rhodes
Radiotracer studies of free radicals using muonium (the second hydrogen radioisotope)
 Progress in Reaction Kinetics and Mechanisms **25** 219 (2000)
- M A Ricci, M Rovere
Studies of water in confinement by experiments and simulations
 J Phys IV **10** 187 (2000)
- A D Robertson, A R Armstrong, P G Bruce
Low temperature Co doped spinel intercalation electrodes
 J Power Sources **97** 332 (2001)
- A D Robertson, A R Armstrong, P G Bruce
Layered Li_xMn_yCo_{1-y}O₂ intercalation electrodes – influence of ion exchange on capacity and structure upon cycling
 Chem Mater **13** 2380 (2001)
- P Sittner, P Lukas, D Neov, M R Daymond, V Novak, G M Swallowe
Stress induced martensitic transformation in CuAlZnMn polycrystals investigated by two in situ neutron diffraction techniques
 Mat Sci Eng A-Struct **324** 225 (2002)
- D S Sivia
The number of good reflections in a powder pattern
 J Appl Crystallogr **33** 1295 (2000)
- N T Skipper, J K Walters, C Lobban, K McKewn, R Mukerji, G J Martin, M de Podesta, A C Hannon
Neutron diffraction studies of graphite-potassium-methylamine: Staging transitions and structure of new graphite intercalation compounds
 J Phys Chem B **104** 10969 (2000)
- I Sosnowska, W Schafer, W Kockelmann, I O Troyanchuk
Neutron diffraction studies of the crystal and magnetic structures of BiMn_xFe_{1-x}O₃ solid solutions
 Mater Sci Forum **378-381** 616 (2001)
- I Sosnowska, R Przenioslo, W Schäfer, W Kockelmann, R Hempelmann, K Wysocki
Possible deuterium positions in the high temperature deuterated proton conductor Ba₃Ca_{1+y}Nb_{2-y}O_{9-δ} studied by neutron and X-ray powder diffraction
 J Alloy Compd **328** 226 (2001)
- L Soubiran, E Staples, I Tucker, J Penfold, A Creeth
Effect of shear on the lamellar phase of a dialkyl cationic surfactant
 Langmuir **17** 7988 (2001)
- T Steiner, I Majerz, C C Wilson
First O-H-N hydrogen bond with a centred proton obtained by thermally induced proton migration
 Angew Chem-Int Edit **40** 2651 (2001)
- A Steuerer, P J Withers, J R Santisteban, L Edwards, G Bruno, M E Fitzpatrick, M R Daymond, M W Johnson, D Q Wang
Bragg edge determination for accurate lattice parameter and elastic strain measurement
 Phys Status Solidi A **185** 221 (2001)
- V G Storchak, D G Eshchenko, J H Brewer, S P Cottrell, S F J Cox, E Karlsson, R W Wappling
Electron transport in cryocrystals
 J Low Temp Phys **122** 527 (2001)
- J-B Suck
Dependence of the dynamics of metallic glasses on quenched-in density fluctuations and on temperature
 J Non-Cryst Solids **293-295** 370 (2001)
- D Sun, F Gingl, H Enoki, D K Ross, E Akiba
Phase components of the sintered Mg-X wt% LaNi₅ (X=20-50) composites and their hydrogenation properties
 Acta Mater **48** 2363 (2000)
- M G Taylor, S F Parker, K Simkiss, P C H Mitchell
Bone mineral: evidence for hydroxyl groups by inelastic neutron scattering
 Phys Chem Chem Phys **3** 1514 (2001)
- C Tengroth, J Swenson, A Isopo, L Borjesson
Structure of Ca_{0.4}K_{0.6}(NO₃)_{1.4} from the glass to the liquid
 Phys Rev B **64** 224207 (2001)

- N Torikai, M Seki, Y Matsushita, M Takeda, K Soyama, N Metoki, S Langridge, D G Bucknall, J Penfold
Comparison between interfacial structures of a block copolymer and two-component homopolymers by neutron reflectivity measurement
J Phys Soc Japan **70** Suppl A344 (2001)
- G V Vajenine, G Auffermann, Yu Prots, W Schnelle, R Kremer, A Simon, R Kniep
Preparation, crystal structure and properties of barium pernitride
Inorg Chem **40** 4866 (2001)
- L Vocadlo, K S Knight, G D Price, I G Wood
Thermal expansion and crystal structure of FeSi between 4K and 1173K determined by time-of-flight neutron powder diffraction
Phys Chem Minerals **29** 132 (2002)
- J C Wasse, S Hayama, N T Skipper, H E Fischer
Structure of a metallic solution of lithium in ammonia
Phys Rev B **61** 11993 (2000)
- G A Webster
Role of residual stress in engineering applications
Mater Sci Forum **347-349** 1 (2000)
- G A Webster
Neutron diffraction measurements of residual stress in a shrink-fit ring and plug
VAMAS report no 38 ISSN 1016-2186 (2000)
- G A Webster
Development of a standard for the measurement of residual stress by neutron diffraction
Proc 6th Int Conf on Residual Stress (Oxford: Institute of Materials) p189 (2000)
- R L Witnens, Y Tabira, J S O Evans, I J King, A W Sleight
A new three-dimensional incommensurately modulated cubic phase (in ZrP_2O_7) and its symmetry characterisation via temperature-dependent electron diffraction
J Solid State Chem **157** 186 (2001)
- A C Wright, B A Shakhmatkin, N M Vedishcheva
The chemical structure of oxide glasses: a concept consistent with neutron scattering studies?
Glass Phys Chem **27** 97 (2000)
- A C Wright, C E Stone, R N Sinclair, N Umesaki, N Kitamura, K Ura, N Ohtori, A C Hannon
Structure of pressure compacted vitreous boron oxide
Phys Chem Glasses **41** 296 (2000)
- A C Wright
X-ray and neutron diffraction
Insulating and Semiconducting Glasses, Ed P Boolchand (World Scientific) Chap 5(A) p147 (2000)
- A C Wright
Defect-free vitreous networks: the idealised structure of SiO_2 and related glasses
Defects in SiO_2 and Related Dielectrics: Science and Technology, Eds G Pacchioni, L Skuja, D L Griscom (Kluwer) p1 (2000)

ISIS Seminars 2001 – 2002

Protein Crystallography at the SRS

Dr. Liz Duke (SRS, Daresbury Laboratory)
22nd May 2001

Experimental Realization of a 2D Fractional Quantum Spin Liquid

Dr. Radu Coldea (University of Oxford)
12th June 2001

Polarised ³He for neutron spin filters and other applications

Prof. Tim Chupp (Univ. of Michigan)

The NIST-Indiana-Hamilton Polarised ³He Neutron Spin Filter Program

Dr. Tom Gentile (National Institute of Standards and Technology)

Recent developments on ³He polarisation using fibre lasers – some applications

Dr. Pierre-Jean Nacher
(L'Ecole Normale Supérieure)
28th June 2001

Long wavelength magnetic excitations in correlated compounds: the case of UGe₂

Dr. A. Yaouanc (CEA Grenoble)
3rd July 2001

How to solve the mystery of Exchange Anisotropy

Dr. G. P. Felcher (Argonne National Laboratory)
9th July 2001

High-energy X-ray diffraction studies of disordered materials

Dr. Shinji Kohara (Japan Synchrotron Radiation Research Institute)
10th July 2001

Modelling V₂O₃

Dr. Martin Long (University of Birmingham)
24th July 2001

Field induced transitions in kagome antiferromagnet

Dr. Mike Zhitormiski (ESRF)
7th August 2001

A New Integrated Facility for High Pressure Physics at the Advanced Photon Source

Dr. Daniel Häusermann (HPCAT and Carnegie Institution of Washington, Advanced Photon Source, Argonne National Laboratory)
29th October 2001

Chirality in two dimensions: an electrochemical approach to characterising asymmetric reactions using heterogeneous catalysts

Prof. Gary Attard (Cardiff University)
13th November 2001

Composite spin degree of freedom in the corner-sharing tetrahedra ZnCr₂O₄

Dr. Seung-Hun Lee
(Center for Neutron Research, NIST)
26th November 2001

Insights into heavy-Fermion behavior from scattering experiments

Dr. G. H. Lander (European Institute for Transuranium Elements, Germany and Los Alamos National Laboratory, USA)
11th December 2001

Quantum spin chains in high magnetic fields

Dr. Mechthild Enderle
(Institut Laue-Langevin, France)
13th December 2001

Quantum Critical Points: When electrons lose their integrity

Prof. Piers Coleman (Rutgers University, USA)
20th December 2001

From atomic scale holography to real space images of atoms

Prof. Gerhard Materlik
(Chief Executive, Diamond Project, RAL)
15th January 2002

ZETA, the new spectrometer at ILL for measuring phonon lifetimes

Dr. Roland Gähler
(Institut Laue-Langevin, France)
25th January 2002

Exploring the capabilities of X-ray absorption spectroscopy for determining the structure of electrolyte solutions: Computed spectra based on molecular dynamics which uses first-principles interaction potentials

Prof. Enrique Sánchez Marcos
(Universidad de Sevilla, Spain)
12th February 2002

Science Discussion Group Meetings 2001 – 2002

Science Discussion Group Meetings are informal gatherings held during ISIS running for the presentation and discussion of new ideas, latest results and recent developments.

Hydrophobic effects in alcohol water solutions

Daniel Bowron
3rd May 2001

Liquid helium in confinement

Bjorn Fak
31st May 2001

Float glass surfaces and coatings studied by X-ray and neutron techniques

Rob Dalgleish
14th June 2001

Evidence for unusual superconductivity in La_3Ni

Adrian Hillier
20th September 2001

Protein adsorption and deformation at interfaces

Stephen Holt
4th October 2001

Understanding disorder in crystals using diffraction data

David Keen
18th October 2001

Caving in the land of the King

Steve King
8th November 2001

Hydrogen in nitride semiconductors, studied by muon spin resonance

Steve Cox
22nd November 2001

An interpretation of resonant X-ray diffraction in V_2O_3

Stephen Lovesey
13th December 2001



Preparations being made for the installation of the GEM radial collimator (01RC4033).

Ken Anderson (ISIS, now ILL) installing polarising components on OSIRIS (01RC4007).



David Follows (Oxford University) preparing his surfactant samples for reflectometry studies (01RC3985).



Bella Lake (Oxford University) during her investigations of dimensional crossover in a spin-5/2 quasi-1D antiferromagnet (01RC4428).



Emulsion samples being prepared for investigation on LOQ by Mark Henderson (Australian National University) (01RC4027).

Paolo Radaelli (ISIS) with the Gem oscillating radial collimator. As described on page 77, this device substantially reduces background scatter from sample environment equipment.

Steve Cottrell (ISIS) shows visitors from the London International Youth Science Forum around the facility (02RC3076).

Students at the 7th Oxford Summer School on Neutron Scattering visiting ISIS in September (01RC3676).

Uschi Steigenberger (ISIS) explains the workings of ISIS to visiting teachers (01RC4512).

Dave McPhail from the ISIS Project Engineering Group and Nigel Rhodes from the ISIS detector group with the new GEM bank 6 detector array (02EC3173).